Development and Application of Modular Light-Induced Ligation Techniques in Polymer Science

Zur Erlangung des akademischen Grades eines

DOKTORS DER NATURWISSENSCHAFTEN

(Dr. rer. nat.)

Fakultät für Chemie und Biowissenschaften

Karlsruher Institut für Technologie (KIT) - Universitätsbereich

genehmigte

DISSERTATION

von

Dipl. Chem. Jan Ole Müller

aus

Worms, Deutschland

On the arid lands there will spring up industrial colonies without smoke and without smokestacks; forests of glass tubes will extend over the plains and glass buildings will rise everywhere; inside of these will take place the photochemical processes that hitherto have been the guarded secret of the plants, but that will have been mastered by human industry which will know how to make them bear even more abundant fruit than Nature, for Nature is not in a hurry and mankind is. And if in a distant future the supply of coal becomes completely exhausted, civilization will not be checked by that, for life and civilization will continue as long as the sun shines!

Giacomo Ciamician (1912)

ABSTRACT

The development of new modular photochemical conjugation techniques as well as the use of light-induced cycloaddition chemistry for applications in various fields of polymer science is reported.

The present thesis thus includes investigations towards the development of advanced light-driven ligation processes enhancing the performance of photochemical tools, e.g., nitrile imine-mediated tetrazole-ene cycloaddition (NITEC), azirine-based ligation, photoenol chemistry, and Paternò–Büchi reactions. The advanced photochemical features enable access to novel applications in polymer science, such as a light-driven step-growth polymerization technique, polymer end group modification induced by visible light, reversible encoding of polymer termini, generation of block copolymers, and crosslinking of polybutadienes.

First, a novel class of photoreactive profluorescent monomers which efficiently polymerize at ambient temperature adhering to Carothers' kinetics, generating strongly fluorescent polymers, is introduced. The newly designed monomers, which carry a tetrazole and a dipolarophile unit respectively, are readily prepared and photo-triggered to polymerize with easily accessible and inexpensive light sources. The structure of the new polymer class is analyzed in detail via size exclusion chromatography (SEC), nuclear resonance spectroscopy (NMR) and electrospray-ionization mass spectrometry (ESI-MS), evidencing the polymerization mechanism and kinetics.

Moreover, an ultra-rapid visible light-driven avenue for catalyst-free ligation is reported. The highly efficient process is based on photochemistry of azirines and thus suitable for cycloaddition reactions with a multitude of reactants. Small molecules were subjected to the conjugation reaction as well as polymeric materials with a reactive terminus. Both processes were monitored in detail employing, for instance, high-performance liquid chromatography (HPLC) or high-resolution mass spectrometry (high-res ESI-MS).

Next, the suitability of Paternò-Büchi chemistry for reversible encoding of polymer termini was investigated applying an aldehyde-capped poly(ethylene glycol) system. Besides the photochemical generation of oxetane functions, their photosensitized cleavage behavior was explored supported by characterization via collision induced dissociation (CID) ESI-MS. The proof of principle for recodability was demonstrated by performing three consecutive photochemical end-group transformations.

Furthermore, a novel polymer conjugation reaction for non-activated dithioesters was established, which is based on a light-triggered hetero Diels–Alder reaction with a highly reactive photoenol diene. The enhanced activity of the photochemically generated reactive species enables nearly quantitative coupling of polymer blocks without a catalyst on very short timescales.

Finally, the crosslinking of unsaturated polymers featuring non-activated double bonds via NITEC that functions in sunlight is reported. Developing a tetrazole-containing di-functional linker moiety allows for the transformation of linear 1,2-polybutadienes into insoluble networks with fluorescent properties, enabling the fabrication of fluorescent patterned surfaces and designs.

ZUSAMMENFASSUNG

Die vorliegende Arbeit behandelt die Neuentwicklung modularer photochemischer Konjugationsmethoden, sowie die Weiterentwicklung bereits etablierter Photoligationsmethoden basierend auf lichtinduzierten Zykloadditionsreaktionen in deren Anwendung auf verschiedenste Bereiche der Polymerwissenschaft.

Diese Arbeit enthält Untersuchungen die auf verbesserte Leistungsfähigkeit diverser photochemischer Synthesewerkzeuge, wie zum Beispiel die Nitrilimin-vermittelte Tetrazol-Ene Zykloaddition (NITEC), Ligation basierend auf Azirinchemie, Photoenolchemie und Paternò–Büchi Reaktionen abzielt. Die dadurch erreichten fortgeschrittenen Möglichkeiten der photochemischen Methoden eröffnen Zugang zu deren neuartiger Anwendung im Bereich der Polymerchemie, wie beispielsweise in auf Licht basierender Stufenwachstumspolymerisation, der Modifikation von polymeren Endgruppen mittels sichtbaren Lichts, der reversiblen Kodierung von Polymerendgruppen, die Herstellung von Blockcopolymeren sowie die Vernetzung von Polybutadienen.

Zu Beginn wird eine neuartige Klasse photoaktivierbarer, profluoreszenter Monomere vorgestellt, die bei Raumtemperatur polymerisiert werden können, dabei die Carothers Kinetik erfüllen und stark fluoreszierende Polymere erzeugen. Diese neuentwickelten Monomere, die eine Tetrazolkomponente sowie eine entsprechende Dipolarophileinheit enthalten, sind einfach herzustellen und mit leicht zugänglichen preisgünstigen Lichtquellen photochemisch zu polymerisieren. Um Polymerizationsmechanismus und -kinetik zu untermauern wird die Struktur der dargestellten neuartigen Polymere mittels Größenausschlusschromatographie, Kernresonanzspektroskopie und Elektrospray-Ionisations Massenspektrometrie detailliert charakterisiert.

Desweiteren wird eine extrem schnelle, durch sichtbares Licht induzierbare Variante zur katalysatorfreien Ligation behandelt. Der höchsteffiziente Prozess basiert auf der Photochemie von Azirinen und ist daher für Zykloadditionsreaktionen mit einer

Vielzahl an Reaktionspartnern geeignet. Kleine Moleküle wurden der Konjugations-methode ebenso unterzogen wie polymere Materialien mit reaktiven Endgruppen. Beide Prozesse wurden detailliert charakterisiert, zum Beispiel mittels Hochleistungs-flüssigkeitschromatographie (HPLC) oder hochaufgelöster Massenspektrometrie.

Als nächstes wurde die Eignung von Paternò–Büchi Chemie zur reversiblen Kodierung polymerer Termini unter Verwendung eines Aldehyd-funktionalisierten Polyethylenglykols untersucht. Außer der photochemischen Erzeugung von Oxetanfunktionalitäten wurde deren photosensibilisiertes Spaltungsverhalten erforscht, unterstützt durch kollisionsinduzierte Dissoziations-Massenspektrometrie. Durch drei aufeinanderfolgende photochemische Endgruppenumwandlungen wurde der Beweis für wiederholte Kodierung erbracht.

Des weiteren wird eine neuartige Reaktion von Dithioestern zur Konjugation von Polymeren etabliert, die auf der lichtinduzierten hetero Diels–Alder Reaktion hochreaktiver Diene beruht. Die erhöhte Aktivität der photochemisch erzeugten, reaktiven Spezies ermöglicht die schnelle, nahezu quantitative Kupplung von polymeren Bausteinen ohne Zusatz von Katalysatoren.

Abschließend wird von der Vernetzung ungesättigter Polymere, die nicht-aktivierte Doppelbindungen enthalten, mittels NITEC im Sonnenlicht berichtet. Durch die Entwicklung eines Tetrazol-basierenden difunktionalen Linkers konnte die Umwandlung von linearen 1,2-Polybutadienen in unlösliche, fluoreszierende Netzwerke erreicht werden, die die Erzeugung von fluoreszenten Mustern auf Oberflächen ermöglichen.

PUBLICATIONS ARISING FROM THE PRESENT THESIS

4. b) **Durch sichtbares Licht induzierte Klick-Chemie**

J. O. Mueller, F. G. Schmidt, J. P. Blinco, C. Barner-Kowollik, *Angew. Chem.* **2015**, DOI: 10.1002/ange.201504716R1.

4. a) **Visible-Light-Induced Click Chemistry**

J. O. Mueller, F. G. Schmidt, J. P. Blinco, C. Barner-Kowollik, *Angew. Chem. Int. Ed.* **2015**, DOI: 10.1002/anie.201504716.

3. **Fluorescent Polymers from Non-Fluorescent Photoreactive Monomers**

J. O. Mueller, D. Voll, F. G. Schmidt, G. Delaittre, C. Barner-Kowollik, *Chem. Commun.* **2014**, *50*, 15681-15684.

2. **Sunlight-Induced Crosslinking of 1,2-Polybutadienes: Access to Fluorescent Polymer Networks**

J. O. Mueller, N. K. Guimard, K. K. Oehlenschlaeger, F. G. Schmidt, C. Barner-Kowollik, *Polym. Chem.* **2014**, *5*, 1447-1456.

1. b) **Lichtinduzierte Modulare Ligation von Konventionellen RAFT Polymeren**

K. K. Oehlenschlaeger,[‡] **J. O. Mueller**,[‡] N. B. Heine, M. Glassner, N. K. Guimard, G. Delaittre, F. G. Schmidt, C. Barner-Kowollik, *Angew. Chem.* **2013**, *125*, 791-796. [‡] both authors contributed equally.

1. a) **Light-Induced Modular Ligation of Conventional RAFT Polymers**

K. K. Oehlenschlaeger,[‡] **J. O. Mueller**,[‡] N. B. Heine, M. Glassner, N. K. Guimard, G. Delaittre, F. G. Schmidt, C. Barner-Kowollik, *Angew. Chem. Int. Ed.* **2013**, *52*, 762-766. [‡] both authors contributed equally.

ADDITIONAL PUBLICATIONS

10. b) Effiziente Photochemie für die räumlich aufgelöste Oberflächen-funktionalisierung

G. Delaittre, A. S. Goldmann, **J. O. Mueller**, C. Barner-Kowollik, *Angew. Chem.* **2015**, *in press*.

10. a) Efficient Photochemistries for Spatially Resolved Surface Functionalization

G. Delaittre, A. S. Goldmann, **J. O. Mueller**, C. Barner-Kowollik, *Angew. Chem. Int. Ed.* **2015**, *in press*.

9. Photo-Induced Sequence Defined Macromolecules via Hetero Bifunctional Synthons

N. Zydziak, F. Feist, B. Huber, **J. O. Mueller**, C. Barner-Kowollik, *Chem. Commun.* **2015**, *51*, 1799-1802.

8. A Disulfide Intercalator Toolbox for Site-Directed Protein Chemistry

T. Wang, Y. Wu, S. L. Kuan, O. Dumele, M. Lamla, D. Y. W. Ng, M. Arzt, J. Thomas, **J. O. Mueller** , C. Barner-Kowollik , T. Weil, *Chem. Eur. J.* **2014**, *21*, 228-238.

7. Adaptable Hetero Diels–Alder Networks for Fast Self-Healing under Mild Conditions

K. K. Oehlenschlaeger, **J. O. Mueller**, J. Brandt, S. Hilf, A. Lederer, M. Wilhelm, R. Graf, M. L. Coote, F. G. Schmidt, C. Barner-Kowollik, *Adv. Mater.* **2014**, *26*, 3561-3566.

6. Photochemical Design of Functional Fluorescent Single-Chain Nanoparticles

J. Willenbacher, K. N. R. Wuest, **J. O. Mueller**, M. Kaupp, H.-A. Wagenknecht, C. Barner-Kowollik, *ACS Macro Lett.* **2014**, 574-579.

5. **Photo-Patterning of Non-Fouling Polymers and Biomolecules on Paper**

T. Tischer, C. Rodriguez-Emmenegger, V. Trouillet, A. Welle, V. Schueler, **J. O. Mueller**, A. S. Goldmann, E. Brynda, C. Barner-Kowollik, *Adv. Mater.* **2014**, *26*, 4087-4092.

4. **Controlled Cell Adhesion on Polydopamine Interfaces Photo-patterned with Non-Fouling Brushes**

C. Rodriguez-Emmenegger, C. M. Preuss, B. Yameen, O. Pop-Georgievski, M. Bachmann, **J. O. Mueller**, M. Bruns, A. S. Goldmann, M. Bastmeyer, C. Barner-Kowollik, *Adv. Mater.* **2013**, *25*, 6123-6127.

3. **Fast and Catalyst-Free Hetero-Diels-Alder Chemistry for Cyclable Bonding/Debonding on Demand Material Design**

K. K. Oehlenschlaeger, N. K. Guimard, J. Brandt, **J. O. Mueller**, C. Y. Lin, S. Hilf, A. Lederer, M. L. Coote, F. G. Schmidt, C. Barner-Kowollik, *Polym. Chem.* **2013**, *4*, 4348-4355.

2. **Harnessing Entropy to Direct the Bonding/Debonding of Polymer Systems on Reversible Chemistry**

N. K. Guimard, J. Ho, J. Brandt, C. Y. Lin, M. Namazian, **J. O. Mueller**, K. K. Oehlenschlaeger, S. Hilf, A. Lederer, F. G. Schmidt, M. L. Coote, C. Barner-Kowollik, *Chem. Sci.* **2013**, *4*, 2752-2759.

1. **Highly Orthogonal Functionalization of ADMET Polymers via Photo-Induced Diels-Alder Reactions**

M. Winkler, **J. O. Mueller**, K. K. Oehlenschlaeger, L. Montero de Espinosa, M. A. R. Meier, C. Barner-Kowollik, *Macromolecules* **2012**, *45*, 5012-5019.

TABLE OF CONTENTS

1

INTRODUCTION

"Is it time to shoot for the sun?" was the title of an article addressing global energy concerns published ten years ago.[1] It is a fair question which the Italian visionary Giacomo Ciamician had answered for himself already at the beginning of the last century. With an unparalleled clear-sightedness, he envisaged the future of mankind to be dependent on solar energy.[2] Although solely relying on the fundamental knowledge of organic and photochemistry at the beginning of the 20th century, Ciamician's vision was highly accurate: He predicted an increasing need for clean energy and efficient industrial processes. Furthermore, mankind would be destined to solve this technological challenge for its survival. In a nutshell, he had actually commenced the debate on sustainability about 100 years before scientists of the modern era have stepped in.

Awakened by global warming and other unambiguous evidence for our destructive dealing with Nature, the contemporary scientific society – including research, industry, and education – is dominated by aspects concerning environmental and energy issues. However, attempting to solve the energy challenge in the context of a Ph.D. thesis would be quite ambitious. Yet, Ciamician's optimistic enthusiasm was not exclusively restricted to employing solar radiation for providing humanity with energy. Being an active photochemist himself, he was convinced that photochemical techniques based on solar radiation would evolve to constitute future industrial

processes. A modern and progressive philosophy coinciding with Ciamician's inspiration by Nature's photosynthesis – the gold standard of efficient systems – is termed green chemistry.[3] Consequently, green chemistry represents simple, efficient, feasible, and environmentally benign processes.[4] Despite the research and development efforts in this area, Nature still exceeds the photoscientists by far, since the efficiency and predominantly the sustainability of its photosynthesis is currently out of reach for every synthetic chemist. Thus, the motivation for today's photochemical research is obvious: The exploration of novel light-induced techniques requires acceleration in order to address the challenges of contemporary society.

Since photochemistry and its application are a wide field, it is critical to define the foci of research for the present thesis. The general aim, however, is set by the previously formulated motivation of stepwise improving the existing state-of-the-art techniques in photochemical science. More specifically, the photochemical tools themselves are to be enhanced, for instance, in terms of accessible excitation wavelengths. Sunlight-induced or – to be even more demanding – visible light-triggered ligation systems are just commenced to be developed and shifting established photochemical methods from the UV region to ubiquitously present radiation is highly desirable. Another opportunity for improving a system's performance stems from highly reactive species which can be generated upon irradiation. Thus, accessing novel pairings is possible and the current work seeks to establish the corresponding protocols. Finally, to demonstrate a broadened scope of photochemical methods, e.g., photoenol,[5] azirine,[6] tetrazole,[7] and Paternò–Büchi chemistry,[8-9] it is important to target novel applications for established as well as improved techniques, retaining a good balance between industry related requirements and the academic need for fundamental research.

In order to present photochemical achievements on a broad platform, polymer science forms the fundamental basis of the current thesis. The extensive and rapidly progressing field of macromolecular chemistry provides a variety of aspects from which the polymerization process, post-polymerization modification of polymer termini, the generation of block copolymers, and polymer crosslinking for surface patterning were chosen to be closely investigated. Merging photochemistry-based endeavors with applications for polymer science results in the following intended advances, ordered by increasing size of the polymeric system: *(i)* A step growth

polymerization process based on tetrazole-ene cycloaddition demonstrating the efficiency and feasibility of this photochemical tool to generate fluorescent polymeric materials from non-fluorescent photoreactive monomers. *(ii)* By designing a novel chromophore-azirine conjugate, a visible light-induced ligation method is developed and applied for polymer end group modification. *(iii)* Reversible end group encoding of polymers may be attempted using the Paternò–Büchi approach. An exploratory study trials the retro Paternò–Büchi reactions for its applicability. *(iv)* Photoenol chemistry allows for accessing poorly activated polymer termini involving a conventional reversible addition-fragmentation chain transfer agent. Thus, the enhanced reactivity of the photo-induced moieties broadens the scope of applied photoenol conjugation. *(v)* Advanced tetrazole design enables to increase their activity towards non-activated dipolarophiles. Hence, spatially controlled surface patterning via crosslinking of polybutadienes is demonstrated in the current thesis.

Each of the single projects alluded to above is categorized in the following scheme depending on its respective photochemical technique as well as its role in the field of polymer science (*Figure 1*).
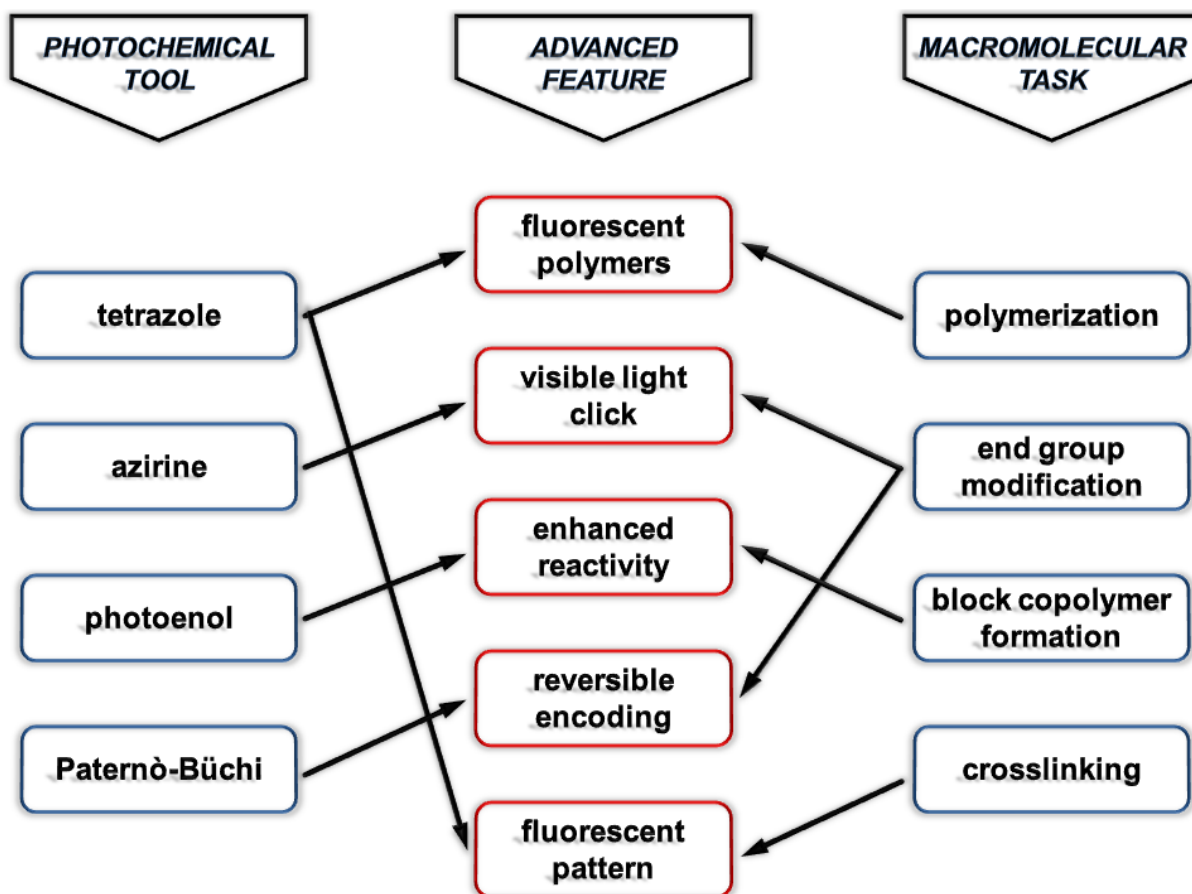
Figure 1: Overview of projects addressed in the current thesis. In each project a macromolecular challenge (right side) is approached via a particular photochemical technique (left side), introducing specific features (middle).

2

PHOTOCHEMISTRY IN POLYMER SCIENCE – A LITERATURE REVIEW

The current thesis covers a large area of aspects in the fields of polymer science and photochemistry. Although the combination of two such large disciplines provides the opportunity to discuss a diversity of aspects and develop various novel systems, neither of the single topics should be addressed cursory. Thus, it is essential for the reader to possess a solid theoretical background in both fields. Nevertheless, the rapid evolution of research requires a more detailed knowledge in the particular directions the various specialized topics the present thesis is addressing. Therefore, it is the purpose of the current chapter to provide on the one hand the very fundamentals in the fields of polymer science and photochemistry, which constitute the first two sections and on the other hand the up-to-date state-of-the-art developments in the area which combines the two extensive disciplines in the final section of this chapter. Thus, it is intended to provide a summary of all the required information allowing the reader to follow the scientific discussions of the subsequent chapters.

2.1 Polymer Science

Synthetic polymeric materials are ubiquitously present in today's society. It was inevitable that polymer science has become the basis for a major industrial branch due to the exceptional developments of the past century. Even before the molecular understanding of what a polymer is emerged, rubbers were an important industrial product and a highly required material with unique properties.[10] In 1929, Hermann Staudinger proposed an initially controversial theory in which polymers were assumed to be macromolecules.[11] His initial studies on the simplest polymeric materials, as well as their physical and chemical properties, are a benchmark in the history of polymer chemistry since they provide the first idea about the molecular constitution of macromolecules.[12-17] Therefore, Staudinger was awarded the Noble Price in 1953. From the 1950s on, the increasing knowledge and experience led to further improvements of the material's performance and thus, a steady increase in the annual industrial production (*Figure 2.1*). By today, polymer industry has reached a level where macromolecular materials are an essential ingredient in the majority of products.
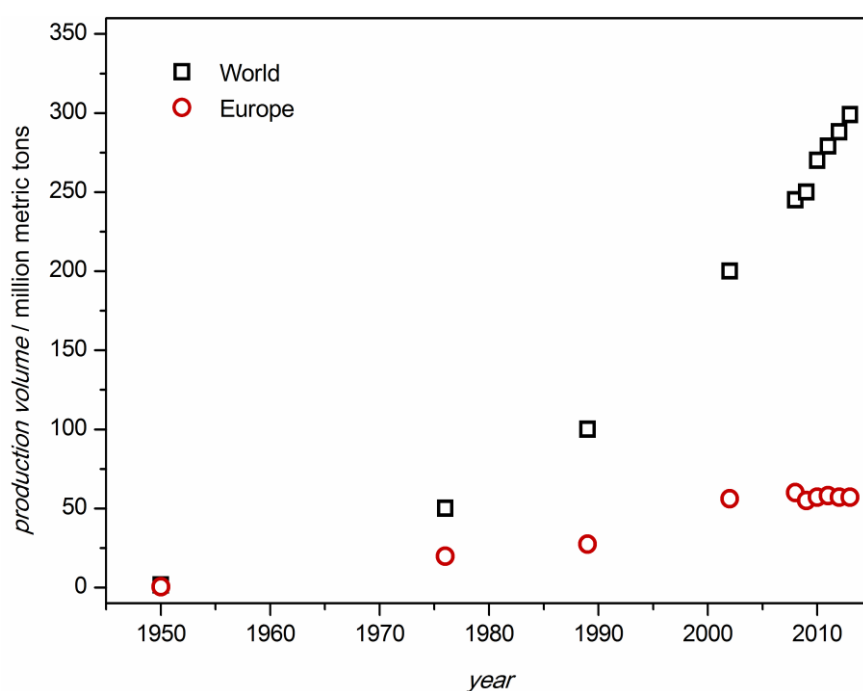
Figure 2.1: Worldwide production of macromolecular materials from 1950 to 2013. Data was reproduced from ref.[18]

Nevertheless, the demands for modern materials become continuously more challenging, emphasizing the importance of our research. Although controlling polymer functionality, topology, and designing architectures for tailor-made functional materials are standard procedures for the synthetic chemist,[19] the need for improved synthetic tools and increasing efficiency, which can broaden the scope of application and enhance the material's performance, is always present.

In the current chapter the reader will be introduced to the fundamentals of polymer chemistry. The following sections contain basic knowledge about polymerization kinetics, as well as more specialized aspects in the field of macromolecular science. The main foci of discussion are, for instance, step-growth and chain-growth polymerization processes, as well as modern polymerization techniques. Thus, the essential knowledge about polymers with regard to the explicit topics addressed in the present thesis is provided.

2.1.1 Step-growth Polymerization

The variety of polymers concerning their constitution, size, monomer type, synthesis, functionality, physical, chemical, and mechanical properties appears to be almost infinite. The attempt to classify polymers – which is not generally feasible – into two categories can be somewhat confusing.[20] In contrast to Wallace H. Carothers' initial classification of polymers into condensation and addition polymers,[21] which was not entirely well engineered, Paul J. Flory's approach to distinguish polymers by their generation mechanism was broadly acknowledged although he applied the same terminology as Carothers.[22] The most recent terminology employs the terms step-growth and chain-growth polymers, where step-growth includes condensation (formation of a low molecular weight side-product during the polymerization) and addition (no formation of side-products) polymers. Chain-growth polymers, which are mostly – yet not exclusively – made of vinyl type monomers, are the subject of discussion in the subsequent section (*2.1.2*). The most prominent of synthetic step-growth polymers are polyesters, polyamides, polycarbonates, polyurethanes, and polysiloxanes, where Nylon – a polyamide – is by far the most popular product.

In a typical step-growth polymerization, the reaction of two different reactive groups, for instance a carboxylic acid and an alcohol, form the linkage between two monomer units. Thus, monomers containing at least two functional groups are required for macromolecular growth. These monomers can be of two different types: They either carry the same function at both ends (A-A, B-B), a case in which it is essential that the two monomers are deployed in the same molar ratio, or one monomer unit contains both functionalities. In the latter case, the problem of equal molarity for the functional groups is eliminated. The schematic representation for both options is depicted in *Scheme 2.1.1-1*.

$$n\ A\text{-}A\ +\ n\ B\text{-}B\ \longrightarrow\ \left[A\text{-}AB\text{-}B \right]_{2n}$$

$$n\ A\text{-}B\ \longrightarrow\ \left[A\text{-}B \right]_{n}$$
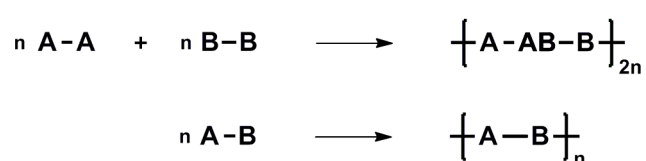
Scheme 2.1.1-1: Step-growth polymerization for two types of monomers: top A−A + B−B, bottom A−B.

Taking a closer look at the kinetics of step-growth polymerization is necessary for two reasons: The kinetics are of importance for the practical use of this type of polymerization, enabling the prediction of molecular weight and allowing to adjust the reaction conditions. Knowledge about kinetics also offers insight into the major differences compared to the chain-growth polymerization process.

At first, some preliminary thoughts about the molecular weight of a step-growth polymer are noted, which is the primary concern to the synthetic chemist. The number average degree of polymerization, DP_n, is defined as the initial number of monomer molecules (N_0), divided by the number of molecules present at a certain reaction time (N_t). In combination with the conversion p, which represents the fraction of monomers converted to polymer (Eq 2.1-1), the resulting equation is known as the Carothers equation (Eq 2.1-2).

$$p = 1 - \frac{N_t}{N_0} \qquad\qquad \text{Eq 2.1-1}$$

$$DP_n = \frac{N_0}{N_t} = \frac{1}{1 - p} \qquad\qquad \text{Eq 2.1-2}$$

Assuming the two functional groups are not present in an equimolar amount, the Carothers equation complicates to Eq 2.1-3, where q is the fraction of functional groups, which is defined to be smaller than unity.

$$DP_n = \frac{1+q}{1+q-2qp}$$
Eq 2.1-3

An alternative version of the Carothers equation (Eq 2.1-4) connects conversion, the molar mass of the monomer (M_{mon}) and weight average molar mass of the polymer (M_w), which is of importance to the discussion in Chapter 3.

$$M_w = M_{mon}\ \frac{1+p}{1-p}$$
Eq 2.1-4

In order to generate kinetic equations for the polymerization process, the elementary reactions need to be identified and evaluated. Firstly, the monomers present in the reaction mixture react with each other to form dimers. The newly formed dimer can itself react with another monomer unit, a dimer, or a trimer, generating a trimer, tetramer, or pentamer, respectively. It becomes obvious that in the case of for example a simple polyesterification, the number of elementary steps is infinite and the resulting kinetic equations for the polymerization process are complex. Therefore, a feasible simplification is required, which can be achieved by assuming that each single reaction step is independent from the size of the monomer/ oligomer/ polymer. Experimental experience, as well as theoretical calculations confirm this assumption to be reasonable since the mobility of the reactive function itself decreases not as much as the mobility of the entire molecule.[23-24] Thus, the polymerization reaction can be summarized by the following reaction scheme (*Scheme 2.1.1-2*).

$$\text{—COOH} \quad + \quad \text{HO—} \quad \underset{k_{-e}}{\overset{k_e}{\rightleftharpoons}} \quad \text{—COO—} \quad + \quad H_2O$$
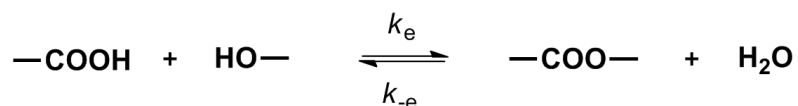
Scheme 2.1.1-2. General reaction scheme for a polyesterification.

The reversibility of esterification reactions causes not only problems with solving the kinetic equations, but it also needs to be suppressed in an actual polymerization system since high conversions must be achieved to obtain molar masses of reasonable value. Therefore, the generated water is typically removed in a polyesterification. The resulting equation for the consumption of functional groups (**COOH** and **OH**) is displayed in the following equation (Eq 2.1-3):

$$-\frac{d\,\textbf{COOH}}{d\,t} = -\frac{d\,\textbf{OH}}{d\,t} = k_e \cdot \textbf{cat} \cdot \textbf{COOH} \cdot \textbf{OH}$$
Eq 2.1-5

Furthermore, the addition of an external catalyst accelerates the reaction and further simplifies the kinetic equation, since k_e and **cat** can be combined to k_c. In addition, if equimolarity of both functional groups is given, **COOH** and **OH** can be termed **M**, resulting in Eq 2.1-4.

$$-\frac{d\,\mathbf{M}}{d\,t} = k_c \cdot \mathbf{M}^2 \qquad\qquad \text{Eq 2.1-6}$$

By integrating from starting time $t = 0$ to reaction time $t = t$ and substitution in the Carothers equation, Eq 2.1-5 is obtained.

$$DP_n = \frac{1}{1-p} = 1 + \mathbf{M} \cdot k_c \cdot t \qquad\qquad \text{Eq 2.1-7}$$

Hence, the degree of polymerization is proportional to the reaction time for an externally catalyzed system.

2.1.2 Chain-growth Polymerization

One of the simplest and most popular polymerization techniques is free radical polymerization (FRP). FRP follows a chain-growth mechanism, which is distinctly different from the step-growth polymerization discussed above.[20] In a chain-growth polymerization an initiator generates a starting radical, anion, or cation, which reacts with a monomer moiety – typically vinyl monomers – by transferring the reactive center to the monomer unit. Thus, additional monomers are consecutively added to the so-called propagating chain. Therefore, the greatest differences to the step-growth process are on the one hand that there are only three types of species present in a chain-growth polymerization mixture: monomer, polymer, and propagating chains. On the other hand, high molar mass material is produced from the very beginning of the polymerization. Due to its simplicity, FRP is a cost-saving process and therefore the most industrially applied polymerization technique. Close to 50 % of the annual polymer production is generated by FRP.[25]

The kinetics of free radical polymerization are determined by four elementary steps: initiation, propagation, termination, and chain transfer. The initiation reaction itself can be divided into two steps (*Scheme 2.2-1*). Initially, radicals are produced from an initiator moiety, which dissociates yielding two radicals. The dissociation reaction can

be triggered under variable conditions, including heat, irradiation, or electrochemical processes, where the first two triggers are more frequently employed. A more detailed discussion of photoinitiators is provided in Section 2.3.2. In the second step of the initiation process the newly generated radical reacts with the first monomer molecule, which represents an important step in polymerization kinetics.

$$I-I \xrightarrow{k_d} I^\bullet + I^\bullet$$

$$I^\bullet + M \xrightarrow{k_i} R_1^\bullet$$
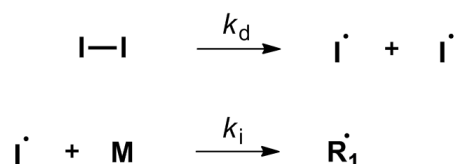
Scheme 2.1.2-1: The first two steps in free radical polymerization consist of the initiator dissociation reaction (top) and monomer addition to the initiating species (bottom).

The rate coefficient of the decomposition of the initiator, k_d, varies with the reaction conditions and is typically in the order of $10^{-5}\,s^{-1}$. In contrast, the transfer reaction to the first monomer unit is of second order ($k_i \approx 10^4\,M^{-1}\,s^{-1}$). The propagation reaction describes the subsequent addition of monomer molecules to the radical species generated from the initiation process (*Scheme 2.1.2-2*). Therein, the rate coefficient of propagation, k_p, is dependent on the properties of the monomer. The value of k_p is in the order of $10\,M^{-1}\,s^{-1}$ for very slowly polymerizing monomers, such as dicyclohexyl itaconate, and $10^5\,M^{-1}\,s^{-1}$ for acrylates, which are fast polymerizing monomers.[26]

$$R_n^\bullet + M \xrightarrow{k_p} R_{n+1}^\bullet$$

Scheme 2.1.2-2: General propagation reaction in FRP.

Termination reactions remove radical species from the polymerization mixture. There are two pathways how the propagation of growing chains can be terminated: combination or disproportionation (*Scheme 2.1.2-3*). The combination process describes the collision of two radicals or macro-radicals, resulting in a dead polymer chain with the combined molar mass of the macro-radicals. Disproportionation, on the other hand, occurs via hydrogen abstraction by one macromolecule from another. In contrast to the combination process, disproportionation produces two dead polymer chains, each one of the same molar mass as the corresponding macro-radicals. The termination process in general is a statistical process, which involves polymer chains of different lengths in the reaction mixture. It is diffusion controlled and thus strongly dependant on the viscosity of the reaction medium[27] as well as the chain length of

the polymer.[28] Therefore, an increasing viscosity and chain entanglement with conversion leads to a decreasing termination reaction rate which can lead to a so-called auto acceleration behavior.[28]
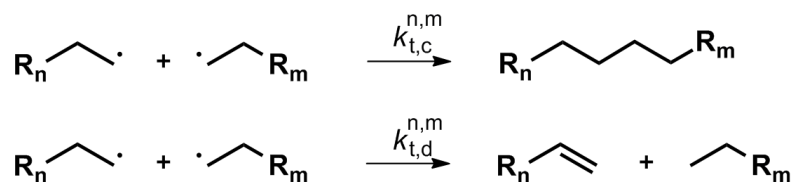
Scheme 2.1.2-3: Termination step of FRP. Termination can occur via combination of two polymer chains (top) or through a disproportionation reaction (bottom).

A further step in conventional free radical polymerization is the chain transfer reaction (*Scheme 2.1.2-4*). Similar to the termination reaction, chain transfer also results in the formation of inactive polymer chains. However, in contrast to the termination reaction, the radical concentration remains constant. The radical is transferred from one polymer chain to another moiety, which can subsequently re-initiate propagation. The moiety the radical is transferred to is either the initiator, the solvent, a monomer molecule, another polymer chain, or a transfer agent that is deliberately added. Radical transfer to polymer chains gives rise to branched polymers, if the generated radical is positioned within the chain.[29]
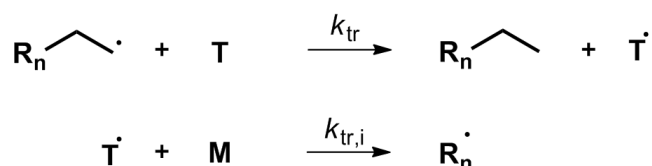
Scheme 2.1.2-4: Chain transfer in FRP. The top reaction depicts the chain transfer to molecule 'T', which could be solvent, initiator, monomer, polymer, or a transfer agent. The bottom reaction depicts the addition of monomer to the re-initiating radical.

Although FRP is a very robust process and therefore the most commonly implemented polymerization technique, it includes some significant limitations. Products produced via FRP are highly unsuitable for advanced applications, the design of polymeric architectures, or simply post-polymerization modification of the resulting polymer, due to a lack in end group functionality and poor control over molecular weight and dispersity. Thus, more advanced polymerization techniques need to be applied.

12

Opposing the properties of FRP, anionic polymerization is the prime example for a living polymerization process.[30] Since no chain termination events occur, it consequently provides perfect control over molecular weight and end group functionality. Further characteristics are a linear evolution of molar mass with conversion and low dispersity values. Moreover, living polymerization enables to produce blockcopolymers by simply adding another monomer after complete consumption of the one initially present. Despite these advantages, anionic polymerization has limited use in industrial processes due to the small number of suitable monomers and very stringent reaction conditions.[31] Thus, the development of novel polymerization techniques was highly important and during the last decades polymer chemists attempted to combine the simplicity of radical polymerization with the advantageous properties of living polymerization techniques.

2.1.3 Modern Polymerization Techniques

Looking for the ideal polymerization process, polymer chemists developed controlled radical polymerization techniques, termed reversible-deactivation radical polymerization (RDRP) by the International Union of Pure and Applied Chemistry (IUPAC). The term 'controlled' will be used from now on, as truly living radical polymerization is impossible since radical-radical termination can never be completely suppressed. However, control over a radical polymerization process can be gained via two generic mechanisms: reversible termination of the propagating species or reversible degenerative chain transfer. Either way, the key to a controlled polymerization is the rapid exchange between dormant and propagating species allowing all polymer chains to grow simultaneously. An alternative approach to produce well defined polymers can be achieved via ring opening polymerization (ROP). ROP features similar advantageous properties and will be introduced subsequent to the introduction of the radical-based techniques.

2.1.3.1 Nitroxide-Mediated Radical Polymerization

Nitroxide-mediated radical polymerization (NMP) was first introduced by Solomon in 1985.[32] The concept behind NMP is that propagating chains are reversibly terminated by a stable radical control reagent. Nitroxide moieties are employed as stable radicals forming alkoxy amines upon combination with the propagating macro-radicals.[33] The dormant species – depicted on the right side of the reaction equilibrium (*Scheme 2.1.3-1*) – is not affected by termination or propagation events, which provides the controlled character of the polymerization method.[34] On the opposite side of the equilibrium, the free radical species reacts naturally with the present monomer compounds.[35] NMP can either be induced via dissociation of a preliminarily present alkoxy amine, or by a typical radical initiator, which requires the addition of a free nitroxide control agent. A commonly employed stable and commercially available radical control reagent is 2,2,6,6-tetramethylpiperidine-1-oxyl (TEMPO).
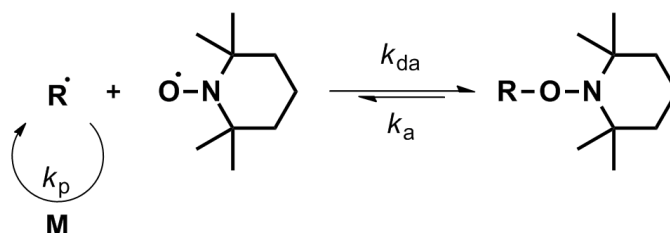
Scheme 2.1.3-1: General reaction equilibrium for NMP. The propagating radical is reversibly terminated by the nitroxide radical, generating a dormant species that is not affected by termination.

In order to obtain controlled polymerization it is important that the rate coefficient of the deactivation (k_{da}) reaction is much larger than the one of the activation step (k_a). If this is not the case, the radical concentration in the reaction would be too high, causing the termination reaction to proceed to a significant extent.

Although NMP is able to produce narrowly distributed polymers of defined chain length, it involves numerous disadvantages. The reaction temperature, for instance, must often be high (up to 130 °C) to accelerate the activation reaction. Moreover, only styrene could initially be polymerized with this controlled radical polymerization system, before the development of advanced control agents enabled to improve the selection of monomers and reduce the polymerization temperature.[36] The most significant and yet unsolved problem is the long reaction time – up to 72 hours – which is necessary for the reaction to proceed caused by the low radical

concentration. In order to further reduce the amount of side reactions caused by high temperatures, photo-induced NMP was established enabling ambient temperature polymerization.[37-39]

2.1.3.2   Atom Transfer Radical Polymerization

Atom transfer radical polymerization (ATRP), first reported by the groups of Matyjaszewski[40] and Sawamoto,[41] is one of the most investigated controlled radical polymerization techniques in terms of mechanism and synthesis.[42-43] The key feature of ATRP is identical to that of NMP: free radicals are reversibly trapped to protect them from termination. To gain control over the polymerization process, ATRP employs redox chemistry, most commonly a Cu^I/Cu^{II} system, to generate an equilibrium between deactivated (i.e., dormant) and activated species (*Scheme 2.1.3-2*). Therein, the initial alkyl halide is reduced via single electron transfer from the copper(I) species to form the free radical, which undergoes propagation steps upon its release. The resulting copper(II) halide re-traps the free radical as alkyl halide (most commonly bromine). Again, for a well controlled process, it is important that the deactivation rate coefficient (k_{da}) is significantly larger than its counterpart (k_a).[44]

$$R^{\cdot} + CuX_2\,(L) \;\; \underset{k_a}{\overset{k_{da}}{\rightleftharpoons}} \;\; R-X \;\; + \;\; CuX\,(L)$$

$$\circlearrowleft k_p$$

$$M$$
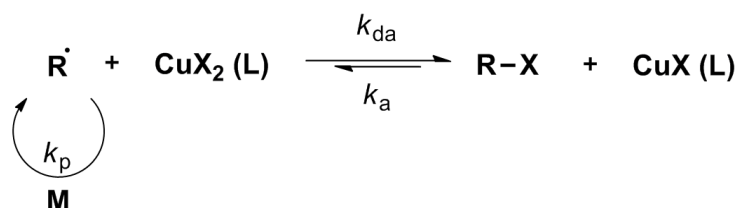
Scheme 2.1.3-2: General activation/deactivation equilibrium for ATRP. L = ligand; X = halide.
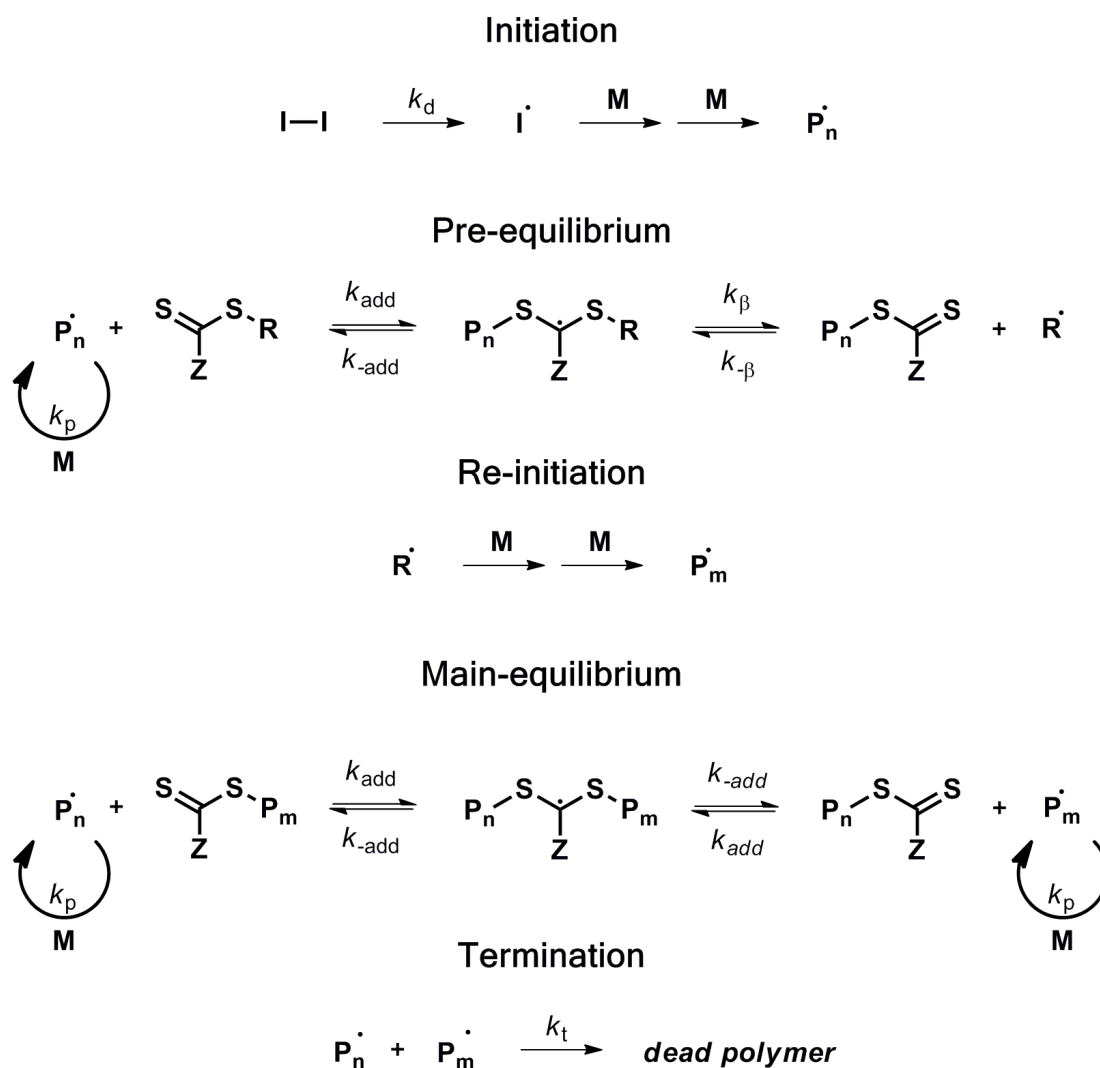
Although the copper-catalyzed process appears to be the most robust technique, other transition metals (Ru,[41] Fe,[45] Ni,[46] Pd,[47] Rh[48]) have been successfully employed for controlling ATRP reactions.[49] Reduced end group functionality, as observed for higher conversions,[50] can be improved by a modern modification of ATRP called activator regenerated by electron transfer (ARGET).[51] By adding a reducing agent, only a minimum amount of copper catalyst is required and enhanced functionality can be achieved.[52] Nevertheless, removal of the cytotoxic copper is a crucial step in performing ATRP. A very recent approach to elegantly eliminate the

copper contamination was successfully conducted applying an electrochemical technique.[53] ATRP has also been conducted via photo-initiation,[54] however, the mechanism of photo-ATRP is still under investigation.[55]

It is worthy to note that the ATRP technique results in halide functional polymers, which is highly advantageous, as it can be further employed as a synthetic handle for post-polymerization modifications. In combination with the wide variety of alkyl halide initiators, ATRP has proven to be a versatile synthetic tool for generating divers macromolecular architectures.[56]

2.1.3.3 Reversible Addition-Fragmentation Chain Transfer Polymerization

Reversible addition fragmentation chain transfer (RAFT) polymerization was first reported by a group from the Commonwealth Scientific and Industrial Research Organization (CSIRO) in 1998.[57] They observed that a regular free radical polymerization could be controlled by the intentional addition of a transfer agent (RAFT agent), in their case a dithioester. At the same time, a French research group invented a similar polymerization method using xanthates as control agents.[58] The RAFT process differs from the previously introduced methods in the way it prevents the radicals from undergoing termination.[59-62] In the presence of a RAFT agent, the termination reaction competes with the radical transfer to the RAFT agent.[63] Consequently, the rate of the latter reaction has to be several orders of magnitude larger than the termination reaction rate in order to achieve a well controlled process. Thus, the probability of single polymer chain termination is transferred from one polymer chain to all chains. Moreover, the main equilibrium also causes all chains to grow simultaneously – a crucial criterion for controlled polymerization and narrow dispersities.[59, 64] A graphical description of the entire process is depicted in *Scheme 2.1.3-3.*

Initiation

$$I\!-\!I \quad \xrightarrow{k_d} \quad I^{\bullet} \quad \xrightarrow{M} \xrightarrow{M} \quad P_n^{\bullet}$$

Pre-equilibrium

Re-initiation

$$R^{\bullet} \quad \xrightarrow{M} \xrightarrow{M} \quad P_m^{\bullet}$$

Main-equilibrium

Termination

$$P_n^{\bullet} \;+\; P_m^{\bullet} \quad \xrightarrow{k_t} \quad \textit{dead polymer}$$

Scheme 2.1.3-3: General reaction scheme for the RAFT process.[65]

The choice of a suitable RAFT agent is crucial for an efficient process. The stabilizing effect of the Z-group has to be adapted based on the monomer reactivity, as well as the stability and re-initiating properties of the R-group radical. In case of an inappropriate choice, retardation or reduced control over the polymerization can occur.[66]

The advantage of the RAFT process is that a large variety of monomers, ranging from styrene to vinyl acetate, can be polymerized, especially when the RAFT agent is chosen judiciously.[67] The formation of block copolymers can only be achieved if the monomer reactivity of the monomer building the first block does not differ too much from the reactivity of the subsequently utilized monomer.[68] Another advantageous aspect of RAFT polymerization is the resulting end group functionality of the produced material. The dithio-terminus can serve as synthetic handle for instance for

aminolysis[69-70] or RAFT-OH exchange.[71-73] Moreover, electron withdrawing Z-groups activate the C=S-double bond for hetero Diels-Alder reactions.[74-75] The so-called RAFT-HDA technique is a highly efficient and versatile tool for the design of challenging polymeric architectures[76] and smart materials.[77-78] The RAFT-HDA concept will be discussed in detail in Section 6.1.

2.1.3.4 Ring Opening Polymerization

Ring opening polymerization (ROP) is disparate from the techniques presented above, as there are three different induction methods for ROP, i.e., radical, cationic, and anionic initiation. However, radical and cationic ROP are both susceptible to termination events[79] – unless control agents are added intentionally[80] – and thus, only anionic ROP is suitable to be conducted in a controlled manner. Therefore, water-free conditions as well as an absence of protic impurities are required. An anionic ROP process, however, which is conducted under inert conditions is a convenient technique for producing polyethers, polyesters, and polyamides of low dispersity with well-defined end groups.[81] A typical anionic polymerization process is depicted in *Scheme 2.1.3-4*. The driving force of the polymerization reaction is derived from the ring strain of the cyclic monomers. Typical monomers are for example, ε-caprolactam, ε-caprolactone, or ethylene oxide, yielding polyamides (i.e., Nylon), polyesters, or poly(ethylene glycol), upon polymerization.
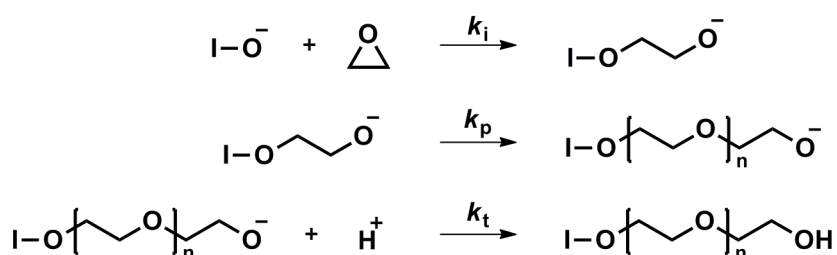
Scheme 2.1.3-4: Exemplary anionic ROP process for ethylene oxide: Initiation (top), propagation (middle) and termination (bottom).

In general, the ROP process is beset with a series of possible disadvantages: The propagation step is reversible and, thus, depolymerization can occur, which is not only a disadvantage, but a required feature for degradable materials;[82] cyclization reactions can produce dead material resulting in broad distributions; long reaction times are not only time consuming, yet also increase the risk of harmful

18

contamination. In order to solve all these problematic issues at once several catalytic systems have been developed. The main mechanisms proceed via small organic molecules,[83] metal-catalysis,[84] or enzymatic catalysis.[85] Either way, backbiting – the intramolecular reaction of the chain terminus with the polymer backbone – is suppressed and the reaction time drastically reduced by coordination to (organic and metal catalysis) or activation of (enzyme) the cyclic monomer. Thus, well defined polymers with narrow dispersity can be obtained. Despite the restriction to a few cyclic monomers, ROP represents a feasible and powerful tool for customized polymer synthesis.[86]

2.2 Photochemistry

The photochemistry section constitutes the basis for understanding the following description of research projects with regard to processes resulting from light-induction. Initially, an introduction to the history of photochemistry in general will be given and the importance of ongoing progress of research in the field of photochemistry is pointed out. Subsequently, a more detailed look into the processes which occur upon the irradiation of matter with light will be provided. In particular, the phenomena of absorption, radiationless transitions, and photoluminescence will be concisely discussed on a molecular level. Finally, an example for a multistep photochemical process will conclude the photochemistry section.

2.2.1 Introduction and History of Photochemistry

Photochemistry and -physics describe the interaction between matter and light. The first results on photochemical transformations were reported by Trommsdorff in 1834, who observed a change of color when santonin was exposed to blue or violet light.[87] Later, Max Planck's work on the black body radiation was the groundbreaking step into the investigations of photo physics.[88] Following Planck's findings was the discovery of the photoelectric effect in 1905[89] by Albert Einstein, who also formulated the quantum equivalence law.[90] It was the first attempt to quantify photochemical processes, a task which was later optimized by Stark and Bodenstein.[91] The first experimental success in photochemistry was achieved by Ciamician and Silber,[92-94] who were not only pioneers in synthetic photochemistry, yet also visionaries. The motivation of Ciamician was to employ light in general (or sunlight in particular) in order to solve environmental problems, supply humanity with clean energy and additionally trigger industrial processes directly by solar radiation.[2] His inspiration was provided by Nature and its photosynthesis, a process which is the demonstration of sustainability since water and carbon dioxide are transformed into glucose and oxygen under use of solar energy. Although Ciamician's ideas were honorable, photochemistry did not take over substantial parts of industrial applications.

Nevertheless, photoscientists were focused on obtaining insights into photochemical processes of biological origin or artificially triggered ones.

The first group to systematically study photochemical reactions in solution was Norrish and coworkers. Employing advanced analytical and experimental techniques for the investigation of the decomposition of carbonyl compounds, they set a milestone for the detailed understanding of photochemical processes.[95-97] Thus, it was possible to unravel, for example, the mechanisms of photosynthesis in Nature or the need of sunshine for human beings.

The challenges that need to be overcome for establishing photochemical synthetic processes in industry – as proposed by Ciamician – are still immense. Not only is the required power a costly factor, but also the intensity gradient in larger vessels is an obvious problem. Nevertheless, current technology is more dependent on photochemistry than ever before, since the age of light-emitting diodes has begun just recently. The importance of this novel technology is well justified since former illumination sources were by far less efficient and the need for heavy metals has expired in the context of lighting. Additional industrial applications for photochemistry are for example surface coatings, which will be discussed in section 2.3.6. Furthermore, surface coatings and sealing materials mostly rely on photo-induced polymerization processes (section 2.3.2).

By now, synthetic photochemical methods provide a platform for a large variety of applications. In addition, the rapidly expanding interest in photo-induced processes is also proof for the potential of photochemistry and its relevance for the future. An entirely novel field of application, for instance, is encouraged by the evolution in the field of laser-technology. Based on a steadily increasing performance of laser setups three dimensional structures can be generated on micro- or nano-scale.[98] Underpinning the unique advantage of photo-induced chemistry, i.e., spatial resolution, direct laser writing (DLW) is the prime example for utilizing this property for producing nanostructures with remarkable precision.[99]

2.2.2 Photochemical Processes

The current section is devoted to the theoretical aspects of photochemistry and is therefore of immediate interest to the scientist keen on understanding photochemical processes on a molecular level. In order to describe the phenomena occurring upon irradiation of matter, Jablonski developed a clear way of graphically displaying the various transitions,[100] i.e., absorption, radiationless transitions, luminescent transitions, and bond cleavage (*Figure 2.2-1*), which will each be discussed in detail in the following subsections.
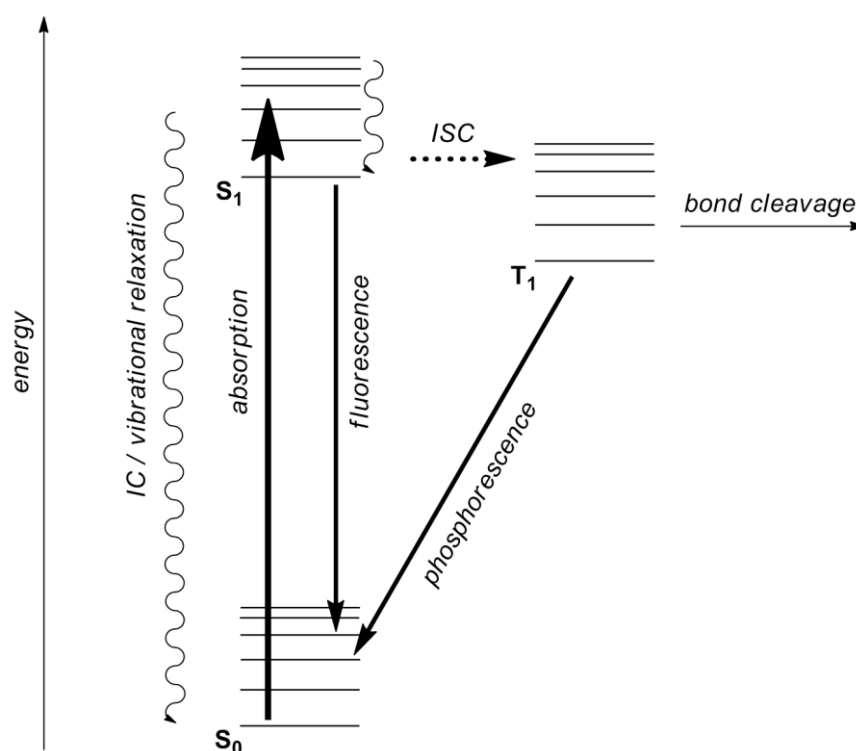
Figure 2.2-1: Jablonski diagram. The possible photochemical processes are absorption, internal conversion (IC), inter system crossing (ISC), vibrational relaxation, fluorescence, and phosphorescence. S_x = singlet states, T_1 = first excited triplet state.

2.2.2.1 Absorption and Excited States

The absorption of radiation by materials – or molecules, to be more specific – is a crucial process in photochemical applications. It describes the excitation of the molecules from their electronic ground states to excited states. Thus, the absorption process precedes all the different transitions which the compounds undergo when partaking in photoreactions. The most delicate challenge in controlling the absorption

process is to trigger the desired transition. Various electronic and vibrational states can be reached upon irradiation of molecules and the consecutive transitions depend on the initial energy absorbed by the molecule. Therefore, the excitation wavelength – presenting the ultimate handle in controlling the absorption process – is of exceptional importance and thus, it needs to be chosen judiciously. For ordinary carbonyl compounds, for example, transitions to excited singlet states like n-π^*, π-π^*, and n-σ^* can occur as well as the less likely transitions to triplet states.[101-102] Absorption spectroscopy is the suitable tool for retrieving useful information about the transitions and excited states experimentally. Thus, data on physical properties of excited states can be provided.[103] Quantum chemical calculations serve as theoretical approach to gain information about the energy levels of different states of a system. Whereas it is straightforward to obtain reliable data about the ground state of molecules,[104] determining energies of excited states is more sophisticated and can be achieved via Hartree-Fock calculations based on molecular orbital theory,[105] internally contracted multiconfiguration-reference configuration interaction,[106] or single reference *ab initio* methods for the calculation of large molecules.[107]

2.2.2.2 Radiationless Transitions

Once the molecule has been excited by absorbing energy, several transitions can occur. One group of transitions is termed radiationless transitions, including a molecule's change in excited state without emission of radiation. Assuming the transition occurs with a change in spin multiplicity, i.e., singlet to triplet or triplet to singlet, the process is termed intersystem crossing (ISC), whereas transitions between states of equal spin multiplicity are referred to as internal conversions (IC). In case chemical bonds are broken, the process is called predissociation. The following general properties of radiationless transitions have been observed experimentally:[108] (*i*) emission of radiation only occurs from the lowest electronically excited level of polyatomic organic molecules, implying rapid radiationless transitions between higher excited states, (*ii*) radiationless transitions are first-order processes, (*iii*) the rate of radiationless transitions decreases with an increasing energy gap between the electronic terms of the initial and final state, (*iv*) the rate of radiationless transitions is greatly reduced upon deuteration of molecules containing C-H bonds, causing increased lifetimes of the excited states, (*v*) the impact of radiationless

processes increases at elevated temperatures, (*vi*) unlike the behavior of small molecules, the phenomenon of radiationless transitions for structures of higher complexity occurs exclusively intramolecularly – in the absence of perturbing collisions.

In order to provide theoretical calculations for backing up these experimental results, a large variety of approaches have been published. A detailed overview of this extensive field of physical chemistry would exceed the scope of the present thesis by far. Thus, the reader is referred to the respective literature.[109]

2.2.2.3 Photoluminescence

The term luminescence was introduced by Eilhard Wiedemann in 1888.[110] It describes the phenomena where radiation is emitted by materials not resulting from heat. Thus, luminescence is an example for cold-body radiation and photoluminescence complements the radiationless transitions discussed above (Section 2.2.2.2). The luminescence of materials can be triggered in a variety of different ways, i.e., (bio- / electro-) chemically, electrically, mechanically, thermally, or by radiation. The latter version is the so-called photoluminescence, which describes the relaxation of molecules from an excited electronic state under emission of radiation. Importantly, the initial excitation was achieved by the absorption of radiation. Among other rare examples, the most common types of emission are fluorescence and phosphorescence, differing in their initial excited state. As fluorescence occurs between two singlet states and is therefore a favored transition, typical lifetimes are in the region of nanoseconds. Phosphorescence, on the other hand, represents a 'forbidden' transition between an excited triplet state and a singlet ground state, implying an ISC which occurs earlier. Therefore, phosphorescence can last from milliseconds up to hours.

Ironically, the term 'phosphorescence' is derived from phosphorus, yet white phosphorus does not exhibit phosphorescence, since emission of phosphorus is based on chemiluminescence. The role of phosphorescence is of rather reduced impact, compared to wide applicability of fluorescent materials. Mainly composed of inorganic compounds, phosphorescent materials are employed for 'glow-in-the-dark' toys, paints, or similar applications.[111]

Although the first fluorescent materials were discovered in the 16th century,[112] the phenomenon known as fluorescence was established and named by George Gabriel Stokes in 1852, who was investigating the luminescence of calcium fluorites.[113] One of his key experiments was the irradiation of a quinine solution with UV-light – generated through a prism – yielding blue light. A measure for the fluorescence intensity is the quantum yield. It displays the number of absorbed photons divided by the number of emitted photons.

There are several general rules, which can serve as a guideline to fluorescence phenomena, yet there are also exceptions and the rules do not always apply:

(*i*) Kasha's rule. The rule states that photon emission from an electronic excited state occurs predominantly from the lowest vibrational state. The theoretical background behind this rule is based on the difference in timescale of vibronic transitions (differing electronic and vibrational wavenumber of initial and final state) compared to the relaxation among vibrational levels. Since the rate of a transition is dependent on the overlap of vibrational wavefunctions, which is expressed in the Franck-Condon factors, the transition between two neighboring vibrational states with similar energy is much faster than any vibronic transition. The Kasha-Vavilov rule – a corollary of Kasha's rule – states that the fluorescence quantum yield is independent of the excitation wavelength, also relating to the fact that non-radiative transitions to the vibrational ground state occur much faster than the radiative relaxation.

Exceptions of the Kasha rule occur when large energy gaps or more than the first electronic excited state are involved.

(*ii*) Mirror image rule. For a broad range of fluorophores, the emission spectrum resembles the mirror image of the absorption spectrum.[114] This observation is supported by the Franck-Condon principle, which stipulates vibronic transitions to be of a vertical nature since they occur in a much shorter timeframe than the distance of two nuclei changes. Therefore, the shape of the absorption and emission spectra depend on the vibrational states of the final states of the respective transition, which are often similar.

(*iii*) Stokes shift. Except for a few examples, the wavelength of the emitted radiation is longer than the wavelength of the absorbed light. Therefore, a difference of the maxima in the corresponding absorption/emission spectra is observed, which is

known as Stokes shift.[114] The energy loss associated with the increasing wavelength, results from radiationless transitions, vibrational relaxation and perturbation events (see also: Kasha's rule and Franck-Condon principle, above).

Fluorescent materials are of high interest to not only chemists but for example in all areas of life sciences or for lighting techniques. The typical fluorescence lamp tube – commercially available since 1939 – consists of a fluorescent inner coating of the tube, which converts the UV light into visible light. Therein, the UV light is generated by the emission of mercury vapor. Continuing in the field of optoelectronics, a modern approach and application for fluorescent materials is based on light-emitting diodes (LEDs). Effort for the development of LED techniques and materials is constantly increasing and inorganic, organic, as well as polymeric systems are competing to set new records for efficiency. Additional information on LED materials will be provided in section 2.3.6. In the life sciences, fluorescent markers are particularly interesting for labeling applications. Attached to cells, proteins, or DNA fluorescent materials allow to track substances in living organisms. Moreover, fluorescence is suitable for providing access to additional characterization techniques. Due to the high sensitivity of fluorescent spectrometers, fluorometry is of high impact in biological applications. A more sophisticated analytical technique is, for instance, Förster Resonance Energy Transfer (FRET), where non-radiative dipol-dipol coupling between two chromophores is involved. FRET is highly sensitive to distance changes and thus provides information about the interaction of different reactive groups, changes in conformation, or concentration of substances.[115]

2.2.2.4   Example for a Light-Induced Chemical Process

In order to complete the picture of photochemical processes, this section provides an example about the interplay of the single transitions in an actual system. The current example is devoted to the irradiation of *ortho*-alkyl benzophenone, an aromatic carbonyl compound. This species was not chosen randomly since the photochemical process yields a highly reactive moiety and applications of the herein described mechanism will later be subject of several subsections in Section 2.3 as well as Chapter 6.

In the years before 1970, the photoreaction of 2,4-dimethyl benzophenone was a mystery to chemists since the typical photo-induced pinacolization did not occur,[116] yet oxidation of the *ortho*-methyl group or an anthraquinone moiety were observed.[5] The mechanism was the subject of a debate even after Tchir and Porter succeeded to investigate the irradiation process of the benzophenone derivative by laser flash photolysis. Since the irradiation time in flash photolysis is extremely short, lasting just 10^{-9}-10^{-15} s, flash experiments allow the operator to take snapshots of the current state of a system and determine its lifetime. Thus, Tchir and Porter were able to identify five transients and proposed an according mechanism for the irradiation of 2,4-dimethyl benzophenone (*Scheme 2.2-1*).
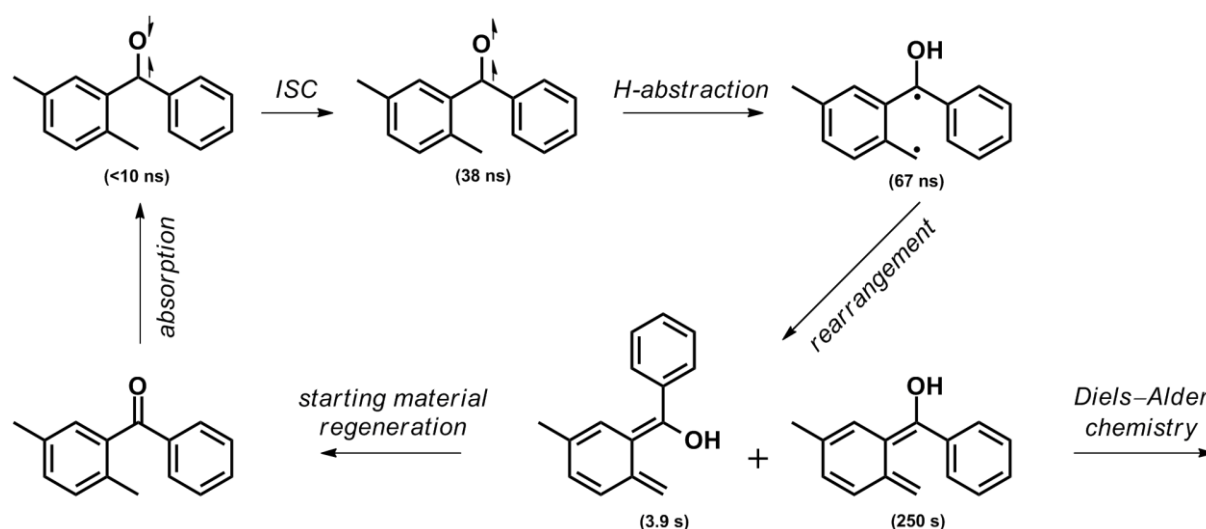
Scheme 2.2-1: Mechanism of the photoenolisation as reported by Tchir and Porter.

Firstly, absorption occurs followed by a *n*-π* transition from the singlet ground state to the first excited singlet state (τ < 10 ns). This process demonstrates the typical behavior of most carbonyl compounds. ISC to the lowest excited triplet state was found to occur subsequently, agreeing with the predicted progress (τ = 38 ns). The next step involves the inevitable formation of radicals, yet instead of intermolecular radical coupling and the formation of the pinacol product, rapid hydrogen abstraction occurs, yielding a biradical intermediate with a lifetime of 67 ns. in a final step, the aromatic system is cleaved, giving rise to the generation of two final enol derivatives. With typically close to 5 s and 250 s, respectively, the lifetime of these highly conjugated enols is comparably high, enabling further reactions such as the formation of anthraquinone or – more relevant to future applications – Diels–Alder reactions with suitable dienophiles. The light-triggered Diels–Alder ligation,

particularly its properties and advantages, is discussed in detail in Section 2.3.1.1 of the current thesis.

2.3 Applications for Light-Induced Chemistry in Polymer Science

The purpose of the above two sections (2.1 and 2.2) was to provide the very fundamentals of two extensive fields of chemistry: macromolecular science and photochemistry. Given the basic knowledge about photochemical processes and polymerization techniques, the current section is devoted to introduce light-induced modification methods applied to polymeric systems in more detail. Besides the demonstration and evaluation of versatile photochemical tools, examples from state-of-the-art research of light-induced chemistry in polymer science are included.

Previous to the detailed discussion of photochemical techniques, some general remarks on the impact of light-triggered applications are noteworthy. The developments in the photochemical section of polymer science have evolved immensely during the last decades. Since light was simply applied for the initiation of radical polymerizations, photochemists have achieved substantial progress in both understanding the ongoing processes and introducing powerful photoreactions to alter properties, modify structures, or generally enhance the performance of customized polymers. The introduction of light-induced ligation reactions set a milestone in the field of photochemistry directing the research to efficient usage of radial energy. A set of atom economic reactions, sometimes termed *click* reactions,[117-118] has addressed the distinct challenges in macromolecular design. Unrivaled among the advantageous features of photochemical tools is the possibility for spatial and temporal control on a scale far off the limits for thermally induced chemistry. Moreover, a modern field of research concerns pushing the limits in terms of resolution employing sophisticated laser setups.[99]

In the following subsections, the most prominent photochemical tools for polymer ligation will be presented, followed by consecutively discussed projects of the present thesis: polymerization via light-sensitive monomers, visible light-triggered conjugation reactions, reversible photochemical reactions, generation of versatile polymer architectures via photoligation, and the photocrosslinking processes for surface patterning. Thus, a literature review containing detailed information particularly on the topics of the subsequently following research chapters is provided.

## 2.3.1 Modern Light-Induced Ligation Techniques

As alluded to above, modern light-induced ligation methods aim for efficiency and sustainability. Therefore, contemporary research is obliged to tackle the challenges of green chemistry.[4] Consequently, the perfect photoreaction is sunlight-induced, bioorthogonal, highly selective, synthetically feasible, conducted in water, and importantly atom efficient. Although fulfilling all of these desirable properties at once is a tall order, chemists have made great advances, and continuously improved and evaluated possible candidate systems. A very promising reaction class is the pericyclic reaction, or specifically, Diels–Alder and dipolar cycloaddition reactions. Both of them include examples which have been termed *click* reactions and, thus, they have been proven useful in macromolecular design,[119-123] in the modification of substrates,[124] or the generation of smart materials.[125-126] Despite the success of the thermal representatives, photochemical versions of Diels–Alder and dipolar cycloaddition systems are required to further improve the properties of the existing thermal methods particularly due to a lack of spatial control in thermal reactions.

Photochemical Diels–Alder chemistry opposes with the common knowledge about the Woodward-Hoffmann rules.[127] 6π-electron systems such as Diels–Alder chemistry are photochemically disfavored, which might cause confusion since they are actually applied for light-induced ligation. Yet, taking a closer look at all of these – for a reason – efficient conjugation tools, the actual cycloaddition step is never based on a photochemical process. Instead, the primary formation of the reactive species, i.e., the diene or the dienophile, is generated upon irradiation whereas the cycloaddition itself is indeed a rapid thermally induced reaction. Therefore, the precursors capable of releasing the reactive moieties for Diels–Alder reactions are sometimes termed 'caged dienes/dienophiles'. However, the rate determining step is in every case the photochemical release of the reactive species. The same rules apply for photo-induced 1,3-dipolar cycloadditions.

2.3.1.1 Photoenol Chemistry

The first conjugation tool presented here is the photoenol technique. It is based on *ortho*-methyl benzaldehyde or *ortho*-methyl benzophenone derivatives, which form *ortho*-quino dimethanes – so-called photoenols – upon irradiation. A detailed description of the photoenolization process is provided in section 2.2.2.4. The general reaction scheme for the photoenol-based ligation reaction is depicted in *Scheme 2.3-1*.
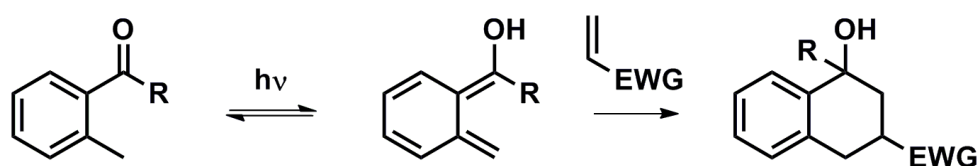
Scheme 2.3-1: General photoenol reaction. R = H, Ph; EWG = electron withdrawing group.

After excitation, the resulting photoenol is a highly reactive diene. It undergoes rapid cycloaddition with electron deficient alkenes, for instance, maleimide, acrylate, or similar groups. In contrast to the photochemical excitation step, the cycloaddition is irreversible. Thus, the diene species forms the desired product, provided that a suitable reaction partner is in close range. Yet – assuming the reaction partner is consumed – it returns to the non-activated species (starting material) without forming any side-products. Although the cycloaddition behavior of photoenols was introduced about 40 years ago,[128] their application was just recently introduced into the realm of polymer science by the group of Barner-Kowollik. In an initial study *ortho*-methyl benzophenone, a photoenol precursor, was attached to a polymer chain and subsequently conjugated with a maleimide end-capped polymer in a light-triggered process.[129] Inspired by the success of this block copolymer formation, photoenol chemistry was combined with thermal *click* methods, i.e., cyclopentadiene/maleimide Diels–Alder chemistry and the copper catalyzed azide-alkyne cycloaddition (CuAAC). Thus, ABA as well as ABC block copolymers could be generated.[130] An advanced version of the photo Diels–Alder reaction was enabled by a second generation of photoenol moieties. Based on an *ortho*-methyl benzaldehyde derivative, the reactivity of the intermediate diene could be increased and thus acrylate-type double bonds were accessible for the ligation. Consequently, the difference in reactivity between the two photoenol moieties could be employed to perform orthogonal photoenol reactions. Therefore, a polymer building block with an acrylate end group and a first

generation photoenol moiety attached to the opposite side was synthesized by acrylic diene-metathesis (ADMET). Next, the polymer was irradiated in the presence of a polymer building block (PEG) containing a maleimide end group. Due to the reactivity differences, only the desired coupling between the photoenol and the maleimide-terminal polymer was observed, enabling a subsequent photoreaction between the residual acrylate terminus and a second generation photoenol-bearing poly(ε-caprolactone) (PCl).[131]
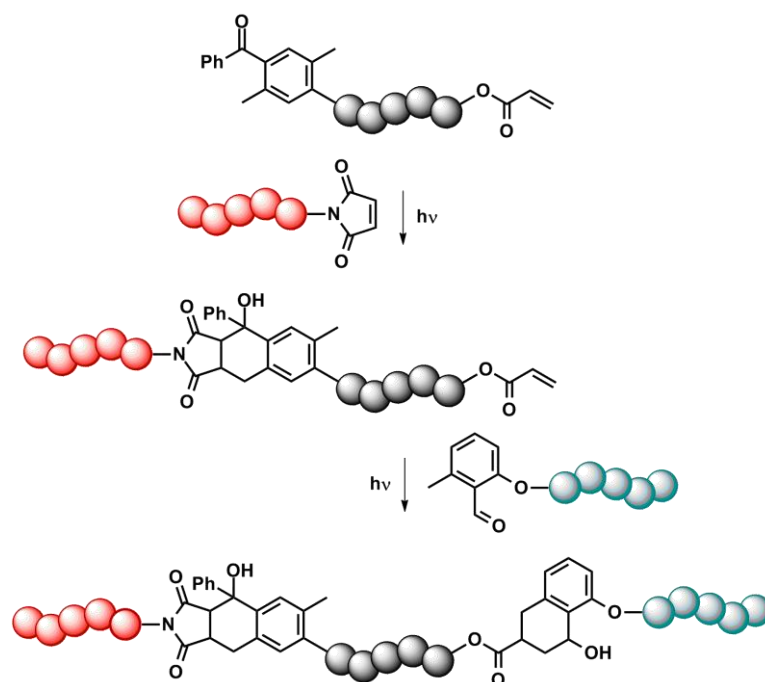
Figure 2.3-1: Photochemical strategy to ABC-triblock copolymers via orthogonal photoenol chemistry. Red polymer: PEG; black polymer: ADMET; green polymer: PCl. The figure was adapted from Ref.[131] with permission from the American Chemical Society (ACS).

A further study in solution focused on the design of single-chain nanoparticles (SCNPs). By introducing a statistical distribution of photoenol and maleimide functionalities into a polymer backbone, SCNPs could be generated by irradiating a diluted solution of the multifunctional polymer.[132] The same principle of self-reacting polymer chains was applied for the preparation of cyclic polymers. In order to obtain purely monocyclic structures, a linear polymer containing a second generation photoenol and an acrylate group was synthesized by ROP. In high dilution the polymer end-caps undergo an intramolecular cycloaddition and the resulting cycles can be readily isolated.[133] Due to the UV light present in solar irradiation, the cycle formation was also feasible in sunlight.[134]

The photoenol technique was also applied for the spatially resolved modification of surfaces. Due to the light-induced nature of the photoenol process, locally constrained functionalization of silicon substrates could be achieved using a shadow mask. Therefore, the surfaces were modified with bromine components, polymers, and peptides, each synthetically altered to contain a maleimide component.[135] Moreover the combination of 3,4-dihydroxyphenyl alanine (DOPA) with photoenol chemistry leads to a mussel adhesive mimicking substrate capable of being modified by photo Diels–Alder reactions.[136] Not only silicon substrates were suitable for patterning, also biosubstrates, such as cellulose and hyaluronan are accessible for modification with photoenol moieties and subsequent spatially resolved functionalization with model peptides.[137]

Micro- and nanoparticles also provide interesting features and applications where light-induced Diels–Alder chemistry can serve as a versatile tool. For example the surface of silver nanoparticles could be covered with photoenol moieties via a linker compound containing a silver anchoring group (benzotriazole).[138] Moreover, the generation of polymeric Janus spheres of micrometer scale could be realized by a combination of photoenol chemistry and RAFT polymerization.[139]

2.3.1.2 Naphthoquinone Methides

Similar to the photoenol process introduced above, another highly reactive diene species can be generated by light. *Ortho*-naphthoquinone methides (NQM) result from irradiating (hydroxymethyl)naphthalene-2-ol – the NQM-precursor (NQMP). The general reaction scheme for the NQM-ligation is given in *Scheme 2.3-2*.
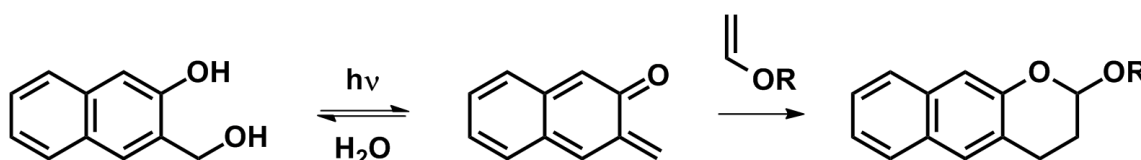
Scheme 2.3-2: General NQM reaction. R = organic substituent.

A detailed look at the reaction mechanism reveals that similar to the photoenolization process the NQM formation is also based on an equilibrium. During the irradiation process a water molecule is released which can rapidly react with NQM to form the initial NQMP. However, in the presence of a suitable reaction partner the NQM has

the tendency to undergo a hetero Diels–Alder (HDA) reaction. The HDA reaction itself is an irreversible process which causes full conversion of the starting component. In contrast to the photoenol process, the diene is electron deficient requiring an electron rich dienophile for an efficient Diels–Alder reaction. Inverse electron demand is for instance fulfilled for vinyl ether dienophiles, which were found to react rapidly with NQMs.[140] This photochemical technique – introduced by the group of Popik – has been mostly employed for surface patterning. Fluorescence markers synthetically connected to NQMs could for instance be immobilized on glass substrates in a spatially resolved fashion.[141] Moreover, photoreactive polymer brushes on silica surfaces were patterned with variable fluorescent markers proving the orthogonality of the photochemical tool towards the CuAAC method.[142]

NQMs are not only capable of HDA reactions. The activated diene species is sensitive to nucleophiles, which is also the general deactivation step in water. By intentionally adding thiol components, for instance thiol containing peptides, the formation of thiol ether linkages occurs rapidly. In addition, this process can be reversed under irradiation in high dilution.[143] The versatility of this approach for modular surface modification was demonstrated by attaching, replacing, and removing different photoreactive NQMs on thiol functionalized substrates.[144]

2.3.1.3   Thioaldehydes

In contrast to the two reactive diene species discussed previously, thioaldehyde derivatives behave like dienophiles. Generated from irradiation of phenacyl sulfides, thioaldehyde moieties are efficiently released, giving access to rapid HDA reactions. The general reaction scheme is depicted below (*Scheme 2.3-3*).
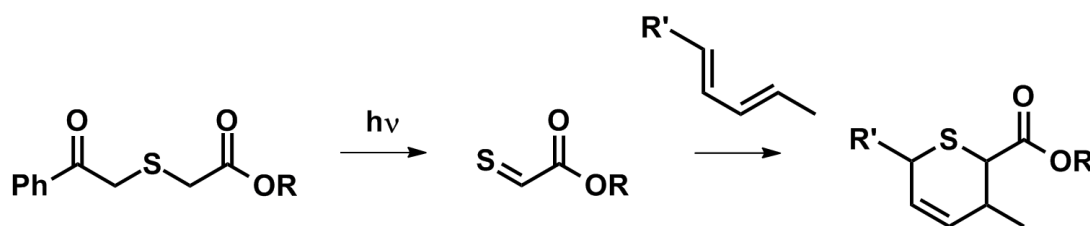
Scheme 2.3-3: General photo induced thioaldehyde reaction. R = alkyl, polymer substituent; R' = organic substituent.

Our team introduced the thioaldehyde technique to polymer chemistry.[145] The synthesis of a phenacyl sulfide terminated poly(ethylene glycol) was shown to be a feasible procedure and the resulting photosensitive polymer could be employed to screen the HDA reaction with versatile dienes. Therein, efficient photochemical conjugation of the functionalized polymer with 2,3-dimethyl butadiene, *trans,trans*-2,4-hexadien-1-ol, cyclohexadiene, cyclopentadiene, and *trans,trans*-2,4-hexadienoic acid was demonstrated. Ultimately, phenacyl sulfide moieties, covalently attached to silicon wavers, were shown to react with cyclopentadiene end-capped poly(ethylene glycol). Thus, site-specific immobilization of polymeric material was enabled. In a subsequent study, the thioaldehyde precursor was synthetically attached to cellulose surfaces. By irradiation of the biosubstrate in the presence of a diene modified peptide or polymer, spatially resolved surface patterning could be achieved.[146]
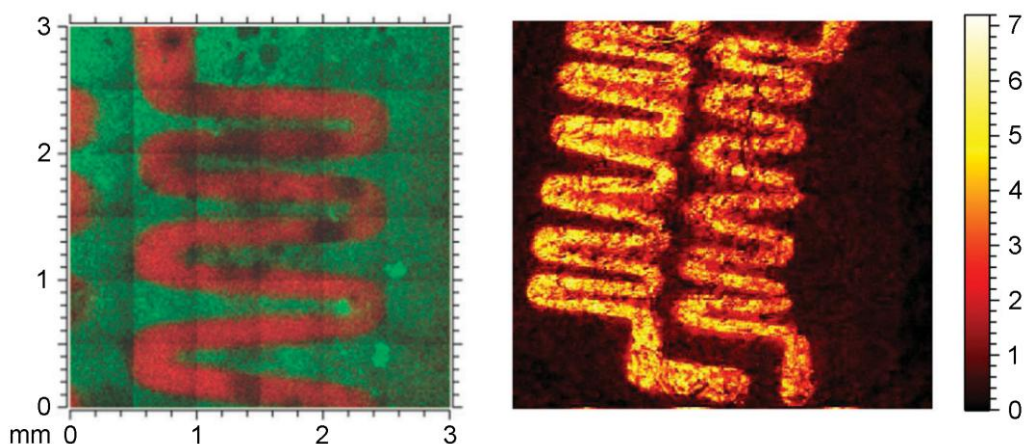
Figure 2.3-2: Time-of-flight secondary ion mass spectrometry (ToF-SIMS) images produced via thioaldehyde chemistry. Left: pattern of PEG (red) immobilized on a silicon substrate (green); right: pattern of fluorine containing polymer (bright) on cellulose (dark). Images were adapted from Ref.[145] and Ref.[146], respectively with permission from the Royal Society of Chemistry (RSC) and Wiley-VCH.

An elegant solution for the synthesis of versatile phenacyl sulfide terminated polymers was demonstrated via the design of a functional RAFT agent. By synthetic conjugation of a trithiocarbonate with the photosensitive phenacyl sulfide, a novel substance was generated which is suitable for controlling radical polymerization and simultaneously installs the thioaldehyde precursor at the chain end. In combination with diene functional polymeric microspheres or planar surfaces, grafting reaction as well as photo patterning were enabled.[147]

Similar to the previously mentioned NQM method, thioaldehyde compounds are also sensitive to nucleophiles. The resulting products for the reaction of thioaldehyde

moieties with amines, hydroxyl amines, and thiols were investigated. Subsequently the technique was applied for site-specific trapping of functional nucleophiles on phenacyl sulfide carrying silicon surfaces.[148]

2.3.1.4 Tetrazole Chemistry

The behavior of tetrazoles under irradiation has been studied extensively for the last 50 years. In the beginning the light-induced cycloaddition, first developed in 1967 by Huisgen and coworkers,[149] has been investigated mainly for its mechanism. In various studies, the nitrile imine could be isolated as an intermediate.[149-153] Therefore, the tetrazole cycloaddition was later termed NITEC (nitrile imine-mediated tetrazole-ene cycloaddition).[154] The general reaction scheme of the NITEC ligation method is depicted in *Scheme 2.3-4.*
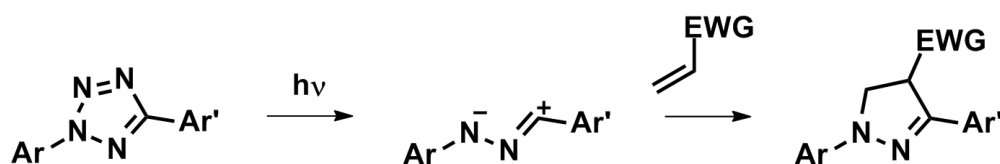
Scheme 2.3-4: General light-induced tetrazole-ene reaction. EWG = electron withdrawing group; Ar, Ar' = general aromatic substituents.

The literature about tetrazole chemistry is too wide to be discussed in detail, yet the most important applications are considered in the following. A pioneer in the field of photo-induced tetrazole chemistry is Qing Lin. He and his team published an enormous quantity of articles and countless different diaryl tetrazole structures were synthesized by his group. Studies on the effect of substituents, solvents, and dipolarophiles were carried out, whereas most of the targeted applications were in the field of peptide modifications. Thus, Lin introduced NITEC chemistry as a modular and biocompatible ligation technique.[155-164]

In our group, the focus of research was on application-related projects. An initial study on the functionalization of surfaces also involves the synthesis of block copolymers by linking maleimide and tetrazole functional polymers. Optimized reaction conditions were applied for the grafting of polymers onto silicon wavers and spatially resolved surface grafting was performed on photoreactive cellulose material.[154] In another study concerning functional cellulose, filter paper was

synthetically modified to contain tetrazole moieties. Subsequently, a meander pattern was produced in a light-induced process using a model peptide as well as an ATRP initiator. By surface-initiated ATRP poly(carboxybetaine acrylamide) could be grafted from the surface, evidenced by high resolution Fourier transform infrared microscopy (FT-IR).[165] A similar approach where a polymer with anti-fouling properties – poly(oligoethylene glycol methyl ether methacrylate) (PMeOEGMA) – was grafted from polydopamine (PDA) surfaces resulted in an accurate pattern of cells after the final anti-fouling tests. Due to the structured nature of the grafted polymer, the growing cells follow the meander line, only growing in non-functionalized areas. The basic light-triggered chemistry that was necessary to obtain the spatial control was NITEC.[166] Moreover, photoresponsive azobenzene surfaces[167] and functional gold nanoparticles were accessible by NITEC chemistry.[168]
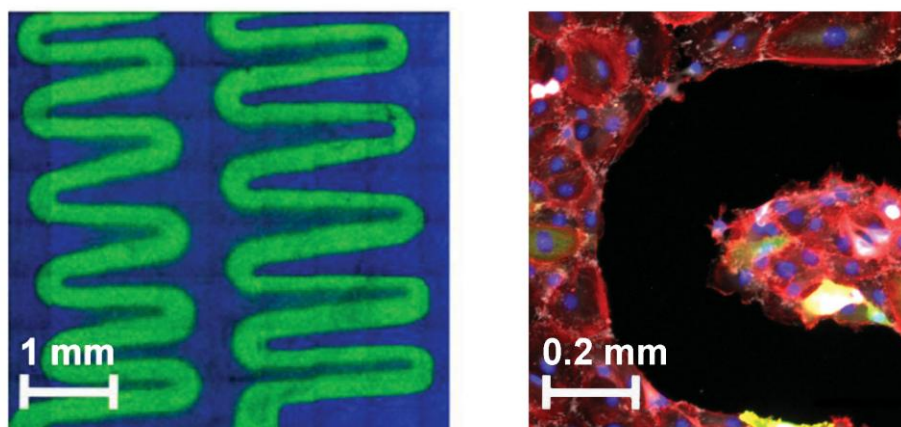
Figure 2.3-3: ToF-SIMS image of photo-patterned PMeOEGMA on a PDA surface (left). Image of cell pattern after 7 h culture, fixation, and staining (right). Images were adapted from Ref.[166] with permission from Wiley-VCH.

A solution-based study on the formation of block copolymers from acrylonitrile rubbers gave interesting insight into the reactivity of a tetrazole component which was previously used for surface grafting. Synthetic rubbers with one tetrazole end group were subjected to a light-induced reaction with a di-linker containing two maleimide units. Efficient block copolymer formation could be shown, evidencing the suppression of crosslinking/polymerization by side reactions of the tetrazole with the pendant nitrile units.[169] In another study involving tetrazoles, cellulose was also the basic material: In an ionic liquid solution, cellulose could be modified to contain tetrazole units, which were subsequently employed to graft poly(*N-iso*-propyl acrylamide) side chains in a light-triggered process. Thus, a renewable, fluorescent,

and thermoresponsive material was produced.[170] Tetrazoles were additionally applied in biological applications for the post-modification of DNA by Wagenknecht and coworkers,[171] as well as for introducing a photochemical tool to disulfide intercalators by our team and the group of Weil.[172]

2.3.1.5 Azirine Photoligation

The photochemistry of *2H*-azirines has been extensively investigated in the 1970s. Former studies of Padwa and coworkers in the first place concerned the behavior of the three-membered heterocycles.[173] Upon irradiation nitrile ylide species are generated via a ring-opening mechanism[6] in very high quantum yields.[174] Naturally, nitrile ylides – representing highly reactive 1,3-dipoles – react with electron deficient multiple bonds in a cycloaddition reaction.[175] The general reaction scheme is presented in *Scheme 2.3-5*.
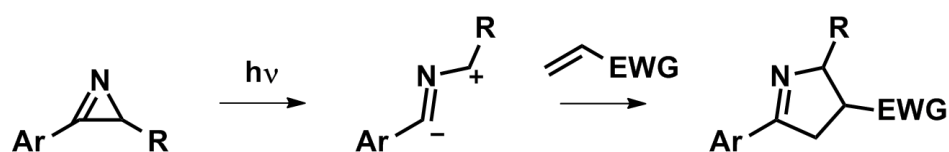
Scheme 2.3-5: General reaction scheme of the light-induced azirine reaction. Ar = aromatic substituent; R = H, alkyl, aromatic substituent.

Thus, an efficient and feasible route to Δ-pyrrolines is provided, whereas its scope and the properties of this synthetic pathway have already been studied.[176-178] Moreover, theoretical work has been conducted on activation energies and reaction kinetics.[179]

Although the azirine-based cycloaddition is an atom-efficient process, Lin and coworkers were the only ones to employ azirines in polymer science. In order to evaluate the scope of the ligation method, five diaryl *2H*-azirine compounds with varying substituents were synthesized and tested for their reactivity towards methyl acrylate and dimethyl fumarate in an ethanol/water mixture. Promising yields of mostly more than 90 % intensified the motivation to use this technique for polymer-peptide ligation. Therefore, a fumarate terminus was installed at a poly(ethylene glycol) chain and an azirine moiety was synthetically anchored to lysozyme. The

resulting bioconjugate was obtained in 41 % conversion according to densitometry analysis.[180]

2.3.1.6 Light-Triggered Azide-Alkyne Cycloaddition

The copper(I)-catalyzed azide-alkyne cycloaddition (CuAAC) has been the most prominent of all *click* reactions.[181] Its efficiency and versatile applicability was demonstrated in a large variety of applications, ranging from materials design,[119, 182-183] chemical biology[184-185] to drug discovery.[186-187] However, the drawback of this technique is the necessity of cytotoxic copper.[188] Therefore, a copper-free version of the azide-alkyne cycloaddition was developed employing cyclooctynes.[189] Due to the strain of the 8-membered ring, the alkyne is more reactive towards azides and thus, the strain promoted azide-alkyne cycloaddition (SPAAC) was established.[190] In 2009, Popik and coworkers introduced a strategy to produce cyclooctynes via photo-induction (photo-SPAAC).[191] Therein, cyclopropenones serve as precursors for the photo-chemical generation of the reactive alkynes. Their thermal stability and insensitivity to organic solvent or water make them suitable for applications and a two step synthesis provides synthetic feasibility.[192] Under irradiation, cyclopropenones release a carbon monoxide unit and the desired ring strain activated alkyne is generated.[193] Rapid cycloaddition occurs at ambient temperature in the presence of azide moieties (*Scheme 2.3-6*).
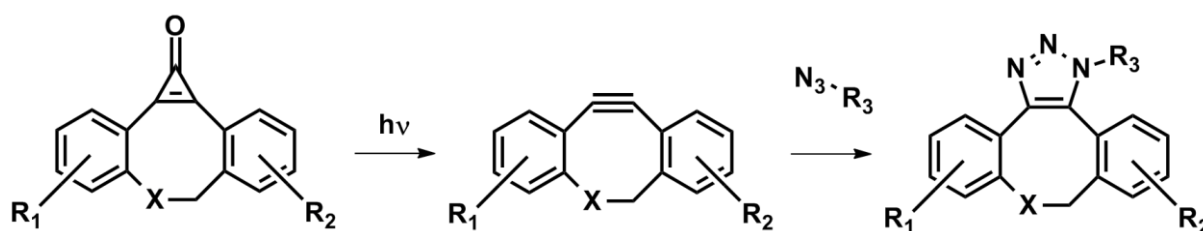
Scheme 2.3-6: General reaction scheme for photo-SPAAC. R_1, R_2, and R_3 are varying organic substituents.

The initial work of Popik and coworkers on photo-SPAAC demonstrated the successful formation of triazole cycles by light-triggered reaction of cyclopropenones and azide compounds. Moreover, labeling of living cells with fluorescence markers was shown. In addition, cyclopropenones anchored to silicon surfaces were employed to generate multicomponent containing pattern. In a two step process,

rhodamin B (RB) and flavin azido (FL) compounds could be immobilized on the surface using a shadow mask.[194]
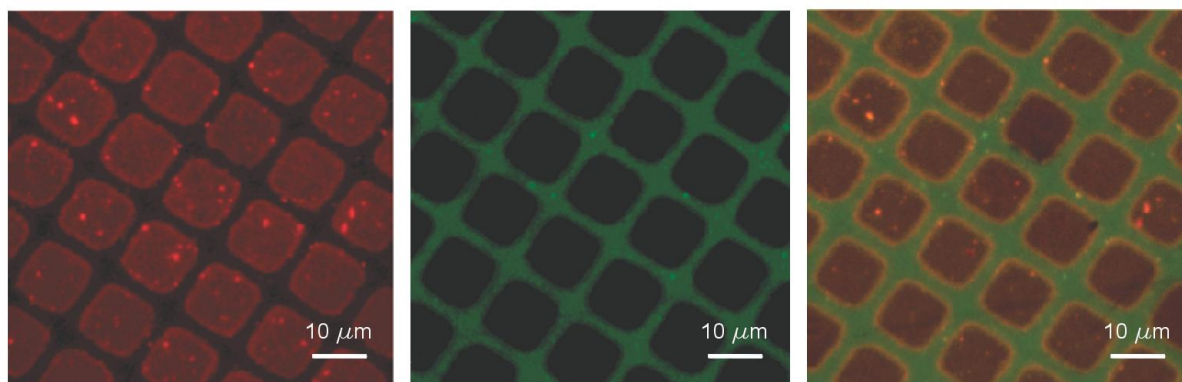
Figure 2.3-4: Fluorescence microscope images of a sequentially photopatterned surface. Left: RB; middle: FL; right: RB and FL. Figure was adapted from Ref.[194] with permission from the ACS.

In order to further increase the reactivity of the alkyne component, particularly in aqueous media, oxa-dibenzocyclooctenones were developed. Their enhanced performance was proven in a kinetic study of the involved photochemical process. Rapid cycloaddition with different azides was demonstrated in water, methanol (MeOH), and mixtures of both solvents.[195]

2.3.1.7 Paternò–Büchi Chemistry

The combined work of Paternò in 1909 and Büchi in 1954 introduces one of the most famous photochemical processes of all time.[8-9] It describes the photo-induced cycloaddition of a carbonyl compound (i.e., aldehyde or ketone) with an alkene via a radical mechanism (*Scheme 2.3-8*). Since its discovery, the Paternò–Büchi (PB) reaction has been subject to a large range of studies mostly concerning mechanistic issues[196-200] or – to be more specific – the selectivity of the reaction with varying reactants and reaction conditions.[201-207]
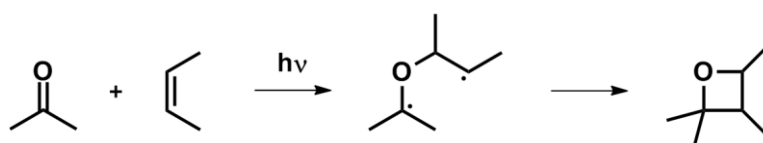
Scheme 2.3-7: General reaction scheme for a Paternò–Büchi reaction.

Another important step for the PB reaction in terms of application was the work of Junkers and coworkers who introduced this photochemical tool to polymer science.[208] In a first study, a benzaldehyde terminated ATRP-polymer was applied for a reaction condition screening. Using the versatility of alkenes, the PB reaction was proven to proceed to high conversions in the presence of, however, a large excess of the alkene moiety. Besides for polymer end group modifications, the reaction could also be proven useful for functionalizing nanoparticles[209] and advanced reaction setups were developed by employing a flow reactor.[210]

The stability of oxetanes – the products of typical PB reactions – is the topic of numerous publications especially with regard to the cycloreversion reaction.[211-213]
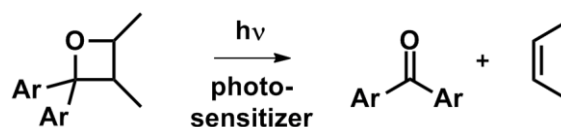
Scheme 2.3-8: General reaction scheme for the photosensitized ring cleavage of oxetane compounds. Ar = aromatic substituent.

Furthermore, the reversible PB chemistry is also of interest for biochemists since DNA lesions – caused by UV-irradiation – are caused by [2+2] cycloaddition reactions. By investigating the repair of such DNA lesions, a photosensitized ring cleavage reaction triggered by photolyases was found.[214-215] Thus, photosensitized ring cleavage of oxetane moieties – proceeding via a radical cationic mechanism – appears to be an applicable tool to reverse the PB reaction.[216] The mechanistic issues of the retro PB reaction were addressed in several studies.[213, 217-218]

A further important tool involving PB chemistry was introduced in a recent exploration of lipid characterization, where oxetane cleavage is the key chemistry for the detection of double bonds by collision induced dissociation electrospray-ionization mass spectrometry (CID ESI-MS).[219] Therein, CID ESI-MS was presented to be an efficient method for cleaving oxetanes on an analytic scale and thus it represents a useful method for investigating their retro PB behavior.

2.3.1.8 Additional Techniques

The current subsection contains ligation methods which have been rarely employed in polymer or materials science, yet they are very suitable for spatially resolved surface modification.

The first example – from our team – is based on an initial, thermal Diels–Alder reaction between phencyclone and maleimide derivatives. The resulting cycloadduct is sensitive to UV irradiation and undergoes efficient decarbonylation and dehydrogenation yielding a large aromatic structure sensitive to nucleophilic addition. This irradiation step is suitable for introducing spatial control as the irradiated positions can be functionalized subsequently. Thus, peptides can be immobilized in distinct positions via a mild and catalyst-free procedure.[220] The reaction sequence is depicted in *Scheme 2.3-7*.
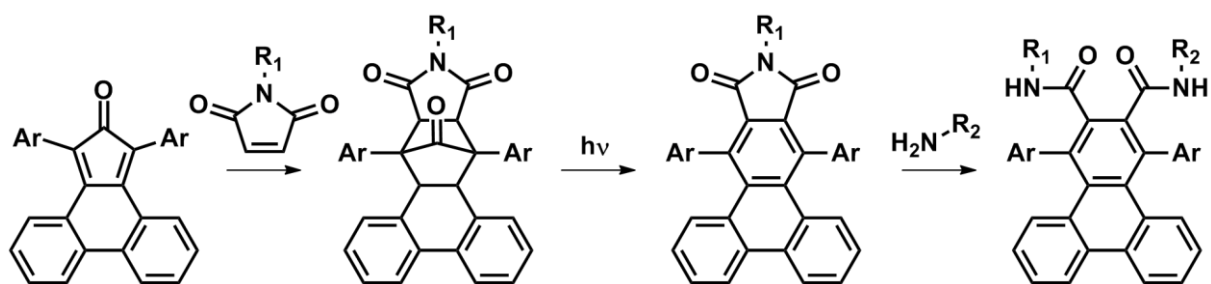
Scheme 2.3-9: General scheme for the phencyclone reaction sequence. Ar = p-Ph-OMe; R₁ = peptide; R₂ = organic substituent

Another highly efficient method to produce patterned structures on surfaces is the photo-induced oxime ligation also introduced by us. *Ortho*-nitrobenzyl acetals quantitatively release benzaldehyde derivatives upon irradiation with wavelengths in the range of 370 nm. The resulting benzaldhyde moiety can subsequently be modified with reactive nucleophiles such as hydroxyl amines yielding highly resolved patterns of the substitution product.[221] The reaction scheme is presented in *Scheme 2.3-8*.
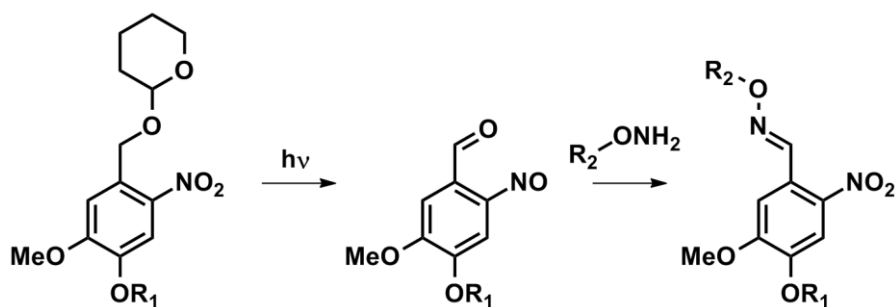
Scheme 2.3-10: General reaction scheme of photo-triggered oxime ligation. R_1 = substrate, R_2 = labelling component.

2.3.2 Light-Induced Polymerization Mechanisms

Inducing polymerization reactions by light is a well-known technique for radical polymerization. Great importance has been given to the investigation of the photoinitiation processes since it determines not only the initiation rate, yet also critically influences the properties of the final polymer.[222] The photoinitiator itself plays a major role in this context, as it produces the initiating radical and thus, the terminus of the resulting polymer. Examples for the most common photoinitiators are depicted in *Scheme 2.3.2*. Four major issues influence the initiation efficiency of a typical photoinitiator: absorbance at the desired wavelength must be provided, intersystem crossing from the first excited singlet state to the excited triplet state is required, fragmentation into radicals must occur (in most cases by α-cleavage), and finally, the generated radicals need to initiate the polymerization.[223] Therefore, the early steps of the initiation process have been studied for instance by femtosecond pump-probe experiments supported by density functional theory (DFT) calculations,[224] whereas initiation efficiencies of the resulting radicals are typically determined by post mortem ESI-MS analysis of polymers produced via pulsed-laser polymerization (PLP).[225-226] Extensive studies combining femtosecond spectroscopy with the insights of PLP-ESI-MS experiments draw a detailed image of the entire photoinitiation process for radical chain-growth polymerization.[227]
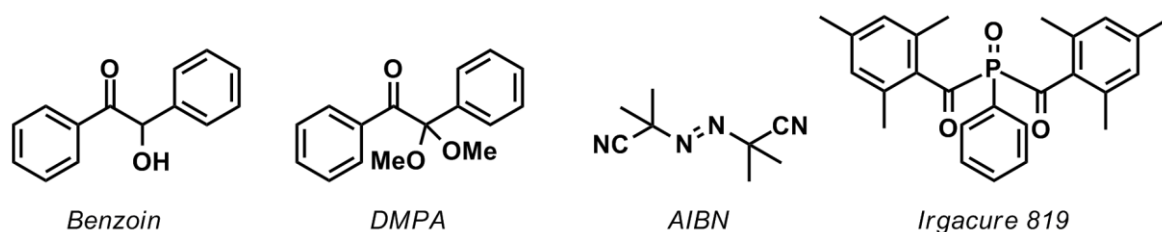
Scheme 2.3.2: Typical radical photoinitiators. DMPA = 2,2-dimethoxy-2-phenyl acetophenone; AIBN = azo-bis-(isobutyronitirile).

Although it requires more synthetic effort than a radical polymerization, step growth polymerization reactions can also be induced be light. There exist few examples where light-triggered cycloaddition reactions have been applied to trigger polymerization processes. The photoenol approach, for instance, has attracted attention of the National Aeronautics and Space Administration (NASA). Along with a corresponding publication, a patent was filed on the light-induced reaction between bismaleimides and difunctional photoenol moieties.[228-229] Thus, polyimides with a number average molecular weight of up to 80,000 g mol^{-1} could be produced. An alternative pathway to generate polyimides was reported based on the photo-induced cycloaddition reaction of bismaleimides with benzene.[230] Moreover, the dimerization reactions of coumarin or cinnamate groups were shown to be feasible for polymerizing oligo(ethylene glycol) monomers.[231] Additional information and a detailed discussion of dimerization reactions is provided in Section 2.3.4.

2.3.3 Visible Light-Induced Chemistry

As discussed above, light-induced chemistry in general has become one of the most rapidly growing fields of contemporary research. A particularly challenging discipline in photochemistry is based on a very special set of photoreactions, presenting very recent developments and a modern approach to apply photochemical tools: visible light-induced chemistry. Since inducing chemical reactions with visible light is a highly attractive topic in terms of sustainability, a variety of approaches has been published lately. Versatile methods and systems provide powerful tools particularly on the platform of synthetic organic chemistry. More specifically, the trends in modern organic chemistry concerns the design of novel catalysts and their use for synthetic challenges. In order to provide an overview of the diversity of photocatalytic

approaches, the current section addresses divers examples for ligation reactions, including metal-based as well as organic dye catalysts. In addition, a more detailed description of a highly interesting metal-free photocatalytic example for a formal [3+2] cycloaddition reaction based on azirines will be discussed. A collation of accessible ligation reactions is depicted in *Scheme 2.3.3*.

Since the first examples of organic synthesis catalyzed by visible light have been reported,[232] increasing attention has been paid to this field of photochemistry. By now, the literature is extensive and the versatility of reactions and catalysts has been summarized in multiple review articles.[233-235] Besides the diversity of investigated processes, where detailed reaction mechanisms have been formulated, the focus of the following examples is on the synthetic aspects. For instance, the addition of α-aminoalkyl compounds to electron deficient double bonds has been reported. The radical-mediated reaction between methyl diphenylamine and diethyl ethylidene malonate was found to proceed catalyzed by 1 mol% of an iridium-based or eosin Y catalyst. High yields up to 97 % were achieved at ambient temperature in 18 h.[236] A metal-free system for the direct C-H arylation of heteroarenes was reported using the photoredox catalyst eosin Y under visible light irradiation. Therein, diazonium salts were employed as starting materials and a single electron transfer mechanism produces the desired products in up to 86 % yield.[237] A very popular transition metal for visible light redox catalysis is ruthenium. It can for instance be applied for the generation of cyclobutane adducts from bis-enone moieties via a [2+2] cycloaddition. By reductive quenching of an excited Ru-complex, the resulting dimer is formed in high yields and excellent diastereoselectivity.[238] Moreover, [3+2] cycloaddition reactions are accessible by photoredox catalysis of ruthenium complexes. Cyclopropyl amines were reported to react with alkenes in a regioselective fashion. The formation of the resulting cyclopentene derivatives is compatible with a multitude of functional groups and proceeds under mild conditions.[239] 1,3-Dipolar cycloadditions can also be activated by visible light catalysis. Irradiation of tertiary amines in the presence of suitable iridium or ruthenium pyridyl complexes leads to the formation of a mediating azomethine ylide. Subsequently, cycloaddition with electron deficient double bond containing moieties results in a newly formed 5-membered heterocycle.[240] This photochemical technique has also been applied for the synthesis of pyrrolo isoquinolines via a catalytic oxidation/cycloaddition/oxidative aromatization sequence.[241] The final example employs azirines as starting material

for photoredox catalytic synthesis of pyrrole derivatives. In the presence of an organic dye photocatalyst, *2H*-azirines were demonstrated to undergo [3+2] cycloaddition reactions with activated carbon-carbon triple bonds. Thus, a series of highly functional pyrrole moieties could be generated utilizing white or blue LEDs.[242]
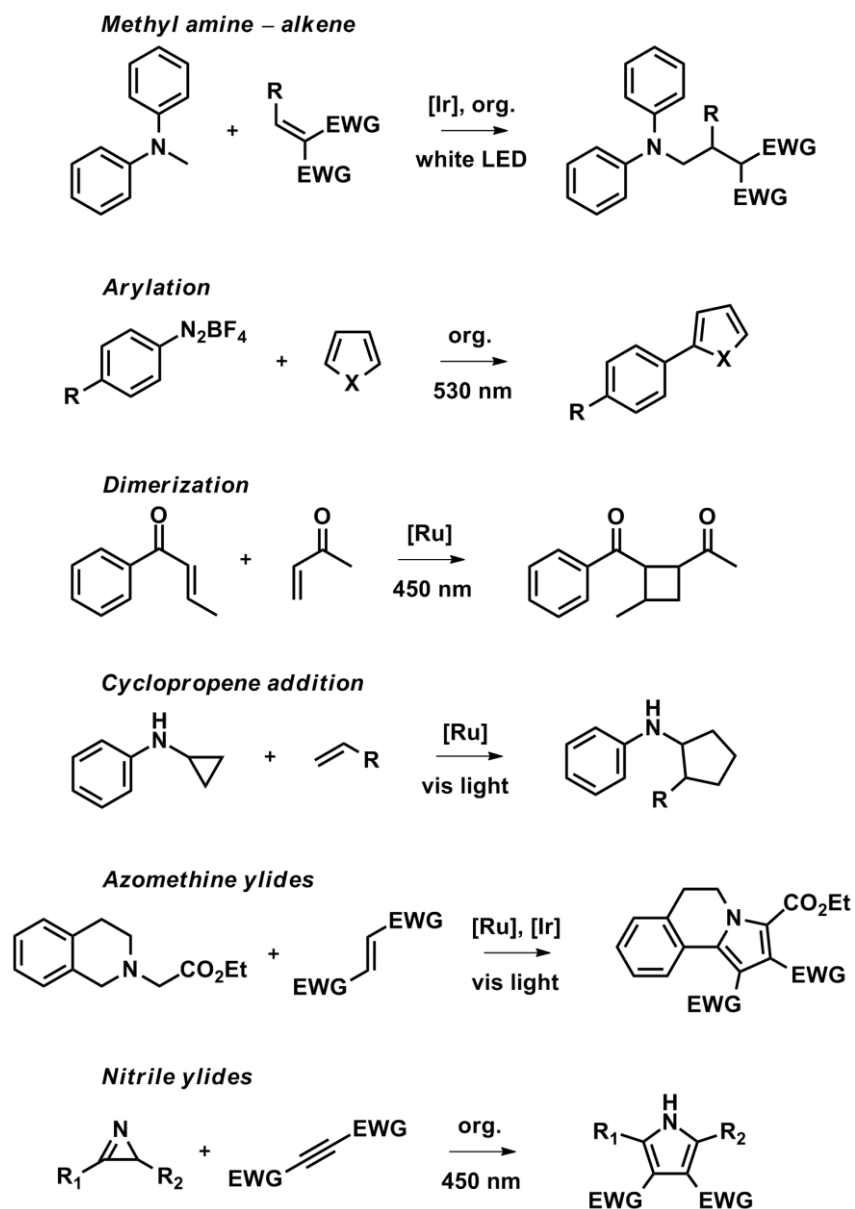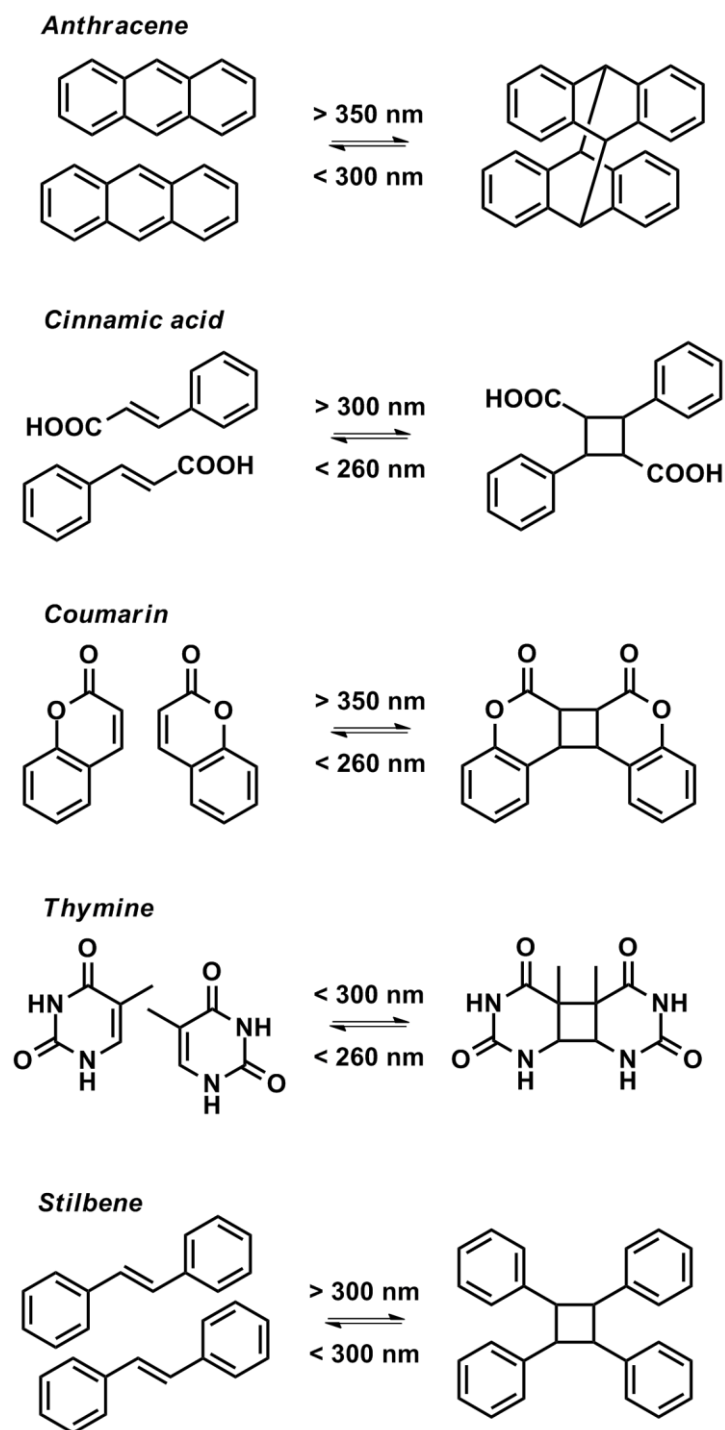

Scheme 2.3.3: Collation of ligation reactions induced by visible light catalysis. EWG = electron withdrawing group; R1, R2 = organic substituents; org. = organic dye catalyst.

2.3.4 Reversible Photoreactions

A particular set of photochemical reactions has the property of being reversible. Photoreversible reactions are especially appealing, as they do not only introduce spatial resolution and precise temporal control over a single photoreaction, but further enable the reverse reaction for designing materials properties. Thus, the range of applications for reversible photochemical techniques is immense, particularly in the field of polymer chemistry and material science.[243] So-called photoresponsive materials are for instance applied in photoresists, where crosslinking of polymeric material enables the generation of 2D and 3D structures.[244] In Section 2.3.6 photoresists will be discussed in more detail. By introducing hydrophilic groups to the polymeric structure, photoresponsive hydrogels can be produced.[245] They consist of crosslinked polymer chains capable of absorbing large amounts of water.[246-247] Recent studies have confirmed that reversible photochemistry is also suitable for applications in the field of self-healing materials, designed to repair cracks or fractures by an external stimulus.[248] A more biological application is the production of nanocarriers. Polymeric micelles formed by amphiphilic block copolymers can be crosslinked photochemically and decrosslinked when desired, which makes them ideal for drug delivery applications.[249-251] The final application of this list is the less complex idea of reversible linear polymers. This concept allows to control the polymerization and depolymerization by light induction.[252]

The chemistry these applications (above) are based on, are dimerization reactions.[253] Their characteristic property is the reversibility of the reaction. Depending on the wavelength, either the dimer formation or the dissociation into monomers is triggered. The following scheme depicts the most popular photoreversible dimerization reactions, including anthracene,[254] cinnamic acid,[255] coumarin,[256] thymine,[257] or stilbene derivatives[258] (*Scheme 2.3.4*).

Anthracene

> 350 nm

< 300 nm

Cinnamic acid

HOOC

COOH

> 300 nm

< 260 nm

HOOC

COOH

Coumarin

> 350 nm

< 260 nm

Thymine

< 300 nm

< 260 nm

Stilbene

> 300 nm

< 300 nm

Scheme 2.3.4: Collation of photoreversible dimerization reactions.

2.3.5 Complex Polymeric Architectures via Light-Induced Chemistry

Materials engineering is a complex field and important for applications in contemporary chemistry. A more detailed investigation of the properties of materials reveals that molecular structures – predominantly macromolecular structures – have a very significant impact. Thus, controlling macromolecular structures and careful design of polymeric architectures are key to modern material science. The tools for producing macromolecular designs rely on a combination of controlled polymerization techniques and efficient conjugation and modification reactions, including light-induced methods. An overview of these tools has already been given in the current chapter (Section 2.3.1). The following examples for the generation of polymeric designs are determined to provide an idea of the applicational scope light-triggered methods possess. Besides the smart usage of one photochemical tool, especially the combination of two different methods can result in synthetic advantages.

The advantages of NITEC chemistry were already highlighted in Section 2.3.1.4. Yet, a more detailed description how NITEC chemistry can be utilized for modern materials design is given by introducing the work of Willenbacher *et al.* from our team. Therein, a peptide mimicking substrate was generated, which is additionally suitable for fluorescence labeling. The approach, therefore, is based on single-chain nanoparticles, a modern and extensive field of chemical research.[259] SCNPs are typically formed by folding polymers, in this case irreversibly by NITEC chemistry. In order to produce a suitable folding precursor polymer, polystyrene with pendant tetrazole and furan-protected maleimide groups was synthesized by NMP. By light-induced folding of the resulting precursor polymers, fluorescent as well as profluorescent nanoparticles could be obtained. The size of the respective SNCPs can be finely adjusted by changing the tetrazole/maleimide ratio along the polymer backbone. In addition, pro-fluorescent SCNPs were produced using the nitrile imine dimerization reaction[7] to generate the folded material. Thus, residual tetrazole units were applied for subsequent conjugation reactions with for instance functional microspheres. Since neither the SCNPs, nor the microspheres were fluorescent prior to the final conjugation reaction, the success of the coupling process – yielding a fluorescent pyrazoline linkage – could be monitored by the discernable fluorescence.[260]
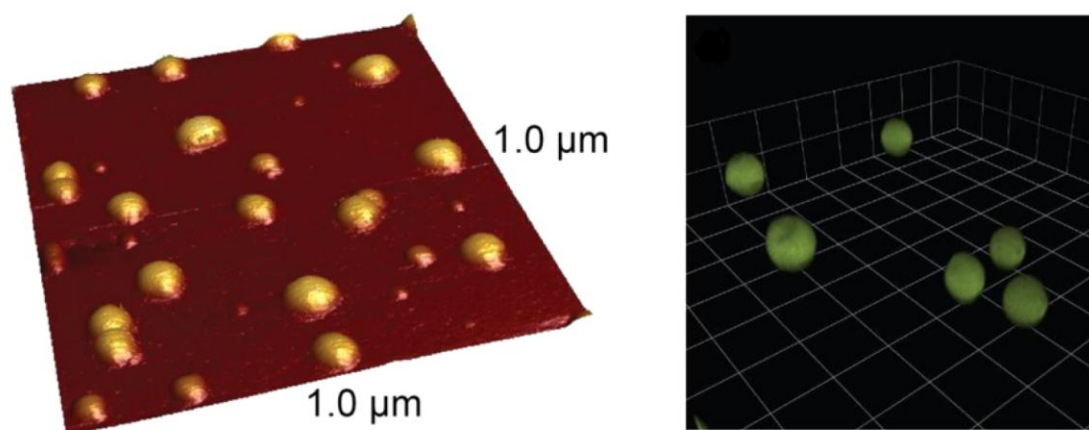
Figure 2.3-5: Three-dimensional atomic force microscopy (AFM) image of SCNPs folded via NITEC (left). Three-dimensional reconstruction of a confocal image stack depicting SCNP-functionalized microspheres (right). Images were adapted from Ref.[260] with permission from the ACS.

Sophisticated architectures are accessible when not only one, but two different photochemical methods are combined. Moreover, by smartly designing the respective photoconjugations a novel type of orthogonality can be introduced. Hiltebrand *et al.* from our group demonstrated that photoenol and NITEC chemistry are suitable for so-called λ-orthogonal ligation, which is also applicable to surface modifications.[261] An α,ω-functional building block containing a tetrazole as well as a photoenol terminus represents the core compound of the study. Since the photoenol can be excited above 310 nm, where the tetrazole group does not absorb when the substituents are chosen appropriately, successful photoenol ligation can be induced without altering the tetrazole end group. The latter can be activated at wavelengths shorter than 310 nm in a second conjugation step. Thus, by choosing the initiation wavelength, a macromolecular construct could be site-selectively encoded with small molecules (maleimides), fluorescent markers, functional polymers – yielding triblock copolymers – or peptides.[262]

It is considered one of the most challenging tasks in contemporary macromolecular chemistry to achieve sequence control in synthetic polymers.[263-264] A photochemical protocol to approach synthesizing macromolecules with exactly defined molar mass, was reported by us. In the respective study, altering photoenol and thioaldehyde ligation chemistry was employed to consecutively conjugate two photoreactive synthons. Commencing from a difunctional maleimide unit, a photoenol reaction was conducted, generating a compound with two open chain diene termini. A subsequent light-induced thioaldehyde ligation yielded two furan-protected maleimide end

groups, which – upon deprotection – were available for repeating the reaction cycle. Thus, a macromolecule containing 10 monomer units with a molar mass of 3231.58 g mol^{-1} and a dispersity of 1.00 could be produced.[265]

2.3.6 Light-Induced Crosslinking Techniques for Surface Patterning

Surface encoding is one of the major applications for photochemical methods. In contrast to the techniques previously alluded to, where the photosensitive compounds were covalently connected with the surface material, the current section addresses an entirely different approach. Despite the advantages of covalently binding photoligation precursors to substrates, a feasible and established method for surface modifications is based on crosslinking the desired material on the surface. Polymer networks are typically insoluble and can thus not be removed by washing procedures. To break the adhesive interaction between crosslinked material and the substrate, mechanical force is required. In addition, the crosslinking approach for surface patterning is applicable to almost any substrate since the properties of the surface do not necessarily affect the crosslinking reaction.

In the context of crosslinking polymeric materials, photochemical methods play a vital role. In order to gain spatial control over the network formation process, various light-induced approaches have been explored. This section introduces the most common crosslinking techniques, ranging from typical radical crosslinking polymerization to advanced *click*-type ligation chemistry. Multifunctional acrylate photoresists, for instance, can be radically crosslinked whereas epoxide based photoresists are similar to the crosslinking polymerization of oxetane functionalized polymer backbones. The above mentioned photochemical dimerization reactions are also suitable techniques to achieve efficient crosslinking which will be demonstrated in a few examples. Light-induced click chemistry has also entered the stage of crosslinking chemistry and methods such as thiol-ene, photoenol, or NITEC significantly increase the available chemical toolbox. All entries from the above list of chemical approaches to build polymeric networks have been employed for a large variety of applications, ranging from 3D structures with attached fluorescent dyes,[266]

to the generation of light-emissive pattern,[267] or dental care materials.[268] To demonstrate the current state-of-the-art in light-induced surface modification via crosslinking, a selection of examples will be presented for each crosslinking method. An overview of the respective crosslinking chemistry is depicted in *Scheme 2.3.6*.

Radical intiation

Oxetane ring opening

Dimerization

Thiol-ene

Photoenol
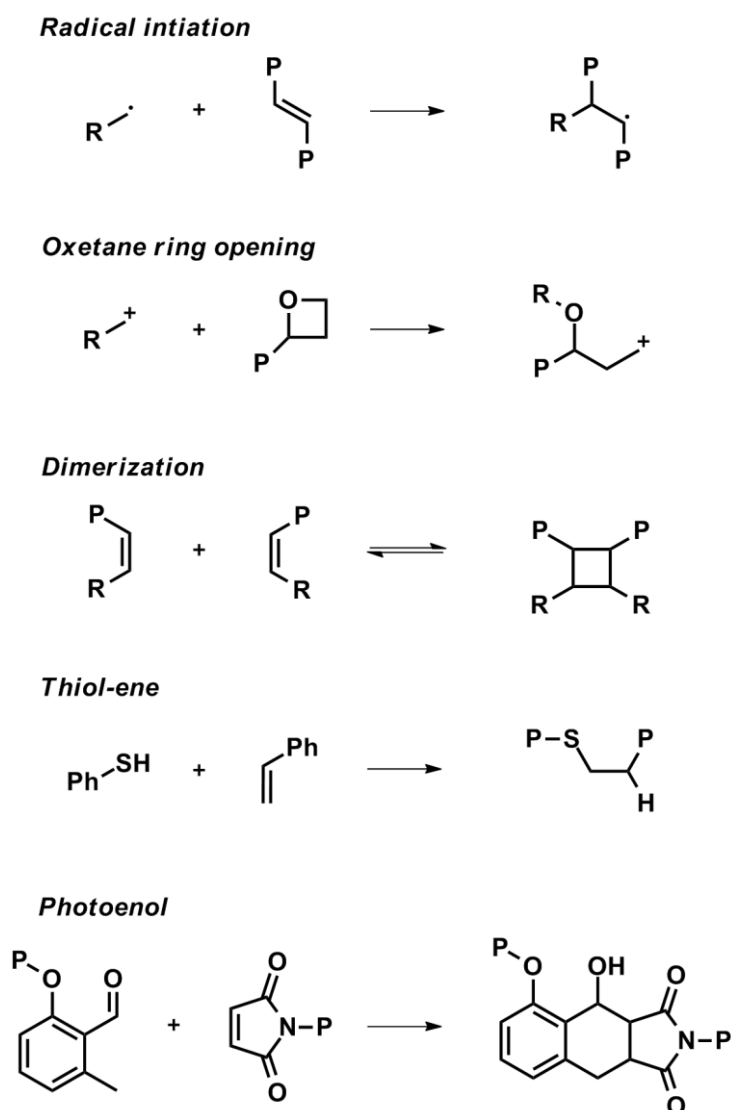
Scheme 2.3-6: Schematic depiction of the crosslinking chemistries. P = connection to polymer or linker; R = organic substituent

Radical polymerization of multifunctional double bond containing compounds is arguably the most feasible route to produce crosslinked material. To induce the polymerization process, benzophenone − or other typical photoinitiators − can be employed to either initiate the polymerization of mixtures of multifunctional monomers, so-called photoresins,[269] or crosslink polymer chains by hydrogen abstraction.[270] Dental care, where UV-initiated curing of viscous material is targeted to yield a robust surface coating,[268] was the first field of application for radical

photoresins. Radical crosslinking was further explored and established particularly with respect to the mechanical properties of crosslinked polymer blends,[271] polyethylene surfaces[272] and melts,[273] as well as multiphase systems.[274] Immobilization of biomolecules onto polymer surfaces could be obtained by introducing functional compounds into crosslinked films, for example azide moieties.[275] The first examples for producing patterned substrates were achieved by employing a shadow mask, which restricts the crosslinking to proceed only in the illuminated areas. Thus, crosslinking monolayers of amphiphilic block copolymers yielding patterns of Langmuir-Blodgett films[276] or the production of light-emissive patterns on micrometer scale by incorporation of fluorescent species were achieved.[277] Moreover, optoelectronics are applications with constantly increasing impact, motivating studies on, e.g., hole-transporting materials via radical photocrosslinking triphenylenes,[278] modulated optical diffraction gratings through photolithographic patterning of electroactive polymer films,[279] or photocrosslinking of conjugated polymers to produce three color polymer light-emitting diodes.[280]

A further famous type of polymeric network formation is based on epoxy resins and proceeds via photoinitiated polymerization of multifunctional epoxide moieties. SU-8, a development of IBM in 1989,[281] is a commercially available photoresist which appears in a large number of patents and journal articles concerning micro electromechanical systems (MEMS) or photolithography in general. The extensive literature about applications involving SU-8 is summarized in multiple review articles.[282] Although SU-8 is more popular, a related type of crosslinking technique has been demonstrated to be suitable for producing optoelectronic materials. By cationic ring-opening of multifunctional oxetane compounds – small molecules, or pedant on polymer backbones – crosslinking can be readily induced. Thus, networks of conjugated polymer could be generated[283] and blue light-emitting diodes via polymerization of a difunctional oxetane monomer were produced.[284] Moreover, the fabrication of a pixelated RGB matrix display was achieved by consecutive crosslinking of oxetane functionalized polymers luminescent in red, green, and blue.[267]
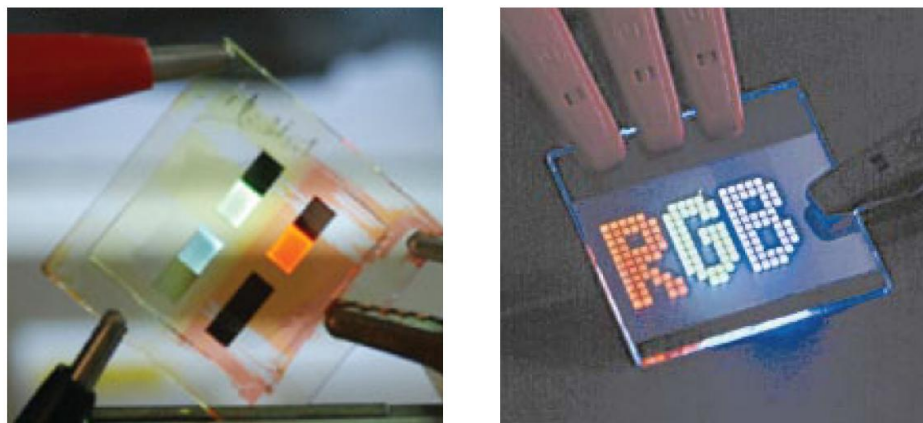
Figure 2.3-6: Picture of an electroluminescent RGB color emitting device (left) produced via radical crosslinking. Photograph of a pixelated RGB device (right) generated by oxetane crosslinking. Images were adapted from Ref.[280] and Ref.[267] with permission from Wiley-VCH and the Nature Publishing Group (NPG)

From a molecular point of view, the above noted crosslinking techniques are based on cross-polymerization mechanisms yielding materials with hardly characterized linking points. Dimerization reactions, on the other hand, are well understood, in-depth analyzed processes. As alluded to in the reversible photoreactions section (2.3.1.4), dimerization approaches can also be utilized to generate networks.[253] Here, selected examples for surface patterning via crosslinking are presented, proving these techniques to be an advanced tool for producing surface modifications via interconnecting polymer chains. For example the light-triggered dimerization of coumarin based polyesters is suitable for generating complementary surface patterns, depending on the excitation wavelength which controls whether crosslinking (350 nm) or decrosslinking and polymer chain scission (254 nm) occur.[285] Reversible crosslinking utilizing anthracene derivatives enables the production of honeycomb structured films, which can be photochemically crosslinked and subsequently patterned on an additional level by reversing the dimerization reaction.[286] In order to enter water based media, thymine pendant groups can be incorporated into polymers. Thus, an aqueous medium approach for surface coating via photocrosslinking of environmentally benign copolymers could be achieved,[287] as well as the development of water based photoresists for patterning copolymers[244] and terpolymers.[288] The cinnamate approach, however, is today's most widely applied photochemical dimerization system for surface encoding. Initially, polymer crosslinking via cinnamate functionalities was employed for incorporating fluorescent acidic dyes,[289] whereas nowadays most efforts are directed to the development of

optoelectronics, e.g., patterns of hole-transport material for light-emitting diodes,[290] optical writing in liquid crystal cells,[291] blue light-emitting copolymers,[292] electrochromic conjugated films,[293] and organic transistors.[294]

Figure 2.3-7: Scanning electron microscopy (SEM) image of the top of a woodpile structure fabricated via thiol-ene-induced DLW (left). Patterning of the respective three-dimensional structure with a fluorescene maleimide component (right). Images were adapted from Ref.[266] with permission from Wiley.

Since the era of click chemistry has begun, the set of efficient light-triggered reactions have proven to be a valuable tool for surface crosslinking. For instance, the photoinitiated thiol-ene reaction was employed for designing novel photoresists applied for surface patterning of ultrathin films[295] or rapid prototyping of multilayer thiol-ene fluidic chips.[296] In addition, electroluminescent networks could be photopatterned by crosslinking polyfluorenes via thiol-ene chemistry[297] and conjugated polymer networks with tunable bandgaps could be generated.[298] Moreover, solution-processed multilayer light-emitting diodes were produced, representing hole-transporting surface coatings.[299] Another advanced application for light-induced techniques in general, i.e., thiol-ene chemistry, is direct laser writing (DLW). For instance, 3D photofixation of furan-maleimide Diels–Alder networks could be realized by laser induced thiol-ene reaction.[300] Processable 3D microstructures – woodpile photonic crystals – could also be generated using the thiol-ene reaction itself for the crosslinking process. Precise patterning of the written surfaces with a fluorescent dye was additionally accessible since the resulting surface of the structures still contains residual photoreactive groups.[266] Apart from the thiol-ene reaction, other light-induced click reactions have been subjected to surface crosslinking. A combination which had already attracted industrial attention,[301] is a photosensitive mixture of multifunctional photoenol and polymeric maleimide species suitable to form a photoresist. The latter was employed to generate woodpile

photonic crystals via DLW with a rod distance of 500 nm. Again, the residual surface exposed photoenol moieties were subsequently employed for site-specific patterning of surface markers.[302]

3

STEP-GROWTH POLYMERIZATION VIA NITEC – FLUORESCENT POLYMERS FROM NON-FLUORESCENT PHOTOREACTIVE MONOMERS

The development of novel polymerization techniques requires a judicious design of the targeted system. First of all, the mechanism for connecting the monomer units needs to be selected. When cycloaddition reactions are utilized for the propagation step, the polymerization mechanism is typically characterized by step-growth behavior. Modern and efficient conjugation tools have recently revived the concept of step-growth polymerization. *Click* chemistry enabled, for instance, accessing conjugated polymers,[303] polyferrocenes,[304] or palladium containing polymers[305] via step-growth polymerization. The current chapter focuses on two issues, the first one being the suitability of NITEC chemistry for step-growth polymerization. As alluded to

---

in the theoretical background section, the conversion in step-growth polymerization processes is required to be well above 90 % to obtain polymeric material of reasonably high molar mass. Therefore, side-reactions must be absent in order to achieve such high conversion values. The most important reasons to conduct the study presented in the current chapter are the properties of the final product. Since tetrazoles themselves are not fluorescent in contrast to the NITEC cycloaddition product, the approach leads to fluorescent polymers from non-fluorescent monomers. Thus, a novel platform technology for fluorescent polymers is established applying a biocompatible and light-induced conjugation method. The following figure describes the idea of the project in a graphical fashion (*Figure 3-1*).
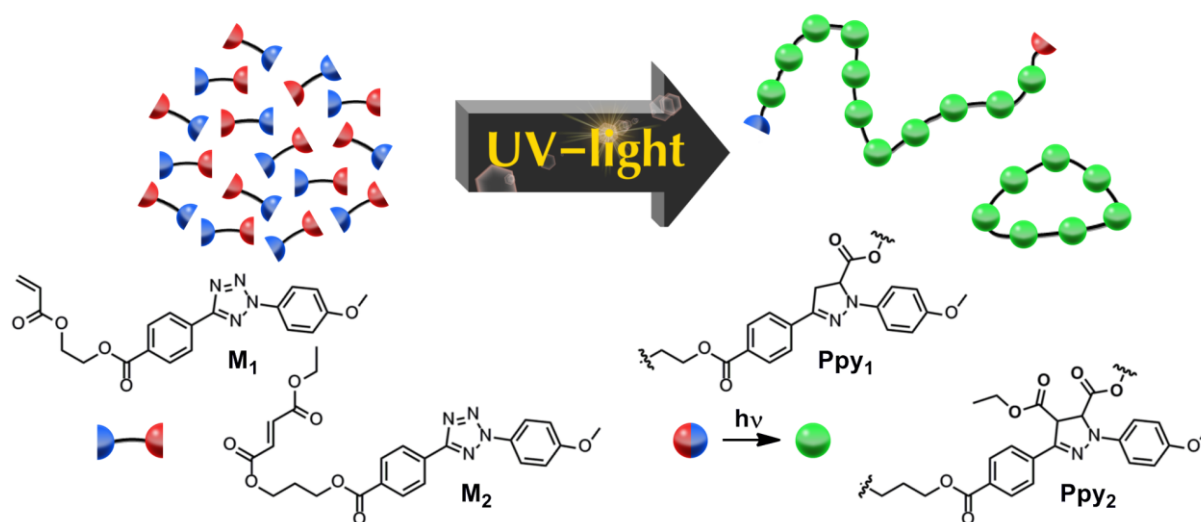
Figure 3-1: Overview of the polymerization strategy for producing fluorescent polymers from profluorescent monomers.

3.1 Design of Photoreactive Monomers

To allow for the development of a novel light-induced polymerization technique, the photoreactive monomers themselves had to be designed (*Scheme 3.1-1*). In step-growth polymerization, linear and non-branched polymers can only be obtained with monomers carrying two functional groups. Moreover, the monomers were designed to contain both functional groups (i.e., tetrazole and dipolarophile) in one molecule – an A-B-type monomer – which provides equimolarity of both functions and thus simplifies the polymerization setup (*Scheme 3.1-1*).
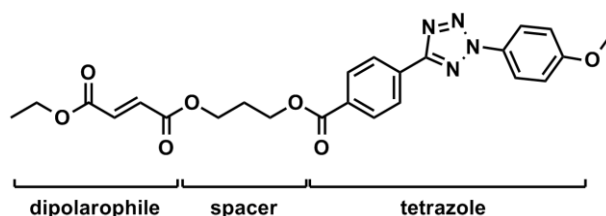
Scheme 3.1-1: Photoreactive monomer M_2.

In order to enable the investigation of the effect of different dipolarophiles, two monomers were prepared carrying different electron deficient double bond moieties, i.e., acrylate as well as fumarate functionalities were included in the monomer design. Besides the photoreactive functionality and its counterpart, the monomers also contain a spacer, which is in both cases a short alkyl chain. The spacer is on the one hand necessary for the monomer synthesis and on the other hand it increases the mobility of the entire compound, to improve the monomers solubility. The synthetic pathway to both monomers is straightforward: A carboxylic acid-functionalized diaryl tetrazole (synthesis is reported in literature),[166] which will be subject of a detailed discussion in Chapter 7, is esterified by transformation into the corresponding acyl chloride. The acrylate dipolarophile is commercially available carrying a hydroxyl ethyl substituent, which readily reacts with the tetrazole acyl chloride to yield the first monomer (M_1) (*Scheme 3.1-2*).
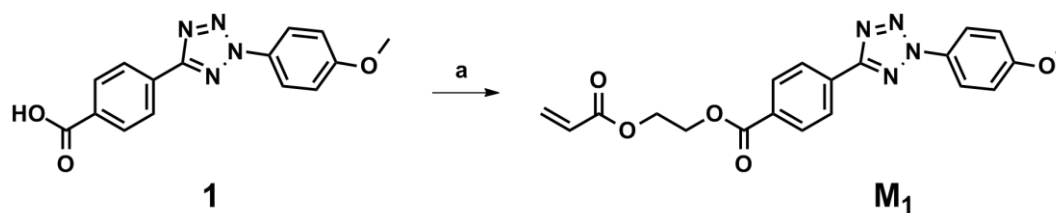
*Scheme 3.1-2: Synthesis of **M₁**. a) 1. SOCl₂, THF, 4 h, 75 °C, 2. hydroxyethyl acrylate, pyridine, dry THF, 0 °C – RT, overnight.*

The synthetic pathway for the second monomer (**M₂**) requires an additional preparative step for connecting the monoethyl fumarate with propanediol. Thus, a compound (**2**) bearing a terminal hydroxyl function for the final esterification step with **1** is generated (*Scheme 3.1-3*).
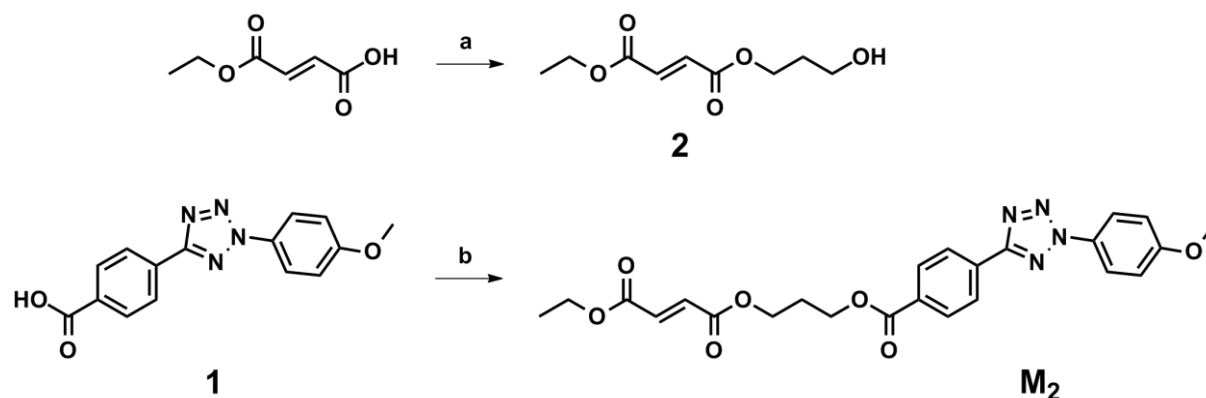
*Scheme 3.1-3: Synthesis of **M₂**. a) 1,3-propanediol, EDC-HCl, DMAP, THF, 0 °C – RT, overnight. b) 1. SOCl₂, THF, 4 h, 75 °C, 2. **2**, pyridine, THF, 0 °C – RT, overnight.*

Hence, two photoreactive monomers, designed for step-growth polymerization, with a molar mass of 394.4 g·mol^{-1} (**M₁**) and 480.5 g·mol^{-1} (**M₂**) were prepared via straightforward organic synthesis.

3.2 Light-Induced Polymerization of Photoreactive Monomers

Upon completed preparation of the two novel monomers, their behavior in light-induced polymerization processes was investigated. Due to the novelty of the light-driven polymerization approach, the reaction parameters including concentration, total batch size, irradiation time, and irradiation intensity had to be explored and optimized. The general preparation of the samples is facile since the NITEC reaction is insensitive to oxygen or water as evidenced in earlier studies.[164] Thus, the monomers simply had to be dissolved in a suitable solvent, the sample vials were crimped airtight to avoid evaporation of the solvent and irradiated in a custom-built photoreactor (refer to the Methods section for details regarding the photoreactor). In order to establish the optimal conditions, **M₁** was subjected to the polymerization process and the monomer concentration as well as the total amount of monomer were screened (*Scheme 3.2-1*).
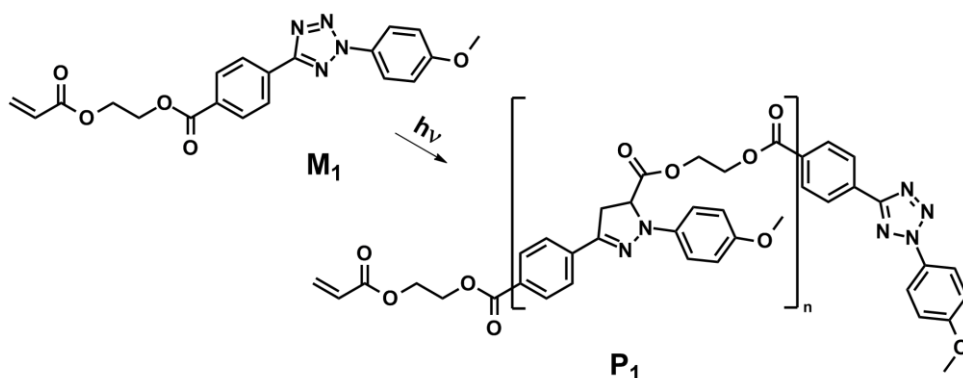
*Scheme 3.2-1: Light-triggered polymerization of **M₁**.*

When the monomer solution is exposed to UV light (λ_{max} = 320 nm), the excited tetrazole moieties form highly reactive nitrile imine species by releasing a nitrogen molecule. The resulting 1,3-dipols react rapidly in a [3+2]-cycloaddition with the dipolarophile units present in an equimolar amount. The newly formed cycloadduct represents the connection between the monomer units in the propagation step and can potentially either be positioned between two monomers, oligomers, or polymeric species. If the cycloaddition proceeds intermolecularly, a step-growth polymerization process takes place, whereas an intramolecular reaction leads to a cyclic termination

product. The inevitable termination reaction via α,ω-cycloaddition is subject to discussion in Section 3.3.

The first parameter to be varied was the concentration. High concentrations were expected to increase the molar mass of the resulting step growth polymer since the probability for intermolecular reaction between two different polymer chains is more likely in concentrated systems. In contrast, formation of cyclic low molar mass material should be favored in diluted media. The initial concentration study reveals this assumption to be correct (*Figure 3.2-1*, left). The amount of higher molar mass material increased when the polymerization medium was concentrated.
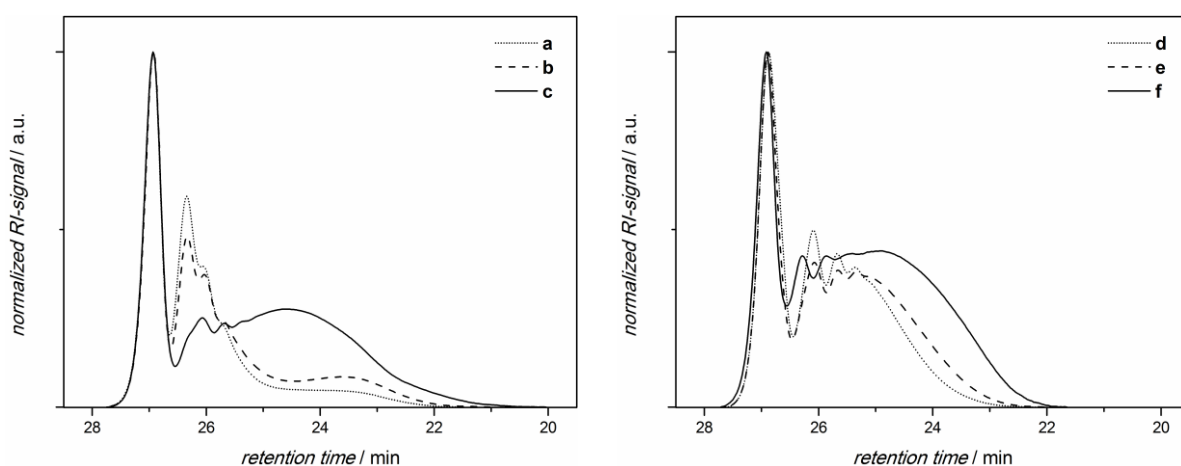
Sample	M_n [g·mol^{-1}]	M_w [g·mol^{-1}]	$Đ$
a	1600	2700	1.69
b	1800	3700	2.07
c	2400	6000	2.56
d	2100	3300	1.56
e	2300	4000	1.73
f	2600	5400	1.73

Figure 3.2-1: Concentration (left) and total batch size (right) study conducted by light-induced polymerization of M_1. Bottom: Collation of molar mass values. Reaction conditions: DMAC, 36 W, 24 h, a) 2 mg·mL^{-1}, 2 mg; b) 10 mg·mL^{-1}, 2 mg; c) 40 mg·mL^{-1}, 2 mg; d) 100 mg·mL^{-1}, 10 mg; e) 100 mg·mL^{-1}, 5 mg; f) 100 mg·mL^{-1}, 2 mg.

Consequently, all further polymerization reaction were conducted with a concentration of 100 mg·mL^{-1} which is close to saturation. Moreover, the optimum scale of a single polymerization batch needed to be investigated. It was found that the reaction time scales with the total amount of monomer employed for the polymerization (*Figure 3.2-1*, right). Since the best results were obtained for the smallest batch size and in order to consume resources responsibly, all future

polymerizations were carried out with the minimum amount of material required for common analytical techniques (NMR, SEC, ESI-MS).

Compared to **P₂**, the solubility of **P₁** was found to be reduced in organic solvents suitable for analytic methods. Consequently, the polymerization process of **M₂** was monitored closely and the kinetic study as well as detailed characterization of the final product were conducted with polymeric material stemming from polymerizing the second monomer (*Scheme 3.2-2*).
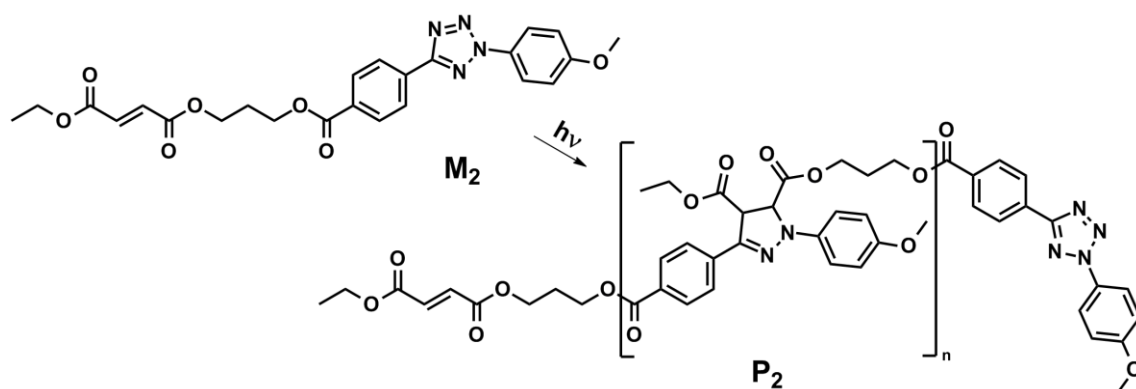
*Scheme 3.2-2: Light-driven polymerization of **M₂**.*

Improved solubility of polymer **P₂** in volatile organic solvents, for instance THF, facilitates isolation and enables to subject the product to versatile analytic methods, such as size-exclusion chromatography (SEC), nuclear magnetic resonance (NMR) spectroscopy, electrospray-ionization mass spectrometry (ESI-MS), UV-visible spectroscopy (UV-vis), and fluorescence spectroscopy. NMR analysis gives detailed insight into the molecular composition of the material. By comparing the proton NMR spectra of **M₂** and the corresponding polymer **P₂**, a shift of the aromatic protons (a, b, c, d) to lower ppm values (a', b', c', d') can be detected (*Figure 3.2-2*, top). In addition, a new set of resonances corresponding to the pyrazoline moieties appears (e', e''), whereas the resonance assigned to the fumarate group (e) vanishes completely. Moreover, all product resonances are relatively broad compared to the monomer spectrum which is a typical observation for polymeric samples. Furthermore, the exceptional purity of the crude spectrum of **P₂** evidences a very clean polymerization process which proceeds without any detectable side-reactions.
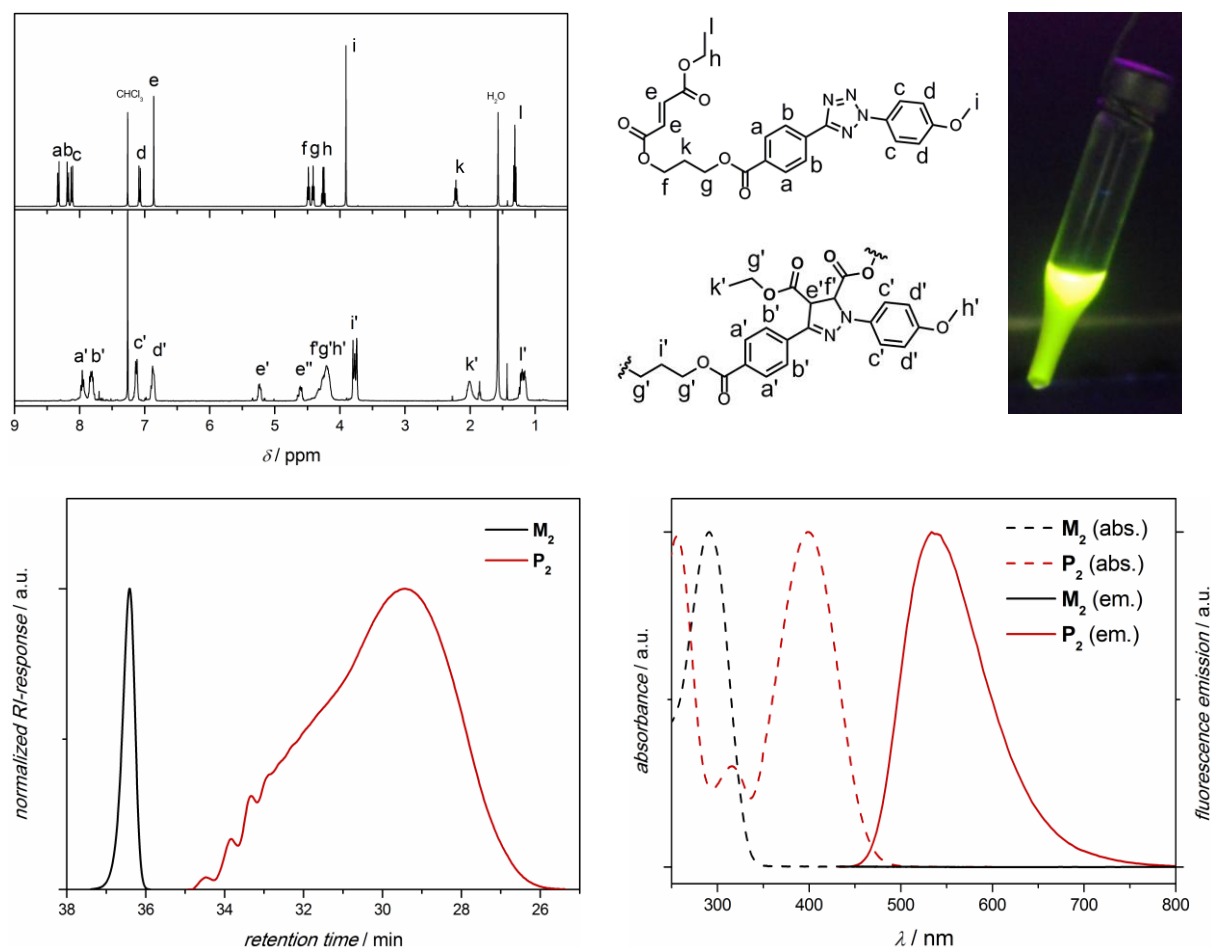
*Figure 3.2-2: Analytic results of the product from the light-driven polymerization of **M₂**. Top left: ¹H NMR spectrum with the corresponding structures; top right: picture of the fluorescent vial containing **P₂** under excitation with a handheld TLC-lamp (λ_{ex} = 365 nm); bottom left: SEC; bottom right: UV-vis and fluorescence spectroscopy.*

SEC is an ideal tool to prove the existence of macromolecules. Since the material is separated by its hydrodynamic radius, polymers can be well distinguished from residual monomer or oligomeric material. *Figure 3.2-2* (bottom, left) demonstrates the difference in retention time of **M₂** (36-37 min) and the polymer **P₂** (26-34 min), which was purified by precipitation. Although molar mass values determined by SEC have to be treated carefully due to the required calibration which is not available for the novel type of polymer, molar mass values of M_n = 7400 g·mol⁻¹ and M_w = 12900 g·mol⁻¹ indicate the success of the light-driven polymerization. A more detailed discussion of the SEC results follows in a subsequent section (Section 3.4). The current polymerization method was developed because of the properties of the polypyrazolines which can be detected by UV-vis and fluorescence spectroscopy. A dramatic change in the absorption properties of the material can be observed during the polymerization process. The absorption of the tetrazole with a maximum of close

to 300 nm (*Figure 3.2-2*, bottom right, black dashed line) differs significantly from the pyrazoline absorption spectrum (350-500 nm) (*Figure 3.2-2*, bottom right, red dashed line). Despite the clear evidence from UV-vis analysis, the success of the desired cycloaddition is even more obvious by evaluating the fluorescence spectroscopy data. The fluorescence spectrum of the tetrazole monomer does not show any emission (*Figure 3.2-2*, bottom right, black plain line), whereas **P₂** fluoresces intensely, emitting a broad spectrum in the visible range (450-750 nm) (*Figure 3.2-2*, bottom right, red plain line).

Summarizing the above noted results, it is evident that a well defined polycycloaddition can be induced by irradiation, resulting in a reasonably large step-growth polymer which exhibits strong fluorescence.

3.3 Characterization of the Termination Product

Due to the assumed cyclization reaction, the step-growth polymerization presented in the current chapter is susceptible to termination. In order to confirm the hypothesis of cyclic low molecular weight material produced throughout the polymerization process, it is worth investigating the products in more detail. First of all, it is important to note that the monomer (black plain line) is completely consumed since the RI-signal intensity in the monomer region is reduced to baseline level subsequent to irradiation (*Figure 3.3-1*). However, besides the desired polypyrazoline (34-26 min), SEC analysis of the crude polymerization product (dashed line) reveals a significant amount of low molar mass material (34-36 min) in the reaction mixture. The overall molar mass values of the crude material are $M_n = 2500$ g·mol^{-1} and $M_w = 12000$ g·mol^{-1}, hence significantly smaller than the purified polymer. Fortunately, the polymer can be readily separated from the termination product by precipitation in cold methanol. Thus, both types of product could be isolated yielding 60 wt% polymer and 40 wt% cyclic oligomers. Subsequent SEC analysis of the single precipitation fractions demonstrates the success of this facile separation method, since the precipitated material (red plain line) is almost quantitatively free of the oligomeric species in the non-precipitating fraction (dotted line).
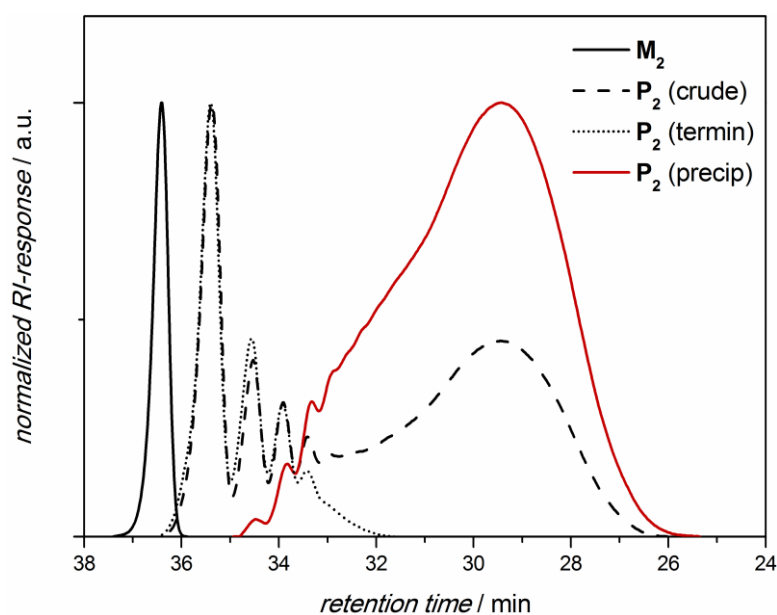
Figure 3.3-1: SEC chromatograms corresponding to M₂ (black plain), its crude polymerization product (black dashed), as well as the separated low molar mass termination product (black dotted) and the isolated polymer (red) generated by light-induced polymerization of M₂.

In order to verify the cyclic structure of the termination product, the low molar mass material was additionally analyzed by ESI-MS (*Figure 3.3-2*). The respective ESI-MS spectrum clearly depicts three signals in the region below 2000 *m/z*. The experimental values of the respective signals correspond well to the predicted masses for the cyclic dimer, trimer, and tetramer. Moreover, linear oligomers which would still contain an intact tetrazole unit are not detected. In addition, the absence of linear material confirms the NMR results, which suggest that full conversion of the tetrazole units to the pyrazoline species was achieved.
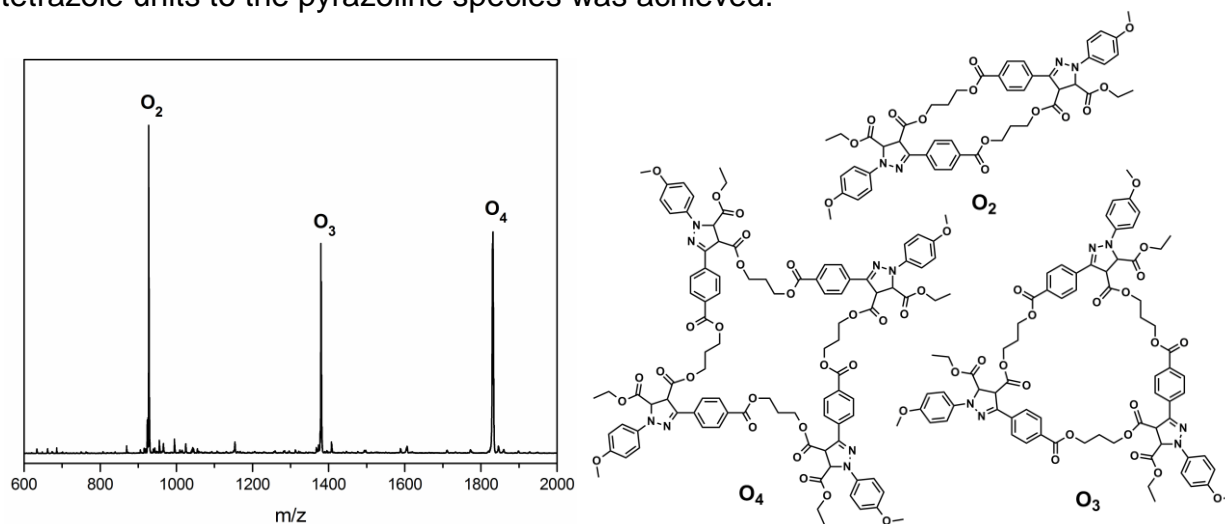
signal	m/z_{exp}	m/z_{theo}	$\Delta\ m/z$	sum formula
O_2	927.50	927.31	0.19	$C_{48}H_{48}N_4O_{14}Na^+$
O_3	1379.58	1379.46	0.12	$C_{72}H_{72}N_6O_{21}Na^+$
O_4	1831.50	1831.63	0.13	$C_{96}H_{96}N_8O_{28}Na^+$

Figure 3.3-2: ESI-MS spectrum of oligomers accumulated during the polymerization process of monomer M₂ (left). Right side: Structures corresponding to the signals in the ESI-MS spectrum. Bottom: Experimental and theoretical m/z values of the low molecular weight termination product.

3.4 Investigation of the Polymerization Kinetics

A crucial aspect for establishing a novel polymerization technique is the investigation of the reaction kinetics. Therefore, the conversion as well as the molar mass need to be monitored throughout the polymerization process. As part of the kinetic study, the influence of the irradiation intensity was investigated by varying the number of UV-lamps employed for the polymerization between 1, 3, and 5 (for lamp specifications as well as photoreaction setups see Methods section 8.3). In the case of the current investigation, NMR is a suitable analytic tool for following the progress of the reaction since the signals of starting material and product can be assigned and integrated without significant overlap. In order to visualize the reaction progress, the resonances in the aromatic region (a, b, c, a', b') are depicted in *Figure 3.4-1*.
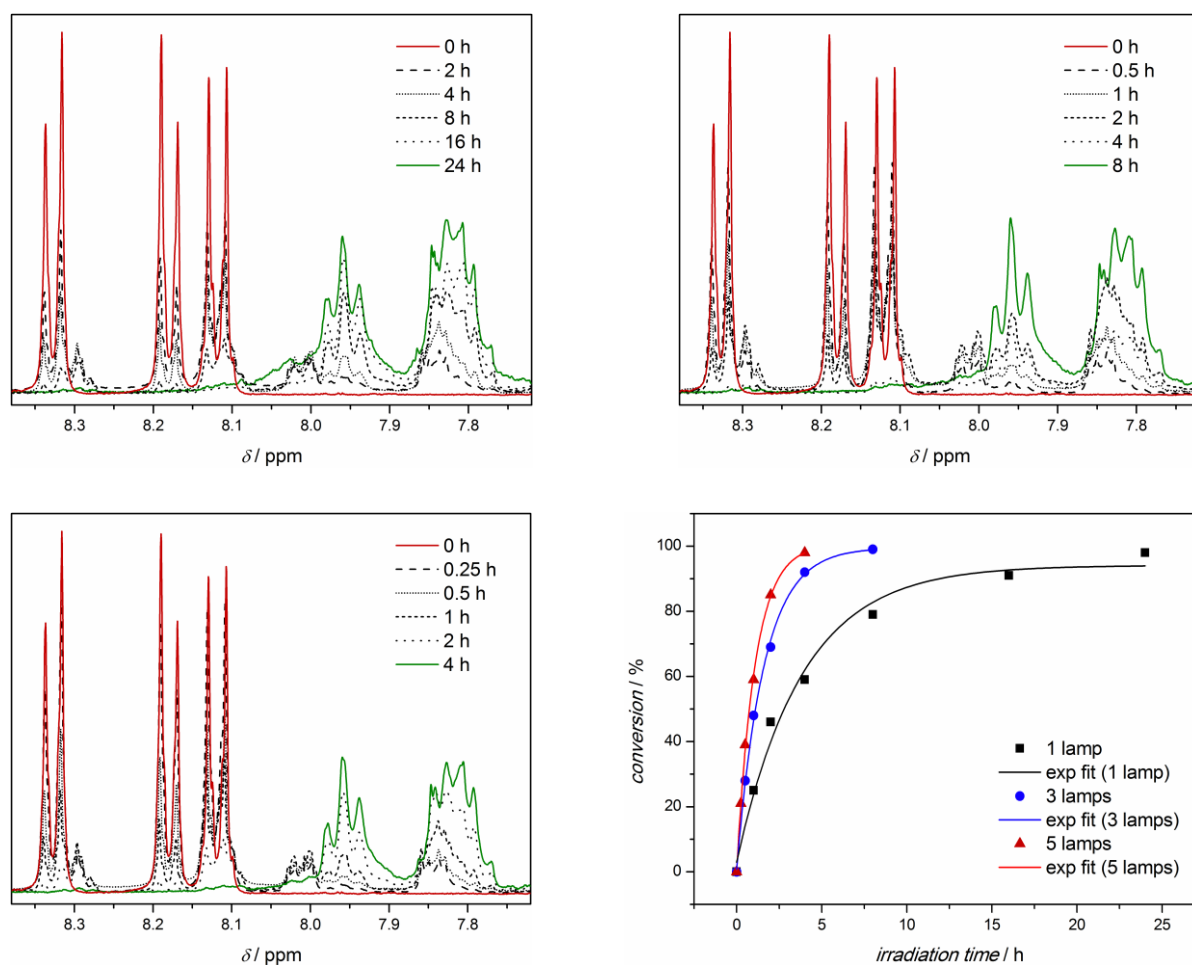
Figure 3.4-1: Aromatic region of the NMR spectra for samples of the kinetic study conducted with different irradiation intensities. Top left: 1 lamp; top right: 3 lamps; bottom left: 5 lamps; bottom right: plot of the conversion values against the irradiation time.

For integration and subsequent calculation of monomer to polymer conversion, the signals *a*, *b*, *a'*, *b'* can be employed as can the pyrazoline signals (*e*, *e'*) or the resonances corresponding to the spacer (*k*, *k'*) (compare *Figure 3.2-2*). Either integration method yields conversion values within an error margin of 5 % which is a typical uncertainty for NMR analysis. The conversion values were calculated according to equation Eq 3.4-1 which includes the product signal (*x'*) and the corresponding signal of the starting material (*x*). To obtain the exact values plotted in *Figure 3.4-1* the integration values for *a* and *a'* were inserted in the following equation.

$$\text{conversion [\%]} = \frac{100 \cdot x'}{x + x'} \qquad \text{Eq 3.4-1}$$

Consequently, the resulting conversion values were plotted as a function of reaction time under variation of the irradiation intensity (1, 3, or 5 lamps, each 36 W). The results coincide with the expectation of a reduced reaction time for increasing irradiation intensity. Thus, the reaction time to achieve full conversion is 24 h applying one UV lamp (36 W), whereas the monomer is fully converted into polymer in 4 h when the photoreactor is equipped with 5 lamps (180 W). Noteworthy is the excellent agreement of the experimental data points with the exponential fit, evidencing a reaction with pseudo first-order kinetics for all employed irradiation intensities.
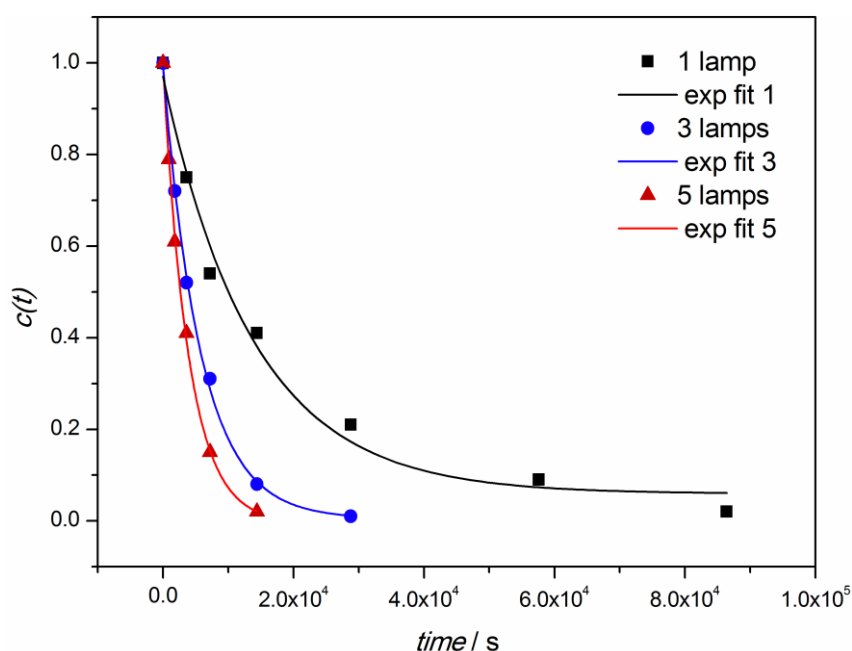
Figure 3.4-2: Kinetic plot representing the experimentally determined tetrazole concentration values for the polymerization of M_2 in correspondence to the reaction time for three different irradiation intensities.

In order to determine the kinetic parameters, a different form of displaying the conversion values is required (*Figure 3.4-2*). Therefore, the molar fraction of tetrazole present in the reaction mixture was plotted against the reaction time (displayed in seconds). An exponential fit – according to the Arrhenius equation (Eq 3.4-2) – to each data set gives access to the kinetic parameters k and A.

$$c_t = c_0 \cdot e^{-kt} + A \qquad\qquad \text{Eq 3.4-2}$$

Table 3.4: Collation of kinetic parameters and their standard deviation (σ). The entries were determined by the plot in Figure 3.4-2.

entry	c_0	$\sigma(c_0)$	A	$\sigma(A)$	k [s^{-1}]	$\sigma(k$ [s^{-1}])
1 lamp	0.911	$5.92 \cdot 10^{-2}$	$5.92 \cdot 10^{-2}$	$3.48 \cdot 10^{-2}$	$7.23 \cdot 10^{-5}$	$1.03 \cdot 10^{-5}$
3 lamps	0.988	$1.94 \cdot 10^{-2}$	$4.56 \cdot 10^{-3}$	$1.55 \cdot 10^{-2}$	$1.73 \cdot 10^{-4}$	$8.80 \cdot 10^{-6}$
5 lamps	1.000	$1.76 \cdot 10^{-2}$	$4.77 \cdot 10^{-3}$	$1.63 \cdot 10^{-2}$	$2.56 \cdot 10^{-4}$	$1.22 \cdot 10^{-5}$

In order to obtain a molar mass vs. conversion plot, information about the molar mass is required. SEC analysis provides such information, yet the data has to be treated cautiously. Evaluating the polypyrazolines of the current study via SEC is problematic since this analytic technique – particularly when it is coupled to an RI-detector – requires calibration with polymers of the same type and defined molar mass. The absence of Mark-Houwink parameters for polypyrazolines further decreases the accuracy of the absolute molar mass values determined by SEC. However, the respective error is systematic and as such it is fairly similar for each measurement when the consecutive samples in a kinetic study are compared. Moreover, not the absolute molar mass values, but the overall trend is of major concern in the kinetic analysis. Thus, the same crude polymerization mixtures which were applied for NMR analysis were subjected to SEC analysis. The respective elugrams for the investigation with different irradiation intensities are depicted in *Figure 3.4-3*. For each setup – 1, 3, or 5 UV lamps – a continuous increase of the overall molar mass with irradiation time is observed. Three reactions with different irradiation intensities were conducted and the obtained weight-average molar mass values (M_w) were compared to the respective theoretical molar mass evolution given by Carothers[306] (*Figure 3.4-3*, bottom right). It can be observed that all three sets of experimental data correlate well with Carothers' theory (for detailed information about Carothers' theory refer to Section 2.1.1). An exception are the values associated with very high

conversions where the molar masses of the experimental data still fit the shape of the curve, yet the experimental values are notably lower.
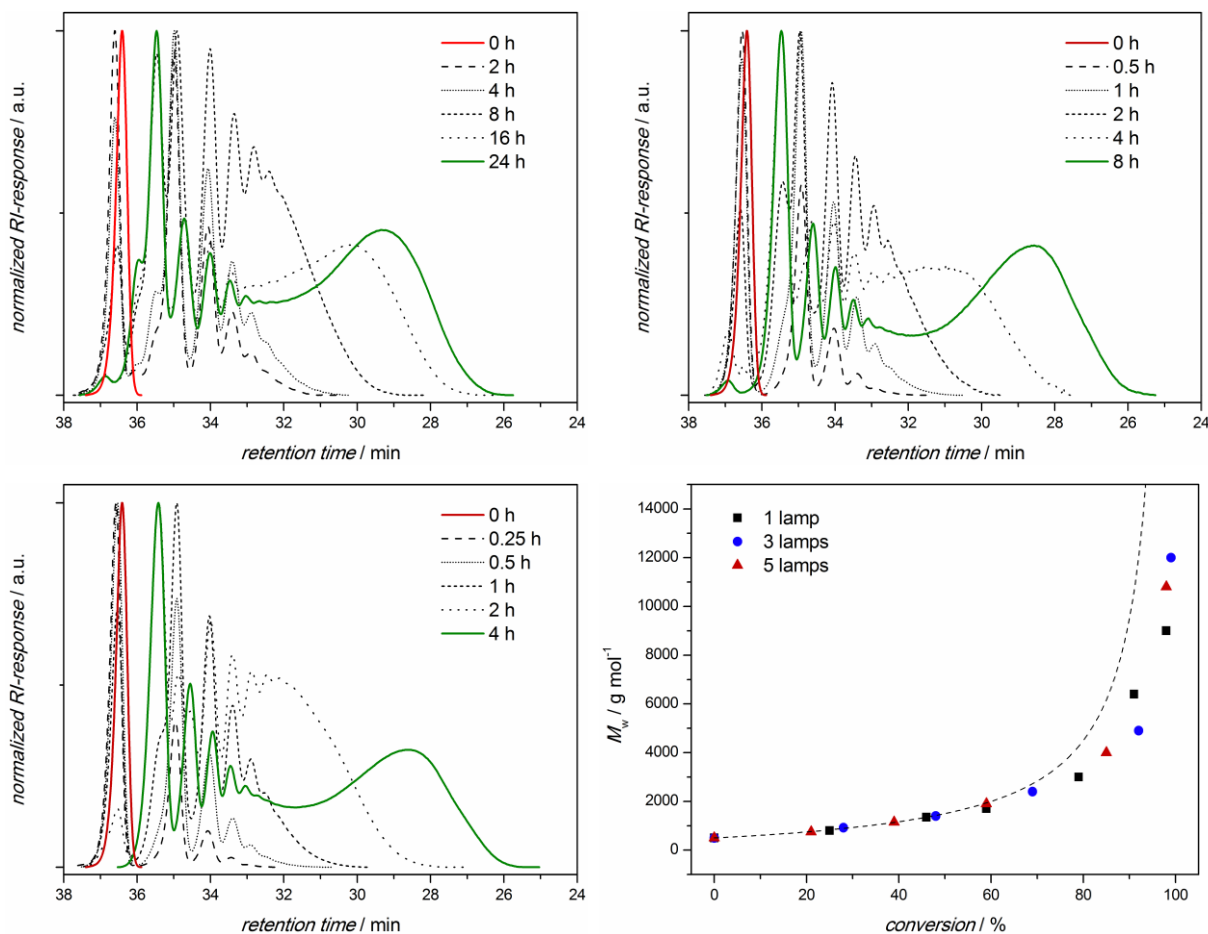
Figure 3.4-3: SEC chromatograms corresponding to the kinetic study conducted with 1 (top, left), 3 (top, right), and 5 UV lamps (bottom, left). Bottom, right: comparison of the experimental molar mass vs. conversion plot with Carothers' theoretical prediction.

Despite the inaccuracy of the SEC molar mass values due to the calibration issue, the slightly lower molar mass values for high conversion values can also be explained by the effect of the termination reaction producing low molar mass material. Due to the termination product which remains in the polymer mixture, the overall molar mass is significantly lowered. In addition, a termination reaction such as the present irreversible ring closure was not taken into account in Carothers' original theoretical work.

3.5 Summary

In conclusion, the study presented in the current chapter demonstrates the suitability of NITEC chemistry for a light-driven step-growth polymerization approach. By designing photoreactive monomers – each bearing a tetrazole as well as a dipolarophile function – light-induced polymerization was enabled. Highly fluorescent polypyrazolines were prepared via a facile polymerization protocol. Due to the advantageous properties of the NITEC reaction, the polymerization can be conducted at ambient temperature and atmosphere without requiring a catalyst. Optimizing the reaction conditions in terms of concentration and total batch size was explored utilizing the acrylate functional monomer. The low molecular weight termination product which accumulates during the light-triggered polymerization of the fumarate-monomer was isolated and determined to be of a cyclic nature via ESI-MS characterization. In addition, the polymerization kinetics were monitored by ^{1}H NMR and SEC analysis. Except for the generation of the low molar mass termination product, the light-triggered step-growth polymerization behaves according to the classical predictions of Carothers. Thus, an efficient light-induced polymerization protocol as a facile avenue to fluorescent polymers from profluorescent monomers is presented. The fluorescence can be induced at wavelengths exceeding 400 nm and might therefore be appealing for imaging applications in living organisms.

4

END GROUP MODIFICATION VIA AZIRINE CHEMISTRY – VISIBLE LIGHT-INDUCED LIGATION

In the current chapter we progress from employing cycloaddition reactions for connecting monomer units to a larger system. Herein, an azirine-based method is applied for the post-polymerization modification of polymer termini. The aim of the current study is the introduction of a catalyst-free visible light-induced ligation chemistry. To date, visible light-triggered reactions require, without exception, a photoredox catalyst as summarized in the literature section. However, by merging a chromophore and a moiety which can readily be activated by irradiation (*2H*-azirine), photoconjugation can be triggered at wavelengths above 400 nm. An initial small molecule study allows for the detailed characterization of the azirine reacting with variable dipolarophiles, e.g. maleimide, fumarate, acrylate and an activated acetylene derivative. Among other characterization techniques, high-performance liquid chromatography (HPLC) was employed to follow the kinetics of the photoreactions and to demonstrate the efficiency of the approach. Besides evidencing the suitability

of the system for organic synthesis triggered by irradiation with low energy light sources, the novel photoreactive compound is additionally subjected to polymer ligation reactions. The advanced demands of polymer ligation reactions are satisfied by the current method via employment of functionalized poly(ethylene glycol) derivatives. High resolution mass spectrometry evidences the rapid and atom economic process. Via visible light induction it is possible to achieve complete end group conversion within only one minute at ambient temperature. Moreover, the insensitivity to moisture or oxygen further emphasize the robust nature of this synthetic tool. The general reaction scheme for the approach is depicted below (*Figure 4-1*).
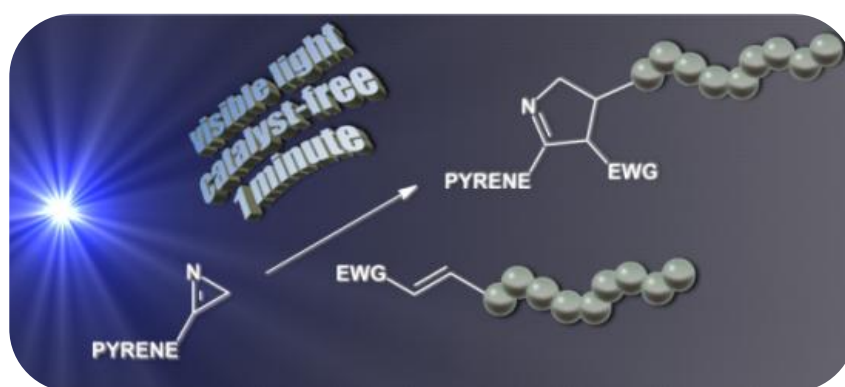
Figure 4-1: General reaction scheme for the visible light-induced polymer ligation. EWG = electron withdrawing group.

4.1 Design of a Visible Light Sensitive Reactant

Two key points must be addressed in order to acquire a photoreactive moiety which can undergo visible light-induced conjugation reactions. Firstly, the compound's absorption spectrum must coincide with the desired excitation wavelength. The second crucial step is the efficient generation of the active species – in this case a nitrile ylide. In order to address the first point, a visible light absorbing chromophore is required. Depending on the substituents, the absorption spectrum of pyrene exceeds the 400 nm benchmark, enabling to excite the compound with low energy visible light. However, the properties of the final photosensitive compound need to be judiciously designed in terms of the absorption wavelength. For instance rapid decomposition of the target compound in the presence of ambient light should be suppressed, although absorption in the region of visible light (400 nm) is indispensable. Thus, a carefully balanced system is required, which absorbs just sufficient light above 400 nm to trigger the desired reaction efficiently. Azirines are known to form a reactive nitrile ylide with high quantum yields (refer to the literature section).[174] By synthetically installing an azirine substituent at the chromophore pyrene (*Figure 4.1-1*), both of the above noted criteria can be fulfilled simultaneously yielding compound **3** in an elegant approach.
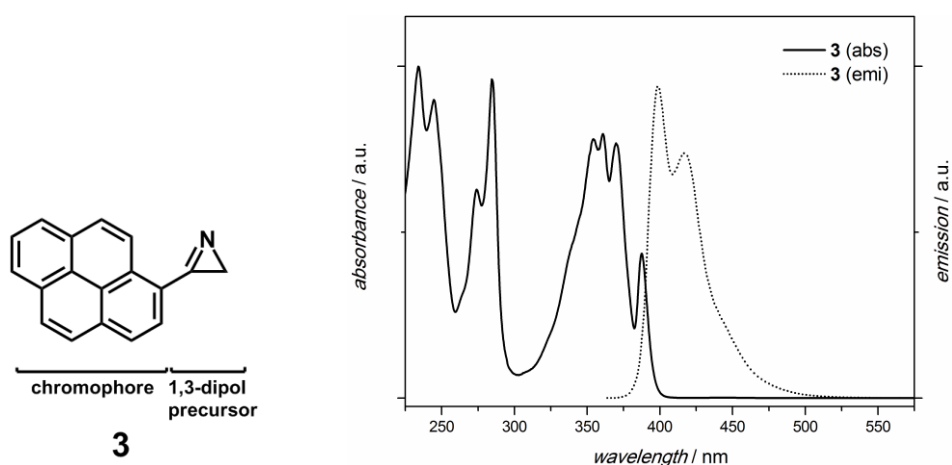
*Figure 4.1-1: Left side: Schematic depiction of the newly designed visible light sensitive compound. Right side: UV-vis (plain) and fluorescence spectra of **3**.*

In addition, the pyrene exhibits fluorescence in the region between 375 nm and 550 nm, which is another advantageous feature for this ligation technique since attaching fluorescence markers to substrates or substances is an important imaging

tool.[307] Furthermore, the pyrene group is not only a fluorophore, yet it can also act as π-π-stacking anchor.[308-310] Both of these additional features remain throughout the light-triggered process and are hence available for applications of the cycloaddition product. The synthetic strategy to prepare **3** is straightforward (*Scheme 4.1-1*): Commercially available acetyl pyrene can be transformed into a hydrazone. Subsequent methylation yields a hydrazonium salt which undergoes a cyclization to the desired azirine in the presence of a strong base. The first two synthetic steps proceed very smoothly, enabling the intermediates to be readily subjected to the subsequent reaction without detailed characterization.
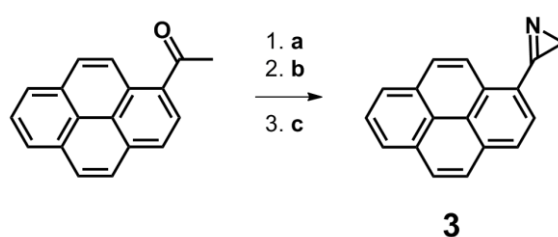
*Scheme 4.1-1: Synthesis of the visible light sensitive compound **3**. Reaction conditions: a) dimethyl hydrazine, TFA, toluene, 120 °C, 5 h; b) MeI, 40 °C, overnight; c) NaH, DMF, 0 °C, 1 h.*

4.2 Small Molecule Conjugation

Subsequent to its preparation and characterization, the novel azirine-pyrene conjugate was subjected to light-induced cycloaddition reactions. In order to provide evidence for the accessibility of diverse types of dipolarophiles and confirm the cycloaddition process to occur, a small molecule study was conducted. As alluded to in the literature review section, the nitrile ylide formation as well as the subsequent cycloaddition of azirines under irradiation have been studied previously. Thus, in the current approach the most common types of dipolarophiles were selected to confirm the novel azirine moiety to behave in a typical manner. Consequently, visible light-induced reactions, employing a light-emitting diode (LED) setup, were performed with derivatives of the following functional group classes: Fumarate, maleimide, and acrylate derivatives represent moieties with electron deficient double bonds, whereas an activated acetylenes allows for the synthesis of pyrrole derivatives. An overview of compounds which are photochemically accessible via the current technique is provided in *Scheme 4.2-1*.
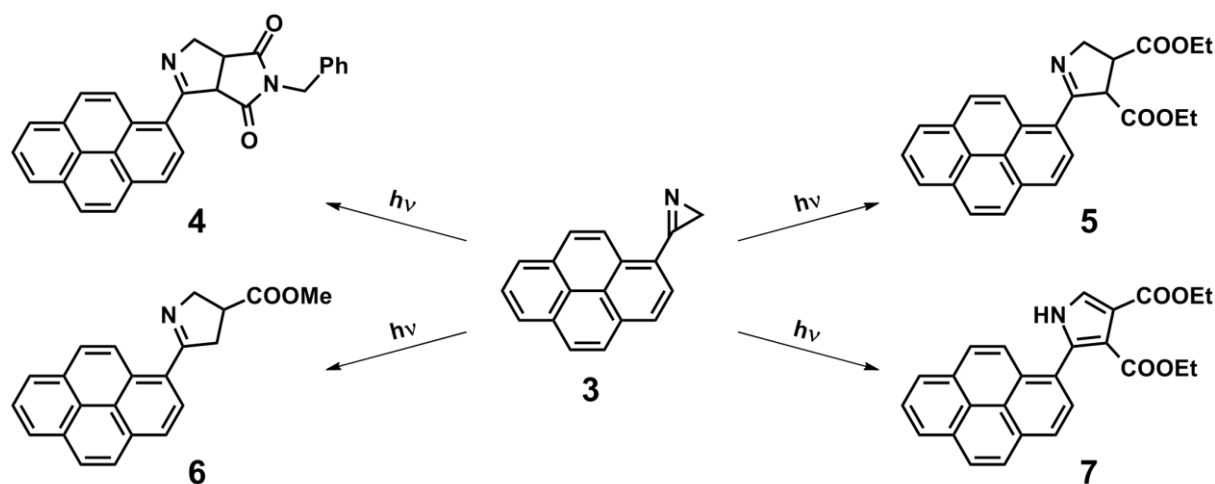
Scheme 4.2-1: Small molecule conjugation reactions of 3 induced by visible light LEDs.

The small molecule study has a distinct advantage compared to polymer ligation: The range of analytic techniques available for characterization of the isolated products is broad. NMR, ESI-MS, UV-vis, and fluorescence spectroscopy can be applied to characterize the cycloaddition products without the interfering effects of a polymer chain. Moreover, the progress of the reaction was monitored by HPLC. The most employed analytic tool of an organic chemist is NMR, providing useful information

about the structure of the analyte. *Figure 4.2-1* displays specific sections of the ^{1}H NMR spectra of **3**, **4**, **5**, **6**, and **7** to facilitate following the occurring changes, whereas the full spectra can be found in the experimental section of the present thesis (Chapter 9).
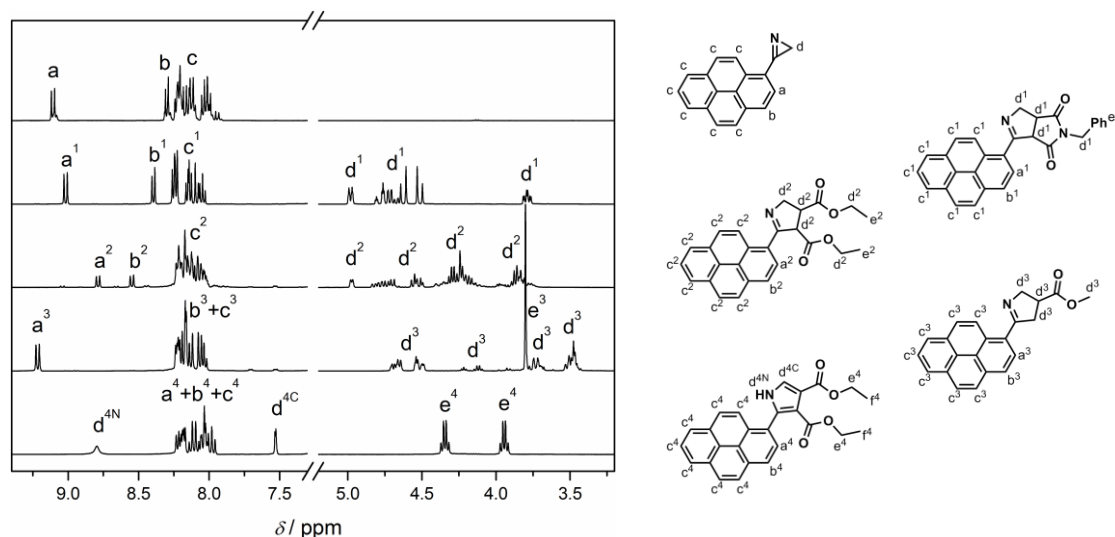
Figure 4.2-1: Left: ^{1}H NMR analysis of 3, 4, 5, 6, and 7. Right: Structures corresponding to the NMR spectra.

The spectrum of **3** contains two doublets assigned to the protons *a* and *b* in the aromatic region (9.5-7.5 ppm), which are predominantly affected by changes to the azirine function. Upon the photoreaction with a maleimide or fumarate derivative, resonance *a*, for instance, is shifted to higher fields (signal a^1 or a^2, respectively). In contrast, a slight shift to lower field can be observed for compound **6**. The signal of proton a^4 is also shifted high-field and cannot be identified between the large number of aromatic resonances b^4 and c^4. Similarly, obvious changes are discernable for proton *b* which was observed to be shifted to lower fields for the compounds **4** and **5**, whereas the same signal for **6** and **7** was found to overlap with the c^3 and c^4 signals. In addition, new sets of signals appear in the region of 5.0-3.5 ppm for all cycloadducts, whereas no such resonances are observed for the azirine. These newly arising signals are labeled d^x and e^x and refer to protons adjacent to the newly generated 5-membered heterocycle or substituents of the dipolarophile. Since unsaturated 5-membered heterocycles bear uncommon bond angles, the resonances in this region are fairly broad and cannot be assigned to particular protons. However, the overall integration values correspond to the correct number of protons. In the case of **7**, a rearrangement which occurs subsequent to the cycloaddition reaction

produces an aromatic pyrrole derivative, a process, which has been reported in literature.[242] Thus, the signals d^4 differ from the other d-signals (**4-6**) since they appear in the aromatic region.

Another powerful analytic tool for the identification of substances is ESI-MS. Hence, ESI-MS spectra of the starting material and the isolated product of the light-triggered process were acquired (*Figure 4.2-2*).
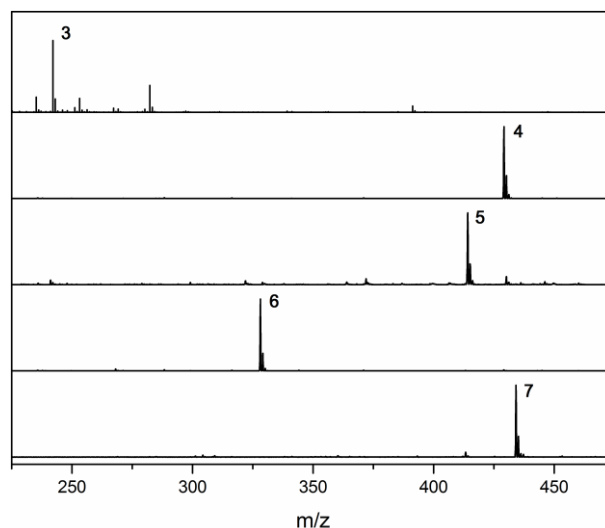
Compound	Sum formula	m/z_{exp}	m/z_{theo}	$\Delta\ m/z$
3	$C_{18}H_{12}N^+$	242.08	242.10	0.02
4	$C_{29}H_{21}N_2O_2^+$	429.16	429.16	0.00
5	$C_{26}H_{24}NO_4^+$	414.16	414.17	0.01
6	$C_{22}H_{18}NO_2^+$	328.12	328.13	0.01
7	$C_{26}H_{21}NO_4Na^+$	434.16	434.14	0.02

*Figure 4.2-2: ESI-MS analysis of **3**, **4**, **5**, **6**, and **7**. Sum formulae as well as the values of exact masses for experimental results, theoretical values and the deviation of both for each compound.*

ESI-MS ionization of the substrate is a crucial issue. A good example is the spectrum of **3**, where a decreased signal-to-noise ratio can be observed. The reduced quality of the spectrum can be explained by the absence of polar functionalities which support the ionization process and increase the total ion count. In contrast to the spectrum of **3**, remarkably clean spectra for **4**, **5**, **6**, and **7** – each carrying at least one polar function – provide unambiguous evidence for the successful generation of the desired products. In addition, the experimentally obtained m/z values coincide almost perfectly with the theoretically calculated exact mass values ($\Delta\ m/z < 0.03$, see table in *Figure 4.2-2*). In combination with the results from NMR analysis, the analytic results provide unambiguous evidence for the success of the light-triggered

reactions. However, to complete the characterization of the photoadducts, UV-vis and fluorescence experiments were conducted (*Figure 4.2-3*).
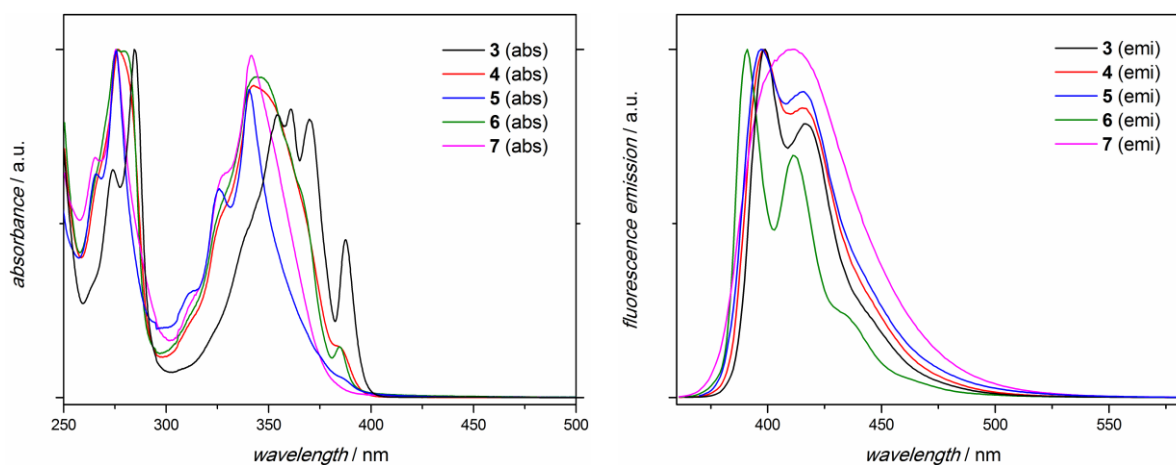
*Figure 4.2-3: UV-vis (left) and fluorescence (right) analysis of the compounds **3, 4, 5, 6**, and **7** recorded in MeCN.*

The structural change of the azirine substituent and the corresponding conjugated π-system can be witnessed by UV-vis spectrometry. By comparing the spectra of *Figure 4.2-3*, it is evident that the initial well-structured absorbance band of **3** between 300 nm and 400 nm changes shape to give rather one broad absorbance upon successful cycloaddition. Interestingly, the entire absorption spectrum is slightly shifted to shorter wavelengths for all four cycloadducts. By recording the fluorescence emission it is obvious that the pyrene system remains intact throughout the photoreaction since strong fluorescence is observed for all compounds. The shapes of **3**, **4**, **5**, and **6** are fairly similar exhibiting two emission maxima, whereas the spectrum of **7** is characterized by a single, broad emission band. The observed difference can be caused by the enlarged aromatic system of the pyrrole substituent. However, the most important message of the fluorescence study is that the pyrene system is potentially still available for imaging applications subsequent to the ligation reaction.

HPLC is a facile, yet highly sensitive technique, which was applied to monitor the reaction conversion. The minimal amount of material that is required for accurate HPLC analysis facilitates the experiments since samples can just be taken from the reaction mixture without altering the conditions significantly. Another advantageous aspect of the current system in combination with HPLC analysis is that UV-vis absorption and fluorescence can both be detected simultaneously enabling detailed

insight of the photoreaction process. A selection of kinetic experiments is provided in *Figure 4.2-3*.
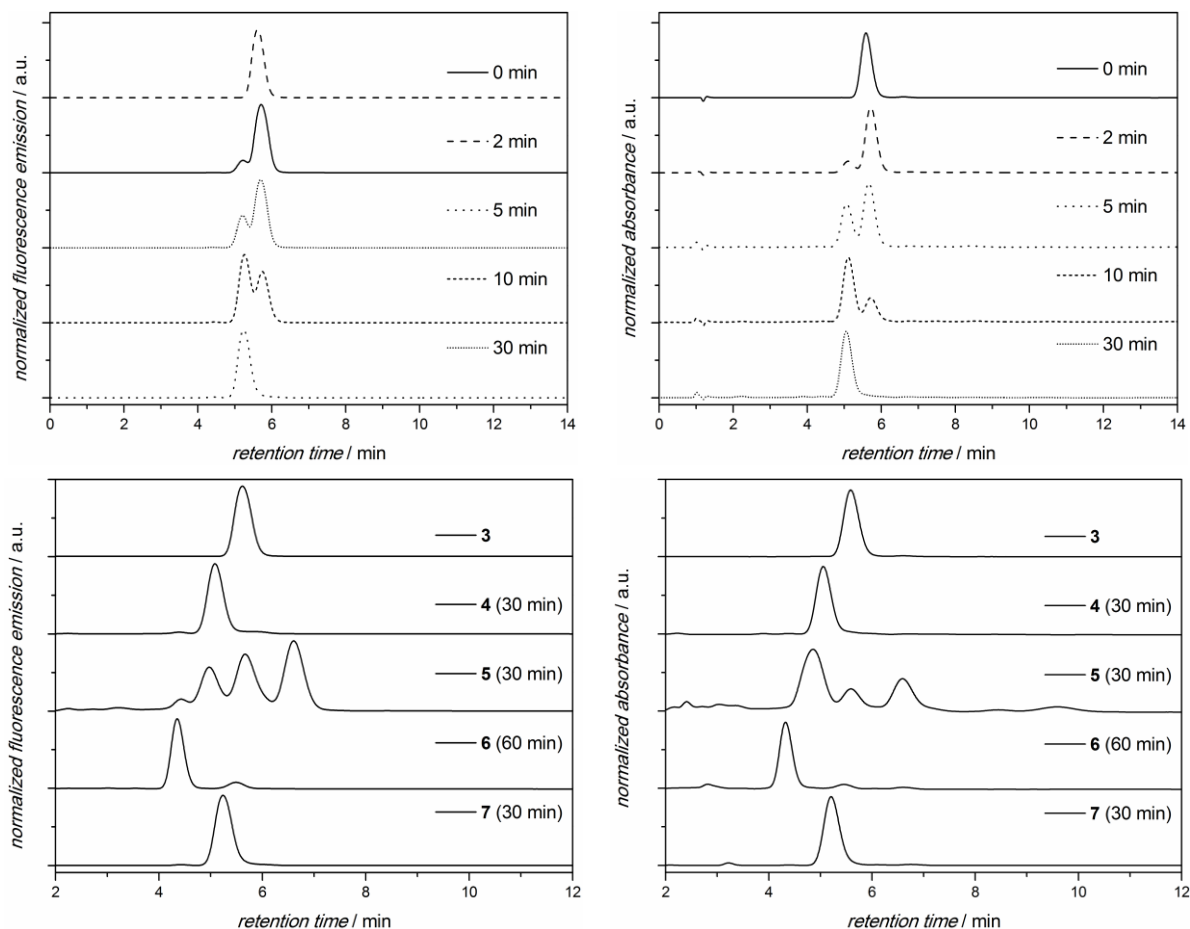
*Figure 4.2-3: HPLC elugrams associated with the small molecule kinetic study. Top left: fluroescence detection at 450 nm (λ_{ex}=350 nm) monitoring the reaction of **3** and diethylester acetylene; top right: absorbance detection at 350 nm monitoring the reaction of **3** and benzyl maleimide; bottom left: fluorescence detection at 450 nm (λ_{ex}=350 nm) for **3** as well as the crude material for the preparation of **4**, **5**, **6**, and **7**; bottom right: absorbance detection at 350 nm for **3** as well as the crude material for the preparation of **4**, **5**, **6**, and **7**.*

Exemplarily, the reactions between **3** and benzyl maleimide (absorbance at 350 nm detected) or diethylester acetylene (fluorescence emission at 450 nm detected) are monitored in detail (top left and right), whereas the final elugrams are depicted by emission and absorption detection (bottom, left and right). The combined results of the HPLC analysis of the crude reaction mixtures demonstrates the properties of the visible light-induced reactions: (*i*) In the kinetic experiments it is obvious that full conversion can be achieved since the intensity of the starting material signal decreases until it disappears completely. (*ii*) The visible light-induced cycloaddition process is highly efficient. Thus, only in the case of the fumarate a significant amount of side product can be detected. (*iii*) Finally, the reaction kinetics can be monitored

either via absorption or fluorescence detection, proving complete formation of **4**, **6**, and **7** after 30 min. In summary, the HPLC results show that the new visible light-induced approach to be remarkably clean enabling highly efficient organic photosynthesis.

4.3 Visible Light-Induced Polymer End Group Modification

In order to achieve efficient post-polymerization end group modification of synthetic polymer strands, the applied ligation techniques have to fulfill a series of demanding criteria.[118] Moreover, the ability to alter polymer termini is a necessity for many subsequent architectural efforts and highly important for a multitude of advanced applications. Therefore, the development of novel (light-induced) techniques is an ongoing process in an attempt to improve the efficiency and synthetic feasibility of the systems. Thus, the capability to perform polymer ligation reactions is a demonstration of the strength of modular conjugation techniques.

A suitable macromolecular system was required to explore the feasibility of the novel visible light-induced cycloaddition approach for polymer ligation reactions. Therefore, a set of comparable polymers containing different dipolarophilic termini is useful. In addition, the polymers should allow for ESI-MS characterization – a powerful tool for polymer characterization. Poly(ethylene glycol) derivatives, for instance, provide a series of beneficial properties which facilitate the preparation of starting materials as well as monitoring the photoreaction: (*i*) Poly(ethylene glycol) chains enable precise ESI-MS measurements due to their unique ionization properties in combination with sodium ions; (*ii*) Poly(ethylene glycol) substrates with versatile end groups are commercially available; (*iii*) Introduction of customized end groups is accessible by esterification of readily available hydroxyl-terminated poly(ethylene glycol) (*Figure 4.3-1*).
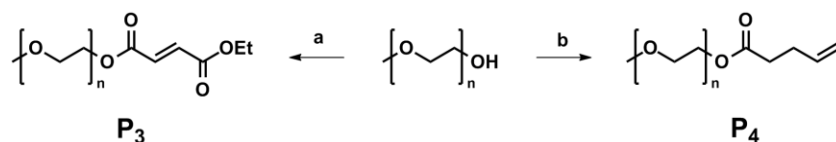
*Figure 4.3-1: Synthesis of polymers **P₃** and **P₄** via esterification of commercially available hydroxyl-terminated poly(ethylene glycol). Reaction conditions: a) monoethyl fumarate, DCC, DMAP, DMF, DCM, RT, 2 d; b) penteneoic acid, DCC, DMAP, DMF, DCM, RT, 2 d.*

Thus, a set of four poly(ethylene glycol) compounds was selected containing end groups with varying reactivity towards dipoles. Besides the synthetically manufactured fumarate (**P₃**) and pentene (**P₄**) terminated moieties, polymers with maleimide (**PEG-mal**) and acrylate (**PEG-acr**) end groups were purchased and the entire set was subjected to the light-triggered process (*Scheme 4.3-2*).
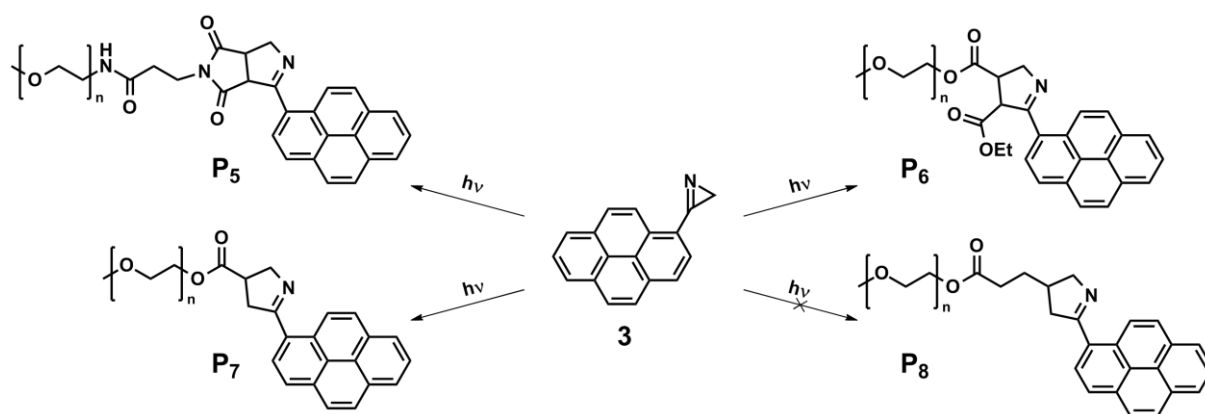
*Scheme 4.3-2: Overview of light-induced reactions of **3** with the polymeric dipolarophiles **P₃**, **P₄**, PEG-mal, and PEG-acr.*

The photo-induced process for the reaction of **3** with **P₃** was monitored in close detail via ESI-MS, CID ESI-MS, NMR, UV-vis and fluorescence analysis. In ESI-MS a shift of the entire polymeric distributions in the single, double, triple and four times charged region is clearly discernible in the overview spectra presented in *Figure 4.3-1*.
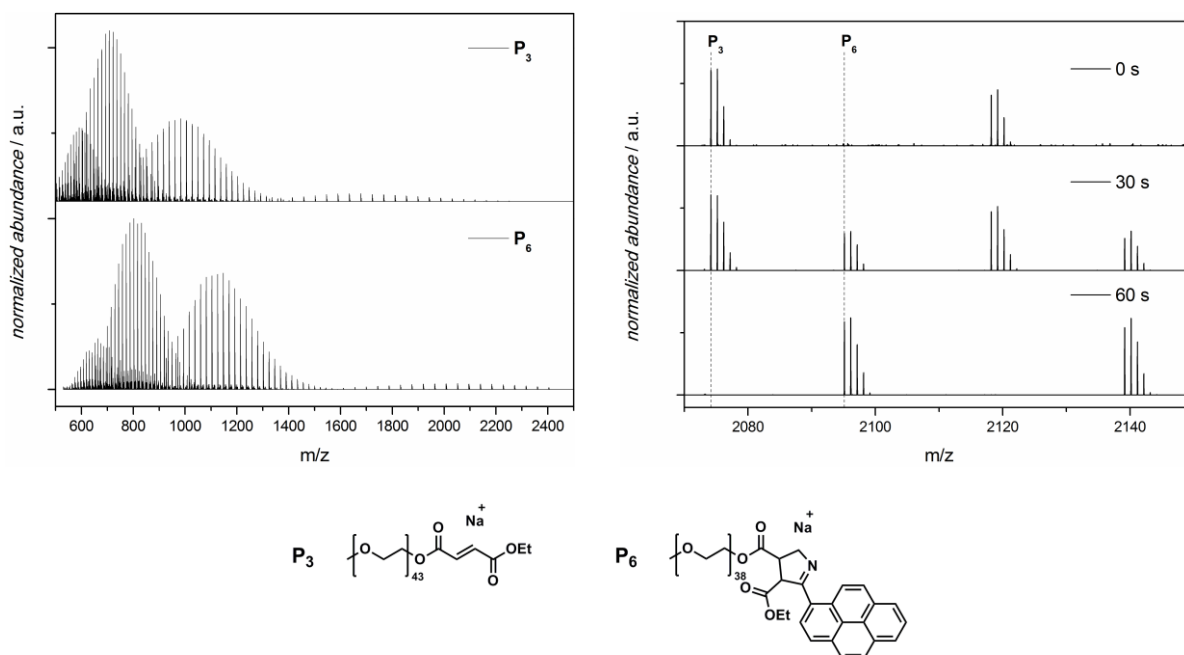
Label	Sum formula	m/z_{exp}	m/z_{theo}	$\Delta\ m/z$
P₃	$C_{93}H_{182}NaO_{47}^{+}$	2074.183	2074.174	0.009
P₆	$C_{101}H_{173}NNaO_{42}^{+}$	2095.142	2095.132	0.010

*Figure 4.3-1: High-res ESI-MS analysis of the reaction between **3** and **P₃**. Left side: overview spectrum of the starting material (**P₃**) and the product (**P₆**). Right side: ESI-MS of the single charged region of the samples after 0, 30, and 60 s. Middle and table: Structures as well as experimental and theoretical exact mass values corresponding to the spectra.*

By inspecting one repeating unit of the single charged region after 0, 30, and 60 s of irradiation it can be observed that the desired reaction proceeds in a remarkably clean fashion. After 30 s, a second distribution arises in addition to the highly pure spectrum of P_3 (0 s). Further 30 s suffice to convert the starting polymer completely into the cycloadduct (P_6), which represents the only signals in the spectrum after 60 s. The extraordinary quality of the spectra underpins the efficiency of the end group modification method, which proceeds without any sign of side product formation. Moreover, the theoretical values coincide excellently with the experimental values.

In order to verify the proposed structure of the product, CID ESI-MS experiments were conducted with the resulting material. Therefore, ions corresponding to a single signal in the double charged region of P_6 were isolated in the ion trap and made to collide with helium ions injected into the ion trap. Thus, the ions were excited with a tunable collision energy, which causes the molecules to decompose above a certain threshold. The resulting spectrum is depicted in *Figure 4.3-2*.

Label	Sum formula	m/z_{exp}	m/z_{theo}	$\Delta\ m/z$
P_6	$C_{111}H_{193}NNa_2O_{47}{}^{2+}$	1169.25	1169.13	0.12
a	$C_{109}H_{189}NNa_2O_{47}{}^{2+}$	1155.17	1155.11	0.06
b	$C_{108}H_{189}NNa_2O_{45}{}^{2+}$	1133.17	1133.12	0.05
c	$C_{87}H_{176}Na_2O_{44}{}^{2+}$	985.67	985.57	0.10
d	$C_{87}H_{174}Na_2O_{43}{}^{2+}$	976.67	976.56	0.11
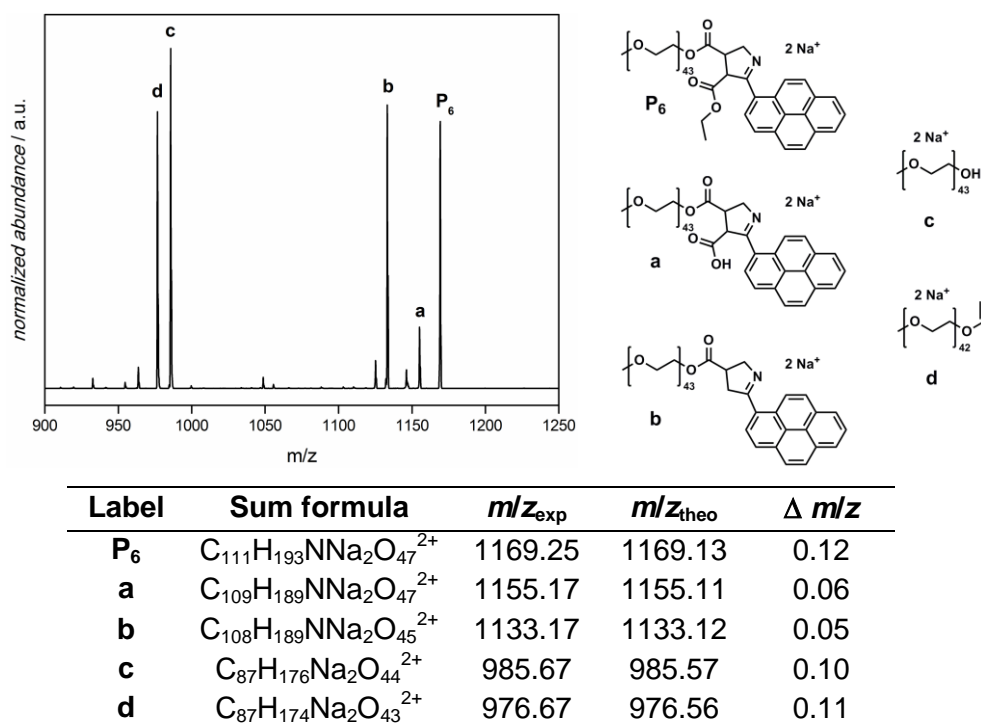
*Figure 4.3-2: CID ESI-MS experiment of **P6** (left). Structures corresponding to the signals (right). Experimental and theoretical exact mass values corresponding to the spectra (bottom).*

The weakest bonds in the structure of the isolated ion P_6 are allocated around the ester groups. Thus, cleavage next to the ester bonds is expected. Consequently, the resulting CID pattern of P_6 exhibits four main signals which correlate perfectly to the

proposed decomposition structures. The few smaller signals in the CID spectrum refer to the loss of monomer units. The results from the CID experiment are in total very conclusive since all signals can be assigned to reasonable cleavage products, which supports the assumption of a successful cycloaddition reaction.

Since the poly(ethylene glycol) chain of P_6 is rather short, NMR characterization is still an accurate tool for determining the polymer end groups. The ^1H NMR spectra of P_3 and P_6 are presented in *Figure 4.3-3*.
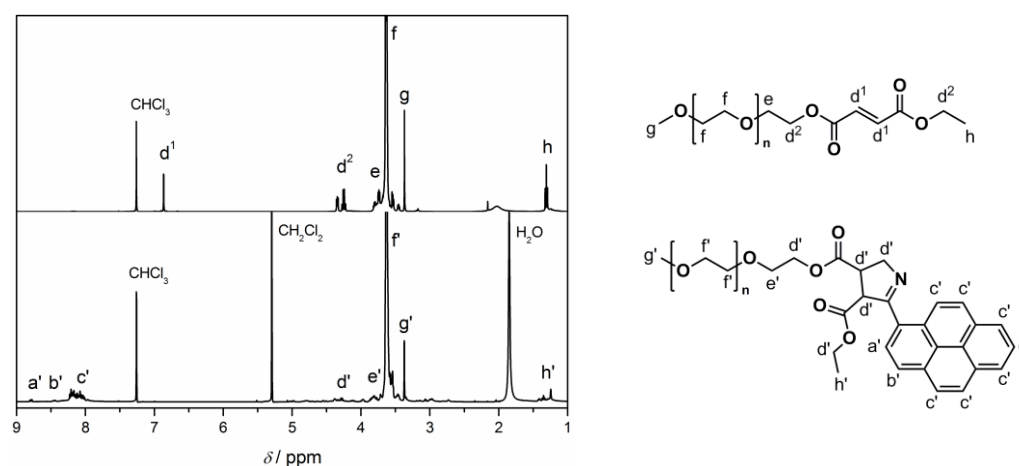
Figure 4.3-3: ^1H *NMR characterization of* P_3 *and* P_6.

The previously assured high purity of P_3, the synthesized starting material for the photoreaction, is confirmed by proton NMR. Therein, the fumarate end group (d^1) is clearly visible as a singlet at 6.87 ppm. Subsequent to irradiation of P_3 in the presence of the azirine, the signal of the fumarate double bond has completely vanished. Therefore, resonances in the aromatic region (8.8-7.9 ppm) arise, which can be assigned to the pyrene protons in agreement with the small molecule study. Assigning additional product signals – for instance the 5-membered heterocycle – is relatively complicated since they can be hardly distinguished from the noise of the baseline. Yet, the NMR results are still very convincing due to the disappearance of the fumarate signals in combination with the apparent pyrene resonances.

Similar to the small molecule study, UV-vis and fluorescence analysis of P_6 should provide twofold information (*Figure 4.3-4*): Firstly, the absorption spectrum of the resulting polymer should differ from the absorption spectrum of **3** since the azirine has undergone the photoreaction. Due to the observed change in absorption behavior, further evidence is given that the azirine compound does not simply adhere to the polymer chain. Fluorescence spectroscopy, on the other hand, confirms the

86

pyrene moiety to be present and intact subsequent to the photochemical ligation. Thus, a fluorescent dye has been successfully installed at the terminus of a poly(ethylene glycol) chain.
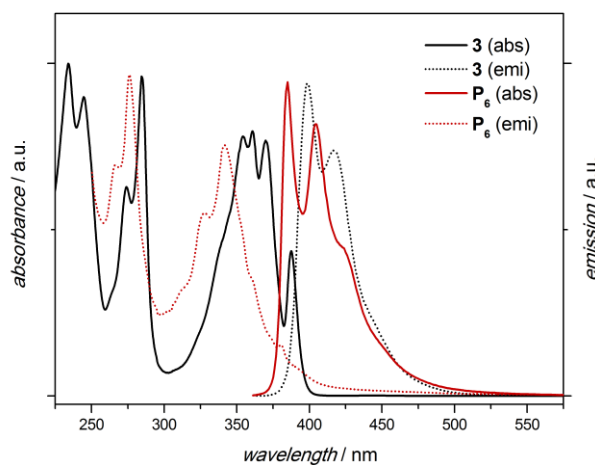
*Figure 4.3-4: UV-vis and fluorescence spectra of **P₆** in comparison to **3**.*

Subsequent to the detailed characterization of **P₆** and given the unambiguous evidence for the occurring cycloaddition by multiple analytic techniques, additional dipolarophile termini were employed for the visible light-triggered process. The light-induced reaction of **3** with **PEG-mal** or **PEG-acr**, respectively, was monitored by high-resolution ESI-MS (*Figure 4.3-5*). In either case, a rapid photochemical conjugation was observed producing the desired cycloaddition product in very high purity. Analogous to the experiment with **P₃**, **P₅** is produced by complete conversion of the starting material after just one minute of irradiation, whereas about 50 % conversion is achieved after 30 s. The reaction of **3** with the commercially available **PEG-acr** of a shorter chain length behaves similarly. After 2 min the signals of the **PEG-acr** were found to disappear completely and two product distributions – proton ionized (**P₇H⁺**) and sodium ionized species (**P₇Na⁺**) – emerge. However, a small amount of impurity (**PEG-acrˣ**), which was already present in the starting material, remains through all spectra due to the absence of the terminal double bond. The reduced reactivity of the acrylate moiety compared to maleimide or fumarate functions leads to an increased reaction time (2 min to full conversion). Again, the experimental values are in excellent agreement with the theoretical predictions (table in *Figure 4.3-5*).
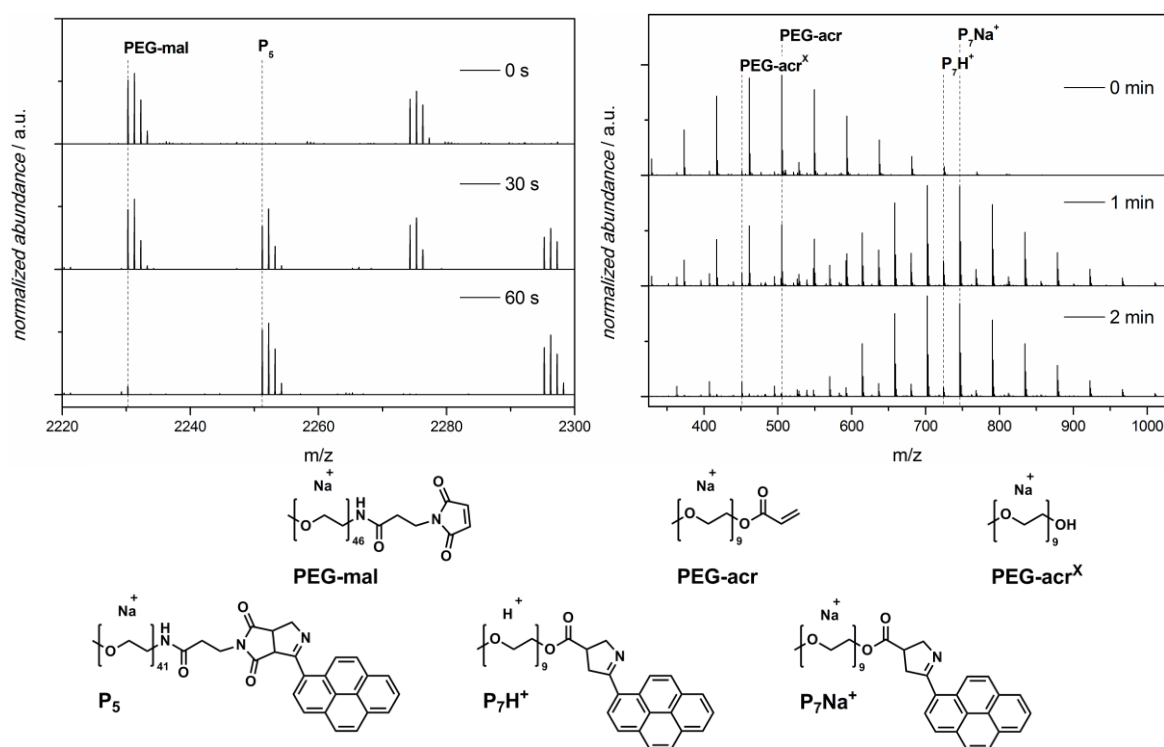
Label	Sum formula	m/z_{exp}	m/z_{theo}	$\Delta\ m/z$
PEG-mal	$C_{100}H_{194}N_2NaO_{49}{}^+$	2230.275	2230.265	0.010
P₅	$C_{108}H_{185}N_3NaO_{44}{}^+$	2251.232	2251.223	0.009
PEG-acr	$C_{22}H_{42}NaO_{11}{}^+$	505.262	505.262	0.000
PEG-acr^X	$C_{19}H_{40}NaO_{10}{}^+$	451.251	451.251	0.000
P₇H⁺	$C_{40}H_{54}NO_{11}{}^+$	724.369	724.370	0.001
P₇Na⁺	$C_{40}H_{53}NNaO_{11}{}^+$	746.351	746.351	0.000

*Figure 4.3-5: High-res ESI-MS analysis of **P₅** (left) and **P₇** (right). The corresponding structures are depicted in the middle, whereas the table collates the experimental and theoretical exact mass values.*

The final experiments of this study on visible light-induced polymer ligation were conducted with **P₄** and **P₂**, respectively (*Figure 4.3-6*). The non-activated double bond, which was installed at the chain terminus of **P₄**, is less reactive towards 1,3-dipolar cycloaddition reactions due to the absence of electron withdrawing substituents and a large resulting energy gap between the highest occupied molecular orbital (HOMO) of the dipol and the lowest unoccupied molecular orbital (LUMO) of the dipolarophile. Thus, the absence of any cycloaddition product after 90 min of irradiation is not particularly surprising, yet it confirms the selectivity of the photochemical technique towards electron deficient double bonds. In addition to the selectivity test with **P₄**, two control reactions without LED irradiation were performed with **P₂**. The first sample was stirred in complete darkness for 1 h, whereas the second sample was allowed to stand on the laboratory bench for the same time. For
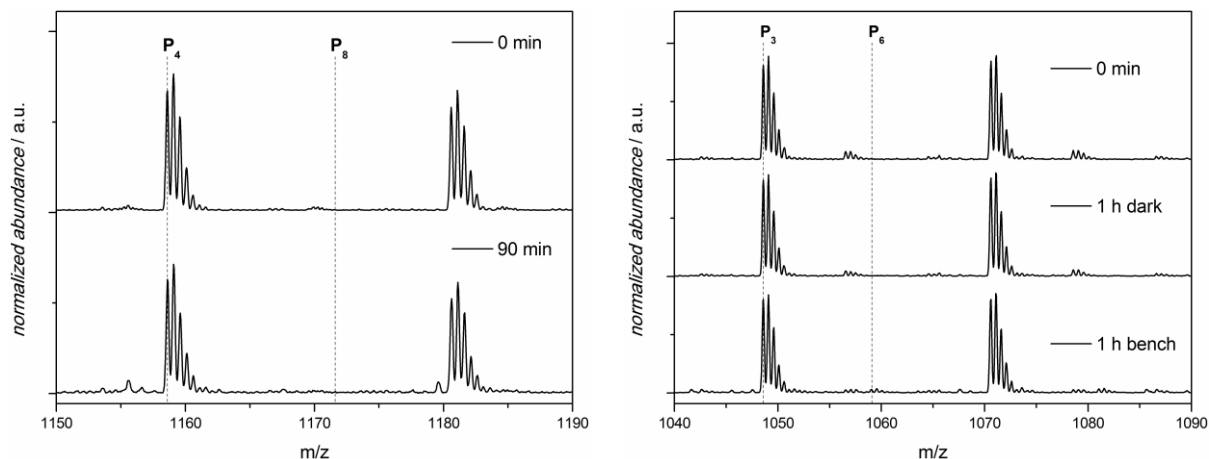
*Figure 4.3-6: ESI-MS characterization of the reaction between **3** and **P₄** (left) as well as the control reactions between **3** and **P₆** without LED irradiation (right).*

clarification, the laboratory illumination remained switched on to simulate typical working conditions, however, the sample was protected from sunlight. Both control samples were subject to ESI-MS analysis, confirming that LED irradiation is crucial for the photoreaction to proceed since no product was discerned. The fact that even one hour on the laboratory bench does not suffice to generate a significant amount of cycloadduct from the photoreactive mixture approves the judicious design of the photolabil component: On the one hand, the material can be handled under ambient conditions and on the other hand it reacts rapidly upon appropriate irradiation.

4.4 Summary

The current chapter introduces an ultra-rapid visible light-driven avenue for catalyst-free ligation – a long sought and thus far not achieved aim in modern modular chemistry. The macromolecular task was the photochemical modification of polymer termini, which was fulfilled via an azirine-based approach. By designing and synthesizing a photoreactive component, the properties of a photolabil *2H*-azirine and the chromophore pyrene could be combined. Thus, a novel substance was developed, which absorbs visible light in the range slightly above 400 nm and immediately produces a nitrile ylide suitable for rapid 1,3-dipolar cycloaddition reactions. The applicability of the visible light-induced azirine ligation was proven in organic synthesis with representatives of the most common reactive groups (maleimide, fumarate, acrylate, and acetylene), which was confirmed via NMR, ESI-MS, UV-vis and fluorescence spectrometry. Moreover, the reaction progress was monitored by HPLC and shown to be highly efficient. The advanced demands of polymer ligation reactions were additionally satisfied by the current system by connecting a fluorescent dye (pyrene) to poly(ethylene glycol) chains with various termini. Furthermore, the selectivity of the current system towards electron deficient double bonds was demonstrated, enabling highly clean and complete end group modification of polymers in irradiation times as short as one minute at ambient temperature.

5

REVERSIBLE END GROUP MODIFICATION VIA PATERNÒ–BÜCHI CHEMISTRY – AN EXPLORATORY STUDY

The next logical progress from post-polymerization modification of end groups in terms of photochemical advancement is to develop a reversible conjugation system. Reversible photochemistry is highly appealing for a multitude of applications as alluded to in the literature section (2.3.4). In the current chapter, two issue are of major concern. On the one hand, the study aims for the establishment of a photochemical tool to encode polymer end groups reversibly, which might – upon success – eventually lead to a technique applicable to reversible surface encoding in a spatially controlled fashion. On the other hand, the strategy is based on Paternò–Büchi (PB) chemistry, a well know process, which is however of limited use in polymer science. The current study was conducted to determine the applicability and thus the scope of PB systems for reversible photochemistry and their applicability. The polymeric frame is – similar to the previous chapter – a benzaldehyde-functionalized poly(ethylene glycol) since it has been proven to be most feasible for

ESI-MS characterization. The initial aldehyde-terminated polymer will be subject of three consecutive photochemical processes: (*i*) A PB reaction with different alkene components resulting in an oxetane-functional polymer, (*ii*) photosensitized ring cleavage of the oxetane unit to yield the initial aldehyde terminus, and (*iii*) a final forward PB reaction to proof the principle of reversible encoding. The entire process can be monitored by ESI-MS as well as NMR analysis. Moreover, a powerful analytic tool – CID ESI-MS – is applied for exploring the stability of oxetane moieties since the cleavage reaction is expected to be the crucial step in the photochemical reaction sequence (*Figure 5-1*).
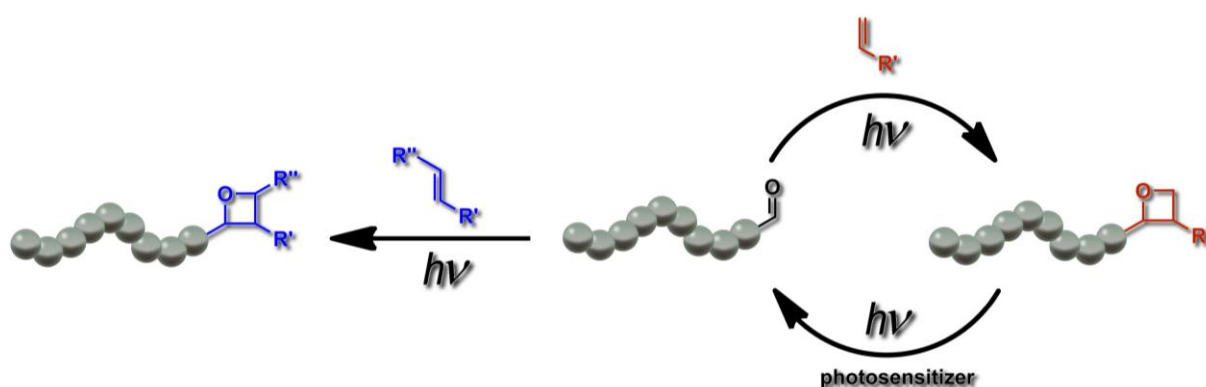
Figure 5-1: Schematic representation of the proposed strategy to demonstrate reversible photo-encoding of polymer end groups. The concept contains three consecutive photochemical steps, each including a modification of the chain terminus.

5.1 Preparation of Oxetane-Functionalized Poly(ethylene glycol)

In the current chapter, a reaction sequence containing three consecutive photochemical reactions is explored: Forward PB, cycloreversion (retro PB), and finally an additional PB reaction with a different reactant compared to the first step. Each single step requires careful analysis and in-depth characterization to understand and optimize the entire system. In order to provide ideal conditions for a detailed characterization, a PEG backbone was selected as polymeric basis for the same reasons as discussed in Chapter 4. In addition, PEG provides good solubility in a variety of organic solvents, which facilitates its handling during the exploration of novel reaction processes. Consequently, the starting material for all photoreactions was synthesized via esterification of PEG-OH with 4-carboxy benzaldehyde (*Scheme 5.1-1*).
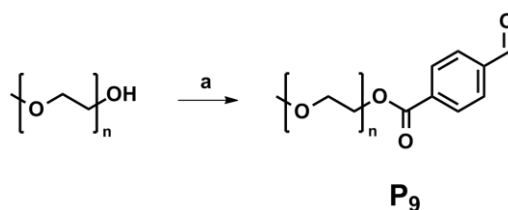
Scheme 5.1-1: Synthesis of benzaldehyde terminal PEG (P₉). a) 4-carboxy benzaldehyde, DCC, DMAP, DMF, DCM, RT, 2 d.

The resulting polymer (**P₉**) was obtained in good quality containing exclusively aldehyde terminal chains, as demonstrated by NMR (*Figure 5.1-1*) and ESI-MS (*Figure 5.1-2*). Work of Junkers and coworkers previously described the photochemical transformation of aldehyde terminal polymers synthesized via ATRP with several alkenes.[208] Nevertheless, detailed characterization of the PB forward reaction for the present system was required due to a diversity of necessary changes compared to the photoreactions reported by Junkers: Extension of the scope of reaction partners to styrenic double bond compounds, change of the polymer backbone, different reaction setup and irradiation conditions. Thus, the photochemical conversion of **P₉** with three styrene derivatives as well as 2-pentene was conducted (*Scheme 5.1-2*).
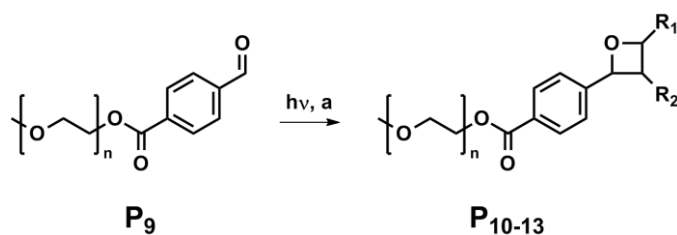
Scheme 5.1-2: The photochemical conversion of **P₉** with various double bond containing moieties yielding **P₁₀** (R_1 = H; R_2 = Ph), **P₁₁** (R_1 = H; R_2 = Ph-pMe), **P₁₂** (R_1 = Me; R_2 = Ph), or **P₁₃** (R_1 = Me; R_2 = C_2H_5). a) toluene, alkene (styrene, p-methyl styrene, trans-methyl styrene, 2-pentene).

Most of the reaction partners for the aldehyde end-capped polymers were chosen to be styrene-based since the resulting oxetanes were expected to be suitable for subsequent cycloreversion reactions.[217] The results of the ^{1}H NMR characterization for **P₁₀** are depicted in *Figure 5.1-1*.
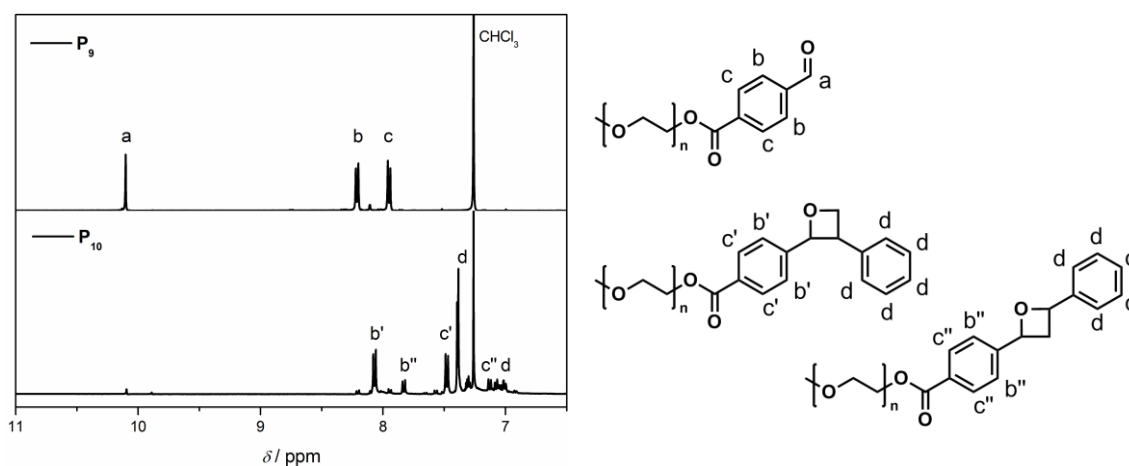
Figure 5.1-1: ^{1}H NMR characterization of **P₉** and **P₁₀**.

Two analytic methods – NMR and ESI-MS – were combined to confirm the success of the photo-induced polymer modification reactions and evaluate the results quantitatively. By comparing the NMR spectra of **P₉** and **P₁₀**, several changes can be witnessed after the irradiation. To facilitate following the changes to the reader, only the aromatic region of the NMR spectra is displayed in *Figure 5.1-1*. Resonance *a*, which corresponds to the aldehyde proton of **P₉**, disappears almost completely – a clear indication for a successful oxetane formation. Moreover, the aromatic protons *b* and *c* are shifted to higher fields for both possible regioisomers (*b'*, *b''*, *c'*, *c''*) and their integrals coincide with the vanishing resonance of the aldehyde. The protons of the newly generated oxetane ring appear in the region of 2-6 ppm due to the unusual bond angle in 4-membered heterocycles and can therefore not be perfectly assigned (for full spectra as well as the spectra of **P₁₁₋₁₃**, see Experimental section).

Nevertheless, an increased number of scans (NS) for the NMR measurement (NS = 256) enables accurate integration of the aromatic region. The evaluation of signal *a*, *b*, and *c* suggests an end group conversion to the resulting oxetane of 90 %.
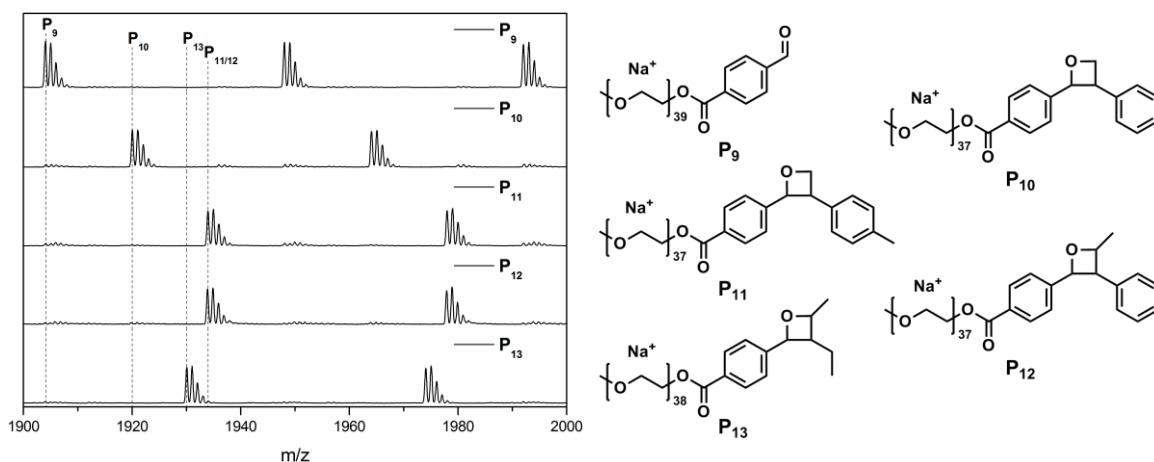
Label	Sum formula	m/z_{exp}	m/z_{theo}	$\Delta\ m/z$
P_9	$C_{87}H_{164}NaO_{42}^+$	1904.17	1904.06	0.11
P_{10}	$C_{91}H_{164}NaO_{40}^+$	1920.08	1920.07	0.01
P_{11}	$C_{92}H_{166}NaO_{40}^+$	1934.08	1934.09	0.01
P_{12}	$C_{92}H_{166}NaO_{40}^+$	1934.08	1934.09	0.01
P_{13}	$C_{90}H_{170}NaO_{41}^+$	1930.17	1930.11	0.06

Figure 5.1-2: ESI-MS spectra depicting two repeating units in the single charged region of P_9 (top) and the crude reaction mixtures of P_9 with styrene (P_{10}, 2nd line), para-methyl styrene (P_{11}, 3rd line), trans-methyl styrene (P_{12}, 4th line), and 2-pentene (P_{13}, bottom). Table: collation of sum formulae and m/z values corresponding to the ESI-MS spectra.

ESI-MS is also a powerful tool for witnessing end group changes of polymer substrates.[311] By judiciously choosing the PEG-chain to be no longer than 2000 g·mol^{-1}, the photoreaction is perfectly suitable for being monitored by ESI-MS. The spectra collated in *Figure 5.1-2* depict the successful PB reaction of P_9 with Styrene (Sty), *para*-methyl styrene (PMS), *trans*-methyl styrene (TMS) and 2-pentene (2-pen). Two repeating units in the single charged region are displayed. In each case, the starting material disappears almost completely (P_9), whereas new signals corresponding to the oxetane-functionalized substrates arise (P_{10}, P_{11}, P_{12}, and P_{13}). Whether quantitative evaluation of ESI-MS spectra is possible for the respective system must be evaluated carefully. Since changing parameters such as the molecular weight or the polarity of the analyst have an effect on the ionization properties of the substrate and therefore on the signal intensity, integration of ESI-MS spectra needs to be conducted judiciously. In the current case, the sodium ion is expected to be attached to the PEG chain which is not altered throughout the

reaction process. On the other hand, the total mass of the product is slightly higher than the starting material's mass, yet the change is only about 10 % of the total mass. Moreover, average integral values including 5 repeating units were applied for determining conversion values from the ESI-MS spectra. Therefore, it is resonable to assume that also quantitative information can be retrieved from ESI-MS analysis for the current system. Moreover, NMR provides an additional analytic method to underpin the accuracy of the ESI-MS results. Integration of the spectra in *Figure 5.1-2* provides conversion values for the PB reaction of more than 90 % in each case. Conversion values calculated from NMR and ESI-MS employing Eq 3.4-1 differ no more than 5 % for the values determined for the photochemical processes, which proves quantitative ESI-MS evaluation to be applicable. Thus, following the kinetics of the photoreaction by ESI-MS is also feasible. *Figure 5.1-3* depicts one repeating unit in the single charged region of samples stemming from the reaction between **P₉** and 2-pentene.
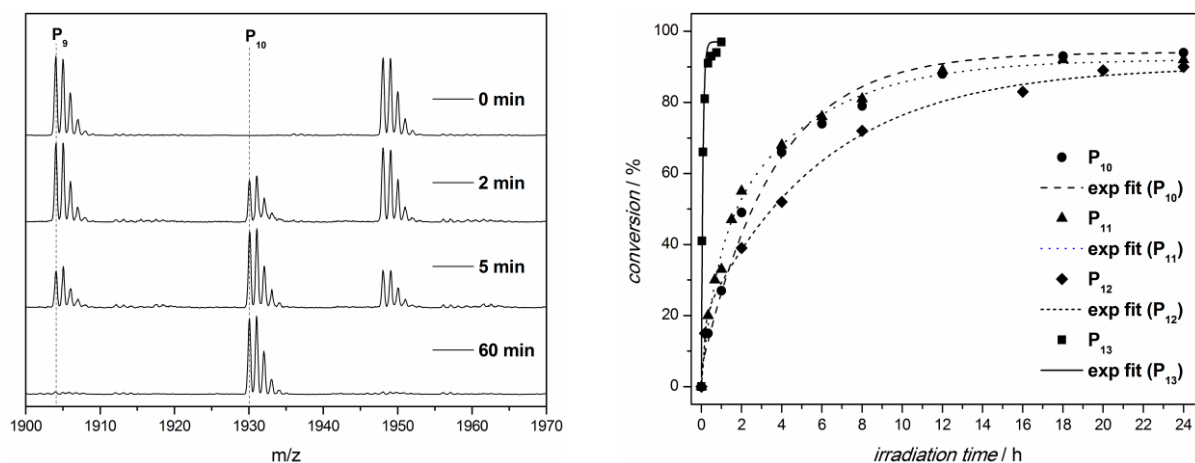
*Figure 5.1-3: ESI-MS spectra representing one repeating unit in a kinetic study of the reaction between **P₉** and 2-pentene (left). Right: Kinetic plot originating from the evaluation of ESI-MS spectra following the reactions of **P₉** with Sty, TMS, PMS, and 2-Pen.*

The samples were taken from the reaction mixture and directly subjected to ESI-MS analysis. Thus, it is remarkable that no side products are discernible and the reaction appears to proceed very cleanly. Finally, the integration values obtained from the kinetic samples were plotted vs. the reaction time (*Figure 5.1-3*, right). The plotted exponential fits match the data points very well in all cases, confirming the expected behavior. It is furthermore notable that the photoconversion takes significantly longer with styrenic types of reaction partners compared to 2-pentene.

5.2 Investigation of the cycloreversion process

Referring to the literature section, CID ESI-MS experiments were expected to give insight into the retro PB behavior of the prepared oxetane-functionalized polymers (*Scheme 5.2-1*). During the CID process, particular polymer ions are isolated and made to collide with helium ions present in the ion trap. Thus, by increasing the collision energy which excites the polymeric species, the mother ion can be fragmented.
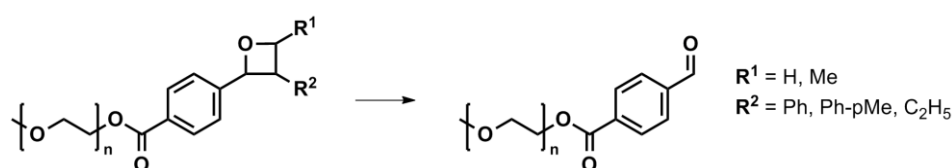
Scheme 5.2-1. The general cycloreversion reaction of the oxetane polymers.

Assuming the weakest bonds to break first, CID experiments are carried out for structure elucidation. In this particular case, the goal was to analyze in which way the oxetane unit – the least stable section of the polymer moiety – would cycloreverse. Therefore, an oxetane species of defined chain length was isolated for each cycloadduct and the decomposition spectrum was recorded (*Figure 5.2-1*).

The CID ESI-MS results reveal a surprisingly clean cycloreversion reaction. For all three oxetane species in both spectra – the medium collision energy and the high collision energy – the only signals of importance are the mother ion (oxetane) and one cycloreversion product. The *m/z* value of the cycloreversion product matches the initial aldehyde species perfectly. In addition, all the spectra are remarkably clean, showing only neglectable side products, which can hardly be distinguished from the baseline noise.
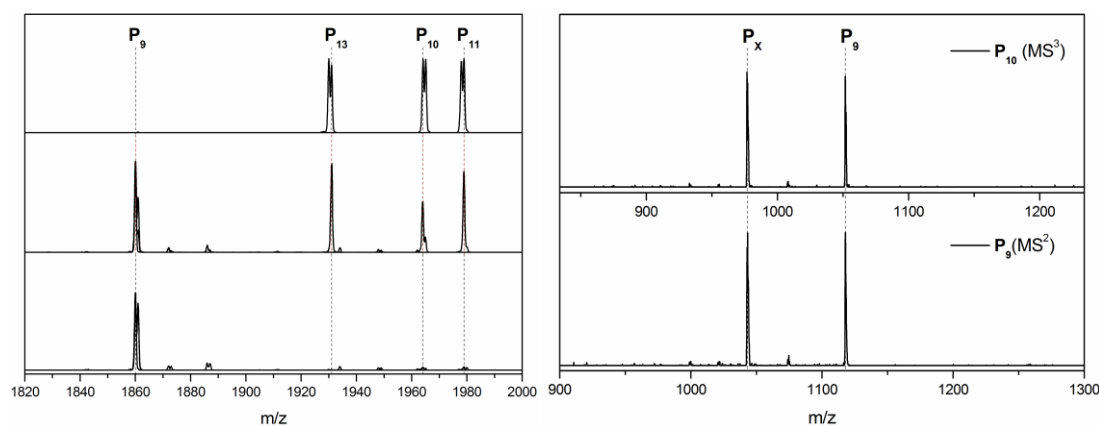
Label	Sum formula	m/z_{exp}	m/z_{theo}	$\Delta\ m/z$
P_9	$C_{85}H_{160}NaO_{41}{}^+$	1860.00	1860.03	0.03
P_{10}	$C_{93}H_{168}NaO_{41}{}^+$	1964.08	1964.10	0.02
P_{11}	$C_{92}H_{166}NaO_{40}{}^+$	1978.92	1979.11	0.19
P_{13}	$C_{90}H_{170}NaO_{41}{}^+$	1930.00	1930.11	0.11
P_9 (MS^3)	$C_{95}H_{180}Na_2O_{46}{}^{2+}$	1051.75	1051.58	0.16
P_X (MS^3)	$C_{87}H_{173}Na_2O_{43}{}^{2+}$	976.75	977.06	0.31
P_9 (MS^2)	$C_{101}H_{192}Na_2O_{49}{}^{2+}$	1117.83	1117.62	0.21
P_X (MS^2)	$C_{193}H_{186}Na_2O_{46}{}^{2+}$	1042.83	1042.51	0.32

Figure 5.2-1. CID ESI-MS experiments. Left, 1st line: Overlay of 3 isolated ions (P_{10}, P_{11}, and P_{13}). PEG species with a chain length of 38 ethylene glycol units were investigated. Left, 2nd line: Overlay of CID pattern corresponding to the top spectra with medium collision energy. Left, 3rd line: Overlay of CID pattern corresponding to the top spectra with high collision energy. Decomposition pattern of the aldehyde signal stemming from the aldehyde signal obtained by CID of P_{10} (top, MS^3) and the initial aldehyde P_9 (bottom, MS^2) are depicted (right). Table: collation of sum formulae and m/z values corresponding to the ESI-MS spectra.

Thus, it appears that the retro PB reaction is a feasible reaction channel for the decay of the oxetane moieties, which is promising for the following synthetic approach to revert the cycloaddition. In an attempt to further verify the retro PB product signal to be the aldehyde moiety, MS^3 experiments were conducted in which the CID product signal was once again subjected to CID (*Figure 5.2-1*). The resulting pattern obtained for medium collision energy (P_{10} (MS^3)) were compared to the CID pattern of the initial aldehyde polymer (P_9 (MS^2)). Although ions with different polymer chain lengths were analyzed, the patterns coincide ideally revealing signals corresponding to the expected elimination of the end group at the ester function.

For the synthetic approach of the cycloreversion, a literature-known process was applied.[216] Due to success reported with naphthalene dinitrile (NDN) as a photosensitizer, it was employed for all retro PB attempts (*Scheme 5.2-2*).
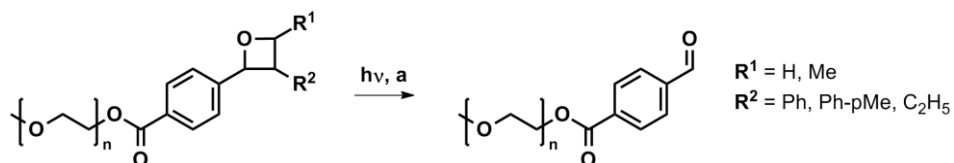
Scheme 5.2-2: General reaction scheme for the photosensitized ring cleavage reaction. a) NDN, MeCN, RT, 3 h.

At first, the reaction conditions needed to be optimized due to changes compared to the literature system: The molar amount of photosensitizer, the dilution of the reagents, as well as the reaction time were varied. The results for a kinetic investigation of the retro PB reaction (P_{10}) with optimized conditions are depicted in *Figure 5.2-2*.
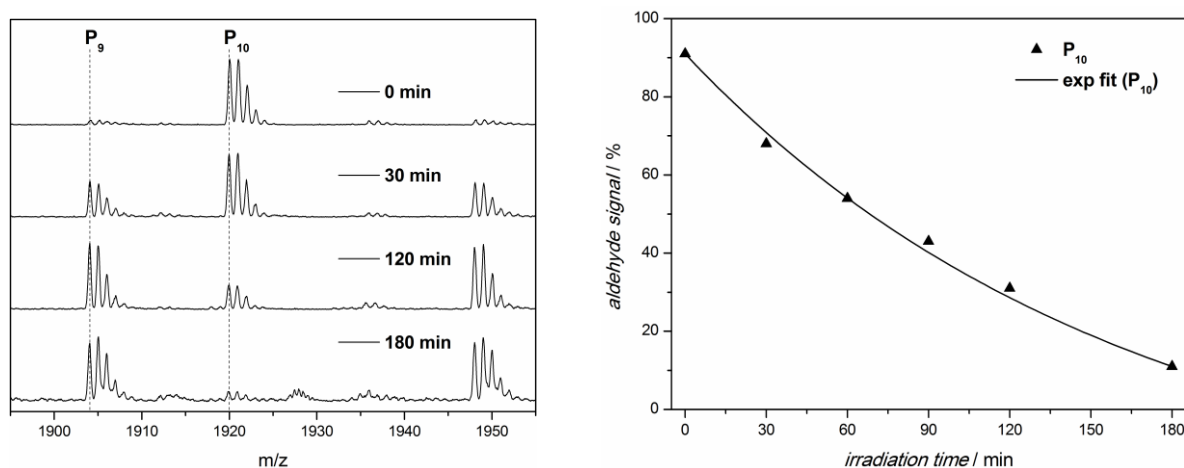
Figure 5.2-2: ESI-MS results of the synthetic cycloreversion reaction of P_{10}. Left: ESI-MS spectra referring to the samples of the kinetic investigation; right: kinetic plot corresponding to the ESI-MS spectra.

The photosensitized cycloreversion reaction appeared to be more delicate than expected. In most cases (P_{11}, P_{12}, and P_{13}), the desired reaction could not be observed. In the case of P_{11}, destruction of the entire polymer chain was found, whereas the product of the P_{12} cycloreversion appeared to be the reduced version of the desired cycloreversion product bearing a benzyl alcohol end group. For P_{13}, no cleavage of the oxetane moiety could be achieved. However, the retro PB results of P_{10} were more promising. As displayed in *Figure 5.2-2*, the ESI-MS spectra evidence an increasing amount of aldehyde end groups up to reaction times of three hours. Simultaneously, the signals for the oxetane derivative decrease until they almost disappear in the baseline noise. The kinetic plot corresponding to the integration values of the ESI-MS spectra is also depicted in *Figure 5.2-2* (right). The conversion

for the photosensitized cycloreversion levels off at 80 % according to ESI-MS. Unfortunately, the NMR results (*Figure 5.3-1*, right, 3rd line) do not coincide with the ESI-MS values as well as for the forward reaction. A maximum amount of 40 % aldehyde functionality can be found after 2 h of irradiation according to NMR and with continued reaction time the value starts to decrease. Since the degradation of the aldehyde group cannot be detected by ESI-MS, it can only be concluded that some sort of rearrangement takes place. A rearrangement would explain the consumption of aldehyde functionalities – as observed by NMR – whereas no changes can be observed via ESI-MS due to the constant *m*/*z* values. Nevertheless, the synthetic approach to cleave the oxetane function photochemically and reproduce aldehyde termini can be conducted. Although a certain amount of side product was found, a detailed study for increasing the efficiency of the cycloreversion was postponed to future studies.

5.3 Proof of Principle – Reversibility

An impure starting material for the third consecutive step in the photoreaction sequence is certainly not ideal, yet the fact that aldehyde end groups could be regenerated allows for the investigation of subsequent photochemical trans-formations (*Scheme 5.3-1*).
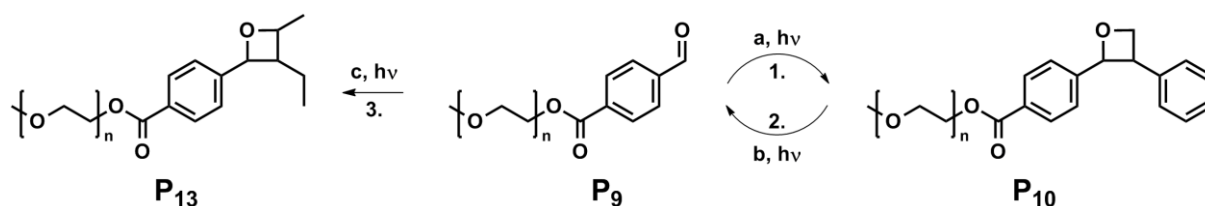
Scheme 5.3-1: Synthetic sequence for the proof of principle for reversible encoding of aldehyde functionalized poly(ethylene glycol). a) styrene, toluene, RT, 24 h; b) NDN, MeCN, RT, 3 h; c) 2-pentene, toluene, RT, 1 h.

The results from the investigation of the first step of the photochemical reaction sequence (Section 5.1) suggest to employ 2-pentene for the final reaction step since it was found to undergo the most rapid and efficient PB reaction with P_9. The reaction conditions and kinetics were carefully explored for the initial step, thus the details of the third reaction step are depicted by collating all three consecutive steps (*Figure 5.3-1*).
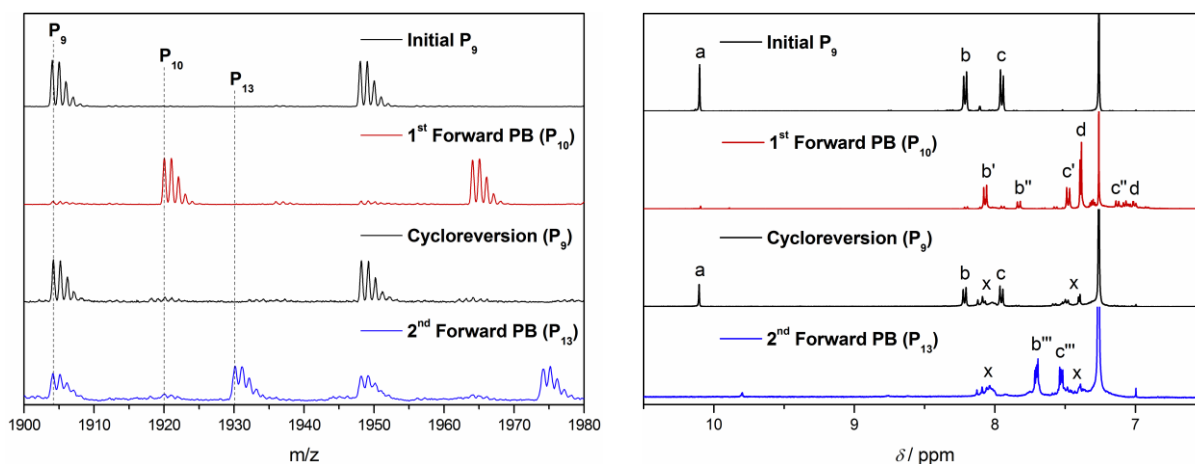
Figure 5.3-1. Left: ESI-MS spectra of P_9 (top) and the three consecutive photoreactions (line 2-4). Right: corresponding NMR spectra.

The three consecutive steps can be clearly followed by ESI-MS: The shift from the initial P_9 (top) to P_{10} (2nd line), the retro PB reaction regenerating P_9 (3rd line), and as final conjugation the subsequent forward PB reaction with 2-pentene yielding P_{13}

(bottom). The first three spectra are of remarkable quality, being highly clean without evidence of side-products. The bottom spectrum however, reveals the side-reaction occurring in the 2nd step. The regenerated aldehyde-functional material was converted into **P$_{13}$**, whereas the rearrangement product remains in the final spectrum at the *m*/*z* value of **P$_9$**. The NMR spectra (*Figure 5.3-1*, right) support this theory: A very clean first forward PB reaction (line 2) is followed by a spectrum for the cycloreversion product which reveals some side-product (signal x). Its signal does not disappear during the final photoreaction, whereas the regenerated aldehyde (line 3, signal a, disappears entirely after the final step. Combining the ESI-MS and NMR results, the final spectra demonstrate that polymer end groups can be reversibly encoded via Paternò–Büchi chemistry. The side-reaction, which can certainly not be neglected, supports the conclusion that the current system requires further optimization. Yet, the proof of concept for a synthetic approach towards a PB/retro PB system is given by the evidence of three consecutive photoreactions.

5.4 Summary

The investigation of the current chapter concerns a light-triggered methodology to produce a reversible system for modifying polymer end groups with versatile oxetane units. Employing poly(ethylene glycol), an aldehyde function was installed at the chain end. An initial forward [2+2] cycloaddition reaction of the polymer with styrene derivatives and 2-pentene yielding oxetane functionalized PEG was monitored in detail by NMR and ESI-MS characterization. Therein, the PB reaction was observed to proceed to conversion values of larger than 90 %. The resulting oxetane end-capped PEG moieties were subjected to CID ESI-MS experiments, where the respective oxetane units could be cleaved to regenerate the aldehyde terminus. A synthetic approach to reverse the PB reaction was attempted by irradiating the resulting oxetane functional polymer in the presence of a photosensitizer (NDN). For the styrene substituted oxetane polymer, reasonable amounts of aldehyde-termini could be regenerated, although a side-reaction was witnessed by NMR. The resulting aldehyde terminal polymer was subjected to a consecutive forward PB reaction with 2-pentene, proving the principal of reversibly encoding polymer end groups. Thus, the presented photochemical switching of polymer end groups provides an option for recoding substrates with different reactants in a catalyst-free fashion. However, the experimental effort for each individual step reduces the applicability of the targeted PB/retro PB approach. In addition, the unexpected side-reaction for P_{10} as well as the unsuccessful cycloreversion results for the polymers P_{11-13} further limit the future prospects of PB chemistry with regard to applications for the reversible encoding of polymeric substrates.

6

BLOCK COPOLYMER FORMATION VIA PHOTOENOLS – ACCESSING NOVEL CONJUGATES

The current chapter is concerned with a light-induced technique applied for the synthesis of block copolymers. The conjugation of two polymer blocks is a highly delicate reaction with extreme demands in terms of efficiency. Thus, the development of ligation techniques enabling block copolymer synthesis is challenging, yet highly valued by synthetic polymer chemists. Herein, a hetero Diels–Alder (HDA) reaction is described connecting a photoenol moiety and a dithioester derivative. In order to introduce the idea behind the investigation presented in the current chapter, the novel conjugation reaction will be discussed with regard to theoretical considerations about the HDA activity of RAFT polymers. Subsequently, the results from block copolymer synthesis proof the suitability of the light-triggered approach to access novel conjugates and apply their formation for macromolecular architecture design.

In detail, a photoenol precursor was installed at the chain end of a poly(ε-caprolactone), which was investigated towards its behavior under irradiation in the presence of RAFT polymers. To further prove the broad scope of the novel synthetic method, RAFT polymers of different molar masses and monomer compositions were synthesized and employed for block copolymer formation, evidenced via SEC. The general reaction scheme depicting the reaction of interest is displayed below (*Figure 6-1*).
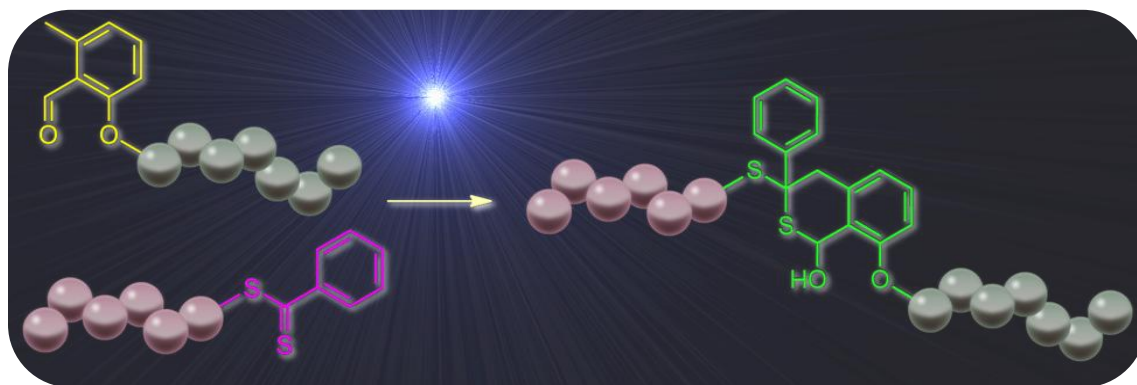
Figure 6-1: General light-induced reaction of the photoenol-based formation of block copolymers employing conventional RAFT polymers.

6.1 Design of an Advanced RAFT-HDA System

Controlled/Living polymerization protocols enable precise preparation of customized polymers. In combination with efficient, modular, and orthogonal post-polymerization modification techniques, the synthetic chemist is provided with powerful tools for the design of advanced macromolecular architectures.[312] One of these suitable concepts is RAFT-HDA chemistry – introduced in Section 2.1.3.3 – which combines the power of RAFT polymerization with the advantageous properties of Diels–Alder cyclo-additions (*Scheme 6.1-1*).[313]

Diene   **RAFT agent**   **HDA adduct**
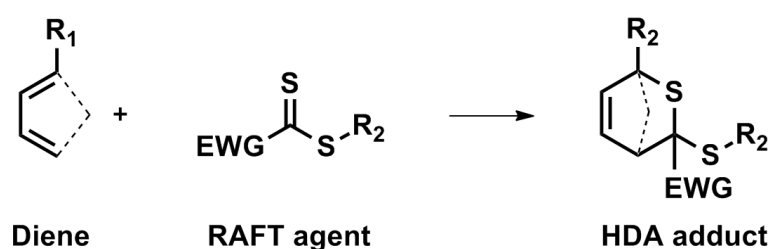
Scheme 6.1-1: General RAFT-HDA reaction. $R_{1,2}$ = polymeric substituents.

The atom-efficient and versatile process makes use of the increased Diels–Alder activity of RAFT agents with electron withdrawing Z-groups. The most prominent examples of HDA-suitable dithioester (DTE) compounds are depicted in *Scheme 6.1-2*.

DTE$_1$ **DTE$_2$**   **DTE$_3$**   **DTE$_4$**
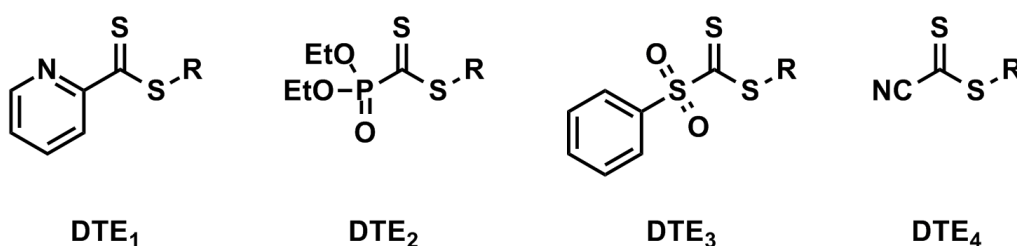
Scheme 6.1-2: HDA-suitable dithioesters. R = organic substituent.

In contrast to the increasing affinity of the DTEs for HDA reaction, the ability to control a radical polymerization process is reduced for strong electron withdrawing substituents. **DTE$_1$** and **DTE$_2$** for instance are relatively good control agents, yet their HDA reaction requires addition of an activating catalyst.[76] **DTE$_3$**, on the other hand, does not require catalysis and enables controlled polymerization of for example isobornyl acrylate. Unfortunately, the strongly electron withdrawing sulfonyl group decomposes upon completed cycloaddition.[314] The remarkably efficient and catalyst-

free HDA reaction of **DTE₄** has been demonstrated in applications such as reversible step-growth polymerizations[125] or self-healing materials.[126] However, a successfully controlled polymerization involving the cyano dithioester has not yet been reported. In summary, the development of a RAFT-HDA system which enables not only the controlled polymerization of a broad variety of monomers but is also suitable for efficient and rapid HDA conjugation is highly desired.

The efficiency and enhanced reactivity of photoenols has already been pointed out in the literature review of the current thesis (Chapter 2). Thus, a promising approach seems to be the combination of the concepts of RAFT-HDA with light-triggered Diels–Alder chemistry. One of the most universally applicable RAFT-agents is 2-cyanopropyl dithiobenzoate (CPDB). It is commercially available and, indeed, enables the controlled polymerization of a diversity of monomers, e.g., styrenics, (meth)acrylates, and (meth)acrylamides.[60-62] Therefore, the investigation reported in the current chapter is based on the reaction of CPDB and the advanced second generation of photoenols (*Scheme 6.1-3*).
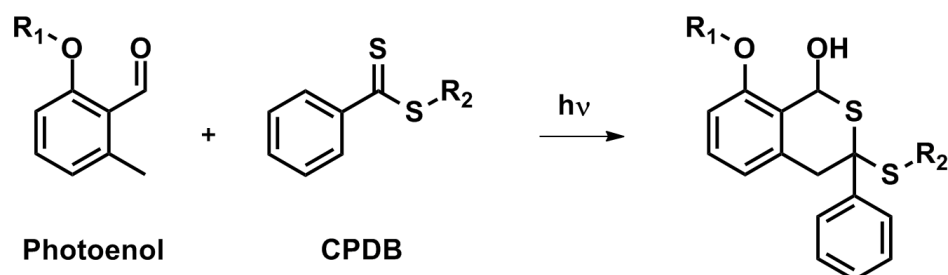
Scheme 6.1-3: Approach for a light-induced RAFT-HDA system involving the universally applicable RAFT agent CPDB. R₁,₂ = polymeric substituents.

A highly demanding task for conjugation techniques is the connection of two polymer blocks. Since separation or polymeric side-products from the reaction mixture is hardly possible, the ligation reaction needs to proceed to complete conversion under entire consumption of both starting blocks. The original RAFT-HDA concept has proven to be suitable for, e.g., ultra-rapid block copolymer formation,[75] the generation of high molecular weight block copolymers,[315] as well as star polymers.[316] The present exploration is focused on the preparation of block copolymers and the detailed analysis of the progress of the photoreaction. Therefore, the two building blocks containing the desired functional groups needed to be synthesized. In terms of the RAFT end group, the synthetic goal could be achieved by purchasing the RAFT

agent and conducting controlled polymerizations of styrene and methyl acrylate (*Scheme 6.1-4*).
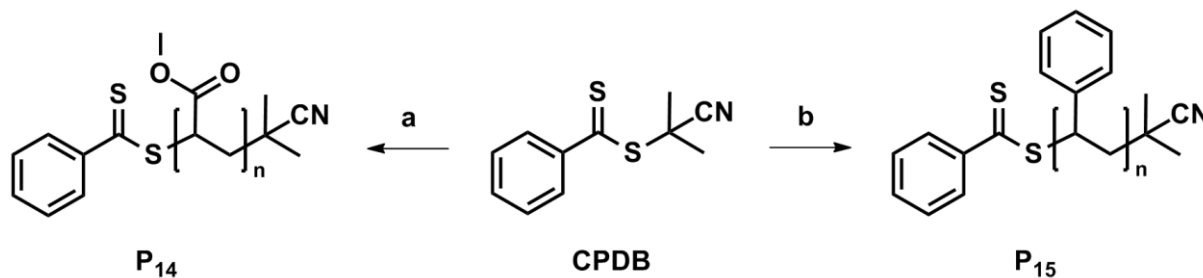
Scheme 6.1-4: General reaction scheme for CPDB-mediated RAFT polymerizations. a) methyl acrylate, AIBN, benzene, 70 °C, 6 h, M_n = 5400 g·mol^{-1}, Đ = 1.05.; b) styrene, AIBN, toluene, 90 °C, 13 h, M_n = 5900 g·mol^{-1}, Đ = 1.05.

For the preparation of a photoenol-capped polymer, a polymerization initiator had to be synthesized. An established synthetic strategy towards an initiator for ring-opening polymerization had been explored in an earlier study by our group (*Scheme 6.1-5*).[131]
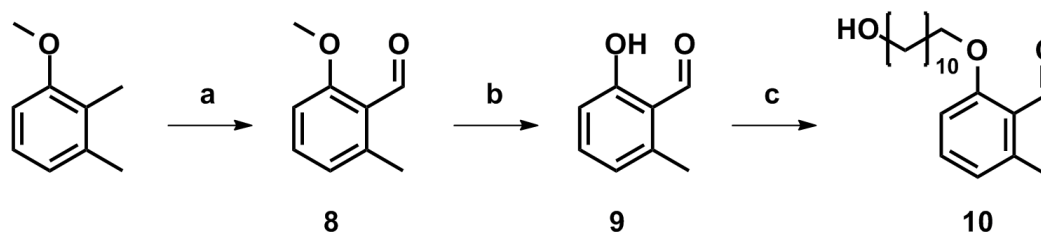
Scheme 6.1-5: Synthetic strategy for a ROP initiator bearing a photoenol precursor species. a) $K_2S_2O_8$, $CuSO_4 \cdot 5\,H_2O$, MeCN/H_2O, 90 °C, 45 min; b) $AlCl_3$, DCM, 0 °C-RT, overnight; c) 11-bromo undecanol, K_2CO_3, DMF, RT, 72 h.

ROP of ε-caprolactone afforded a polymer of narrow dispersity fully functionalized with the photoenol precursor (*Scheme 6.1-6*). The molar mass of the resulting polymer was determined by SEC, while NMR analysis confirmed quantitative end group functionality.
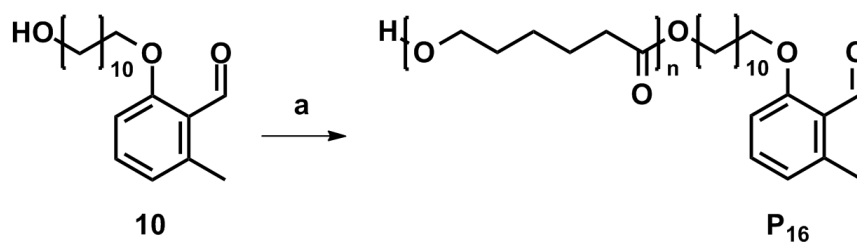
Figure 6.1-6: ROP of ε-caprolactone employing a photoenol functionalized initiator. a) ε-caprolactone, TBD, toluene, benzoic acid, RT, 7 h, M_n = 8500 g·mol^{-1}, Đ = 1.08.

6.2 Generation of Block Copolymers

The investigation of the photo-induced RAFT-HDA conjugation was conducted in two separate parts: Confirming the existence of the expected cycloadduct and exploring the scope of the novel synthetic tool. Detailed information about the initial study concerning the verification of the cycloadducts structure can be retrieved from ref.[317], as well as the Ph.D. thesis of Dr. Kim K. Oehlenschlaeger, as noted above. However, it is noteworthy that a variety of analytic techniques was applied to determine the structure of the isothiopyrane linkage in a model reaction based on a poly(methyl methacrylate) RAFT polymer (PMMA) of short chain length (M_n = 3300 g·mol^{-1}). Thus, SEC/ESI-MS, CID ESI-MS, NMR, and UV-vis spectroscopy could be applied to the conjugation product of PMMA with compound **9**. Moreover, SEC, ESI-MS and NMR were employed for monitoring the light-triggered process of PMMA and photoenol end-capped low molar mass poly(ε-caprolactone) (M_n = 2000 g·mol^{-1}).

The unambiguous evidence – given by the analytic methods noted above – for the modular formation of the desired cycloadduct provides the proof of principle for the idea of photo-induced HDA chemistry. However, the applicability of the novel ligation technique to polymers of higher molar mass and different monomer composition needed to explored. Moreover, an optimization of the reaction times was conducted to assess the limits of the current approach. Therefore, mixtures of the – compared to the previous results – larger ROP polymer **P$_{16}$**, and the RAFT polymers **P$_{14}$** or **P$_{15}$** in acetonitrile (MeCN/DCM for **P$_{15}$**) were prepared containing both functional end groups in equimolar amounts. The respective reaction schemes are provided in *Scheme 6.2-1*. It is important to note that removal of oxygen by three consecutive freeze-pump-thaw cycles is crucial for successful photoenol reactions due to a possible peroxide formation in the presence of oxygen.[318] Upon complete degassing, the photoreactions were conducted, taking samples for SEC analysis after 0, 2.5, 5, 7.5, and 10 min. The corresponding SEC chromatograms are presented in *Figure 6.2-1*.
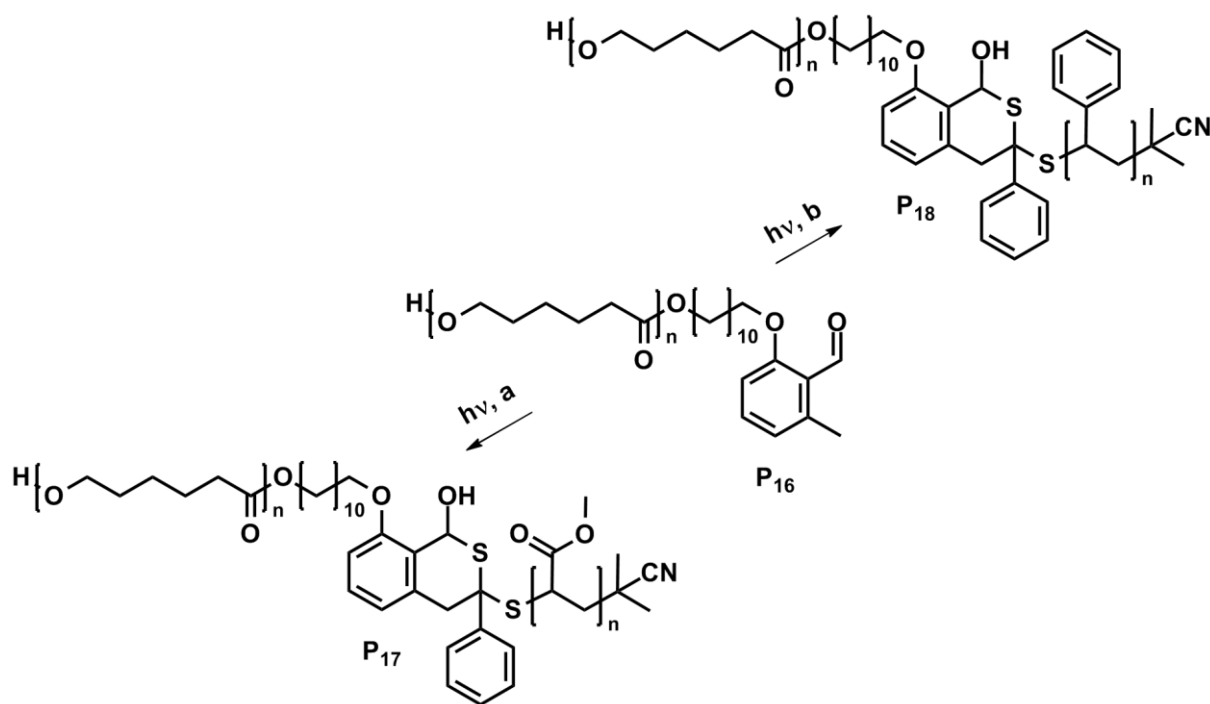
Scheme 6.2-1: Preparation of block copolymers via light-triggered RAFT-HDA. a) **P₁₄**, MeCN, RT, 10 min; b) **P₁₅**, MeCN/DCM, RT, 10 min. Light source: Cosmedico Arimed B6, 36 W.
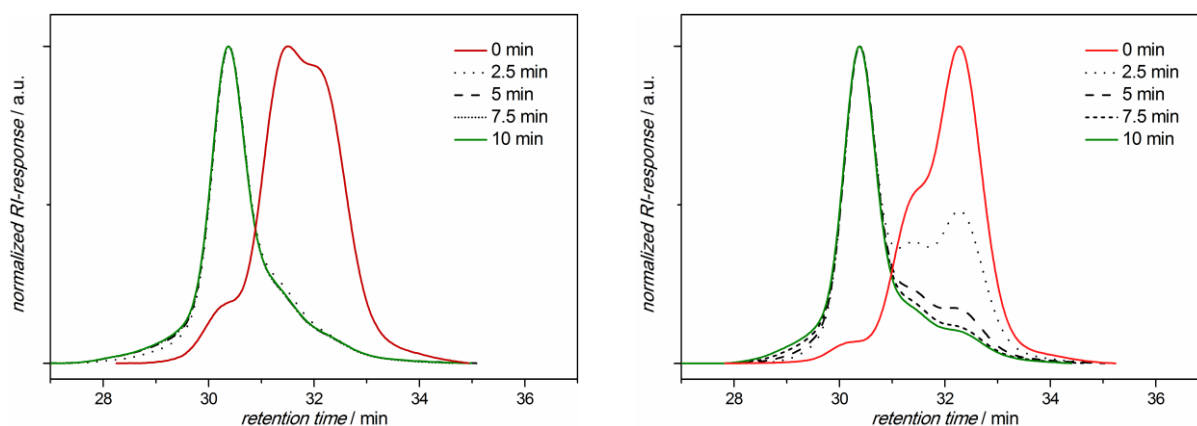
Figure 6.2-1: SEC chromatograms corresponding to the kinetic runs monitoring the preparation of **P₁₇** (left) and **P₁₈** (right).

The SEC chromatograms in *Figure 6.2-1* provide important information about the light-induced block copolymer formation process. The red plain lines represent the mixtures of the initial starting polymers, whereas the green plain lines depict the resulting block copolymers. The preparation of **P₁₇**, which contains the PMA-based RAFT polymer, is almost complete after 2.5 min. The changes compared to the elugram obtained after 5 min irradiation time are insignificant and the chromatograms after 7.5 or 10 min are identical to the one obtained after 5 min. Thus, a rapid conjugation reaction occurs and the resulting product does not decompose upon further irradiation. In contrast to the complete product formation of **P₁₇** after 3 min, the

generation of P_{18} requires about 10 min of irradiation. The prolonged reaction time can be either caused by the polystyrene block, which might absorb some UV-irradiation, or the additionally added DCM due to solubility issues of P_{15} in pure MeCN, causes a reduced reaction rate. However, after 10 min, no further increase of the molar mass of the block copolymer could be observed. A graphic depiction of the number average molar mass evolution for both reaction mixtures is provided in *Figure 6.2-2*.
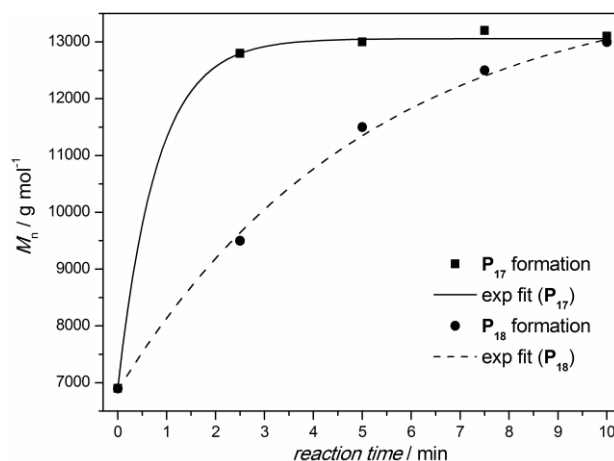
Figure 6.2-2: Kinetic plot corresponding to the SEC results depicted in Figure 6.2-1.

An even more obvious form of displaying the success of the block copolymer formation is provided in *Figure 6.2-3*. The two starting blocks (RAFT polymer in red lines, ROP polymer in black lines), as well as the final block copolymer (green line) are displayed. Compared to the starting materials, a clear shift of the chromatogram for the product to lower retention times and therefore higher molar masses is observed. Although the photo-induced process is rather efficient, little traces of starting material can be discerned in the elugrams of the block copolymers. A possible explanation for the presence of starting material in the final product is the unavoidable termination during the RAFT process. Despite the controlled nature of the polymerization process, the termination reaction cannot be fully suppressed, resulting in non-functional (dead) polymer chains.[49b, 50] Due to a lack of functionality, these termination products are not accessible for Diels–Alder reactions and therefore not only the terminated material itself, but also an equimolar amount of ROP polymer remain in the final product. However, the results of SEC analysis clearly indicate the successful coupling of the single blocks.

	P₁₄	**P₁₅**	**P₁₆**	**P₁₇**	**P₁₈**
M_n [g·mol^{-1}]	5400	5900	8400	13000	13400
Đ	1.05	1.05	1.08	1.21	1.19
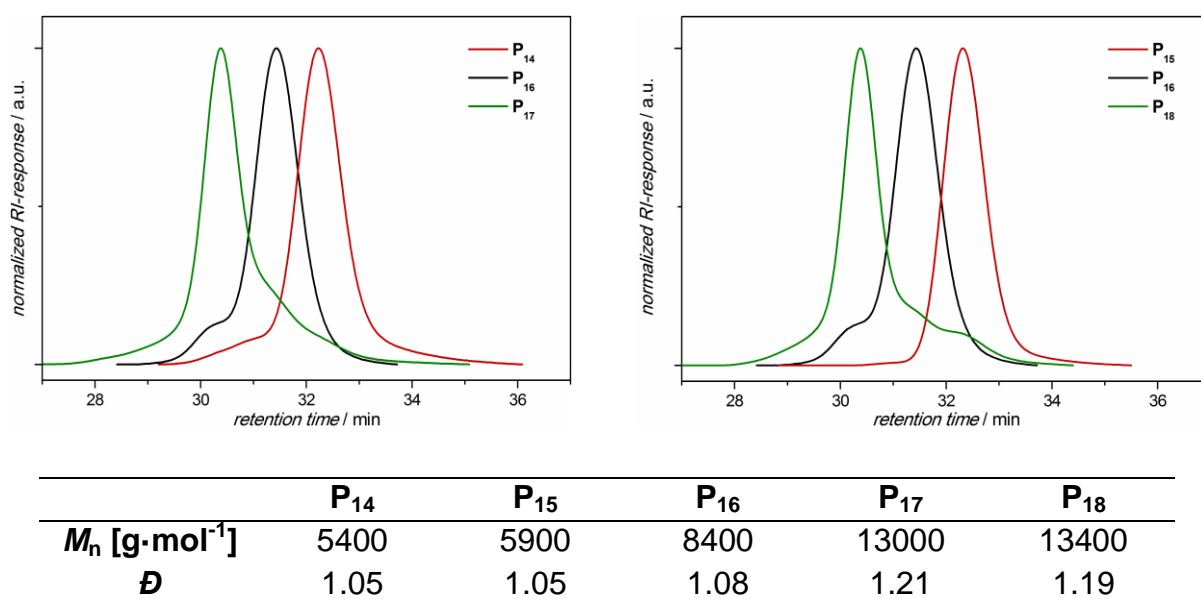
*Figure 6.2-3: SEC analysis of the starting polymers (**P₁₄** and **P₁₆** (left), **P₁₅** and **P₁₆** (right)), as well as the resulting block copolymers (**P₁₇** (left), **P₁₈** (right)). The number average molar mass and dispersity values are collated at the bottom.*

Very high conversions are achieved for both conjugation reactions, which is also underpinned by the good agreement of the measured M_n values with the expected M_n values for the copolymers (Table in *Figure 6.2-3*). The slight differences between the experimental and theoretical values can be explained since the block copolymers possess a different elution behavior due to the differing properties of the two polymer blocks.[319]

6.3 Summary

The current chapter presents the successful combination of two concepts in polymer ligation chemistry. By merging the RAFT-HDA approach and the light-induced photoenol ligation technique it was possible to access the conjugation of a so far unavailable RAFT group for hetero Diels–Alder reactions. The non-activated dithioester functionality in a commercially available RAFT agent allows for the controlled polymerization of a large variety of monomers and is thus one of the most universally applied control agents. Accessing a conventional RAFT agent for HDA reactions broadens the scope of the RAFT-HDA concept and simultaneously demonstrates the abilities of light-induced ligation protocols. The efficiency of the herein introduced light-triggered method was demonstrated by the preparation of block copolymers. Therefore, a photoenol precursor-bearing ring opening polymerization initiator was synthesized and subsequently employed for the polymerization of ε-caprolactone, yielding a well defined and photoenol end-capped polymer. Poly(methyl acrylate) and polystyrene were obtained via RAFT polymerization. The block copolymer formation was investigated in terms of reaction time monitored by SEC. The catalyst-free conjugation requires no more than 10 min to achieve full conversion from an equimolar mixture of starting blocks. The establishment of a modular ligation technique for conventional RAFT polymers greatly expands the synthetic toolbox available to macromolecular chemists.

7

POLYMER CROSSLINKING VIA NITEC – ACCESS TO FLUORESCENT POLYMER NETWORKS

The final project of the current thesis concerns the largest polymeric systems discussed so far: polymer networks. Herein, the establishment of a cycloaddition-based technique for crosslinking polybutadienes is presented. In general, crosslinking pre-existing polymer strands is a powerful method for tuning material properties. For instance the viscosity, solubility, and optical properties can be adjusted by controlling the extent of crosslinking, making it an ideal handle for materials design. Moreover, physical properties of crosslinked materials can be readily modulated, which makes network-based substances valuable for industrial applications.[320-321] Polybutadienes, or in general, unsaturated polymeric materials, are suitable for crosslinking reactions since they contain carbon-carbon double bonds. These double bonds can be readily exploited to further modify the material.[322] The electronically non-activated nature of the double bonds of polybutadienes allows radical crosslinking mechanisms, whereas performing cycloaddition reactions is

---

rather challenging. Thus far, radical thiol-ene chemistry[323-325] or typical radical initiators, such as AIBN,[326] benzophenone derivatives,[327-330] acyl phosphines,[331-332] α-thiocyanato ketones,[333] were successfully employed for crosslinking (1,2-) polybutadienes, as well as UVC light-induced self-crosslinking.[334] A detailed literature overview of crosslinking methods and applications is available in the literature review section (2.3.6).

The photochemical approach for tackling the challenge of crosslinking the non-activated polymers is based on NITEC chemistry. Reactions of nitrile imines with non-activated alkenes have been previously reported[155] and thus, NITEC appears to be a feasible tool for the crosslinking study. By fusing the concepts of NITEC ligation and unsaturated polymer crosslinking, a sunlight-triggered method for transforming linear 1,2-polybutadienes into networks with fluorescent properties is targeted, enabling the fabrication of fluorescent patterned surfaces and designs. Based on a novel di-functionalized linker compound, bearing two diaryl-substituted tetrazole groups, the reaction with vinylic type carbon-carbon double bonds is enabled under UV-irradiation. Similar to other studies described in the present thesis, a small molecule model study was initially performed, in order to explore the efficiency of the NITEC system. Subsequent to the detailed analysis of the characteristics of the light-triggered process, 1,2-polybutadienes were utilized for the generation of fluorescent networks. Ultimately, the crosslinking reaction was performed in sunlight to generate an insoluble fluorescent film with high spatial resolution. The following figure depicts the content of the current chapter graphically (*Figure 7-1*).
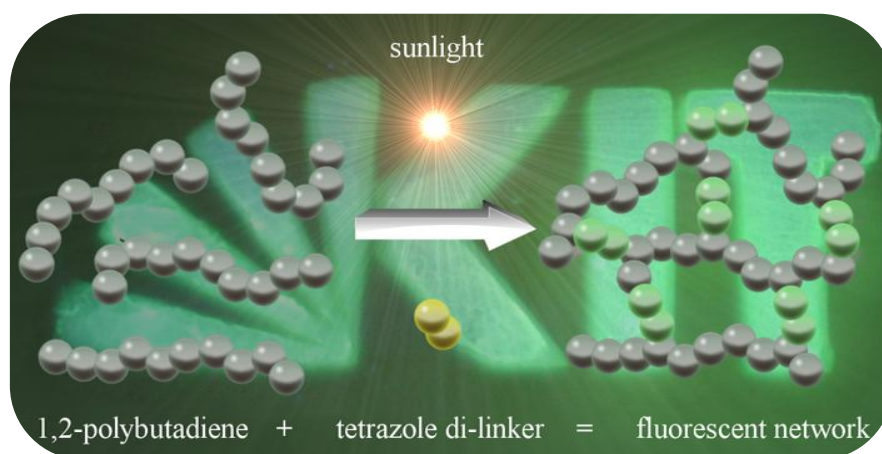
Figure 7-1: Graphic depiction for the sunlight-induced crosslinking of 1,2-polybutadienes (gray polymers) employing a tetrazole di-functional linker molecule (yellow). Due to the resulting fluorescent linkages (green), fluorescent patterns of crosslinked material can be produced (KIT logo in the background).

7.1   Design of a Photoreactive Di-Linker

Light-sensitive crosslinking agents are well known in the literature and are particularly valuable to polymer and biochemists.[335-337] Most of the previously utilized light-induced methods for crosslinking pre-existing polymers are based on carbene and nitrene chemistry[338] or radical processes.[327-328] In contrast to the poorly characterized reaction processes noted above, the current study targets the generation of polymer networks via a well-defined cycloaddition reaction, consistent with the polymer community's growing interest in light-induced cycloaddition chemistry.[339] Therefore, a newly designed light-sensitive linker compound needed to be designed which is capable of NITEC reactions. Various di-functional tetrazole moieties, either directly connected, or separated by an aryl or alkyl spacer, have already been synthesized as reported elsewhere[340-341] and the photochemical generation of their respective bis-nitrile imines were analyzed, for example by different low-temperature spectroscopic methods and in time resolved studies.[150-151, 153, 342] However, a novel customized linker moiety containing two diaryl substituted tetrazoles was designed (*Scheme 7.1-1*) to fulfill two crucial criteria in order to allow for an in-depth characterization of a small molecule model reaction and successful sunlight-triggered crosslinking of polybutadienes: *(i)* good solubility/ionization properties and *(ii)* a suitable excitation wavelength.

12
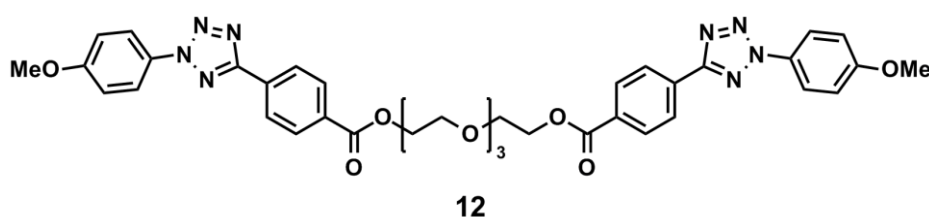
Scheme 7.1-1: Structure of the novel tetrazole di-linker.

The first criterion was addressed by judiciously selecting the spacer connecting the photosensitive tetrazole functions in order to provide good solubility of the entire linker compound. Therefore, a tetraethylene glycol spacer was introduced, offering advantageous properties similar to poly(ethylene glycol) as discussed in Chapters 4 and 5. Moreover, the diol species enables a facile esterification protocol to prepare **12** from a carboxylic acid functional tetrazole derivative (**1**). The synthesis of the novel tetrazole derivative was adapted from literature[343] and upon optimization, the

two step process enabled the preparation of the desired compound in 65 % overall yield. The synthetic strategy is depicted in *Scheme 7.1-2*.
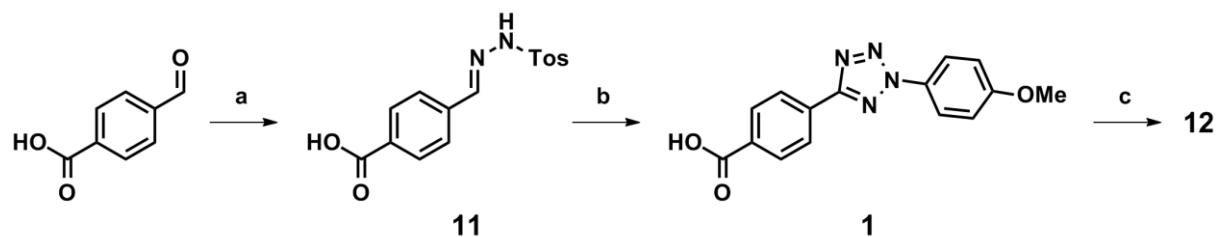
Scheme 7.1-2: Synthetic sequence towards the tetrazole di-linker. a) toluenesulfonyl hydrazide, ethanol, 40 °C, 1 h; b) anisidine, HCl, ethanol/H_2O, THF, 0 °C – RT, overnight; c) 1. thionyl chloride, THF, 75 °C, 4 h, 2. tetraethylene glycole, pyridine, THF, RT, overnight.

The absorption properties of the linker moiety were adjusted by substituting the tetrazole with aryl groups. In detail, the absorption range of the diaryl tetrazoles mostly depends on the aromatic substituents in *para*-position.[158, 164] For the current study, a significant overlap with the solar emission spectrum was required to provide efficient excitation of the photoreactive groups. The two substituents – an electron donating substituent (e.g., OMe) on the N2-phenyl ring and an electron withdrawing substituent (e.g., COOH) on the C5-phenyl ring – were introduced,[344] causing a bathochromic shift compared to formerly employed diaryl tetrazoles.[154, 167] Thus, the resulting absorption spectrum of **12** ranges from 250 nm to 345 nm and permits the usage of a large variety of light sources emitting at different wavelengths, as well as the sunlight, which also exhibits UV-irradiation (*Figure 7.1-1*).
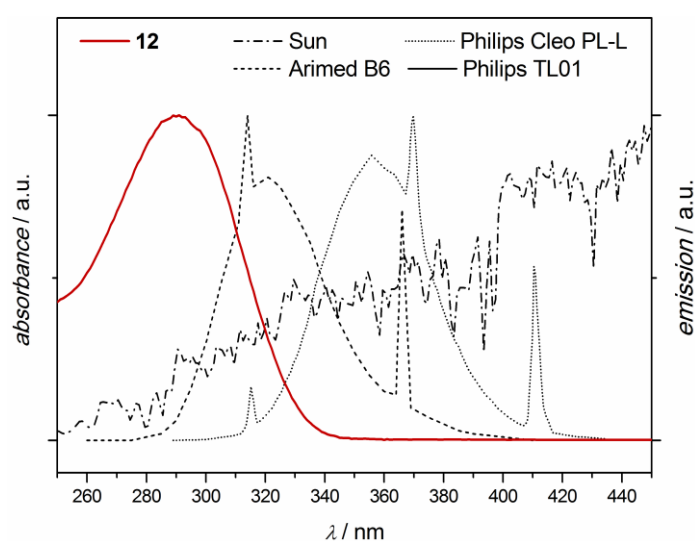
*Figure 7.1-1: UV-Vis analysis of **12**. Emission spectra of various UV-lamps as well as a section of the solar emission spectrum.*

A crucial requirement for high reaction rates as well as efficient conjugation is the overlap of the UV-lamp emission spectra with the absorption spectrum of **12**. However, self-crosslinking of polybutadienes – occurring under irradiation with high energy UVC-light (200-280 nm)[334] – needs to be suppressed and therefore irradiation in the wavelength region of λ_{ex} < 300 nm should be avoided. Although excitation by sunlight is desired for the final application, compact low pressure UV-lamps were employed for most of the following investigations to exclude the influence of environmentally changing irradiation conditions. Light sources such as a typical UVA-emission lamp (*Philips Cleo PL-L*) as well as two UVB-emission lamps (*Arimed B6*, *Philips TL01*) were utilized for investigating the effect of the light source. Detailed lamp specifications are available in the Methods section (9.2).

7.2 Small Molecule Model Study

At first, the reaction of the novel di-linker moiety with non-activated alkenes was investigated in a small molecule reaction (*Scheme 7.2-1*). The small molecule study was conducted to gain detailed knowledge regarding the conditions influencing the efficiency of the NITEC reaction and for elucidating the reaction kinetics of the photochemical process. 1-Pentene is employed as dipolarophile due to the electron density of its the terminal double bond, which is similar to the vinylic double bonds present in the 1,2-polybutadienes used in subsequent experiments. A further advantageous feature of 1-pentene is its facile removal from the reaction mixture simplifying the workup subsequent to the reaction. The majority of the following photoreactions was conducted using a UVB emission lamp (*Arimed B6*), which mimics the high energy section of the sunlight spectrum and provides an emission spectrum overlapping reasonably well with the absorption spectrum of **12**. Thus, reliable and reproducible results could be obtained, since inconsistencies associated with fluctuations in sunlight emission were avoided. A detailed study concerning the irradiation source was subsequently conducted in combination with the kinetic investigations (Section 7.2.2).
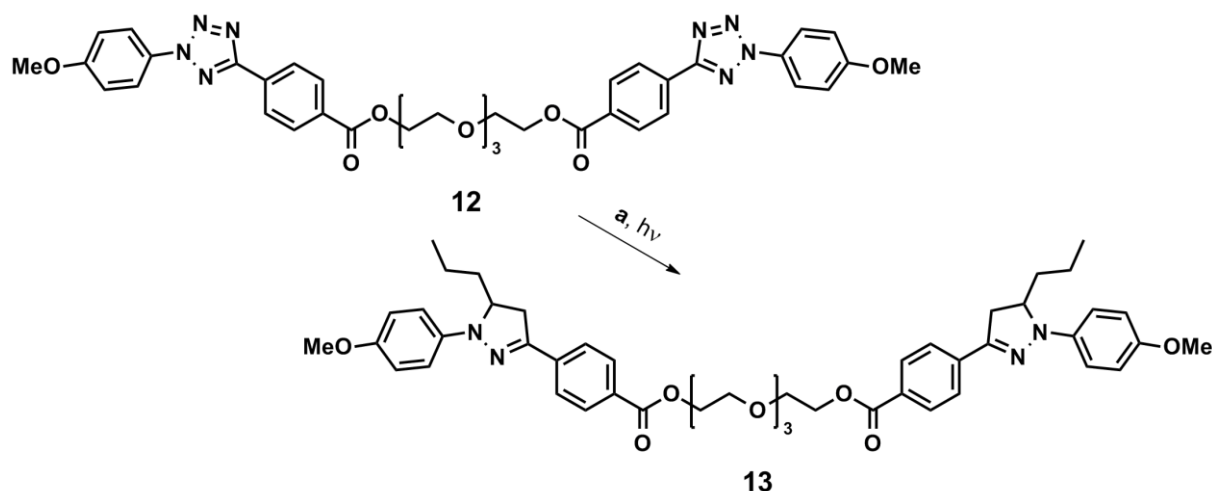
Scheme 7.2-1: Reaction scheme of the small molecule model system.

7.2.1 Investigation of the Cycloadduct

A variety of spectroscopic characterization methods was applied to demonstrate the efficiency of the NITEC reaction. Upon successful cycloaddition the molar mass of the analyte increases, which can for instance be monitored by ESI-MS or SEC. The differing optical properties of the starting material and cycloadduct can be witnessed by UV-vis and fluorescence spectroscopy. Moreover, the structural changes can be followed by ^{1}H NMR characterization.

The m/z values of **14** and **15** are well within the detection range of an LXQ ESI-MS spectrometer, enabling access to the extent to which the light-induced reaction proceeds (*Figure 7.2-1*).

Label	Sum formula	m/z_{exp}	m/z_{theo}	$\Delta\ m/z$
12	$C_{38}H_{38}N_8NaO_9^+$	773.25	773.27	0.02
13	$C_{48}H_{58}N_4NaO_9^+$	857.50	857.41	0.09
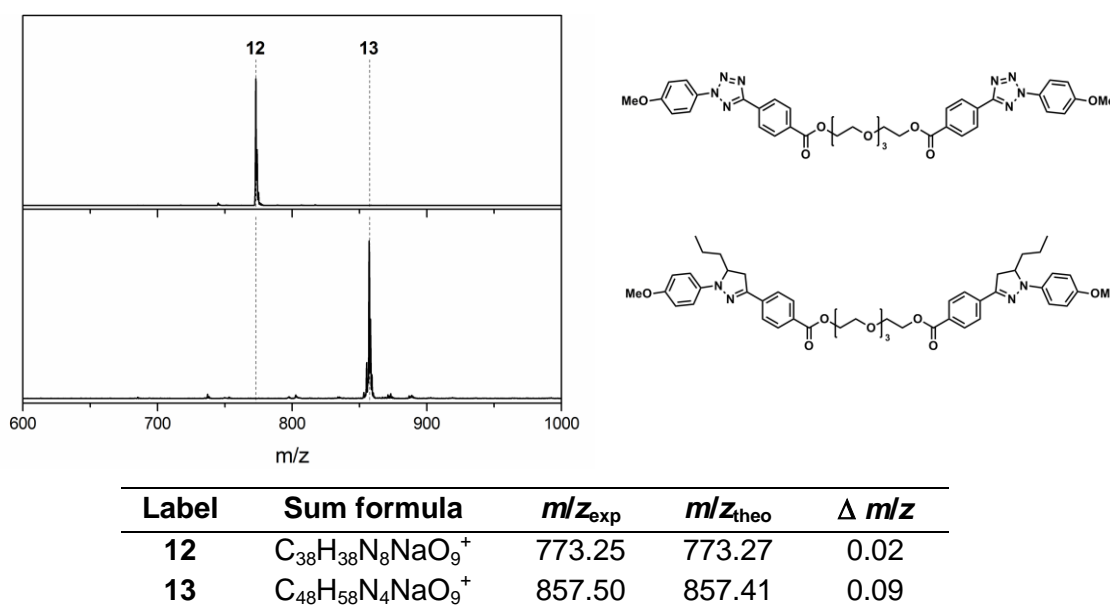
*Figure 7.2-1: ESI-MS spectrum of **12** (top) and **13** (bottom) as well as the corresponding structures (right). Bottom: Collation of sum formulae and m/z values corresponding to the ESI-MS spectra.*

Noteworthy is the excellent purity of the starting material (**12**) appearing at 773.25 amu. Upon two hour irradiation in the presence of 1-pentene, the signal of **12** disappeared completely and the new signal emerging at 857.5 amu corresponds to the addition of two 1-pentene molecules under loss of two nitrogen molecules from the tetrazole units. The ESI-MS spectrum of **13** demonstrates that the reaction occurs without producing any significant amount of side products. A high ion count detected for both spectra indicates the excellent ionization quality of the material which was targeted by introducing the tetra(ethylene glycol) spacer.

The molar mass – and therefore hydrodynamic volume – difference between the starting material and the product also allows for SEC analysis (*Figure 7.2-2*).
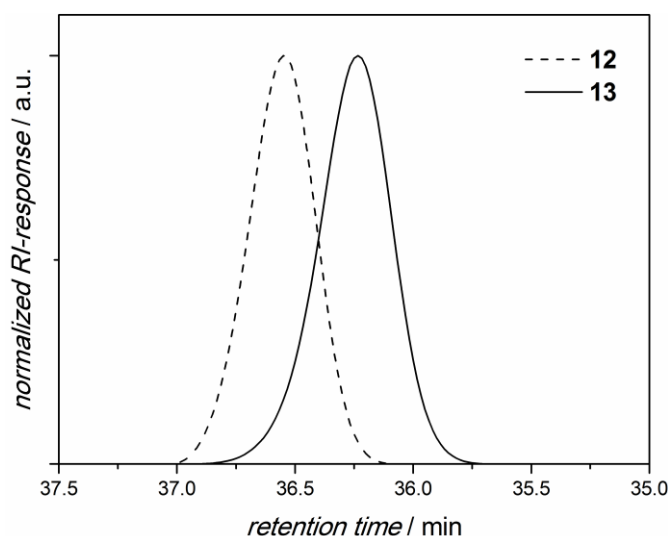
Figure 7.2-2: SEC elugrams of 12 (dashed line, $M_n = 750$ g·mol^{-1}, Đ = 1.01) and 13 (plain line, $M_n = 860$ g·mol^{-1}, Đ = 1.01).

Since both components are monodisperse, narrow molar mass distributions are expected which was confirmed by the measurements. A clear shift to lower retention times and therefore higher molar mass was observed for the cycloadduct in comparison with the starting material. The high purity of both compounds causes a symmetrical shape of the chromatograms indicating that no side reactions, such as nitrile imine dimerization, take place. Although polystyrene calibration was applied for the SEC system, the obtained molar mass values are very accurate.

In addition, the differences in optical properties of **12** and **13** can be determined by UV-vis and fluorescence spectroscopy (*Figure 7.2-3*). Both the tetrazole di-linker as well as the cycloadduct correspond well to the expected behavior reported in literature.[158] The initial tetrazole absorption maximum of $\lambda_{abs} = 290$ nm (plain line) is clearly shifted to an absorption maximum of close to 410 nm for **13** (dashed line). The latter value is within the typical absorbance range of di-aryl pyrazolines.[345] Even more evident for a successful cycloaddition is the observed fluorescence of the product ($\lambda_{em} = 450$ - 750 nm) associated with the presence of pyrazoline moieties (dotted line). The tetrazoles on the other hand, do not fluoresce.
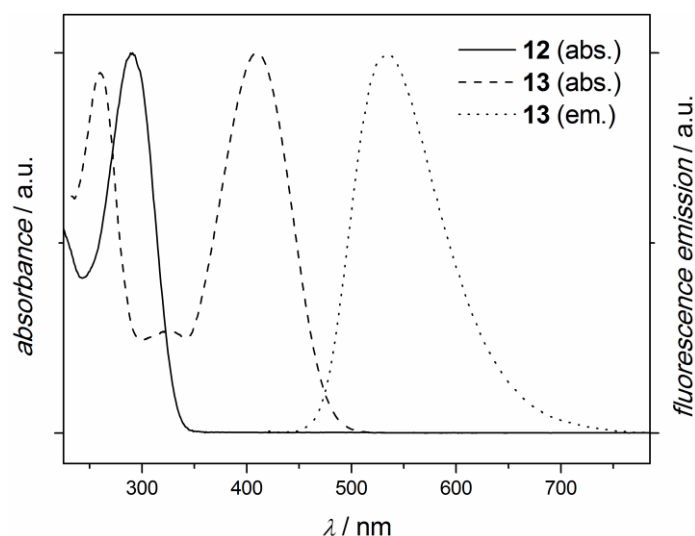
Figure 7.2-3: UV-vis spectra of 12 (plain) and 13 (dashed), as well as the fluorescence emission spectrum of 13 (dotted).

^{1}H NMR characterization of obtained cycloadduct is less simple than it appears to be at first sight (*Figure 7.2-4*). Due to a mixture of regioisomers caused by the cyclo-addition reaction which can occur in two different ways at both nitrile imine sites, the observed spectrum suffers from reduced clarity compared to the previous analytic techniques (ESI-MS, SEC, UV-vis, fluorescence spectroscopy). However, full conversion of the initial tetrazole units upon irradiation in the presence of 1-pentene is confirmed by the ^{1}H NMR results since all aromatic protons (*a-d*) disappear, whereas resonances shifted to higher fields emerge (*a'-d'*). Moreover, all the expected resonances can be assigned to the major cycloaddition product.
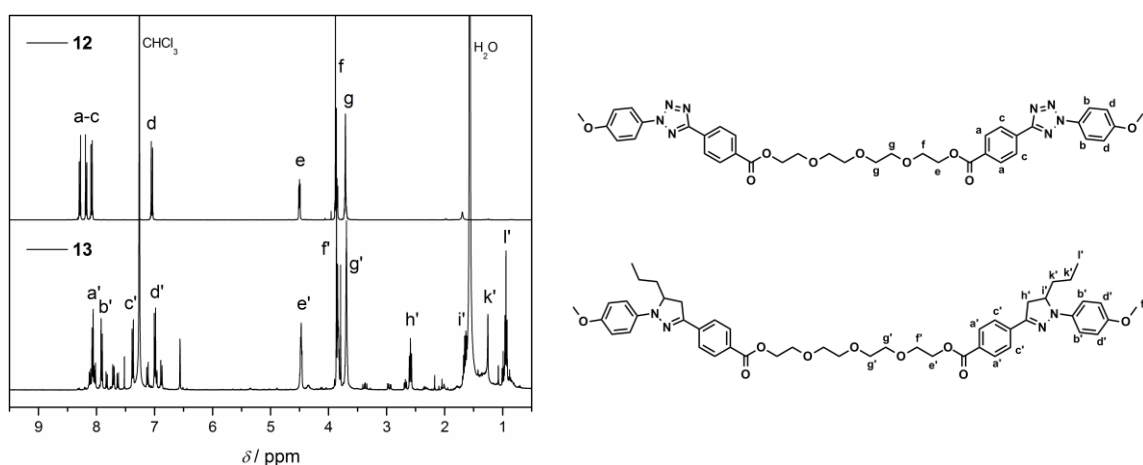
Figure 7.2-4: ^{1}H NMR spectra of 12 (top) and 13 (bottom) as well as the corresponding structures (right).

123

Although evidence for the light-induced tetrazole-ene cycloaddition with terminal non-activated carbon-carbon double bonds exists in contemporary literature,[155, 160] the light-induced reaction of tetrazoles with moieties bearing internal carbon-carbon double bonds has not yet been reported to the best of the candidate's knowledge. If efficient conjugation of tetrazoles with moieties such as *cis*-2-hexene or *trans*-2-octene was provided, the scope of the NITEC ligation technique would be significantly widened as typical 1,4-polybutadienes would also be accessible for crosslinking. Thus, **12** was subjected to photoreactions with several alkene moieties including *cyclo*-hexene, *cis*-2-hexene, and *trans*-2-octene (*Scheme 7.2-2*).
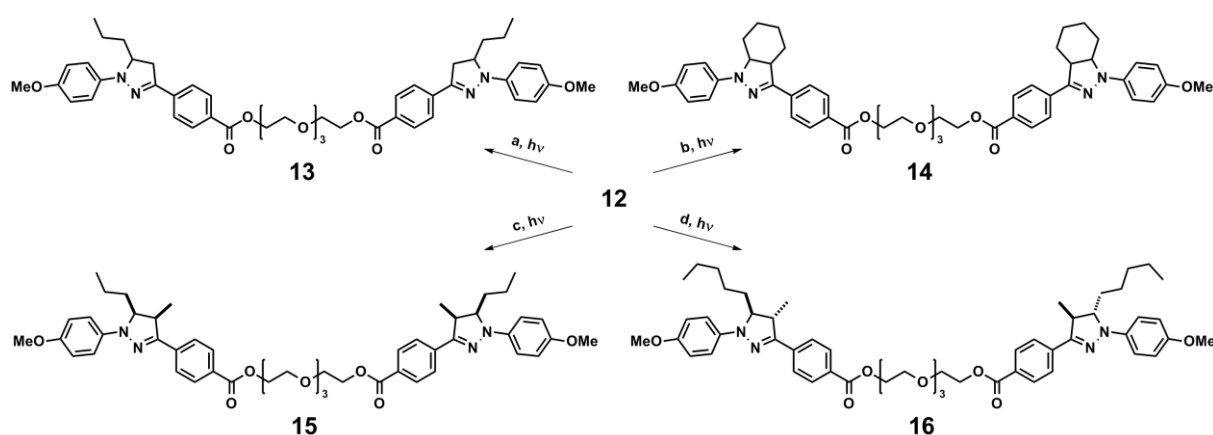
*Scheme 7.2-2: Overview of light-induced synthesis with **12** employing 1-pentene, cyclo-hexene, cis-2-hexene, and trans-2-octene.*

In order to evaluate the efficiency of the light-induced NITEC reaction with non-activated alkenes, the previously established model study was repeated using the above noted components as dipolarophiles applying the same conditions as described above. The results of the light-induced cycloaddition reactions were evaluated by ESI-MS (*Figure 7.2-5*). Regardless of the employed dipolarophile, the formation of the desired product was observed, confirming the high reactivity of the nitrile imine intermediate. However, a clear decrease in the reaction efficiency was found for the reactions conducted with dipolarophiles bearing internal double bonds. Unidentifiable side products appear in the spectra of the reaction mixtures with *cyclo*-hexene, *cis*-2-hexene, and *trans*-2-octene. In contrast, the product generated from the reaction with 1-pentene was highly pure. Integration of the respective ESI-MS spectra was applied to allow for a more quantitative statement about the efficiency of cycloadduct formation based on different dipolarophiles.
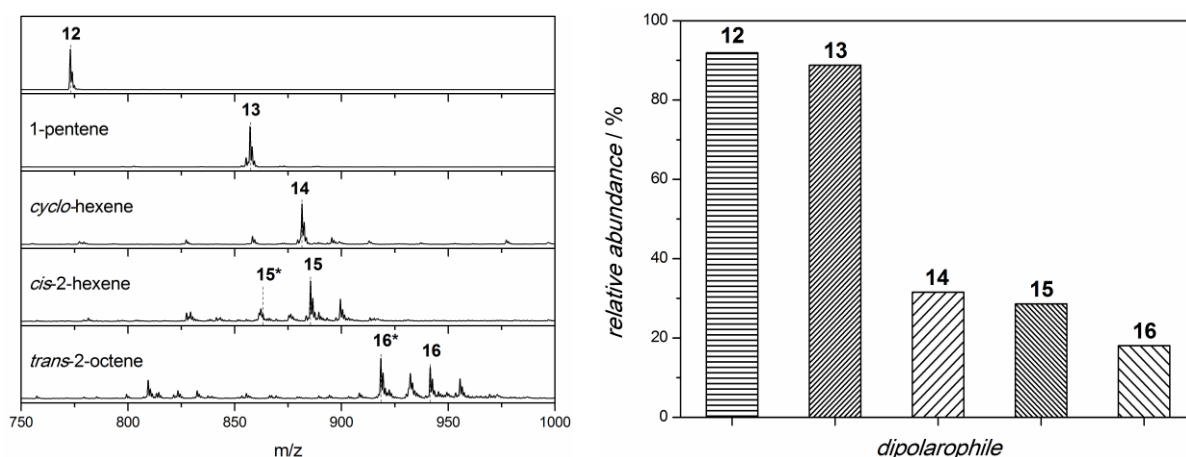
Label	Sum formula	m/z_{exp}	m/z_{theo}	$\Delta\ m/z$
12	$C_{38}H_{38}N_8NaO_9^+$	773.25	773.27	0.02
13	$C_{48}H_{58}N_4NaO_9^+$	857.50	857.41	0.09
14	$C_{50}H_{58}N_4NaO_9^+$	881.50	881.41	0.09
15*	$C_{50}H_{62}N_4O_9^{+\cdot}$	862.17	862.45	0.28
15	$C_{50}H_{62}N_4NaO_9^+$	885.50	885.44	0.06
16*	$C_{54}H_{70}N_4O_9^{+\cdot}$	918.42	918.51	0.09
16	$C_{54}H_{70}N_4NaO_9^+$	941.50	941.50	0.00

Figure 7.2-5: ESI-MS spectra of 12 as well as the crude reaction mixtures of 13, 14, 15, and 16 (left). Integration of the respective signals results in the diagram to the right. The sum formulae and m/z values corresponding to the ESI-MS spectra are collated in the table at the bottom.

Since the integration method includes a noise correction factor, the integration values for **12** and **13** are slightly below 100 %, although the corresponding signals are the only detectable signals. Nevertheless, integration values over 90 % are considered to associate with highly pure products. However, the values corresponding to the integrated product signals of **13**, **14**, **15**, and **16** are significantly lower, with relative abundance values of less than 40 %. The increased extent to which side reactions appear to occur prohibits the use of internal double bond-based polymers for crosslinking applications since high conversion of the photosensitive groups is crucial for efficient network formation. It is worth noting that the large conjugated system of the pyrazoline group is susceptible to oxidation during the electrospray ionization process. Therefore, **15** and **16** can be detected as both the sodium adducts and radical cation species (**15***, **16***).[346] Regardless, the efficiency for the formation of **13** from **12** and 1-pentene provides an excellent opportunity to crosslink 1,2-polybutadienes employing the di-functional tetrazole linker.

Before commencing the upcoming crosslinking reactions, the high excess of dipolarophile required for efficient cycloaddition needs to be discussed. An excess of

1000 equivalents was applied in all reactions included in the small molecule model study. Reducing the excess leads to a clear reduction in efficiency along with the formation of side-products. However, for the targeted application of crosslinking polybutadienes, a high excess of double bonds is operational since the photoreactive linker is present in small fractions.

7.2.2 Kinetic Investigations

Photoreactions depend strongly on various parameters, for example, quantum efficiency, absorbance of the reaction medium, concentrations, molar ratios, size of the reaction vessel, and the power and emission spectrum of the light source. Therefore, to correctly predict the crosslinking rate for applications, these parameters must be considered when investigating a reaction process in detail. In former studies the reaction kinetics for the photochemical decay of tetrazoles have been studied extensively.[53] Thus, the current section focuses on confirming the expected two-step reaction process depicted in *Scheme 7.2-4* as well as on determining the influence of the irradiation source on the reaction time. The di-functional linker molecule of the current system is not expected to react at both photolabile sites at the same time, which implies the intermediate existence of a mono-pyrazoline intermediate. Consequently, a reaction mechanism containing two consecutive cycloaddition reactions is more likely for the conjugation of **12** and two 1-pentene molecules.
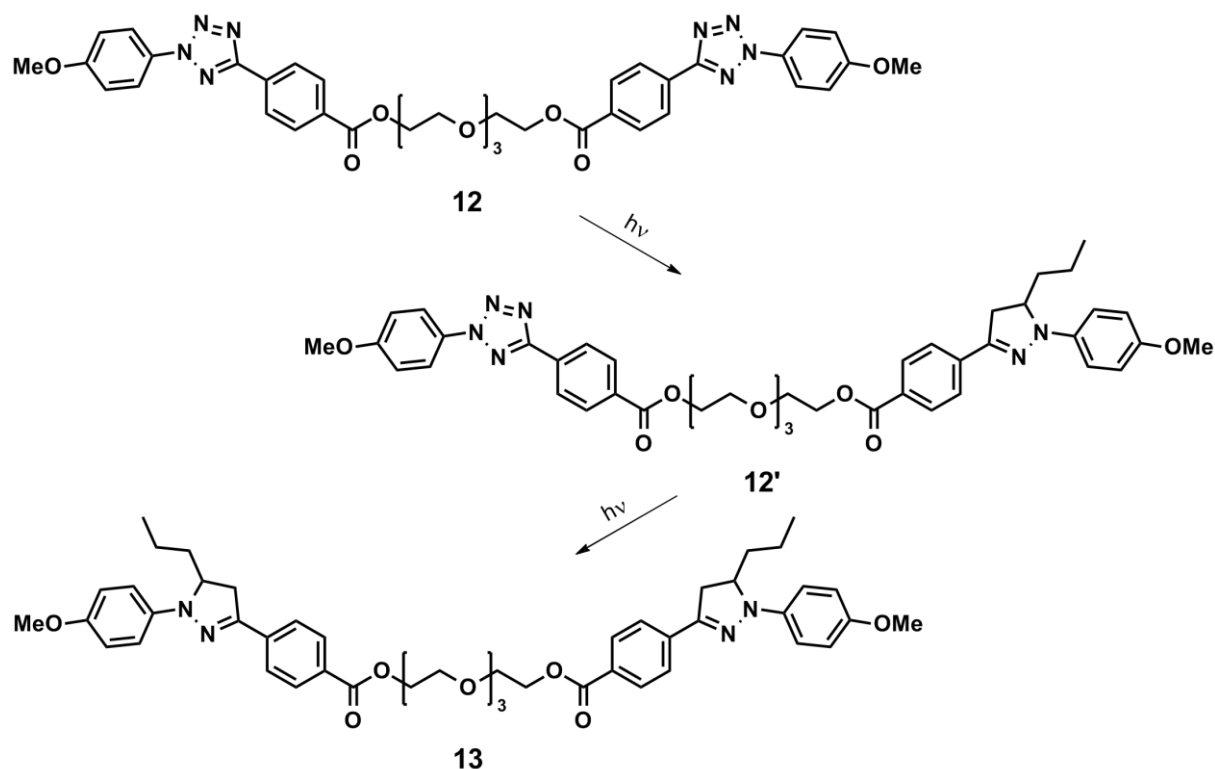
*Scheme 7.2-4: Proposed 2-step reaction process of the light-induced reaction between **12** and 1-pentene.*

In order to confirm the proposed two-step mechanism depicted above, ESI-MS characterization was employed. As previously alluded to (Chapter 4, 5), the reliability of the quantitative evaluation of ESI-MS spectra is highly dependent on the ionization properties of the system to be analyzed. By intentionally selecting a strongly polar tetra(ethylene glycol) spacer, good and reasonably constant ionization is provided, resulting in strong ESI-MS signals. Given these requirements, ESI-MS in combination with a previously established integration method makes this characterization technique a powerful tool for following the reaction processes in detail.[311] Nevertheless, the absolute integration values of signals detected by ESI-MS generally need to be treated carefully. However, the lack of side products in the current study indicates that meaningful trends can be derived from the following kinetic study (*Figure 7.2-6*).
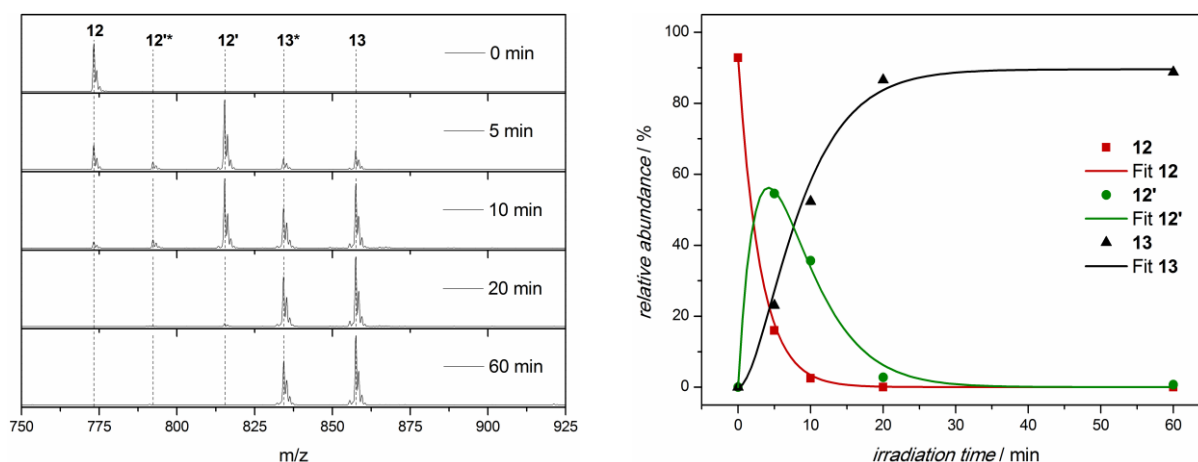
Label	Sum formula	m/z_{exp}	m/z_{theo}	$\Delta\ m/z$
12	$C_{38}H_{38}N_8NaO_9^+$	773.25	773.27	0.02
12'*	$C_{43}H_{48}N_6O_9^{+\cdot}$	792.25	792.35	0.10
12'	$C_{43}H_{48}N_6NaO_9^+$	815.33	815.34	0.01
13*	$C_{48}H_{58}N_4O_9^{+\cdot}$	834.33	834.42	0.09
13	$C_{48}H_{58}N_4NaO_9^+$	857.50	857.41	0.09

Figure 7.2-6: ESI-MS spectra of samples from the kinetic study conducted with the Arimed B6 UV-lamp (left). The integration values as well as the respective fits are depicted on the right.

The light-triggered reaction process of **12** and 1-pentene was first investigated employing the *Arimed B6* UVB lamp. Samples were taken from the reaction mixture after 5, 10, 20, and 60 min and subjected to ESI-MS analysis. The respective ESI-MS spectra indicate the disappearance of **12** after approximately 10 min. After approx. 5 min the relative abundance of the intermediate mono-substituted adduct (**12'** and **12'***) reaches a maximum and subsequently decreases until in vanishes after 20 min. Consequently, the intensity of the signals corresponding to the final product (**13**, **13***) increases constantly with reaction time until a pure bis-pyrazoline spectrum can be observed after 60 min. The respective integral values of the recorded ESI-MS spectra are presented in the form of a kinetic plot confirming the typical two-step reaction behavior.

Analogous to the photochemical experiment described above, the identical reaction was monitored utilizing different UV lamps as well as sunlight for irradiation (*Figure 7.2-7*). The reaction times to achieve full conversion – the point at which all starting material and the intermediate signals have vanished completely – vary from 10 min (*Philips TL01*), 30 min (*Arimed B6*), and 120 min (*Philips Cleo PL-L*) up to 240 min (sunlight). In addition, independent from the employed light source, the product was

always obtained in good purity, proving that variable irradiation conditions are applicable to the present NITEC system.
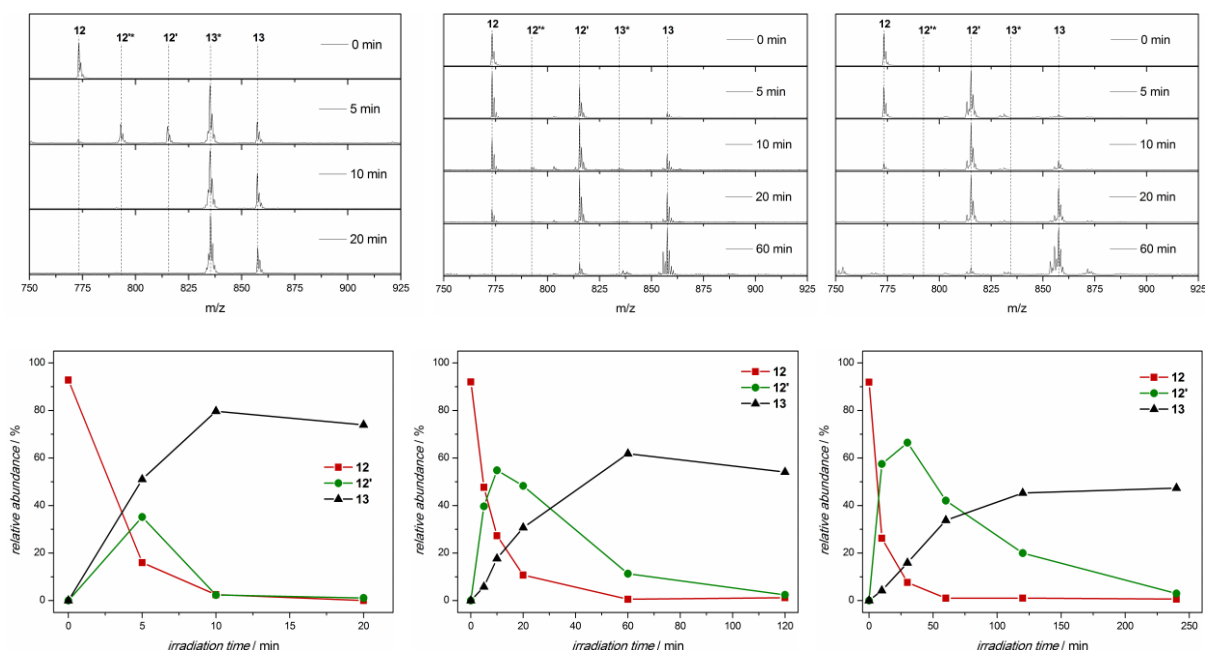
*Figure 7.2-7: Results of the kinetic study for the reaction between **12** and 1-pentene employing different irradiation sources. ESI-MS spectra are depicted on top, whereas the respective kinetic plots are displayed below. Irradiation sources: Philips TL01 (left), Philips Cleo (middle), sunlight (right).*

Fluorescence spectroscopy additionally provides the opportunity to monitor the progress of tetrazole-based cycloadditions. The current NITEC reaction can be triggered at the same wavelength which is required to excite the fluorescence of the newly formed product. Thus, the photoreaction can be induced by the excitation beam of the fluorescence spectrometer, enabling to analyze the reaction process on-line. The optimal wavelength fulfilling the dual function of inducing tetrazole decay as well as pyrazoline fluorescence was determined to be 315 nm. The optimized wavelength is close to the absorption maximum of the tetrazole and is therefore promising to induce an efficient conjugation reaction. Although the ideal wavelength for triggering the fluorescence is above 400 nm and the absorption spectrum of the pyrazoline product is rather low at 315 nm (compare *Figure 7.2-3*), intense fluorescence was observed, enabling accurate product detection. The on-line fluorescence spectrometry experiment was conducted in two detection modes (*Figure 7.2-8*): The fluorescence can either be repetitively recorded between 400 and 800 nm (cycle mode, left) or the fluorescence at 535 nm – representing the emission maximum of **13** – can be detected continuously (right). For both methods constant excitation (λ_{ex} = 315 nm) is provided.
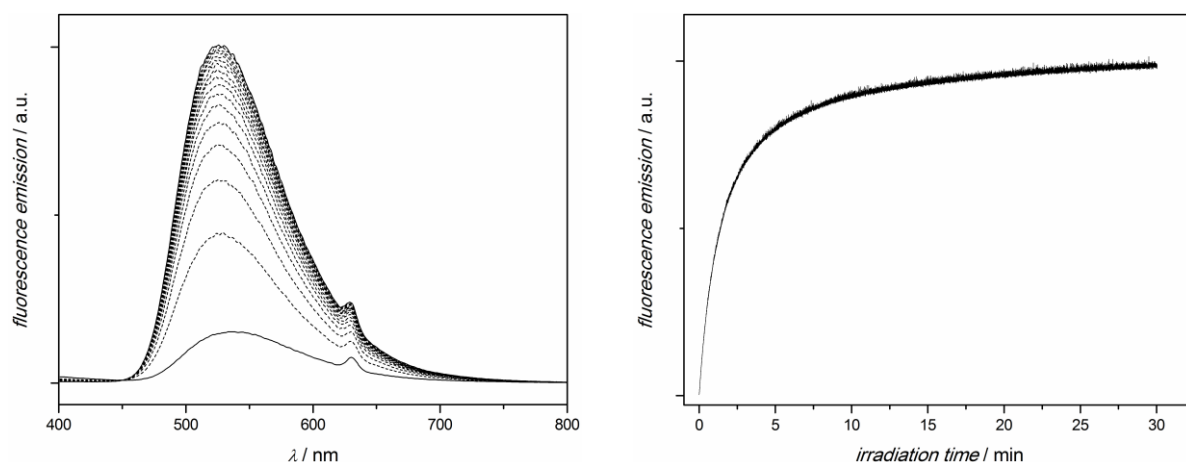
*Figure 7.2-8: On-line fluorescence experiments investigating the reaction between **12** and 1-pentene applying a constant excitation wavelength of 315 nm. Left: Consecutive fluorescence spectra are recorded in the range of 400-800 nm. Right: The fluorescence at $\lambda_{em} = 535$ nm is recorded continuously.*

The first fluorescence spectrum (bottom solid line, *Figure 7.2-8* left) already exhibits the typical broad pyrazoline emission proving the reaction to proceed rapidly at the beginning when a high tetrazole concentration is present. Subsequently recorded spectra each display an increase in fluorescence, witnessing the expected reaction progress with increasing irradiation time. The relative increase of the emission signal becomes smaller with every repetitive cycle (dashed lines) until the spectrum remains constant after 17 runs of the measurement at the highest intensity (top solid line). In total agreement with the first experiment, the fluorescence the signal was found to initially increase with time and then plateau after about 30 min in the second experiment. Thus, the reaction was confirmed to proceed to completion in short timeframes by on-line analysis, providing irradiation at a suitable wavelength occurs.

7.3 Polymer Crosslinking and Patterning

The next step towards the final application of patterning fluorescent materials was to conduct a detailed investigation of the light-induced crosslinking reaction of polybutadienes. Therefore, two commercially available 1,2-polybutadienes, **PBD₁** (Sigma-Aldrich, 3000 g·mol^{-1}, 90 % vinyl content) and **PBD₂** (Japanese Synthetic Rubber Company, RB 820, 100000 g·mol^{-1}, 92 % vinyl content) were employed. The large difference in molar masses was selected to enable two analytic methods for the evaluation of the crosslinking reaction. For the reaction of **12** with **PBD₁**, SEC was employed for monitoring the molar mass, since the resulting material remained soluble. On the other hand, fluorescent gels and films were generated utilizing **PBD₂**. The networks generated from the high molar mass starting material were characterized by gravimetric analysis. In order to optimize the crosslinking process, the reaction parameters needed to be adjusted. Therefore, the reaction time, concentration of the di-linker/polymer mixture as well as the molar composition of the mixture, were varied. First, the short chain length **PBD₁** was reacted with **12** under irradiation of the UVB-lamp *Arimed B6* and subsequently analyzed by SEC (*Figure 7.3-1*).
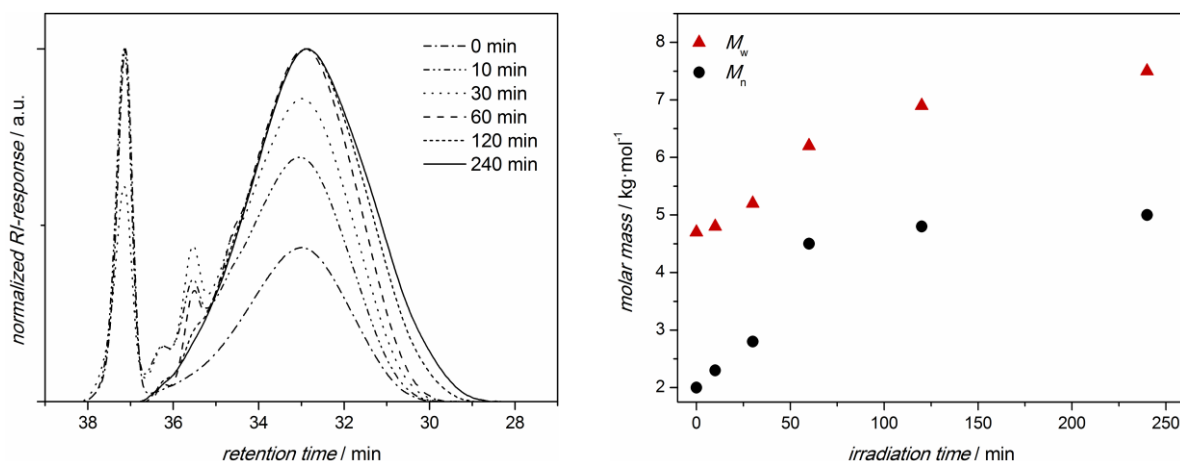
Figure 7.3-1: Dependence on the reaction time of the crosslinking reaction of **PBD₁**. *Left: SEC chromatograms corresponding to the samples taken during the crosslinking process. Right: Plot of the respective M$_n$ and M$_w$ values.*

The influence of the reaction time on the crosslinking reaction was studied by irradiating a mixture of **PBD₁** (10 mg) and **12** (3 mg) at high concentration (300 g·L^{-1}). Samples were collected for reaction times ranging from 0 to 240 min. An advantage

of the current system is that subsequent SEC characterization enables simultaneous detection of the starting materials and the product, providing information about shifted molar masses, as well as the consumption of the di-linker. A rapid decrease of the signal of **12** – detected at a retention time of 37 min – was found at the beginning of the reaction, expressing its incorporation into the polymeric material. After 60 min the signal of free **12** disappeared entirely indicating that the linker compound was completely attached to the polymer chains and, therefore, at least one tetrazole moiety per molecule has reacted with **PBD$_1$**. Thus, at that time during the process, the overall molecular weight exceeds that of pure **PBD$_1$** since it was reduced in the beginning by addition of the low molar mass di-linker. Upon the reaction of the remaining tetrazole groups with the polybutadiene, material of higher molar mass is generated due to the connection of multiple PBD chains. The SEC elugrams for longer reaction times confirm the occurrence of the crosslinking reaction depicting a shoulder which appears on the high molar mass side of the polymer distribution as well as the sudden increase in number average molecular weight (M_n) and weight average molecular weight (M_w) (*Figure 7.3-1*, right). The molar mass of the mixture was observed to increase continuously during the first 2-3 h of irradiation, whereas it was found to stabilize after approximately 4 h, corresponding to the consumption of all tetrazole moieties.

Next, the concentration of the photoreactive di-linker/polymer mixture was altered, which was kept constant for the kinetic study (*Figure 7.3-2*). For a starting mixture with a diluted solution of 8 mg·mL^{-1} the molar mass of the product hardly differed
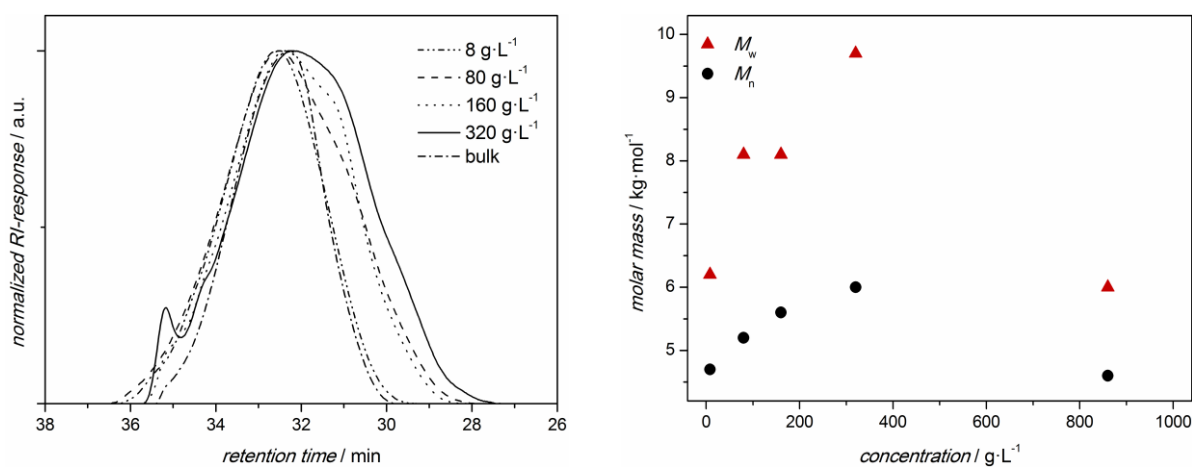
*Figure 7.3-2: Crosslinking reaction of **PBD$_1$** under variation of the concentration. Left: SEC chromatograms corresponding to the samples with varying concentration. Right: Plot of the respective M_n and M_w values.*

from that of the control (i.e., **PBD$_1$** without addition of **12**), suggesting that mostly intramolecular reactions occurred since the probability of the di-linker to react with a single chain twice is drastically increased in a diluted mixture. Thus, as expected, it was found that an increasing concentration of the photosensitive mixture leads to higher molar masses for the respective crosslinking product. Consequently, the material with the highest molar mass was achieved close to the saturation point of **12** (320 g·L^{-1}). Therefore, the only possibility to further increase the concentration and the extent of crosslinking was to perform the reaction in bulk. However, the general reaction rates for photoreactions in bulk are significantly reduced compared to photo-reactions in solution, and thus it was not surprising that only limited crosslinking was achieved in reasonable timeframes. Moreover, the importance of the judicious design of the di-linker component is obvious: Since extremely high starting material concentrations are needed, the linker component must be highly soluble in the polymeric mixture.

Finally, the molar ration between **12** and **PBD$_1$** was varied while the concentration and the reaction time were maintained constant (*Figure 7.3-3*). As expected, an increasing molar mass is observed as the amount of di-linker in the photosensitive mixture increases. The highest molar mass is achieved for a linker fraction of 43 wt%. However, especially for industrial applications, systems with a linker content of 43 wt% are unfortunately far from cost effective.
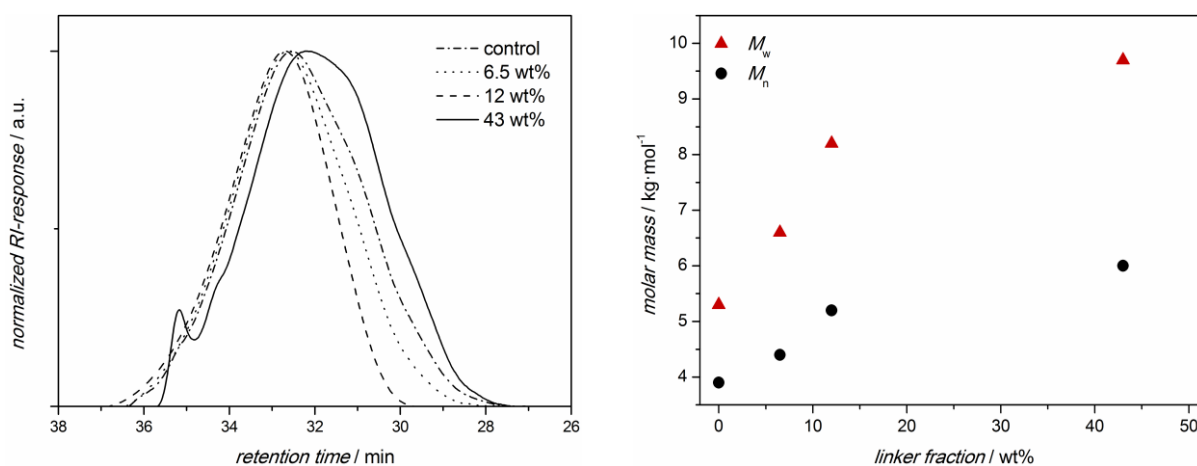
*Figure 7.3-3: Influence of the molar ratio on the crosslinking reaction of **PBD$_1$** with **12**. Left: SEC chromatograms corresponding to the samples with varying linker content. Right: Plot of the respective M$_n$ and M$_w$ values.*

So far, no insoluble material could be obtained from the crosslinking reactions of **PBD₁** during the optimization studies, suggesting that side reactions might interfere with the crosslinking process. As alluded to above, nitrile imines can undergo dimerization reactions resulting in a six-membered heterocycle (i.e., tetrazine)[347] when there is no dipolarophile present or a dipolarophile of reduced activity is not available in high excess. In the current system, the selected dipolarophiles (i.e., 1-pentene or polybutadiene) are less reactive for cycloadditions than typical dipolarophiles, such as maleimides or maleic esters. Therefore, the molar excess of carbon-carbon double bonds compared to tetrazoles needs to be extremely high to minimize the side-reaction. Hence, due to the existence of the side-reactions and the low molar mass of **PBD₁** the number of linkages per polymer chain likely remains low resulting in a poor crosslinking efficiency. In summary, **PBD₁** is not suitable for producing fluorescent gels by the current approach.

In order to generate insoluble polybutadiene-based networks via NITEC chemistry, a 1,2-polybutadiene of high molar mass – **PBD₂** (M_n = 100 kg·mol⁻¹) – was subjected to the light-triggered crosslinking process. The resulting partly insoluble material was analyzed by gravimetric determination of the gel fraction. Due to the fact that the leftover soluble material obstructs syringe filters (0.2 μm) – employed before SEC analysis – immediately, SEC was not available for characterization of the **PBD₂** system. Analogous to the investigation of the crosslinking process of **PBD₁**, the reaction parameters such as the irradiation time, the concentration, and the di-linker fraction needed to be optimized (*Figure 7.3-4*). In agreement with the kinetic investigation of the light-induced crosslinking reaction of **PBD₁**, the gel fraction of a mixture containing **12** (10 wt%) and **PBD₂** (200 g·L⁻¹) was observed to increase steadily at the beginning and plateau after extended reaction times when high conversions are achieved (*Figure 7.3-4*, top left). The maximum possible gel fraction for the mixture (80 %) was obtained after an irradiation time of 20 h. In contrast, the control samples, which were subjected to identical treatment except for the omitted addition of di-linker, stayed completely soluble. Hence, the network formation results from the desired cycloaddition instead of a self-crosslinking mechanism of polybutadiene. However, it is noteworthy that the reaction times for the crosslinking reactions of **PBD₂** are much longer than for the model system with 1-pentene (and longer than with **PBD₁**), which is the expected behavior when expanding a system from small molecules to polymers.[348] As noted in the literature section, the concen-
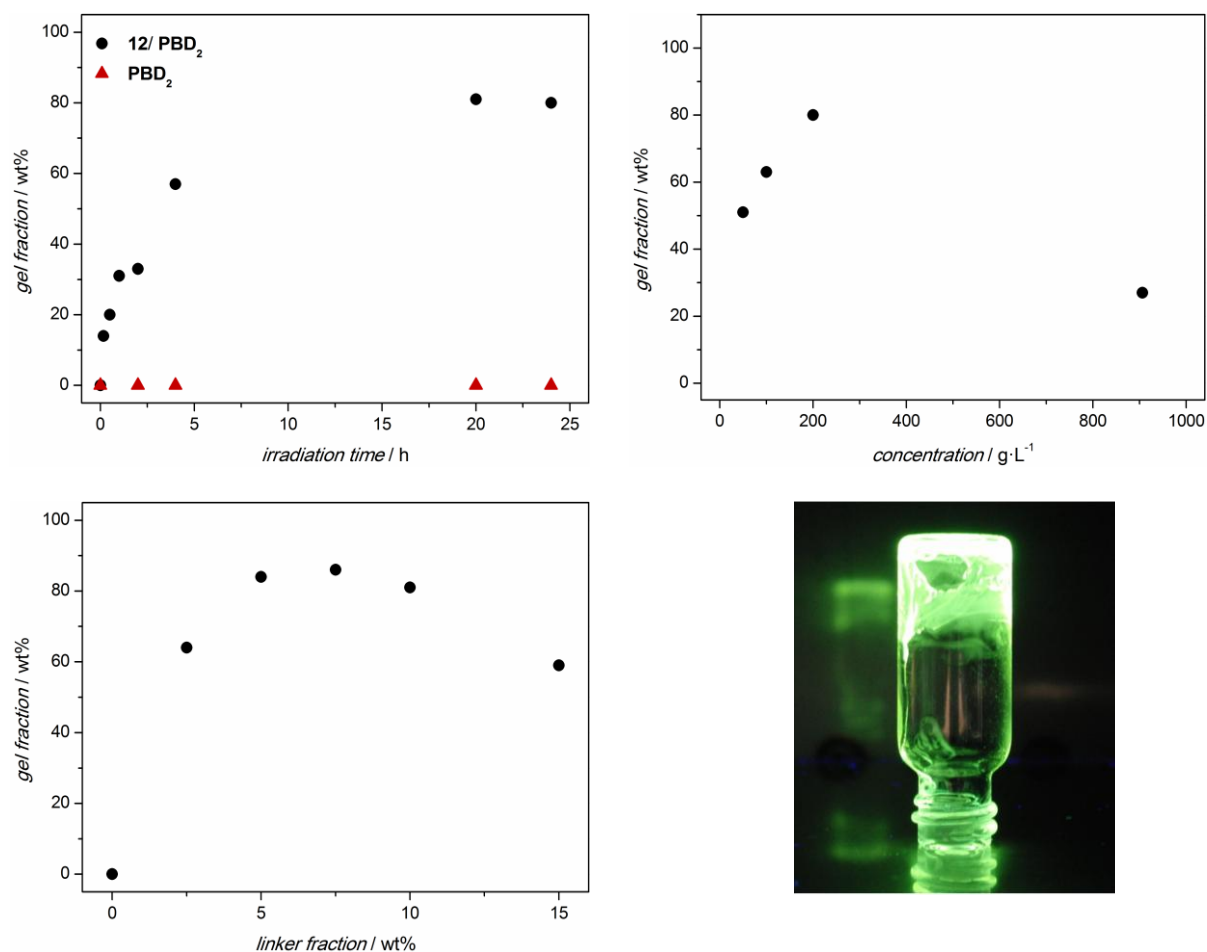
*Figure 7.3-4: Investigation of the crosslinking reaction of **PBD₂** varying the irradiation time (top, left), the concentration (top, right), and the di-linker fraction (bottom, left). Bottom right: images of fluorescent gels under excitation with a handheld TLC lamp (λ = 365 nm).*

tration of the linker/polymer mixture can strongly influence the outcome of the photoreaction. For instance, at high concentrations (50-200 $g \cdot L^{-1}$), crosslinking is more likely than at low concentrations, where single chain folding becomes favored.[132, 260] Importantly, the reaction was found to proceed in a reasonable timeframe when the presence of solvent is provided, whereas only limited conversion (27 % gel fraction) could be achieved in bulk (*Figure 7.3-4*, top right).

Applying the optimized conditions of the previous investigations (high concentration and 24 h of irradiation), the effect of changing linker content present in the reaction mixture was explored (*Figure 7.3-4*, bottom left). In contrast to the linker fraction study conducted with **PBD₁**, the high molecular weight of **PBD₂** enabled using relatively small quantities of **12** (2.5-7.5 wt%) for successful crosslinking. Gel fractions of 64-86 wt% could be achieved since a large molar excess of double bonds exists under optimal crosslinking conditions for **PBD₂**, reducing the possible side-

reactions. Increasing the linker fraction beyond 7.5 wt% (10-15 wt%) results in decreasing gel fractions of 80-59 wt%, which supports the theory that more soluble material-generating side-reactions occur when the amount of di-linker becomes too high. The success of the current crosslinking approach can also be visualized by a tube inversion test of the respective gels under excitation with a handheld TLC lamp (Figure 7.3-4, bottom right). Strong fluorescence is observed as well as insolubility of the gelatinous material which are crucial factors for successfully applying the crosslinking reaction for photo-patterning of substrates.

The spatial resolution of light-triggered reactions – besides excellent temporal control – is one of the primary reasons that (bio)chemists and material scientists apply photochemical methods. In order to demonstrate spatial control for the current crosslinking system, insoluble polybutadiene patterns were generated from a mixture of **PBD$_2$** and **12**. The photosensitive mixture was solvent casted on a glass slide, which was subsequently irradiated in the presence of a shadow mask. Employing shadow masks to introduce spatial control is a typical procedure for patterning surfaces.[142, 344, 349] Surface patterning was finally achieved by irradiating the solvent casted film consisting of **PBD$_2$** and **12** (5 wt%) covered with a shadow mask (depicting the KIT logo) with sunlight. All the non-crosslinked material which was protected from the sunlight was subsequently removed by immersing the entire glass substrate in a tetrahydrofuran (THF) bath. The irradiated – and thus crosslinked – sections of the film remained on the glass substrate exhibiting the fluorescent pattern. Thus, the desired spatial control of crosslinking system could be evidenced on a macroscopic scale (*Figure 7.3-5*). The sample preparation technique, which causes varying film thickness, results in slight irregularities in the light emission of the film. However, the simplicity of the sunlight-induced patterning setup as well as the facile workup emphasize the applicability of the herein reported crosslinking system.

*Figure 7.3-5: Image of fluorescent pattern produced by crosslinking a **12/PBD$_2$** film in the sunlight employing a shadow mask. The fluorescence was visualized using a handheld TLC lamp (λ_{max} = 365 nm).*

7.4 Summary

The current chapter introduces the investigation of a crosslinking system based on NITEC chemistry, which is applicable for the preparation of fluorescent patterns on substrates. A novel tetrazole containing photoreactive di-linker was designed to enable sunlight-induced reactions. Judicious selection of tetrazole substituents allowed to adjust the absorption range to be compatible to the UV emission of the sun. Moreover, the di-linker was designed to be soluble in high concentrations for efficient crosslinking reactions, which could be achieved by installing a tetra(ethylene glycol) spacer. The behavior of the novel tetrazole derivative was explored in a small molecule model study, monitored by ESI-MS, SEC, NMR, UV-vis, and fluorescence spectroscopy. Thus, the reaction of di-linker with 1-pentene was evidenced to yield the desired cycloadduct. A kinetic study revealed rapid progress of the photo-induced process achieving full conversion in 10-240 min depending on the irradiation source. Besides the off-line investigation via ESI-MS, the reaction progress could also be monitored by on-line fluorescence spectroscopy. Subsequent to the small molecule study, the light-triggered reaction of the di-linker with a low molar mass 1,2-polybutadiene was established. Based on SEC results, the reaction conditions were found to yield the best results employing a high molar amount of linker, at high concentrations, in 4 h. Furthermore, highly fluorescent polymer gels were produced via crosslinking of a 1,2-polybutadiene (100 kg·mol^{-1}). Gravimetric determination of the insoluble gel fraction was applied for exploring the crosslinking reaction kinetics, the influence of the molar ratio of di-linker as well as the reagent concentration dependence on the extent of crosslinking. Gel fractions of up to 86 % were obtained under optimized conditions (200 g·L^{-1} concentration, 7.5 wt% di-linker, 24 h irradiation time). Finally, fluorescent patterns were generated by crosslinking a solvent casted film of a polybutadiene/di-linker mixture under irradiation with sunlight for two hours employing a shadow mask. The well resolved pattern confirmed the excellent spatial control of the sunlight-induced NITEC-based crosslinking process.

8

CONCLUDING REMARKS

In contemporary chemical science, efficient and readily accessible conjugation techniques are highly valued. In particular, a continuously increasing impact is assigned to light-induced methods, which are suitable to access rapid and quantitative ligation in a spatially resolved fashion. However, to the best of the candidate's knowledge, few synthetic examples are highly efficient as required for modern polymer based processes. Therefore, continued advances are required to satisfy the increasingly challenging demands of (bio)chemists and material scientists.

The present thesis contains the development of novel light-triggered conjugation techniques as well as the improvement of existing methods by merging photochemistry and polymer science. Combining both of these extensive fields, various photochemical tools, including NITEC, azirine ligation, photoenols, and Paternò-Büchi reactions, were applied for polymerization processes, (reversible) polymer end-group modification, block copolymer synthesis as well as crosslinking of pre-existing polymer strands. Thus, advances are reported with regard to the reactivity of the photoreactive species enabling access to novel conjugates, the available excitation wavelengths, which allows for sunlight and visible light induction, and in general the broadened scope of the respective photo-induced techniques.

In Chapter 3, a novel polymerization procedure based on NITEC chemistry is reported. Therefore, photoreactive and profluorescent monomers were designed bearing a photosensitive tetrazole function as well as a suitable dipolarophile unit. UV-light irradiation of concentrated monomer solutions consequently triggers an ambient temperature step-growth polymerization process, which was found to adhere to Carothers' kinetics. In addition, strong fluorescence was observed for the resulting polymers stemming from the generated pyrazoline units incorporated in the polymer backbone.

Red-shifting the excitation wavelength for conjugation reactions into the visible light region of the electromagnetic spectrum has thus far only been achieved by photoredox catalysis. A catalyst-free system enabling ultra-rapid visible light-driven ligation is described in Chapter 4 of the present thesis. Therein, a photosensitive compound is presented which combines the absorption properties of a chromophore (pyrene) with the reactivity of azirine moieties allowing for efficient cycloaddition reactions with a multitude of reactants. Thus, small molecules were ligated as well as polymeric materials with reactive termini.

Chapter 5 includes an exploratory study evaluating the applicability of the Paternò–Büchi reaction for the reversible encoding of polymer end groups. The investigation is based on a poly(ethylene glycol) system, which was monitored in detail by NMR, ESI-MS and CID ESI-MS. Thus, the efficiency of three consecutive photochemical end group transformations – Paternò–Büchi reaction, photosensitized ring cleavage, an additional Paternò-Büchi reaction – was determined.

In Chapter 6, the extremely high reactivity of photoenols is applied for developing a novel conjugation tool which broadens the scope of controlled/living radical polymerization. Due to the enhanced affinity of the photoenol diene towards dipolarophiles, non-activated dithioesters – present in conventional polymers prepared via the RAFT technique – were accessible for hetero Diels–Alder reactions. The remarkable efficiency of the rapid ligation method enabled the synthesis of block copolymers of different monomer constitutions.

Since spatially resolved crosslinking is a progressive discipline in modern material science, a novel crosslinking system based on NITEC chemistry is provided in Chapter 7. By judiciously designing a di-functional tetrazole linker compound, the

reactivity as well as the excitation wavelength of the photolabil moiety could be adjusted allowing for the sunlight induced reaction with non-activated double bonds present in 1,2-polybutadienes. Thus, the fabrication of insoluble fluorescent surface patterns was enabled.

In summary, the present thesis describes significant advances in the field of light-induced polymer ligation. A series of newly developed techniques and the application of improved methods is demonstrated. By altering absorption properties, making use of substituent effects, and in general combining photochemical tools with contemporary challenges in polymer chemistry, examples for the broad scope of the herein reported systems were given. In particular, the advancement into the direction of sunlight and visible light triggered chemistry, which allows to avoid the biologically harmful UV-irradiation, is a remarkable achievement.

However, the major challenges of the present society remain unsolved. Despite the herein reported successfully improved properties of photochemical techniques, these advancements can only be viewed as a small step in the right direction. A significant amount of photochemical research and technological advances are still required until industrial processes can be driven by solar radiation. Similarly far from success appears the desirable goal of providing mankind with clean solar energy. Nevertheless, exploratory research and continuous advances towards sustainable processes are the crucial requirements for approaching these ultimate aims step by step.

9

EXPERIMENTAL SECTION

The experimental section contains more detailed information related to the synthetic and analytic procedures. Besides a list of materials (Section 9.1), details about the analytic instrumentation and methods are provided (Section 9.2). Finally, Section 9.3 contains the synthetic procedures accompanied with the corresponding analytic data of the species included in the present thesis.

9.1 Materials

Acetonitrile (MeCN, reagent grade, Chem-Supply), 1-acetyl pyrene (97 %, Aldrich), aluminum chloride (anhydrous, >99%, ROTH), anisidine (99 %, ABCR), benzoic acid (99.5 %, Sigma-Aldrich), benzyl maleimide (99 %, Aldrich), 11-bromo-1-undecanol (purum, Fluka), copper sulfate pentahydrate (99+ %, Acros), 2-cyanopropyl dithiobenzoate (CPDB, >97%, Sigma-Aldrich), cyclohexane (VWR, GPR RECTAPUR), dichloromethane (DCM, VWR, AnalaR NORMAPUR), dichloromethane (DCM, extra dry, 99.8 %, Arcos Organics), dicyclohexyl carbodiimide (DCC, 98 %, Aldrich), diethyl ester acetylene (95 %, Aldrich), diethyl ether (Et$_2$O, reagent grade, Fisher Chemical), diethyl fumarate (98 %, Aldrich), 4-dimethyl aminopyridine (4-DMAP, purum, >98 %, Fluka Analytical), 2,3-dimethyl anisole (97 %, Alfa-Aesar), dimethyl hydrazine (98 %, Aldrich), ethyl acetate (EA, VWR, AnalaR NORMAPUR), 1-ethyl-3-(3-dimethylaminopropyl) carbodiimide-hydrochloride (EDC-HCl, ≥99 % Carl Roth), formyl-benzoic acid (96 %, Acros Organics), hydrochloric acid (HCl, 37 %, Carl Roth), 2-hydroxyethyl acrylate (HEA, contains monomethyl ether hydroquinone as inhibitor, 96 %, Aldrich), iodo methane (MeI, stab. with copper foil, 99 %, Chem-Supply), magnesium sulfate (MgSO$_4$, ≥99 %, Carl Roth), methyl acrylate (stab. with monomethyl ether hydroquinone, 98 %, Aldrich), monoethyl fumarate (95 %, Aldrich), pentenoic acid (95 %, Aldrich), p-toluenesulfonyl hydrazide (98 %, Alfa Aesar), polybutadiene predominantly 1,2-addition (**PBD$_1$**, approx. 90 % 1,2-vinyl, Sigma-Aldrich), poly(ethylene glycol) monomethyl ether (M_n = 2000 g·mol^{-1}, Aldrich), potassium peroxodisulfate (97 %, Sigma-Aldrich), 1,3-propanediol (98 %, Aldrich), pyridine (99+ %, Alfa Aesar), silica gel (Geduran Si 60, 40-63 µm, for column chromatography, Merck), sodium chloride (NaCl, >99.8 %, Carl Roth), sodium hydride (65 % with petrol ether, Aldrich), sodium hydrogen carbonate (NaHCO$_3$, ≥99 %, Carl Roth), sodium nitrite (NaNO$_2$, 98 %, Alfa Aesar), sodium sulfate (NaSO$_4$, >99 %, Carl Roth), tetrahydrofuran (THF, extra dry, 99.5 %, stabilized, Acros Organics), thionyl chloride (SOCl$_2$, ReagentPlus, ≥99 %, Aldrich), toluene (reagent grade, Chem-Supply), and 1,5,7-triazabicyclo[4.4.0]dec-5-ene (TBD, Sigma-Aldrich) were used as received.

Methyl methacrylate (MMA, 99+ %, Acros), styrene (99 %, extra pure, Acros), and methyl acrylate (MA, 99+ %, Acros) were passed through a column of basic alumina

(VWR) to remove inhibitor and subsequently stored at -19 °C. 2,2'-Azobis(2-methylpropionitrile) (AIBN, Sigma-Aldrich) was recrystallized twice from methanol (MeOH, VWR) and subsequently stored at -19 °C. ε-Caprolactone (ε-CL, Sigma-Aldrich) was distilled from CaH_2 and stored over molecular sieves. Dichloromethane (DCM, VWR) and *N,N*-dimethyl formamide (DMF, 99+ %, Alfa Aesar) were dried and stored over $CaCl_2$ prior to use. Ethyl acetate (EA, reagent grade, Chem-Supply) and n-hexane (fraction, Chem-Supply) were distilled prior to use for column chromatography. 1,2-Polybutadiene (JSR RB_820, **PBD₂**) was kindly provided by NRC (Nordmann, Rassmann).

For GPC measurements tetrahydrofuran (THF, multisolvent, stabilized with BHT, Scharlau) and dimethyl acetamide (DMAC, CHROMASOLV Plus for HPLC, ≥99 %, Aldrich) were used as solvent as received. For photopolymerization reactions tetrahydrofuran (THF, multisolvent, stabilized with BHT, Scharlau), and dimethyl acetamide (DMAC, CHROMASOLV Plus for HPLC, ≥99 %, Aldrich) were used as solvents as received.

Chloroform-d_1 (CDCl$_3$, EURISO-TOP, 99.8 %,) and dimethyl sulfoxide-d_6 (DMSO-d_6, EURISO-TOP, 99.8 %,) were utilized for NMR measurements.

For ESI-MS measurements tetrahydrofuran (THF, multisolvent, stabilized with BHT, Scharlau), dichloromethane (DCM, ROTISOLV HPLC ultra gradient grade, Carl Roth), and methanol (MeOH, ROTISOLV HPLC ultra gradient grade, Carl Roth) were used as solvent and sodium trifluoro acetate (NaTFA, 98 %, Aldrich) was used as doping agent (5 μmol) as received.

Purification of the monomers of **M₁** and **M₂** as well as the polymerization sample preparation were conducted in a laboratory illuminated by a high pressure sodium lamp (SYLVANIA TWINARC, SHP-S, 50 W, E27) (amber light) due to the photosensitivity of the monomers. The photopolymerization reactions were performed utilizing crimp-top vials (VWR, crimp neck vial, 0.7 mL, 40×7 mm, clear glass, conical) and the corresponding caps (VWR, cap alu 8 mm, silicon white/PTFE red 1.3 mm).

9.2 Methods and Analytic Instrumentation

Nuclear magnetic resonance (NMR) spectroscopy. The synthesized compounds were analyzed *via* ^{1}H- and ^{13}C-NMR spectroscopy using a Bruker Avance 400 spectrometer (^{1}H, 400 MHz; ^{13}C, 101 MHz). Samples were dissolved in CDCl$_3$. The δ-scale was referenced with tetramethylsilane (δ = 0.00) as internal standard. Abbreviations used in the description of the materials' syntheses include singlet (s), doublet (d), triplet (t), quartet (q), broad multiplet (bm), and unresolved multiplet (m).

The synthesized compounds described in Chapter 4 were analyzed via ^{1}H- and ^{13}C-NMR spectroscopy using a Varian INOVA 400 (^{1}H, 400 MHz; ^{13}C, 101 MHz). The samples were dissolved in CDCl$_3$. The δ-scale was referenced with tetramethyl silane (δ = 0.00).

Electrospray ionization - mass spectrometry (ESI-MS). ESI-MS spectra were recorded on a LXQ mass spectrometer (ThermoFisher Scientific, San *J*ose, CA, USA) equipped with an atmospheric pressure ionization source operating in the nebulizer assisted electrospray mode. The instrument was calibrated in the *m/z* range of 195-1822 using a standard containing caffeine, Met-Arg-Phe-Ala acetate (MRFA) and a mixture of fluorinated phosphazenes (Ultramark 1621) (all from Aldrich). A constant spray voltage of 4.5 kV was used. Nitrogen was applied at a dimensionless sweep gas flow-rate of 2 (approx. 3 L·min^{-1}) and a dimensionless sheath gas flow-rate of 12 (approx. 1 L·min^{-1}) were applied. The capillary voltage, the tube lens offset voltage and the capillary temperature were set to 60 V, 110 V, and 300 °C respectively.

Orbitrap Electrospray-Ionization Mass Spectrometry (high-res ESI-MS). Mass spectra were recorded on a Q Excative (Orbitrap) mass spectrometer (Thermo Fisher Scientific, San Jose, CA, USA) equipped with an atmospheric pressure ionization source operating in the nebulizer assisted electrospray mode. The instrument was calibrated in the m/z range 150-2000 using a standard containing caffeine, Met-Arg-Phe-Ala acetate (MRFA) and a mixture of fluorinated phosphazenes (Ultramark 1621) (all from Aldrich). A constant spray voltage of 3.5 kV and a dimensionless sheath gas of 6 and a sweep gas flow rate of 2 were applied. The capillary voltage and the S-lens RF level were set to 68.0 V and 320 °C, respectively.

Size exclusion chromatography (SEC). To determine molecular weight distributions (MWD) a SEC system (Polymer Laboratories PL-GPC 50 Plus) comprised of an auto injector, a guard column (PLgel Mixed C, 50 × 7.5 mm) followed by three linear columns (PLgel Mixed C, 300 × 7.5 mm, 5 μm bead-size) and a differential refractive index detector was employed. THF was used as the eluent at 35 °C, with a flow rate of 1 mL·min^{-1}. The SEC system was calibrated using narrow poly(methyl methacrylate) standards ranging from 600 to 6 × 105 g mol^{-1} (Polymer Standards Service (PSS), Mainz, Germany). The resulting molecular weight distributions were determined by universal calibration using Mark-Houwink parameters for polystyrene ($K = 14.1 \times 10^{-5}$ dL g^{-1}, $\alpha = 0.7$).

Fluorescence and UV-vis spectroscopy. Fluorescence emission spectra were recorded for samples in quartz cuvettes loaded with a sample volume of 230 μL on a Varian Cary Eclipse Fluorescence Spectrometer. UV-visible spectroscopy was performed using a Varian Cary 300 Bio spectrophotometer featuring a thermostatted sample cell holder. Absorption spectra were measured for 1.0×10^{-4} mol L^{-1} samples in acetonitrile solution from 200 to 800 nm with a resolution of 1 nm and slit width of 2 nm in a 1 cm UV cuvette.

Analytical high performance liquid chromatography (HPLC) was carried out on a HPLC system using a Prep-C18 scalar column (4.6 X 150 mm, 10 μm) with a flow rate of 1 mL/min. A solvent mixture of THF/H$_2$O 50:50 was applied.

Photoreactions were carried out in a custom-built photoreactor equipped with 1,3, or 5 low pressure UV-lamps (*Figure 8.3-1*):

Arimed B6, Cosmedico GmBH, Stuttgart, Germany. Compact low-pressure fluorescent lamp, 36 W, λ_{max} = 320 nm (±30 nm).

Philips Cleo PL-L, Philips Deutschland GmBH. Compact low-pressure fluorescent lamp, 36 W, λ_{max} = 355 nm (±50 nm).

Philips TL01, Philips Deutschland GmBH. Philips Medical Therapy UV-B Narrow Band/01, 36W λ_{max} = 312 nm (±5 nm).
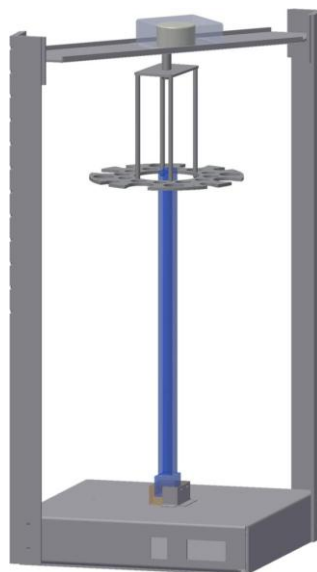
Figure 9.2-1: Illustration of the custom-built photoreactor employed in the current thesis.

The photo-reactions described in Chapter 4 were carried out in Rayonet Photoreactor using an LED system for irradiating the samples. Three light emitting diodes (Avonec, 410-420 nm, 3 W, actinic blue) with an emission angle of 120° grafted on cooling elements (Fischer, SK577-25SA - 50mm x 25mm) were set up triangularly on top of a magnetic stirrer. The samples were positioned above the LED setup at a distance of ~5 cm.

9.3 Synthetic Procedures

Synthesis of 4-((2-tosylhydrazono)methyl)benzoic acid (11). A mixture of 4-formyl-benzoic acid (6.558 g, 43.7 mmol, 1.0 eq) and *p*-toluenesulfonyl hydrazide (8.138 g, 43.7 mmol, 1.0 eq) in ethanol (100 mL) was heated to reflux for 30 min. The solution was diluted with water (100 mL) and the precipitate was filtered off. The solid was washed with aqueous ethanol (100 mL). Yield 14.5 g (98 %) ^{1}H-NMR (DMSO, 250 MHz) δ/ ppm: 13.07 (s, 1H, a), 11.68 (s, 1H, b), 7.96 (s, 1H, c), 7.94 (d, $^3J = 8.3$ Hz, 2H, d), 7.77 (d, $^3J = 8.2$ Hz, 2H, e), 7.66 (d, $^3J = 8.2$ Hz, 2H, f), 7.41 (d, $^3J = 8.3$ Hz, 2H, g), 2.35 (s, 3H, h). ^{13}C-NMR (DMSO, 100 MHz) δ/ ppm: 166.74 (a), 145.63 (b), 143.49 (c), 137.54 (d), 136.01 (e), 131.63 (f), 129.65 (g), 127.12 (h) 126.69 (i), 20.91 (k).
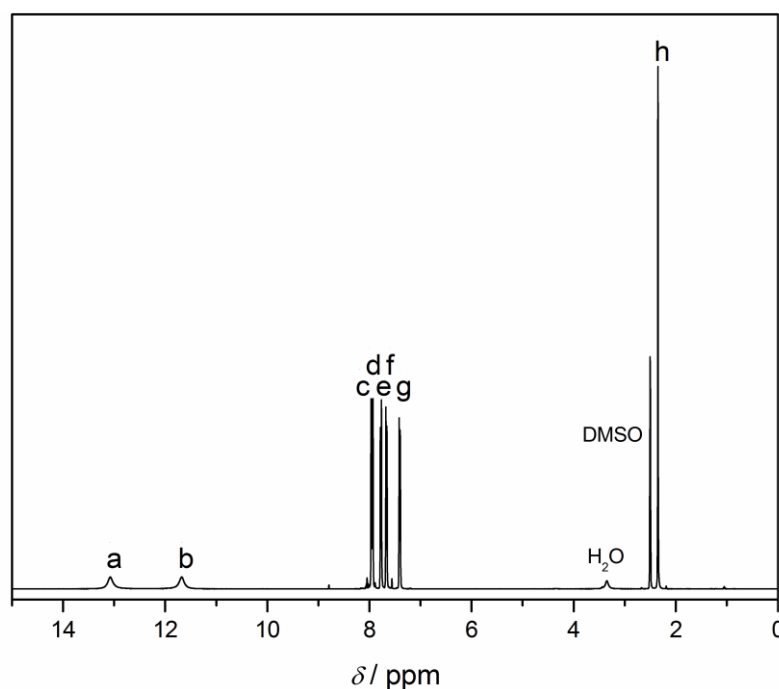
Figure 9.3-1: ^{1}*H-NMR spectrum of* **12** *recorded in CDCl₃.*

4-(2-(4-methoxyphenyl)-2H-tetrazol-5-yl)benzoic acid (1). Preparation of the diazonium salt: Anisidine (4 g, 32.5 mmol, 1.0 eq) was dissolved in a mixture of concentrated HCl (8.46 mL), water (26.9 mL) and EtOH (26.9 mL) and cooled to 0 °C. A cooled solution of sodium nitrite (2.241 g, 32.5 mmol, 1.0 eq) in water (13.45 mL) was added dropwise and stirred for 10 min at 0 °C.

Preparation of the tetrazole: The in situ generated diazonium salt solution was added dropwise to a solution of **12** (10.34 g, 32.5 mmol, 1.0 eq) in pyridine (200 mL) at -10 °C to -5 °C over a period of 45 min. After complete addition the solution was stirred at 0 °C for 30 min and at ambient temperature overnight. The turbid solution was poured into HCl-solution (10 %, 500 mL), the precipitate was filtered off and washed with EtOH (250 mL). Yield: 6.2 g (65 %). ^{1}H-NMR (DMSO, 400 MHz) δ/ ppm: 13.23 (s, 1H, a), 8.24 (d, ^3J = 8.1 Hz, 2H, b), 8.13 (d, ^3J = 8.1 Hz, 2H, c), 8.05 (d, ^3J = 8.8 Hz, 2H, d), 7.20 (d, ^3J = 8.8 Hz, 2H, e), 3.86 (s, 3H, f). ^{13}C-NMR (DMSO, 100 MHz) δ/ ppm: 166.63 (a), 163.43 (b), 160.40 (c), 132.55 (d), 130.24 (e), 130.15 (f), 129.41 (g), 126.59 (h) 121.59 (i), 115.02 (k), 55.62 (k).
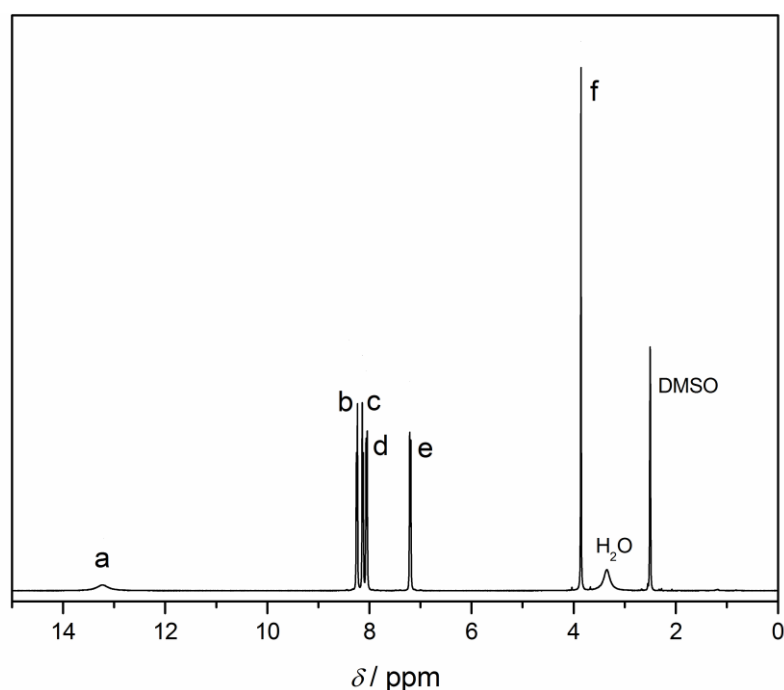
*Figure 9.3-2: ^{1}H-NMR spectrum of **1** recorded in CDCl$_3$.*

Synthesis of (2-(Acryloyloxy)ethyl 4-(2-(4-methoxyphenyl)-2*H***-tetrazol-5-yl)benzoate) (M₁)**. **1** (3.00 g, 10.1 mmol, 1.0 eq) was suspended in dry THF (80 mL) and SOCl$_2$ (12.05 g, 7.34 mL, 101.3 mmol, 10.0 eq) was added under inert atmosphere. The mixture was heated to reflux (75 °C) for 3.5 h and the volatiles were subsequently removed under reduced pressure. The residue was dissolved two times in dry THF (40 mL) and dried in vacuum to remove the excess of SOCl$_2$. The resulting product (3.10 g, 9.86 mmol, 1.0 eq) was dissolved in dry THF (80 mL) and added dropwise to a cooled solution (0 °C) of 2-hydroxyethyl acrylate (HEA, 11.5 g, 11.3 mL, 98.6 mmol, 10.0 eq) and pyridine (2.92 g, 3.00 mL, 37.0 mmol, 3.8 eq) in

dry THF (15 mL). After complete addition, the reaction mixture was stirred at 0 °C for an additional hour before it was stirred at ambient temperature overnight. All purification steps were carried out in a yellow light laboratory using a high pressure sodium lamp (refer to the *Methods section*). The precipitate was subsequently removed by filtration. The solution was diluted with DCM (300 mL) and washed 2 times with HCl (5 %, 2 × 130 mL), water (2 × 130 mL) and brine (2 × 130 mL). The organic phase was dried over $MgSO_4$ and the volatiles were removed under reduced pressure. The crude monomer **M$_1$** was washed two times with cold ethanol and subsequently dried under reduced pressure. The pure monomer M_1 was obtained by column chromatography (silica gel, CH/EA (1:1)) as a white solid; yield: 0.75 g (19 %). ^{1}H NMR (CDCl$_3$, 400 MHz) δ/ ppm: 8.33 (d, J^3 = 8.6 Hz, 2H, a), 8.19 (d, J^3 = 8.7 Hz, 2H, b), 8.11 (d, J^3 = 9.2 Hz, 2H, c), 7.07 (d, J^3 = 9.2 Hz, 2H, d), 6.47 (m, 1H, e), 6.17 (m, 1H, f), 5.88 (m, 1H, g), 4.60 (m, 4H, h, i), 3.90 (s, 3H, k). ^{13}C NMR (CDCl$_3$, 100 MHz) δ/ ppm: 166.08 (C, a), 165.92 (C, b), 164.22 (C, c), 160.85 (C, d), 131.64 (C, e), 130.47 (C, f), 128.13 (C, g), 127.08 (C, h), 121.61 (C, i), 114.89 (C, k), 63.09 (C, l), 62.34 (C, m), 55.83 (C, n). Exact mass: m/z_{theo} = 417.12; m/z_{exp} = 417.25.
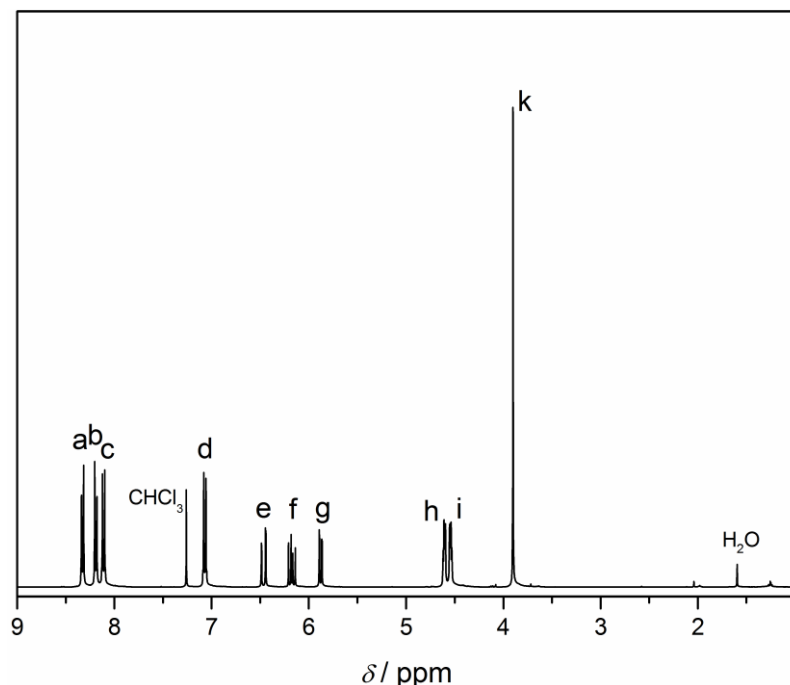
Figure 9.3-3: ^{1}H-NMR spectrum of **M$_1$** recorded in CDCl$_3$.

Synthesis of 3-hydroxypropyl fumarate (2). Monoethyl fumarate (10.0 g, 87.6 mmol, 1.0 eq), 1,3-propanediol (25.3 mL, 26.6 g, 350 mmol, 4.00 eq), and 4-dimethylaminopyridine (DMAP, 214 mg, 17.5 mmol, 0.02 eq) were dissolved in dry THF (200 mL). The solution was cooled to 0 °C in an ice bath and 1-ethyl-3-(3-dimethylaminopropyl) carbodiimide-hydrochloride (EDC-HCl, 21.8 g, 114 mmol, 1.3 eq) was added portion-wise to the stirred solution. After complete addition, the reaction mixture was stirred at 0 °C for an additional hour before it was stirred at ambient temperature overnight. The solvent was removed under reduced pressure and the residue was dissolved in diethyl ether (400 mL). The organic layer was washed two times with HCl (5 %, 3×150 mL), saturated $NaHCO_3$ solution (3×150 mL), and distilled water (3×150 mL). The organic phase was dried over $MgSO_4$ and the volatiles were removed under reduced pressure. The crude product was purified via column chromatography (silica gel, CH/EA (1:1)) to afford a light yellow oil; yield: 4.48 g (25 %). ^1H NMR ($CDCl_3$, 400 MHz) δ/ ppm: 6.83 (s, 2H, a), 4.34 (t, $J^3 = 6.2$ Hz, 2H, b), 4.24 (q, $J^3 = 7.1$ Hz, 2H, c), 3.71 (m, 2H, d), 2.05 (bs, 1H, e), 1.91 (p, $J^3 = 6.2$ Hz, 2H, f), 1.30 (t, $J^3 = 7.1$ Hz, 3H, g). ^{13}C NMR ($CDCl_3$, 100 MHz) δ/ ppm: 165.39 (C, a), 165.03 (C, b), 134.09 (C, c), 133.37 (C, d), 62.34 (C, e), 61.52 (C, f), 59.05 (C, g), 31.64 (C, h), 14.18 (C, i).
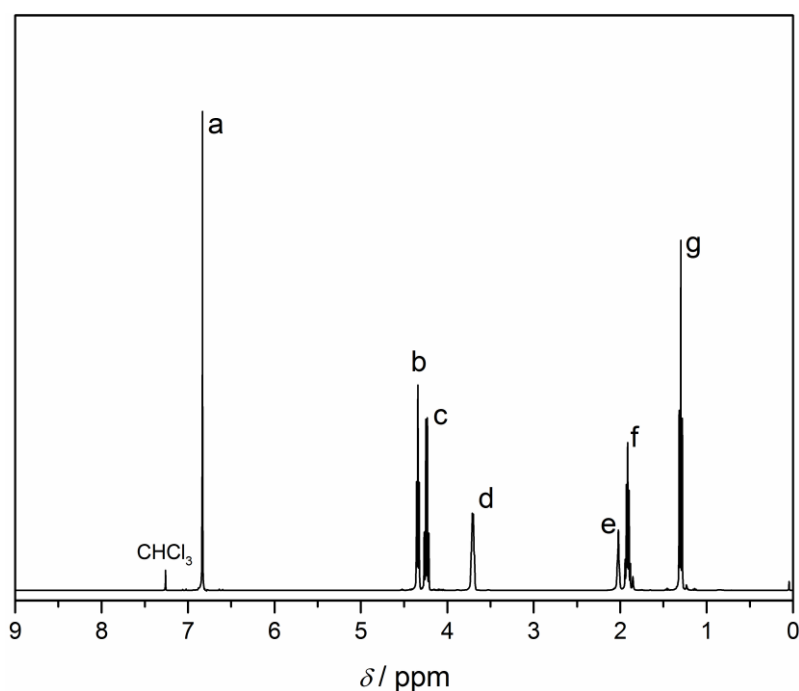
Figure 9.3-4: ^1H-NMR spectrum of **2** recorded in $CDCl_3$.

Synthesis of Ethyl 3-(4-(2-(4-methoxyphenyl)-2*H*-tetrazol-5-yl)benzoyloxy) propyl fumarate (M₂). (3.00 g, 10.1 mmol, 1.0 eq) was suspended in dry THF (80 mL) and $SOCl_2$ (12.05 g, 7.34 mL, 101.3 mmol, 10.0 eq) was added under inert atmosphere. The mixture was heated to reflux (75 °C) for 3.5 h and the volatiles were subsequently removed under reduced pressure. The residue was dissolved two times in dry THF (40 mL) and dried in vacuum to remove the excess of $SOCl_2$. The resulting product (2.30 g, 7.31 mmol, 1.0 eq) was dissolved in dry THF (60 mL) and added dropwise to a cooled solution (0 °C) of ethyl 3-hydroxypropyl fumarate (refer to step 1, 4.43 g, 21.9 mmol, 3.0 eq) and pyridine (2.17 g, 2.21 mL, 27.4 mmol, 3.8 eq) in dry THF (12 mL) via a syringe. After complete addition, the reaction mixture was stirred at 0 °C for an additional hour before it was stirred at ambient temperature overnight. All purification steps were carried out in a yellow light laboratory using a high pressure sodium lamp (refer to the *Materials section*). The precipitate was subsequently removed by filtration. The solution was diluted with DCM (250 mL) and washed 2 times with HCl (5 %, 2 × 100 mL), water (2 × 100 mL) and brine (2 × 100 mL). The organic phase was dried over $MgSO_4$ and the volatiles were removed under reduced pressure. The crude monomer M₂ was washed two times with cold ethanol to remove major impurities and subsequently dried under reduced pressure. The pure monomer M₂ was obtained by column chromatography (silica gel, CH/EA: 1/1) as a white solid; yield: 1.41 g (40 %). ^{1}H NMR ($CDCl_3$, 400 MHz) δ/ ppm: 8.33 (d, J^3 = 8.3 Hz, 2H, a), 8.18 (d, J^3 = 8.3 Hz, 2H, b), 8.12 (d, J^3 = 9.1 Hz, 2H, c), 7.08 (d, J^3 = 9.1 Hz, 2H, d), 6.86 (s, 2H, e), 4.48 (t, J^3 = 6.2 Hz, 2H, f), 4.41 (t, J^3 = 6.2 Hz 2H, g) 4.25 (q, J^3 = 7.1 Hz, 2H, h), 3.91 (s, 3H, i), 2.22 (p, J^3 = 6.2 Hz, 2H, k), 1.31 (t, J^3 = 7.1 Hz, 3H, l). ^{13}C NMR ($CDCl_3$, 100 MHz) δ/ ppm: 166.04 (C, a), 164.99 (C, b), 164.24 (C, c), 160.86 (C, d), 134.26 (C, e), 133.25 (C, f), 131.69 (C, g), 130.36 (C, h), 127.09 (C, i), 121.63 (C, k), 114.91 (C, l), 61.90 (C, m), 55.85 (C, n), 28.17 (C, o), 14.24 (C, p). Exact mass: m/z_{theo} = 503.15; m/z_{exp} = 503.25.
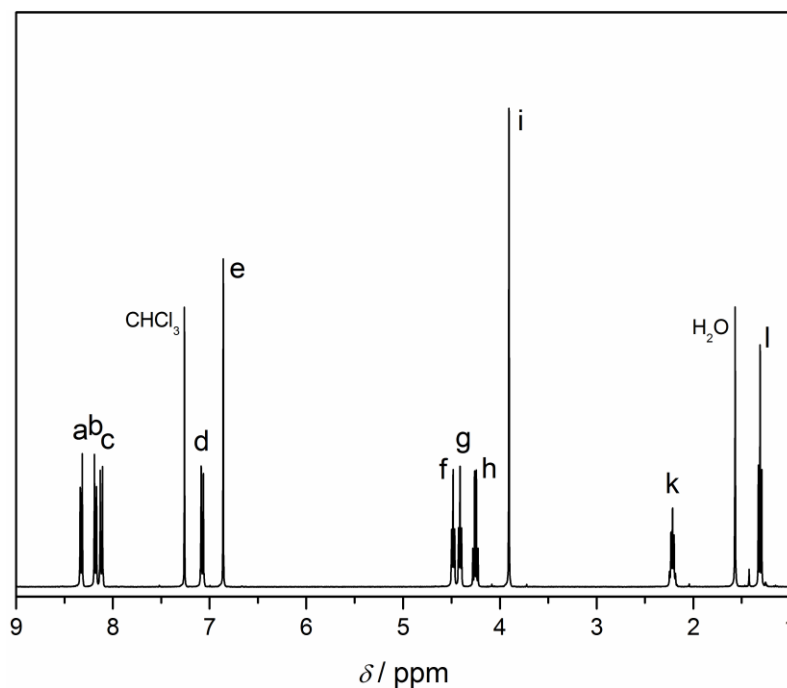
Figure 9.3-5: ^{1}*H-NMR spectrum of* **M$_2$** *recorded in CDCl$_3$.*

General photo-induced polymerization procedure for the monomers M$_1$ and M$_2$ (P$_1$, P$_2$). All photopolymerization samples were prepared in crimp-top vials (refer to the *Materials section*) containing 2 mg **M$_1$** or **M$_2$** and 20 µL THF or DMAC ($c = 100$ mg·mL^{-1}) if not otherwise stated. The vials were sealed with appropriate caps and directly irradiated in a custom-built photoreactor. After the desired reaction time, the solvent of each sample was removed under reduced pressure. Subsequently, NMR spectra (in CDCl$_3$) and GPC (in THF or DMAC) were measured.

Synthesis of 3-(pyren-1-yl)-2*H*-azirine (3). 1-acetyl pyrene (2.00 g, 8.29 mmol, 1.0 eq) was dissolved in toluene (15 mL) before N,N-dimethyl hydrazine (0.98 g, 24.90 mmol, 3.0 eq) and a catalytic amount of trifluoroacetic acid (0.01 mL) were added to the solution. The mixture was heated to reflux for 5 h and allowed to cool to ambient temperature. The solution was diluted with toluene (35 mL), washed with water (3 × 50 mL) and the organic layer was dried over Na$_2$SO$_4$. The volatiles were subsequently removed under reduced pressure. The crude yellow product was used for further synthesis without additional purification.

The crude product of the previous step was dissolved in iodomethane (10 mL) and stirred at 40 °C overnight. The resulting suspension was diluted with diethyl ether

(100 mL). The precipitate was filtered off and washed with additional diethyl ether (100 mL). The crude precipitate was dissolved in dichloromethane (100 mL) before diethyl ether (100 mL) was added dropwise until the product precipitated. The pure product was obtained by filtration as a yellow powder and was of sufficient purity to be used in the next step. Yield: 1.5 g (55 %)

The hydrazonium salt of the previous step (0.70 g, 1.63 mmol, 1.0 eq) was dissolved in DMF (dry, 10 mL) and the resulting solution was cooled to 0 °C in an ice-bath. Sodium hydride (60 %, 0.26 g, 6.50 mmol, 4.0 eq) was added in one portion and the mixture was stirred at 0 °C for 1 h. Diethyl ether (200 mL) was added to the reaction mixture and the insoluble material was removed by filtration. The filtrate was subsequently washed with water (5 × 100 mL), dried over Na_2SO_4 and the volatiles were removed. The crude product was purified by column chromatography using hexane/ethyl acetate (gradient 9:1 to 5:1) as an eluent. The pure product was obtained as yellow powder. Yield: 80 mg (20 %). ^{1}H NMR ($CDCl_3$), δ / ppm: 9.18 (d, J = 9.2 Hz, 1 H, **a**); 8.37 (d, J = 7.9 Hz, 1 H, **b**); 8.38-8.17 (m, 5 H, **c**); 8.09-8.05 (m, 2 H, **d**); 1.96 (s, 2 H, **e**). ^{13}C NMR ($CDCl_3$): δ = 164.84 (s, 1 C); 134.33 (s, 1 C); 131.09 (s, 1 C); 130.89 (s, 1 C); 130.58 (s, 1 C), 129.99 (s, 2 C); 129.59 (s, 1 C); 127.09 (s, 1 C); 126.73 (s, 1 C); 126.65 (s, 1 C), 126.51 (s, 1 C); 124.56 (s, 1 C); 124.37 (s, 1 C); 123.96 (s, 1 C); 123.54 (s, 1 C); 117.27 (s, 1 C); 17.78 (s, 1 C).
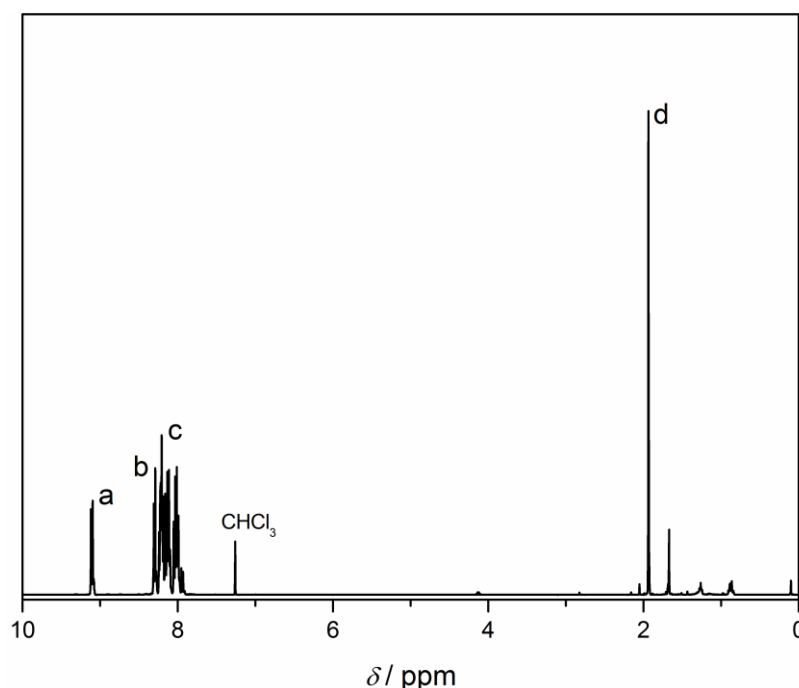
Figure 9.3-6: ^{1}*H-NMR spectrum of* **3** *recorded in CDCl₃.*

Synthesis of fumarate end-capped poly(ethylene glycol) (P₃). Monoethyl fumarate (576 mg, 4.0 mmol, 4.0 eq), poly(ethylene glycol) monomethyl ether (2.00 g, 1.0 mmol, 1.0 eq), DCC (900 mg, 4.4 mmol, 4.4 eq), and DMAP (50.0 mg, 0.4 mmol, 0.4 eq) were dissolved in DCM (dry, 10 mL). The mixture was stirred at ambient temperature for 48 h before the precipitate was filtered off and the solvent removed under reduced pressure. The polymer was purified by threefold precipitation in cold Et₂O yielding 1.6 g (75 %) of pure product. ^{1}H NMR(CDCl₃), δ / ppm: (s, 2 H, **a**); 4.34 (t, J = 4.8 Hz, 2 H, **b**); 4.25 (q, J = 7.1 Hz, 2 H, **c**); 3.82-3.73 (m, 4 H, **d**); 3.63 (bs, 180 H, **e**); 3.55-3.44 (m, 4 H, **f**); 3.37 (s, 3 H, **g**); 1.31 (t, J = 7.1 Hz, 3 H, **h**).
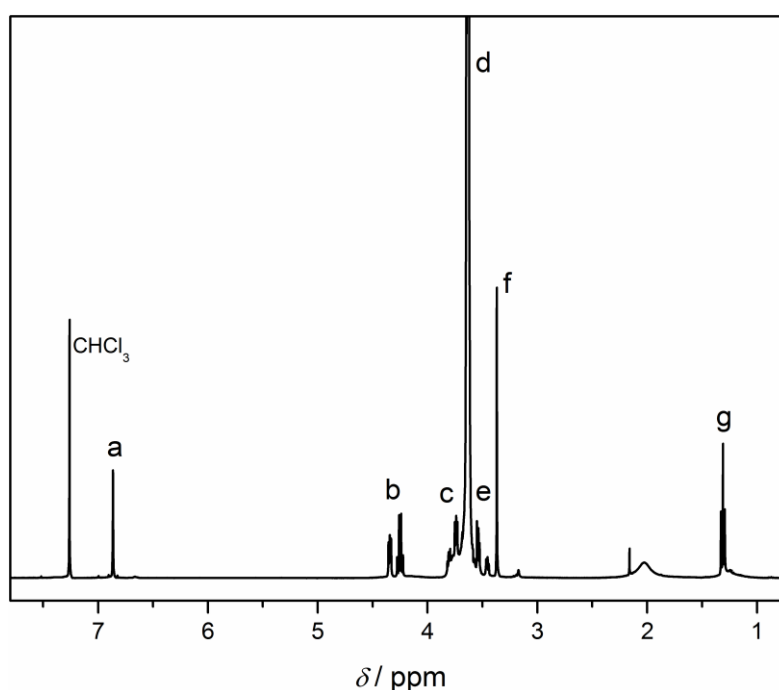
*Figure 9.3-7: ^{1}H-NMR spectrum of **P₃** recorded in CDCl₃.*

Synthesis of alkene end-capped poly(ethylene glycol) (P₄). Petenoic acid (1.10 g, 5.0 mmol, 5.0 eq), poly(ethylene glycol) monomethyl ether (2.00 g, 1.0 mmol, 1.0 eq), DCC (1.13 g, 5.5 mmol, 5.5 eq), and DMAP (62.5 mg, 0.5 mmol, 0.5 eq) were dissolved in DCM (dry, 10 mL). The mixture was stirred at ambient temperature for 72 h before the precipitate was filtered off and the solvent removed under reduced pressure. The polymers were purified by threefold precipitation in cold Et₂O yielding 1.4 g (70 %) of pure product. ^{1}H NMR(CDCl₃), δ / ppm: 5.86-5.76 (m, 1 H, **a**); 5.07-4.98 (m, 2 H, **b**); 4.22 (t, J = 4.8 Hz, 2 H, **c**); 3.82-3.67 (m, 4 H, **d**); 3.63 (bs, 190 H, **e**); 3.56-3.44 (m, 4 H, **f**); 3.37 (s, 3 H, **g**); 2.46-2.34 (m, 4 H, **h**).
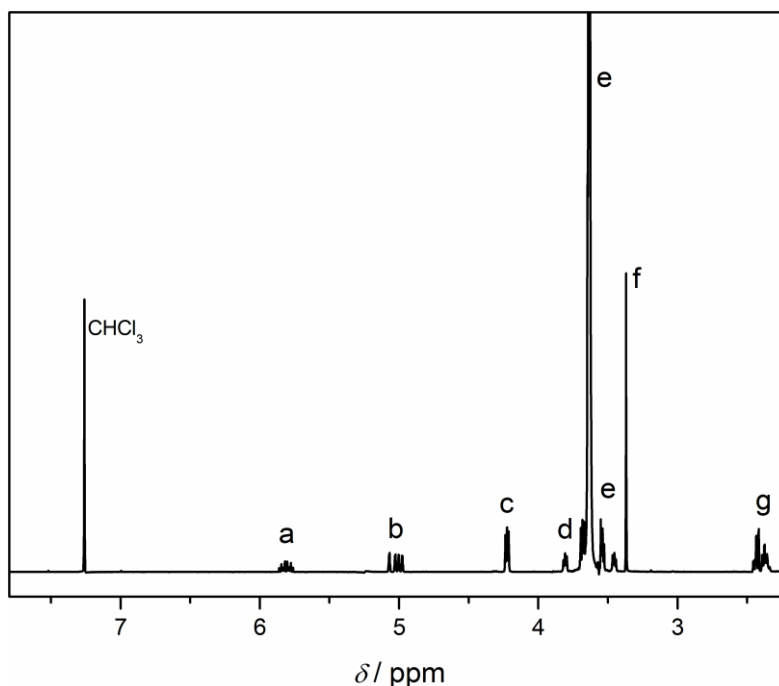
*Figure 9.3-8: ^{1}H-NMR spectrum of **P$_4$** recorded in CDCl$_3$.*

Visible light-induced small molecule synthesis. Dipolarophile (46.0 µmol, 5.0 eq) and **3** (5.0 mg, 9.2 µmol, 1.0 eq) were weighed into 50 mL round bottom flasks. The materials were dissolved in acetonitrile (15 mL) and placed in the photoreactor, where they were irradiated for the desired reaction time under continuous stirring. Samples for HPLC analysis (0.5 mL) were taken from the reaction mixture immediately after dissolving, and subsequently after the required reaction times. The samples were subjected to HPLC analysis without any purification steps. The volatiles were removed under reduced pressure and the product was separated from the excess of dipolarophile by column chromatography. Isolated yields: **4** (90 %), ^{1}H NMR (CDCl$_3$), δ / ppm: 9.02 (d, J = 9.4 Hz, 1 H, a); 8.40 (d, J = 8.1 Hz, 1 H, b); 8.26-8.23 m, 3 H, c); 8.17-8.03 (m, 4 H, c); 7.28-7.14 (m, 5 H, d); 4.99-4.79 (m, 1 H, e); 4.82-4.66 (m, 2 H, e); 4.62 (d, J = 14.2 Hz, 1 H, e); 4.51 (d, J = 14.2 Hz, 1 H, e). ^{13}C NMR (CDCl$_3$), δ / ppm: 177.73 (s, 1 C); 172.89 (s, 1 C); 167.76 (s, 1 C); 135.32 (s, 1 C); 132.92 (s, 1 C); 131.15 (s, 1 C); 131.58 (s, 1 C); 129.99 (s, 1 C); 129.10 (s, 1 C); 129.06 (s, 1 C); 129.00 (s, 1 C); 128.66 (s, 1 C); 128.47 (s, 1 C); 128.19 (s, 1 C); 127.99 (s, 2 C); 127.25 (s, 1 C); 126.23 (s, 1 C); 126.00 (s, 1 C); 125.72 (s, 1 C); 125.60 (s, 1 C); 125.09 (s, 1 C); 124.82 (s, 1 C); 124.38 (s, 1 C); 124.03 (s, 1 C); 64.37 (s, 1 C); 58.50 (s, 1 C); 43.94 (s, 1 C); 42.63 (s, 1 C). **5** (25 %), ^{1}H NMR (CDCl$_3$), δ / ppm: 8.79 (d, J = 9.6 Hz, 1 H, a); 8.55 (d, J = 9.3 Hz, 1 H, b); 8.23-8.02

m, 7 H, c); 4.98-3.76 (m, 8 H, d); 1.38-0.74 (m, 6 H, e). **6** (50 %), ^{1}H NMR (CDCl$_3$), δ / ppm: 9.22 (d, J = 9.4 Hz, 1 H, a); 8.24-8.02 (m, 8 H, b+c); 4.70-4.49 (m, 2 H, d); 3.80 (s, 3 H, e); 3.77-3.68 (m, 1 H, d); 3.53-3.43 (m, 2 H, d). ^{13}C NMR (CDCl$_3$), δ / ppm: 177.73 (s, 1 C); 172.89 (s, 1 C); 167.76 (s, 1 C); 135.32 (s, 1 C); 132.92 (s, 1 C); 131.15 (s, 1 C); 131.58 (s, 1 C); 129.99 (s, 1 C); 129.10 (s, 1 C); 129.06 (s, 1 C); 129.00 (s, 1 C); 128.66 (s, 1 C); 128.47 (s, 1 C); 128.19 (s, 1 C); 127.99 (s, 2 C); 127.25 (s, 1 C); 126.23 (s, 1 C); 126.00 (s, 1 C); 125.72 (s, 1 C); 125.60 (s, 1 C); 125.09 (s, 1 C); 124.82 (s, 1 C); 124.38 (s, 1 C); 124.03 (s, 1 C); 64.37 (s, 1 C); 58.50 (s, 1 C); 43.94 (s, 1 C); 42.63 (s, 1 C), **7** (50 %), ^{1}H NMR (CDCl$_3$), δ / ppm: 8.80 (bs, 1 H, a); 8.23-7.96 (m, 9 H, b); 7.53 (d, J = 2.6 Hz ,1 H, c); 4.34 (q, J = 7.1 Hz, 2 H, d); 3.95 (q, J = 7.1 Hz, 2 H, d); 1.37 (t, J = 7.1 Hz, 3 H, e); 0.77 (t, J = 7.1 Hz, 3 H, e).
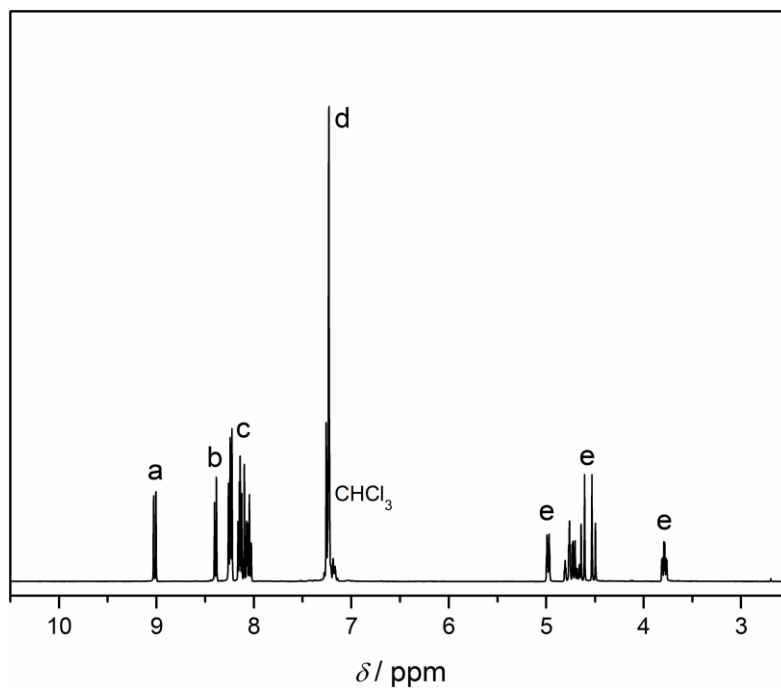
*Figure 9.3-9: ^{1}H-NMR spectrum of **5** recorded in CDCl$_3$.*
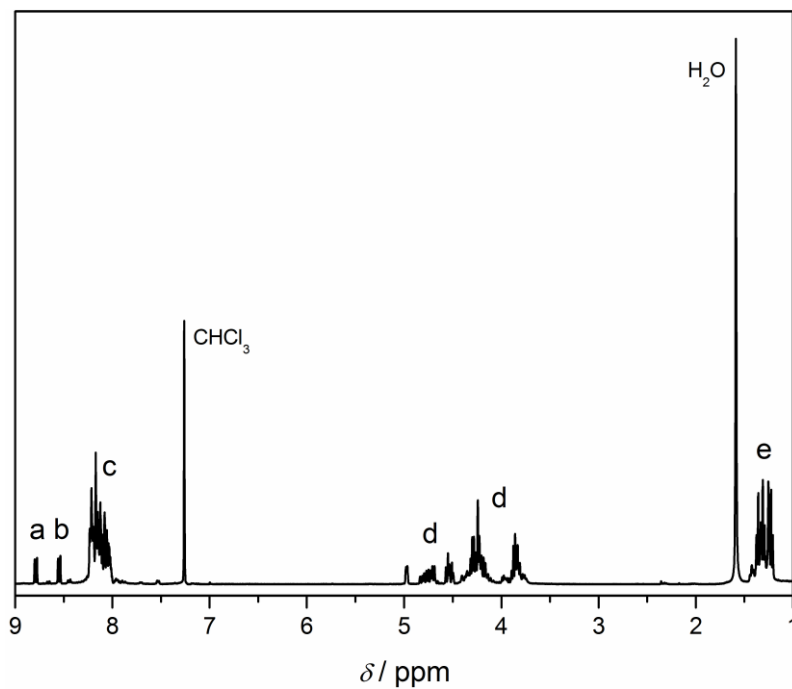
Figure 9.3-10: ^{1}H-NMR spectrum of 6 recorded in CDCl$_3$.
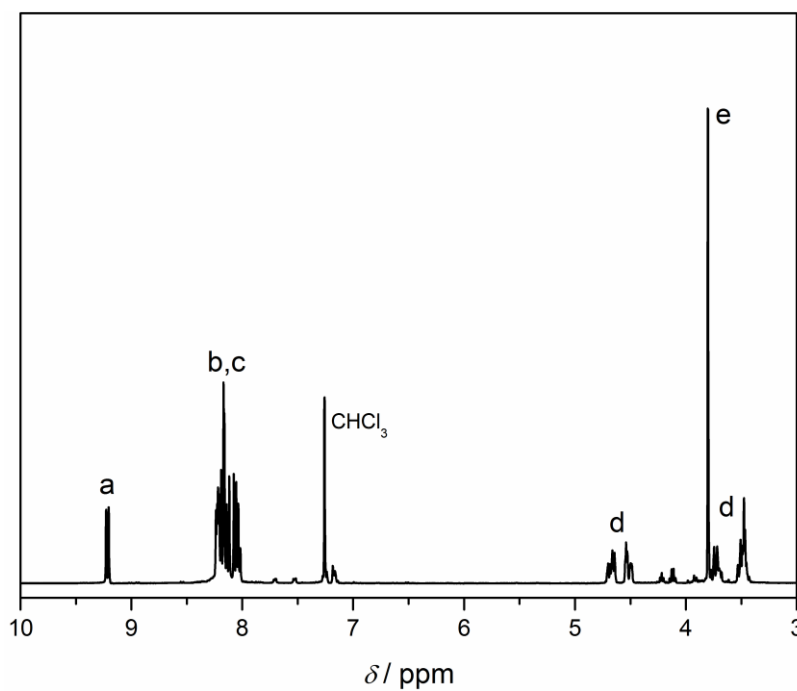
Figure 9.3-11: ^{1}H-NMR spectrum of 7 recorded in CDCl$_3$.

159
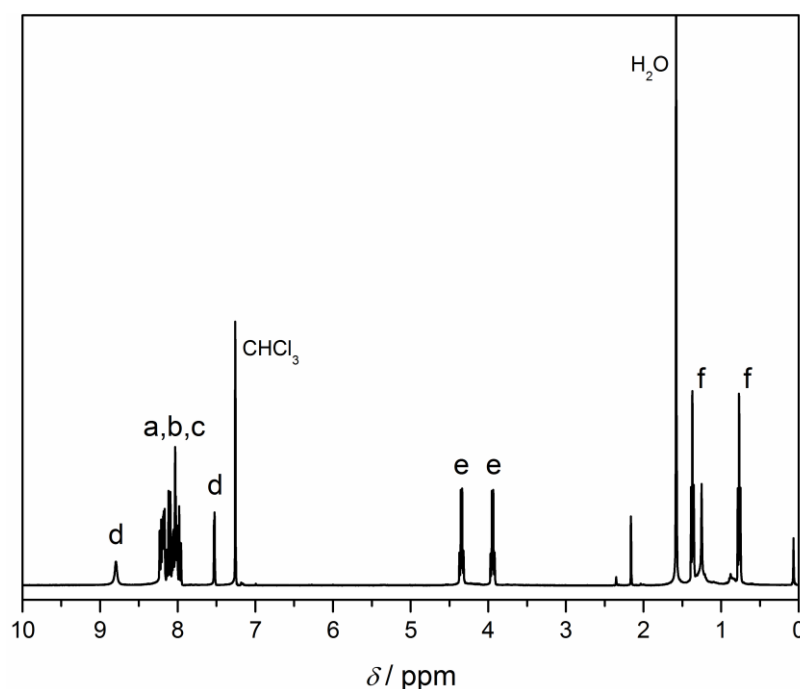
*Figure 9.3-12: ^{1}H-NMR spectrum of **8** recorded in CDCl$_3$.*

Visible light-induced polymer ligation. Functionalized poly(ethylene glycol) (**P$_5$-P$_8$**, 0.45 μmol, 1.0 eq) and **3** (1.0 mg, 2.3 μmol, 5.0 eq) were weighed up into a headspace vial (Pyrex, dia. 20 mm). The vial was sealed with a crimp top containing a PTFE inner liner. The solids were dissolved in acetonitrile (5 mL) and placed in the photoreactor, where they were stirred for 1 h in the dark before the lamps were switched on. Samples for ESI-MS analysis (0.1 mL) were taken from the reaction mixture immediately after dissolving, before the lamps were switched on, and subsequently after the preset reaction times. The samples were subjected to ESI-MS without any purification steps. **P$_6$** was subsequently purified by twofold precipitation in cold Et$_2$O and subjected to NMR analysis. ^{1}H NMR(CDCl$_3$), δ / ppm: 8.81-8.78 (m, 1 H, a); 8.46-8.44 (m, 1 H, b); 8.23-7.97 (m, 7 H, c); 5.07-3.93 (m, 4 H, c); 3.87-3.70 (m, 4 H, d); 3.63 (bs, 180 H, e); 3.57-3.45 (m, 4 H, f); 3.37 (s, 3 H, g); 3.19-2.95 (m, 4 H, h); 1.43-1.16 (m, 3 H, i).
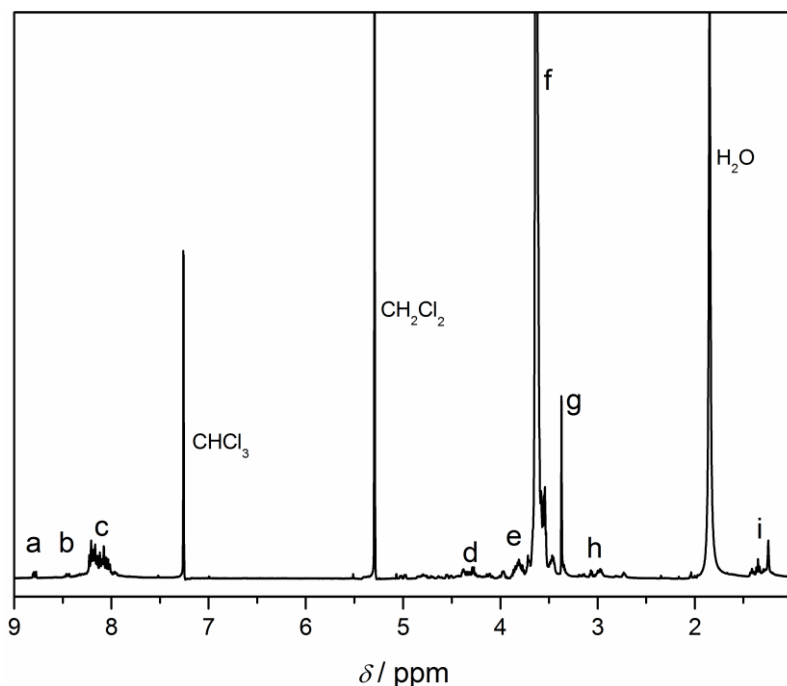
Figure 9.3-13: ^{1}H-NMR spectrum of P_6 recorded in CDCl$_3$.

Synthesis of aldehyde terminal poly(ethylene glycol) (P$_9$). Poly(ethylene glycol) methyl ether (1.00 g, 0.5 mmol, 1.0 eq), 4-carboxy benzaldehyde (300 mg, 2.0 mmol, 4.0 eq), and DMAP (24 mg, 0.2 mmol, 0.4 eq) were dried in vacuum and subsequently dissolved in a mixture of DMF (4 mL) and DCM (4 mL). DCC (450 mg, 2.2 mmol, 4.4 eq) was dissolved in dry DCM (3 mL), added to the dissolved reactants and the mixture was stirred for 48 h at ambient temperature. The solvent was removed under reduced pressure and the residue was suspended in DCM. The dissolved product was purified by twofold precipitation in cold ether (yield: 520 mg, 50 %). ^{1}H NMR(CDCl$_3$), δ / ppm: 10.10 (s, 1 H, a); 8.21 (d, ^3J = 8.3 Hz, 2 H, b); 7.94 (d, ^3J = 8.4 Hz, 2 H, c); 4.50 (t, ^3J = 4.8 Hz, 2 H, d); 3.84 (t, ^3J = 4.8 Hz, 2 H, e); 3.63 (bs, 180 H, f); 3.50-3.42 (m, 2 H, g); 3.37 (s, 3 H, h).
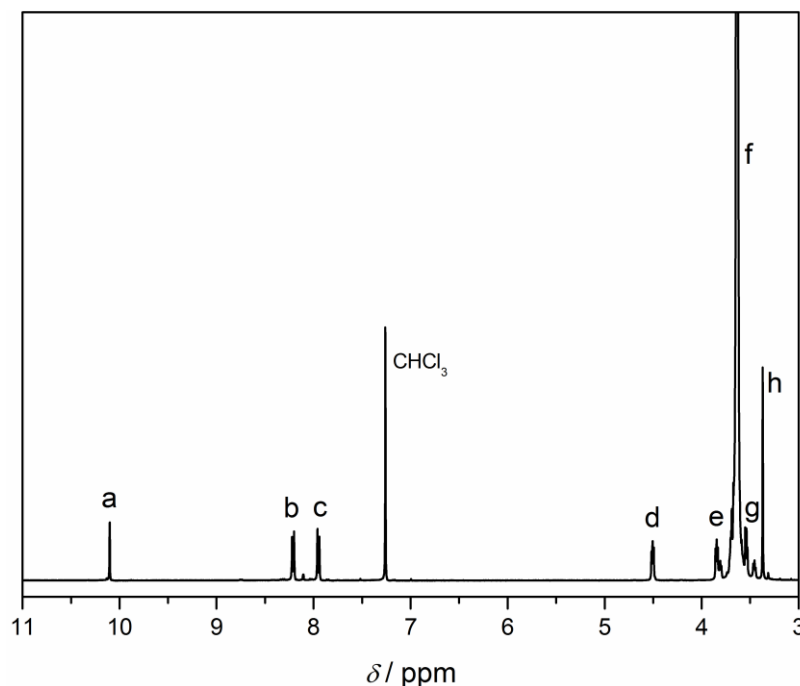
*Figure 9.3-14: ^{1}H-NMR spectrum of **P$_9$** recorded in CDCl$_3$.*

General procedure for light triggered [2+2]-cycloaddition reactions of P$_9$. A stock solution of aldehyde functional poly(ethylene glycol) methyl ether (10 mg) in a mixture of styrene, 4-methyl styrene, or 2-pentene (10 mL) and toluene (10 mL) was prepared and portioned into headspace vials which were crimped airtight. The reaction mixture was subsequently deoxygenated by purging with nitrogen for 15 min. The samples were irradiated for the desired reaction time revolving in a custom built photoreactor equipped with 5 low pressure mercury lamps (Cosmedico Arimed B6, 36 W). The volatiles were removed under reduced pressure. In the cases where styrenics were utilized as enes, polymeric material stemming for self polymerization under irradiation was removed by precipitation in cold methanol. The product was obtained after precipitation in cold ether.

General procedure for the light-triggered cycloreversion of P$_{10}$-P$_{13}$. Oxetane functional poly(ethylene glycol) methyl ether (2 mg, 0.87 mmol, 1.0 eq) and 1,4-naphthalene dinitrile (1.5 mg, 4.3 mmol, 5.0 eq) were dissolved in acetonitrile (1 mL). The reaction mixture was subsequently deoxygenated by purging with nitrogen for 15 min. The sample was irradiated for the desired reaction time revolving in a custom built photoreactor equipped with a low pressure mercury lamps (Cosmedico Arimed

162

B6, 36 W). Subsequent to irradiation, the product was purified by precipitation in cold ether.

2-Methoxy-6-methylbenzaldehyde (8). 2,3-Dimethyl anisole (7.03 g, 51.6 mmol, 1.0 eq), copper sulfate pentahydrate (13.1 g, 52.5 mmol, 1.0 eq) and potassium peroxodisulfate (41.9 g, 154.8 mmol, 3.0 eq) were added to a mixture of MeCN/water (1:1, 500 mL) in a round bottom flask. The suspension was vigorously stirred and heated at 90 °C in a temperature regulated oil bath until thin layer chromatography (TLC) revealed that all the starting material had been consumed. At this point, 45 min after the start of the reaction, the mixture was allowed to cool down to ambient temperature and the non-dissolved copper salt was removed by filtration. DCM (150 mL) was added and the phases were separated. The aqueous phase was extracted two times with DCM (100 mL) and the combined organic layers were dried over magnesium sulfate. After removal of the solvent under reduced pressure, the crude product was purified by flash chromatography (silica gel, hexane/ethyl acetate 5:1 v/v), yielding 5.2 g (68 %) of a yellow solid. ^{1}H-NMR (DMSO, 250 MHz), δ / ppm: 10.51 (s, 1H, a), 7.48 (t, ^3J = 8.0 Hz, 1H, b), 7.04 (d, ^3J = 8.5 Hz, 1H, d), 6.70 (d, ^3J = 7.4 Hz, 1H, e), 3.87 (s, 3H, e), 2.45 (s, 3H, f).
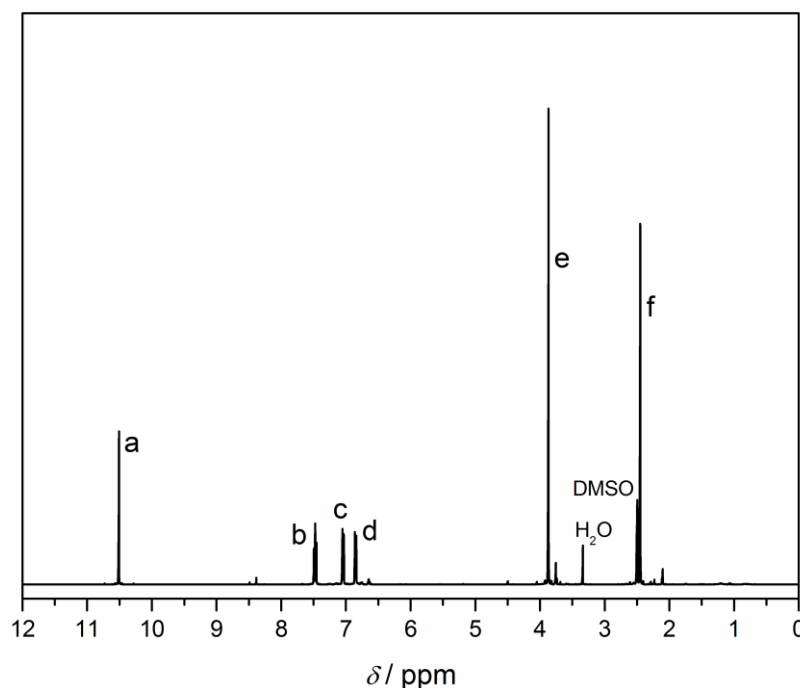
*Figure 9.3-15: ^{1}H-NMR spectrum of **8** recorded in DMSO-d^6.*

2-Hydroxy-6-methylbenzaldehyde (9). 2-Methoxy-6-methylbenzaldehyde (5.20 g, 34.6 mmol, 1.0 eq) was dissolved in anhydrous DCM (75 mL) and cooled to 0 °C. $AlCl_3$ (13.9 g, 103.9 mmol, 3.0 eq) was added and the mixture was stirred at ambient temperature overnight. The reaction was quenched with H_2O and the phases were separated. The aqueous layer was extracted three times with DCM (100 mL). The combined organic layers were dried over magnesium sulfate and the solvent was evaporated. The final purification was carried out by flash chromatography (silica gel, cyclohexane/ethyl acetate 2:1 v/v) yielding 3.9 g (82 %) of a yellow solid. ^{1}H-NMR $(CDCl_3, 250 MHz)$, δ / ppm: 11.91 (s, 1H, a), 10.32 (s, 1H, b), 7.37 (t, $^3J = 7.9$ Hz, 1H, c), 6.81 (d, $^3J = 8.5$ Hz, 1H, d), 6.71 (d, $^3J = 7.4$ Hz, 1H, e), 2.61 (s, 3H, f).
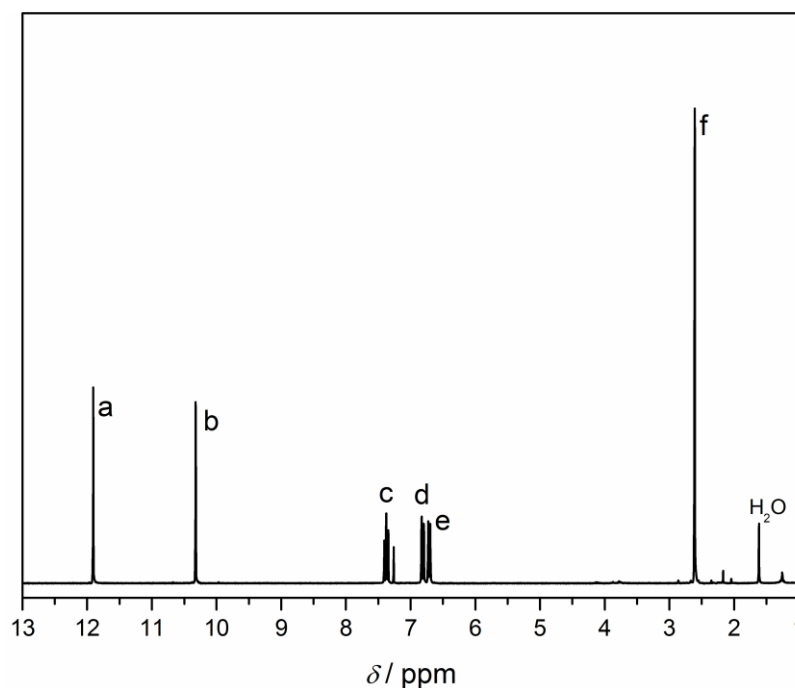
Figure 9.3-16: ^{1}H-NMR spectrum of **9** recorded in $CDCl_3$.

2-((11-Hydroxyundecyl)oxy)-6-methylbenzaldehyde (10). To a suspension of K_2CO_3 (394 mg, 2.85 mmol, 1.7 eq) in anhydrous DMF (5.2 mL) 2-hydroxy-6-methylbenzaldehyde (909 mg, 6.68 mmol, 1.2 eq) was added and the mixture was stirred for 30 min. A solution of 11-bromo-undecanol (1.36 g, 5.47 mmol, 1.0 eq) in anhydrous DMF (2 mL) was added dropwise over a period of 30 min. After stirring for 72 h the reaction was quenched with H_2O (50 mL). The mixture was extracted with diethyl ether three times and the combined organic layers were washed with 5 %

NaOH (2 x 50 mL) and H_2O (2 x 100 mL). After drying over magnesium sulfate and evaporating the solvent, the crude product was purified by flash chromatography (silica gel, cyclohexane/ethyl acetate 2:1 v/v) yielding a yellow solid (0.77 g, 45 %). ^{1}H-NMR (CDCl$_3$, 250 MHz), δ/ ppm: 10.67 (s, 1H, a), 7.34 (t, ^3J = 7.9 Hz, 1H, b), 6.80 (t, ^3J = 8.2 Hz, 2 H, c), 4.03 (t, ^3J = 6.3 Hz, 2H, d), 3.64 (t, ^3J = 6.6 Hz, 2H, e), 2.57 (s, 3H, f), 1.89-1.74 (m, 2 H, g), 1.62-1.25 (m, 16H, h).
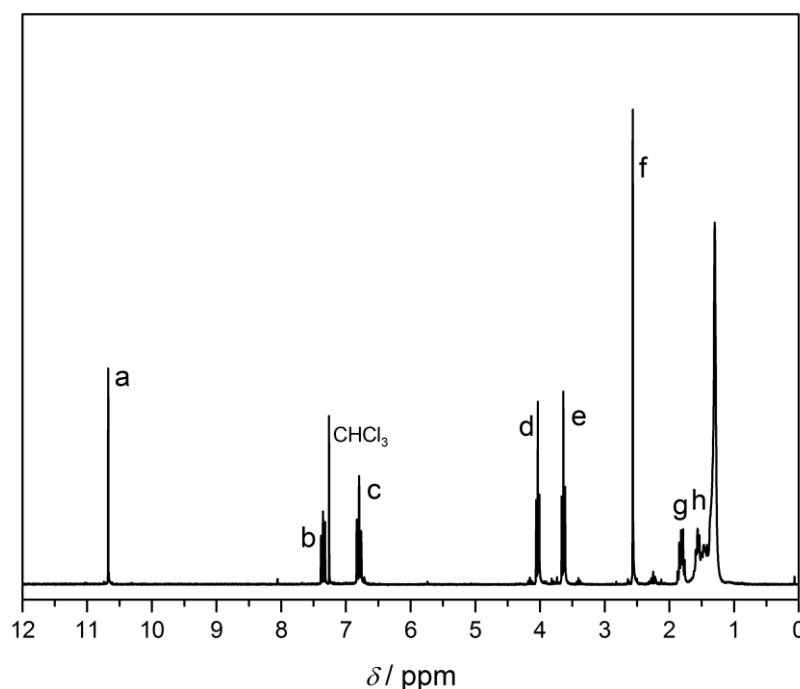
Figure 9.3-17: ^{1}H-NMR spectrum of **10** recorded in CDCl$_3$.

RAFT polymerization of methyl acrylate with CPDB (P$_{14}$). Methyl acrylate (4.016 g, 46.5 mmol, 128 eq), 2-cyanopropyl dithiobenzoate (0.080 g, 0.363 mmol, 1.00 eq) and 2,2'-azobis(isobutyronitrile) (0.0137 g, 0.084 mmol, 0.23 eq), and benzene (3.756 g) were weighed into a round bottom flask. The flask was sealed with a rubber septum, the solution stirred and nitrogen was bubbled through the mixture for 30 min. The mixture was subsequently heated to 70 °C for 6 h, after which it was exposed to air and cooled with an ice bath. Two consecutive precipitations from cold n-hexane yielded 1.108 g of a pink viscous oil which was analyzed via SEC (M_n = 5400 g·mol^{-1}, $Đ$ = 1.05) (conversion determined by NMR: 28 %).

RAFT polymerization of styrene with CPDB (P$_{15}$). Styrene (3.3 mL, 3 g, 0.028 mol, 200 eq), 2-cyanopropyl dithiobenzoate (0.032 g, 0.148 mmol, 1.00 eq) and 2,2'-

azobis(isobutyronitrile) (0.0011 g, 0.0067 mmol, 0.10 eq) were weighed into a round bottom flask and dissolved in toluene (3.3 mL). The flask was sealed with a rubber septum, and the solution was deoxygenated by purging with nitrogen for 60 min. The mixture was subsequently heated to 90 °C. After 13 h the solution was exposed to air and cooled to ambient temperature. Three consecutive precipitations from cold MeOH yielded 1 g of a pink powder, which was analyzed via SEC (M_n = 5900 g·mol^{-1}, $Đ$ = 1.05).

Photoenol end-capped poly(ε-caprolactone) (P$_{16}$): **10** (121 mg, 0.396 mmol, 0.08 eq) and TBD (6.00 mg, 0.043 mmol, 0.008 eq) were dissolved in toluene (2.5 mL) under inert atmosphere. ε-CL (565 mg, 4.95 mmol, 1.0 eq) was added and the solution was stirred under argon atmosphere at ambient temperature for 7 h. The reaction was quenched with benzoic acid (50.0 mg, 0.40 mmol, 0.08 eq) and the polymer was precipitated in cold hexane/Et$_2$O (1:1 v/v, 200 mL). ^{1}H-NMR (CDCl$_3$, 250 MHz), δ/ ppm: 10.67 (s, 1H, a), 7.37 (t, ^3J = 7.9 Hz, 1H, b), 6.80 (t, ^3J = 8.3 Hz, 2H, c), 4.05 (t, ^3J = 6.6 Hz, 2 H along backbone, d), 3.64 (t, ^3J = 6.4 Hz, 2H, e), 2.56 (s, 3H, f), 2.30 (t, ^3J = 7.5 Hz, 2H along backbone, g), 1.86-1.24 (m, 4 H along backbone, h). (M_n = 8500 g·mol^{-1}, $Đ$ = 1.08).
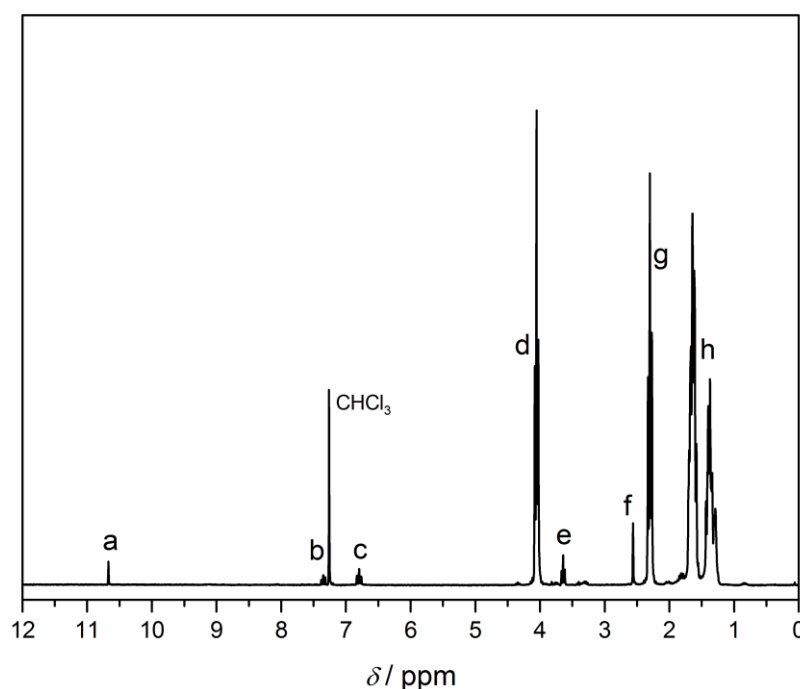
Figure 9.3-18: ^{1}H-NMR spectrum of **P$_{16}$** recorded in CDCl$_3$.

Light-triggered reaction of photoenol end-capped poly-(ε-caprolactone) with the RAFT-poly(methyl acrylate) (P_{17}). Equimolar amounts of both polymers were weighed up in Schlenk-flasks and dissolved in MeCN to give a polymer concentration of 5 g·L^{-1}. The solution was deoxygenated by performing three consecutive freeze-pump-thaw cycles. In an argon glovebox the stock solution was transferred into a headspace vial (Pyrex, dia. 20 mm), which was crimped airtight using a styrene/butadiene rubber seal with a PTFE inner liner. The vial was irradiated (e.g., 5 min) by revolving it around a compact low-pressure fluorescent lamp (Arimed B6, Cosmedico GmbH, Stuttgart, Germany) emitting at 320 nm (±30 nm) at a distance of 40–50 mm in a custom-built photo reactor. After ending the reaction, the solvent was evaporated under reduced pressure and the polymer was dissolved in THF for SEC analysis (M_n = 13000 g·mol^{-1}, Đ = 1.21).

Light-triggered reaction of photoenol end-capped poly(ε-caprolactone) with RAFT-polystyrene (P_{18}). Equimolar amounts of both polymers were weighed up in Schlenck-flasks and dissolved in MeCN/ DCM (1:1) to give a polymer concentration of 5 g·L^{-1} solution. The solution was deoxygenated by three consecutive freeze-pump-thaw cycles. In an argon glovebox the stock solution was transferred into a headspace vial (Pyrex, dia. 20 mm), which was crimped airtight using a styrene/butadiene rubber seal with a PTFE inner liner. The vial was irradiated (e.g., 10 min) by revolving it around a compact low-pressure fluorescent lamp (Arimed B6, Cosmedico GmbH, Stuttgart, Germany) emitting at 320 nm (±30 nm) at a distance of 40–50 mm in a custom-built photo reactor. After ending the reaction, the solvent was evaporated under reduced pressure and the polymer was dissolved in THF for SEC/ESI-MS analysis (M_n = 13400 g·mol^{-1}, Đ = 1.20).

Synthesis of (Oxybis(ethane-2,1-diyl) bis(4-(2-(4-methoxyphenyl)-2H-tetrazol-5-yl)benzoate) (12). (3.00 g, 10.1 mmol, 1.0 eq) was suspended in dry THF (80 mL) and SOCl$_2$ (12.05 g, 7.34 mL, 101.3 mmol, 10.0 eq) was added under inert atmosphere. The mixture was heated to reflux (75 °C) for 3.5 h and the volatiles were subsequently removed under reduced pressure. The residue was dissolved two times in dry THF (40 mL) and dried in vacuum to remove the excess of SOCl$_2$. The

resulting product (1.06 g, 3.374 mmol, 5.0 eq) was dissolved in dry THF (20 mL), a solution of pyridine (134 mg, 136 μL, 1.69 mmol, 2.5 eq) and tetraethylene glycol (131 mg, 116 μL, 0.675 mmol, 1.0 eq) in dry THF (20 mL) was added dropwise at ambient temperature and the mixture was stirred overnight. The reaction was quenched with water (5 mL), the solvent was evaporated, and the resulting residue was suspended in dichloromethane (100 mL). The insoluble, unreacted starting material was filtered off. The filtrate was subsequently washed with aqueous HCl (5 %) and then water. The organic layer was dried over magnesium sulfate and concentrated under reduced pressure. The crude product was suspended in a minimum amount of chloroform, insoluble side-products were filtered off and the dissolved product was precipitated in ethanol at ambient temperature to give the di-linker in 25 % yield (120 mg). ^{1}H-NMR (CDCl$_3$, 400 MHz), δ / ppm: 8.29 (d, ^3J = 8.6 Hz, 4 H, a), 8.18 (d, ^3J = 8.6 Hz, 4 H, b), 8.08 (d, ^3J = 9.1 Hz, 4 H, c), 7.04 (d, ^3J = 9.1 Hz, 4H, d), 4.50 (t, ^3J=4.8 Hz, 4H, e), 3.88 (s, 6H, f), 3.86 (t, ^3J = 4.8 Hz, 4H, g), 3.71 (m, 4H, h). ^{13}C-NMR (CDCl$_3$, 160 MHz) δ /ppm: 165.93 (a), 164.04 (b), 160.63 (c), 131.45 (d), 130.25 (e), 126.80 (f), 121.40 (g), 114.69 (h) 70.71 (i), 69.17 (j), 64.33 (k), 55.64 (l). Exact mass: $m/z_{calculated}$ = 750.28; m/z_{exp} = 750.25.
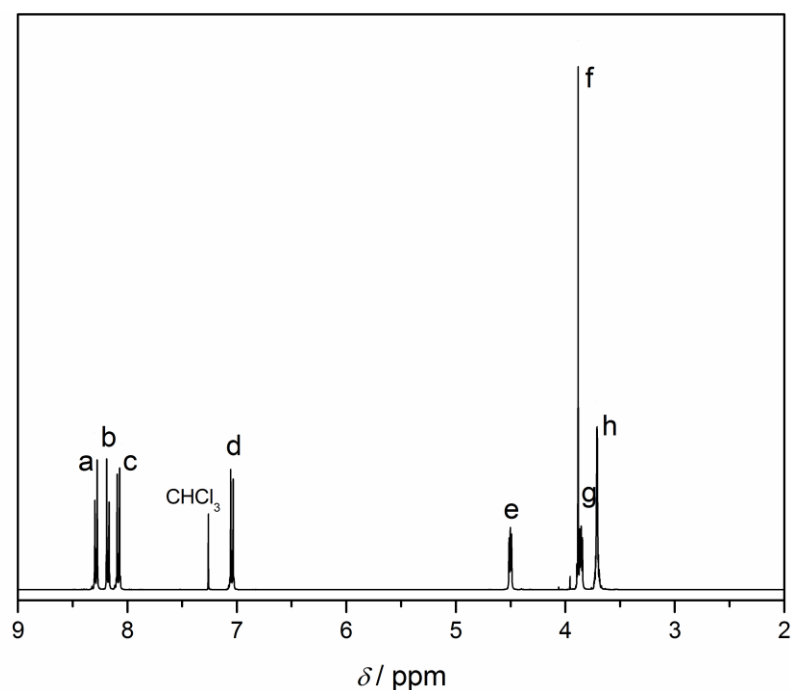
Figure 9.3-19: ^{1}H-NMR spectrum of **12** recorded in CDCl$_3$.

Kinetic study of the light-triggered model reaction of 12 and 1-pentene. **12** (1.0 mg, 1.3 mmol, 1.0 eq) was dissolved in THF (1 mL). 1-Pentene (93.4 mg, 146.0 mL, 1.3 mol, 1000 eq) was added to the mixture and the resulting stock solution was aliquoted into 5 headspace vials (Pyrex, dia. 20 mm), which were crimped airtight using a styrene/butadiene rubber seal with a PTFE inner liner. The vials were irradiated for a given reaction time by revolving them around a compact low-pressure fluorescent lamp (lamp specifications are available in the Methods section) at a distance of 40-50 mm in a custom-built photoreactor (Methods section). After ending the reaction, the solvent and the excess of 1-pentene were evaporated under nitrogen flow and the product was dissolved in THF for ESI-MS, SEC, NMR, UV-vis, and fluorescence analysis.

Typical procedure for the kinetic study of the light-triggered crosslinking reaction of PBD₁. **PBD₁** (70 mg, 1.3 mol(vinyl bonds), 127 eq (vinyl bonds)) and **12** (7.70 mg, 10.2 mmol, 1.0 eq) were dissolved in THF (5 mL). After both components were completely dissolved, equal amounts of the stock solution were aliquoted into headspace vials (Pyrex, dia. 20 mm). The solvent was removed under reduced pressure and THF (50 µL) was added to each vial, before they were flushed with nitrogen and crimped airtight using styrene/butadiene rubber seals with PTFE inner liner. The samples were irradiated for the desired reaction time by revolving around a low-pressure compact UV-lamp (Arimed B6) at a distance of 40-50 mm. After irradiation, the solvent was removed and the samples were characterized by SEC analysis.

Typical procedure for the kinetic study of the light-triggered crosslinking reaction of PBD₂. 1,2-Polybutadiene (70 mg, 1.3 mol(vinyl bonds), 127 eq(vinyl bonds)) and **12** (7.70 mg, 10.2 mmol, 1.00 eq) were dissolved in THF (5 mL) while shaking at 40 °C for 1 h. After both components were completely dissolved, equal amounts of the stock solution were aliquoted into headspace vials (Pyrex, dia. 20 mm). The solvent was removed under reduced pressure and THF (50 µL) was added to each vial, before they were flushed with nitrogen and crimped airtight using styrene/butadiene rubber seals with PTFE inner liner. The samples were irradiated

for the desired reaction time by revolving around a low-pressure compact UV-lamp (Arimed B6 or Philips TL01) at a distance of 40-50 mm. After irradiation, THF (3 mL) was added and the gelatinous mixture was allowed to stand for 3 h. The soluble polymer/linker mixture and the insoluble gel were separated by decanting and both were subsequently dried and weighed.

Light-triggered crosslinking for the preparation of a fluorescent pattern. 1,2-Polybutadiene (**PBD-2**, 200 mg, 3.7 mol(vinyl bonds), 278 eq(vinyl bonds)) was dissolved in THF (5 mL) under stirring at 35 °C. After complete dissolution, **12** (10 mg, 13.3 mmol, 1.0 eq) was added and the mixture was stirred for an additional 10 min. The polymer/linker solution was solvent casted on a glass slide (100 × 50 mm). After evaporation of the solvent, the glass slide was covered with a second glass slide and covered with a shadow mask. This setup was placed into the sunlight for 2 h so that the light shone perpendicularly on the shadow mask. After irradiation, the mask and the top glass slide were removed and the bottom glass slide with the polymer/linker mixture was placed in a THF bath. After complete dissolution of the non-crosslinked polymer, the plate was visualized under a 365 nm TLC lamp to analyze the fluorescent pattern.

LIST OF SCHEMES AND FIGURES

LIST OF ABBREVIATIONS

ACS	American Chemical Society
ADMET	Acrylic diene-metathesis
AFM	Atomic force microscopy
AIBN	Azobisisobutyronitrile
ATRP	Atom transfer radical polymerization
ARGET	Activator regenerated by electron transfer
CH	Cyclohexane
CID ESI-MS	Collision induced dissociation electrospray ionization mass spectrometry
CPDB	Cyanopropyl dithiobenzoate
CSIRO	Commonwealth Scientific and Industrial Research Organization
CuAAC	Copper catalyzed azide-alkyne cycloaddition
DCC	Dicyclohexyl carbodiimide
DCM	Dichloromethane
DFT	Density functional theory
DLW	Direct laser writing
DMAC	Dimethyl acetamide
DMAP	*N*,*N*-Dimethyl aminopyridine
DMF	Dimethyl formamide
DMSO	Dimethyl sulfoxide
DOPA	3,4-Dihydroxyphenyl alanine
DTE	Dithioester
EA	Ethyl acetate
EDC-HCl	1-Ethyl-3-(3-dimethylaminopropyl) carbodiimide-hydrochloride
ESI-MS	Electrospray ionization mass spectrometry
EtOH	Ethanol
FL	Flavin azido
FRET	Förster Resonance Energy Transfer
FRP	Free radical polymerization
FT-IR	Fourier transform infrared microscopy

HCl	Hydrochloric acid
HDA	Hetero Diels–Alder
HEA	2-Hydroxyethyl acrylate
high-res ESI-MS	High resolution electrospray ionization mass spectrometry
HOMO	Highest occupied molecular orbital
HPLC	High-performance liquid chromatography
IBM	International Business Machines Corporation
IC	Internal conversion
ISC	Intersystem crossing
IUPAC	International Union of Pure and Applied Chemistry
KIT	Karlsruhe Institute of Technology
LED	Light-emitting diode
LUMO	Lowest unoccupied molecular orbital
MA	Methyl acrylate
MeCN	Acetonitrile
MeI	Iodo methane
MEMS	Micro electromechanical systems
MeOH	Methanol
MMA	Methyl methacrylate
MWD	Molecular weight distribution
NASA	National Aeronautics and Space Administration
NaTFA	Sodium trifluoro acetate
NDN	Naphthalene dinitrile
NITEC	Nitrile imine-mediated tetrazole-ene cycloaddition
NMP	Nitroxide mediated radical polymerization
NMR	Nuclear magnetic resonance spectroscopy
NPG	Nature Publishing Group
NQM	*Ortho*-naphthoquinone methide
NQMP	*Ortho*-naphthoquinone methide precursor
NS	Number of scans
PB	Paternò–Büchi
PBD	Polybutadiene
PCl	Poly(ε-caprolactone)
PDA	Polydopamine
PEG	Poly(ethylene glycol)
PEG-acr	Acrylate end-capped poly(ethylene glycol)
PEG-mal	Maleimide end-capped poly(ethylene glycol)

PEG-OH	Hydroxyl end-capped poly(ethylene glycol)
photo-SPAAC	Photo-induced strain promoted azide-alkyne cycloaddition
PLP	Pulsed-laser polymerization
PMA	Poly(methyl acrylate)
PMeOEGMA	Poly(oligoethylene glycol methyl ether methacrylate)
PMMA	Poly(methyl methacrylate)
PMS	*Para*-methyl styrene
PSS	Polymer Standards Service
PTFE	Poly(tetrafluoro ethylene)
RAFT	Reversible addition fragmentation chain transfer
RB	Rhodamin B
RSC	Royal Society of Chemistry
RDRP	Reversible-deactivation radical polymerization
RGB	Red-green-blue
ROP	Ring opening polymerization
RT	Ambient temperature
SCNP	Single-chain nanoparticle
SEC	Size exclusion chromatography
SEM	Scanning electron microscopy
SPAAC	Strain promoted azide-alkyne cycloaddition
Sty	Styrene
TBD	1,5,7-Triazabicyclo[4.4.0]dec-5-ene
TEMPO	2,2,6,6-Tetramethylpiperidine-1-oxyl
THF	Tetrahydrofuran
TLC	Thin layer chromatography
TMS	*Trans*-methyl styrene
ToF-SIMS	Time-of-flight secondary ion mass spectrometry
UV-vis	UV-visible spectroscopy

BIBLIOGRAPHY

1   R. F. Service, *Science*, **2005**, *309*, 548.

2   G. Ciamician, *Science*, **1912**, *36*, 385.

3   A. Albini and M. Fagnoni, *Green Chem.*, **2004**, *6*, 1.

4   J. H. Clark, *Green Chem.*, **1999**, *1*, 1.

5   E. F. Zwicker, L. I. Grossweiner and N. C. Yang, *J. Am. Chem. Soc.*, **1963**, *85*, 2671.

6   A. Padwa and J. Smolanoff, *J. Am. Chem. Soc.*, **1971**, *93*, 548.

7   R. Huisgen, *Angew. Chem. Int. Ed.*, **1963**, *75*, 604.

8   E. Paterno and G. Chieffi, *Gazz. Chim. Ital.*, **1909**, *39*, 341.

9   G. Büchi, C. G. Inman and E. S. Lipinsky, *J. Am. Chem. Soc.*, **1954**, *76*, 4327.

10   R. B. Seymour, *J. Chem. Edu.*, **1988**, *65*, 327.

11   H. Staudinger, M. Brunner, K. Frey, P. Garbsch, R. Signer and S. Wehrli, *Ber. Dtsch. Chem. Ges.*, **1929**, *62*, 241.

12   H. Staudinger and H. F. Bondy, *Ber. Dtsch. Chem. Ges.*, **1929**, *62*, 2411.

13   H. Staudinger, K. Frey, P. Garbsch and S. Wehrli, *Ber. Dtsch. Chem. Ges.*, **1929**, *62*, 2912.

14   H. Staudinger, E. Geiger and E. Huber, *Ber. Dtsch. Chem. Ges.*, **1929**, *62*, 263.

15   H. Staudinger and W. Heuer, *Ber. Dtsch. Chem. Ges.*, **1929**, *62*, 2933.

16   H. Staudinger and H. Machemer, *Ber. Dtsch. Chem. Ges.*, **1929**, *62*, 2921.

17   H. Staudinger and O. Schweitzer, *Ber. Dtsch. Chem. Ges.*, **1929**, *62*, 2395.

18   PlasticsEurope, Production of plastics worldwide from 1950 to 2013 (in million metric tons), http://www.statista.com/statistics/282732/global-production-of-plastics-since-1950/.

19   C. Barner-Kowollik, J.-F. Lutz and S. Perrier, *Polym. Chem.*, **2012**, *3*, 1677.

20   G. Odian, *Principles of Polymerization*, John Wiley & Sons, New York, **2004**.

21   W. H. Carothers, *J. Am. Chem. Soc.*, **1929**, *51*, 2548.

22   P. J. Flory, *Principles of Polymer Chemistry*, Cornell University Press, Ithaca, New York, **1953**.

23   E. Rabinowitch, *Trans. Faraday Soc.*, **1937**, *33*, 1225.

24   B. V. B. and J. J. Sudborough, *J. Indian Inst. Sci.*, **1925**, *8A*, 89.

25   K. Matyjaszewski, in *Controlled and Living Polymerizations*, Wiley-VCH, Weinheim, **2010**, 103.

26   A. P. Haehnel, M. Schneider-Baumann, K. U. Hiltebrandt, A. M. Misske and C. Barner-Kowollik, *Macromolecules*, **2013**, *46*, 15.

27   J. Barth, M. Buback, G. T. Russell and S. Smolne, *Macromol. Chem. Phys.*, **2011**, *212*, 1366.

28   C. Barner-Kowollik and G. T. Russell, *Prog. Polym. Sci.*, **2009**, *34*, 1211.

29 T. Junkers, S. P. S. Koo, T. P. Davis, M. H. Stenzel and C. Barner-Kowollik, *Macromolecules*, **2007**, *40*.

30 M. Szwarc, *Nature*, **1956**, *178*, 1168.

31 N. Hadjichristidis, M. Pitsikalis, S. Pispas and H. Iatrou, *Chem. Rev.*, **2001**, *101*, 3747.

32 D. H. Solomon, E. Rizzardo and P. Cacioli, European Patent, EP 135280, **1985**.

33 C. J. Hawker, A. W. Bosman and E. Harth, *Chem. Rev.*, **2001**, *101*, 3661.

34 V. Sciannamea, R. Jérôme and C. Detrembleur, *Chem. Rev.*, **2008**, *108*, 1104.

35 T. Fukuda, T. Terauchi, A. Goto, K. Ohno, Y. Tsujii, T. Miyamoto, S. Kobatake and B. Yamada, *Macromolecules*, **1996**, *29*, 6393.

36 D. Benoit, S. Grimaldi, S. Robin, J.-P. Finet, P. Tordo and Y. Gnanou, *J. Am. Chem. Soc.*, **2000**, *122*, 5929.

37 E. Yoshida, *Colloid. Polym. Sci.,* **2008**, *286*, 1663.

38 E. Yoshida, *Polymers*, **2012**, *4*, 1125.

39 E. Yoshida, *Colloid. Polym. Sci.*, **2013**, *291*, 2733.

40 J.-S. Wang and K. Matyjaszewski, *J. Am. Chem. Soc.*, **1995**, *117*, 5614.

41 M. Kato, M. Kamigaito, M. Sawamoto and T. Higashimura, *Macromolecules*, **1995**, *28*, 1721.

42 M. Ouchi, T. Terashima and M. Sawamoto, *Chem. Rev.*, **2009**, *109*, 4963.

43 K. Matyjaszewski and J. Xia, *Chem. Rev.*, **2001**, *101*, 2921.

44 W. Tang, N. V. Tsarevsky and K. Matyjaszewski, *J. Am. Chem. Soc.*, **2006**, *128*, 1598.

45 G. Moineau, P. Dubois, R. Jérôme, T. Senninger and P. Teyssié, *Macromolecules*, **1998**, *31*, 545.

46 C. Granel, P. Dubois, R. Jérôme and P. Teyssié, *Macromolecules*, **1996**, *29*, 8576.

47 P. Lecomte, I. Drapier, P. Dubois, P. Teyssié and R. Jérôme, *Macromolecules*, **1997**, *30*, 7631.

48 V. Percec, B. Barboiu, A. Neumann, J. C. Ronda and M. Zhao, *Macromolecules*, **1996**, *29*, 3665.

49 K. Matyjaszewski, *Chem. Eur. J.*, **1999**, *5*, 3095.

50 J.-F. Lutz and K. Matyjaszewski, *J. Polym. Sci., Part A: Polym. Chem.*, **2005**, *43*, 897.

51 W. Jakubowski and K. Matyjaszewski, *Angew. Chem. Int. Ed.*, **2006**, *45*, 4482.

52 K. Pahnke, J. Brandt, G. Gryn'ova, P. Lindner, R. Schweins, F. G. Schmidt, A. Lederer, M. L. Coote and C. Barner-Kowollik, *Chem. Sci.*, **2015**, *6*, 1061.

53 N. Jasinski, A. Lauer, P. J. M. Stals, S. Behrens, S. Essig, A. Walther, A. S. Goldmann and C. Barner-Kowollik, *ACS Macro Lett.*, **2015**, *4*, 298.

54 Y. Kwak and K. Matyjaszewski, *Macromolecules*, **2010**, *43*, 5180.

55 M. A. Tasdelen, M. Uygun and Y. Yagci, *Macromol. Chem. Phys.*, **2011**, *212*, 2036.

56 V. Coessens, T. Pintauer and K. Matyjaszewski, *Prog. Polym. Sci.*, **2001**, *26*, 337.

57 J. Chiefari, Y. K. Chong, F. Ercole, J. Krstina, J. Jeffery, T. P. T. Le, R. T. A. Mayadunne, G. F. Meijs, C. L. Moad, G. Moad, E. Rizzardo and S. H. Thang, *Macromolecules*, **1998**, *31*, 5559.

58   P. Corpart, D. Charmot, T. Biadatti, S. Zard and D. Michelet, in *PCT Int. Appl. WO 9858974 A1*, **1998**.

59   G. Moad, Y. K. Chong, A. Postma, E. Rizzardo and S. H. Thang, *Polymer*, **2005**, *46*, 8458.

60   G. Moad, E. Rizzardo and S. H. Thang, *Austr. J. Chem.*, **2005**, *58*, 379.

61   G. Moad, E. Rizzardo and S. H. Thang, *Austr. J. Chem.*, **2006**, *59*, 669.

62   G. Moad, E. Rizzardo and S. H. Thang, *Austr. J. Chem.*, **2009**, *62*, 1402.

63   G. Moad, J. Chiefari, Y. K. Chong, J. Krstina, R. T. A. Mayadunne, A. Postma, E. Rizzardo and S. H. Thang, *Polym. Int.*, **2000**, *49*, 993.

64   L. Barner, T. P. Davis, M. H. Stenzel and C. Barner-Kowollik, *Macromol. Rapid Commun.*, **2007**, *28*, 539.

65   C. Barner-Kowollik, *Handbook of RAFT Polymerization*, Wiley-VCH Verlag, Weinheim, Germany, **2008**.

66   M. L. Coote and L. Radom, *J. Am. Chem. Soc.*, **2003**, *125*, 1490.

67   C. Barner-Kowollik, T. P. Davis, J. P. A. Heuts, M. H. Stenzel, P. Vana and M. Whittaker, *J. Polym. Sci., Part A: Polym. Chem.*, **2003**, *41*, 365.

68   L. Albertin, M. H. Stenzel, C. Barner-Kowollik, L. J. R. Foster and T. P. Davis, *Macromolecules*, **2005**, *38*, 9075.

69   X.-P. Qiu and F. M. Winnik, *Macromol. Rapid Commun.*, **2006**, *27*, 1648.

70   A. P. Vogt and B. S. Sumerlin, *Soft Matter*, **2009**, *5*, 2347.

71   C. Schmid, J. Falkenhagen and C. Barner-Kowollik, *J. Polym. Sci., Part A: Polym. Chem.*, **2011**, *49*, 1.

72   C. Schmid, J. Falkenhagen, T. F. Beskers, L.-T. T. Nguyen, M. Wilhelm, F. E. Du Prez and C. Barner-Kowollik, *Macromolecules*, **2012**, *45*, 6353.

73   C. Schmid, S. Weidner, J. Falkenhagen and C. Barner-Kowollik, *Macromolecules*, **2012**, *45*, 87.

74   S. Sinnwell, A. J. Inglis, T. P. Davis, M. H. Stenzel and C. Barner-Kowollik, *Chem. Commun.*, **2008**, 2052.

75   A. J. Inglis, S. Sinnwell, M. H. Stenzel and C. Barner-Kowollik, *Angew. Chem. Int. Ed.*, **2009**, *48*, 2411.

76   A. J. Inglis, S. Sinnwell, T. P. Davis, C. Barner-Kowollik and M. H. Stenzel, *Macromolecules*, **2008**, *41*, 4120.

77   A. J. Inglis, L. Nebhani, O. Altintas, F. G. Schmidt and C. Barner-Kowollik, *Macromolecules*, **2010**, *43*, 5515.

78   N. K. Guimard, J. Ho, J. Brandt, C. Y. Lin, M. Namazian, J. O. Mueller, K. K. Oehlenschlaeger, S. Hilf, A. Lederer, F. G. Schmidt, M. L. Coote and C. Barner-Kowollik, *Chem. Sci.*, **2013**, *4*, 2752.

79   O. Nuyken and S. Pask, *Polymers*, **2013**, *5*, 361.

80   H. Mori, S. Masuda and T. Endo, *Macromolecules*, **2006**, *39*, 5976.

81   T. Endo, Y. Shibasaki and F. Sanda, *J. Polym. Sci., Part A: Polym. Chem.*, **2002**, *40*, 2190.

82   A. Rodriguez-Galan, L. Franco and J. Puiggali, *Polymers*, **2010**, *3*, 65.

83   N. E. Kamber, W. Jeong, R. M. Waymouth, R. C. Pratt, B. G. G. Lohmeijer and J. L. Hedrick, *Chem. Rev.*, **2007**, *107*, 5813.

84   H. R. Kricheldorf, I. Kreiser-Saunders and A. Stricker, *Macromolecules*, **2000**, *33*, 702.

85   D. Knani, A. L. Gutman and D. H. Kohn, *J. Polym. Sci., Part A: Polym. Chem.*, **1993**, *31*, 1221.

86   A.-C. Albertsson and I. K. Varma, *Biomacromolecules*, **2003**, *4*, 1466.

87   H. Trommsdorff, *Ann. Pharm. Chem.*, **1834**, *11*, 190.

88   M. Planck, *Ber. Verh. Dtsch. Phys. Ges.*, **1900**, *2*, 237.

89   A. Einstein, *Ann. Phys.*, **1905**, *17*, 132.

90   M. Bodenstein, F. Weigert, R. Luther, J. Franck, L. S. Ornstein, F. A. Lindemann, J. Rice, J. A. Christiansen, E. C. C. Baly, Rice, E. K. Rideal, A. J. Allmand, H. von Halban, P. Lasareff, E. J. Bowen, H. S. Taylor, D. L. Chapman, S. C. Roy, S. L. Langedyk, M. Padoa and F. I. G. Rawlins, *Trans. Faraday Soc.*, **1926**, *21*, 515.

91   M. Bodenstein, *Z. physik. Chem.*, **1914**, *85*, 327.

92   G. Ciamician and P. Silber, *Ber. Dtsch. Chem. Ges.*, **1901**, *34*, 2040.

93   G. Ciamician and P. Silber, *Ber. Dtsch. Chem. Ges.*, **1907**, *40*, 2415.

94   G. Ciamician and P. Silber, *Ber. Dtsch. Chem. Ges.*, **1908**, *41*, 1928.

95   R. G. W. Norrish and C. H. Bamford, *Nature*, **1967**, *140*, 195.

96   C. H. Bamford and R. G. W. Norrish, *J. Chem. Soc.*, **1938**, 1544.

97   R. G. W. Norrish and M. E. S. Appleyard, *J. Chem. Soc.*, **1934**, 874.

98   G. von Freymann, A. Ledermann, M. Thiel, I. Staude, S. Essig, K. Busch and M. Wegener, *Adv. Funct. Mater.*, **2010**, *20*, 1038.

99   M. Deubel, G. von Freymann, M. Wegener, S. Pereira, K. Busch and C. M. Soukoulis, *Nat. Mater.*, **2004**, *3*, 444.

100   A. Jablonski, *Nature*, **1933**, *131*, 839.

101   S. Dym, R. M. Hochstrasser and M. Schafer, *J. Chem. Phys.*, **1968**, *48*, 646.

102   W. C. Johnson and W. T. Simpson, *J. Chem. Phys.*, **1968**, *48*, 2168.

103   R. M. Hochstrasser and L. J. Noe, *J. Chem. Phys.*, **1969**, *50*, 1684.

104   L. R. Warren J. Hehre, P. von R. Schleyer, J. Pople, *AB INITIO Molecular Orbital Theory*, John Wiley & Sons, New York, **1986**.

105   J. B. Foresman, M. Head-Gordon, J. A. Pople and M. J. Frisch, *J. Phys. Chem.*, **1992**, *96*, 135.

106   P. Knowles and H.-J. Werner, *Theoret. Chim. Acta*, **1992**, *84*, 95.

107   A. Dreuw and M. Head-Gordon, *Chem. Rev.*, **2005**, *105*, 4009.

108   D. Bryce-Smith, *Photochemistry Vol. 1*, The Chemical Society, **1970**.

109   B. R. Henry and M. Kasha, *Ann. Rev. Phys. Chem.*, **1968**, *19*, 161.

110   E. Wiedemann, *Ann. Phys.*, **1888**, *270*, 446.

111   K. A. Franz, W. G. Kehr, A. Siggel, J. Wieczoreck and W. Adam, *Ullmann's Encyclopedia of Industrial Chemistry*, Wiley-VCH, Weinheim, **2000**.

112   B. Valeur and M. N. Berberan-Santos, *J. Chem. Edu.*, **2011**, *88*, 731.

113   G. G. Stokes, *Phil. Trans. R. Soc. Lond.*, **1852**, *142*, 463.

114   J. R. Lakowicz, *Principles of Fluorescence Spectroscopy*, Springer US, New York, **2006**.

115   J. Zheng, *Ion Channels*, Humana Press, New York City, **2006**, 65.

116   F. Bergmann and Y. Hirshberg, *J. Am. Chem. Soc.*, **1943**, *65*, 1429.

117   H. C. Kolb, M. G. Finn and K. B. Sharpless, *Angew. Chem. Int. Ed.*, **2001**, *40*, 2004.

118   C. Barner-Kowollik, F. E. Du Prez, P. Espeel, C. J. Hawker, T. Junkers, H. Schlaad and W. Van Camp, *Angew. Chem. Int. Ed.*, **2011**, *50*, 60.

119   D. Fournier, R. Hoogenboom and U. S. Schubert, *Chem. Soc. Rev.*, **2007**, *36*, 1369.

120   B. Helms, J. L. Mynar, C. J. Hawker and J. M. J. Frechet, *J. Am. Chem. Soc.*, **2004**, *126*, 15020.

121   O. Altintas, B. Yankul, G. Hizal and U. Tunca, *J. Polym. Sci., Part A: Polym. Chem.*, **2006**, *44*, 6458.

122   H. Durmaz, A. Dag, O. Altintas, T. Erdogan, G. Hizal and U. Tunca, *Macromolecules*, **2007**, *40*, 191.

123   M. Glassner, J. P. Blinco and C. Barner-Kowollik, *Macromol. Rapid Commun.*, **2011**, *32*, 724.

124   A. S. Goldmann, A. Walther, L. Nebhani, R. Joso, D. Ernst, K. Loos, C. Barner-Kowollik, L. Barner and A. H. E. Müller, *Macromolecules*, **2009**, *42*.

125   K. K. Oehlenschlaeger, N. K. Guimard, J. Brandt, J. O. Mueller, C. Y. Lin, S. Hilf, A. Lederer, M. L. Coote, F. G. Schmidt and C. Barner-Kowollik, *Polym. Chem.*, **2013**, *4*, 4348.

126   K. K. Oehlenschlaeger, J. O. Mueller, J. Brandt, S. Hilf, A. Lederer, M. Wilhelm, R. Graf, M. L. Coote, F. G. Schmidt and C. Barner-Kowollik, *Adv. Mater.*, **2014**, *26*, 3561.

127   R. B. Woodward and R. Hoffmann, *J. Am. Chem. Soc.*, **1965**, *87*, 395.

128   S. M. Mellows and P. G. Sammes, *J. Chem. Soc., Chem. Commun.*, **1971**, 21.

129   T. Gruendling, K. K. Oehlenschlaeger, E. Frick, M. Glassner, C. Schmid and C. Barner-Kowollik, *Macromol. Rapid Commun.*, **2011**, *32*, 807.

130   M. Glassner, K. K. Oehlenschlaeger, T. Gruendling and C. Barner-Kowollik, *Macromolecules*, **2011**, *44*, 4681.

131   M. Winkler, J. O. Mueller, K. K. Oehlenschlaeger, L. Montero de Espinosa, M. A. R. Meier and C. Barner-Kowollik, *Macromolecules*, **2012**, *45*, 5012.

132   O. Altintas, J. Willenbacher, K. N. R. Wuest, K. K. Oehlenschlaeger, P. Krolla-Sidenstein, H. Gliemann and C. Barner-Kowollik, *Macromolecules*, **2013**, *46*, 8092.

133   T. Josse, O. Altintas, K. K. Oehlenschlaeger, P. Dubois, P. Gerbaux, O. Coulembier and C. Barner-Kowollik, *Chem. Commun.*, **2014**, *50*, 2024.

134   T. Josse, J. De Winter, O. Altintas, P. Dubois, C. Barner-Kowollik, P. Gerbaux and O. Coulembier, *Macromol. Chem. Phys.*, **2015**, DOI: 10.1002/macp.201500054.

135   T. Pauloehrl, G. Delaittre, V. Winkler, A. Welle, M. Bruns, H. G. Börner, A. M. Greiner, M. Bastmeyer and C. Barner-Kowollik, *Angew. Chem. Int. Ed.*, **2012**, *51*, 1071.

136   C. M. Preuss, T. Tischer, C. Rodriguez-Emmenegger, M. M. Zieger, M. Bruns, A. S. Goldmann and C. Barner-Kowollik, *J. Mater. Chem. B*, **2014**, *2*, 36.

137   T. Tischer, T. K. Claus, M. Bruns, V. Trouillet, K. Linkert, C. Rodriguez-Emmenegger, A. S. Goldmann, S. Perrier, H. G. Börner and C. Barner-Kowollik, *Biomacromolecules*, **2013**, *14*, 4340.

138   L. Stolzer, I. Ahmed, C. Rodriguez-Emmenegger, V. Trouillet, P. Bockstaller, C. Barner-Kowollik and L. Fruk, *Chem. Commun.*, **2014**, *50*, 4430.

139   M. Kaupp, T. Tischer, A. F. Hirschbiel, A. P. Vogt, U. Geckle, V. Trouillet, T. Hofe, M. H. Stenzel and C. Barner-Kowollik, *Macromolecules*, **2013**, *46*, 6858.

140   S. Arumugam and V. V. Popik, *J. Am. Chem. Soc.*, **2011**, *133*, 5573.

141   S. Arumugam and V. V. Popik, *J. Am. Chem. Soc.*, **2011**, *133*, 15730.

142   S. Arumugam, S. V. Orski, J. Locklin and V. V. Popik, *J. Am. Chem. Soc.*, **2011**, *134*, 179.

143   S. Arumugam, J. Guo, N. E. Mbua, F. Friscourt, N. Lin, E. Nekongo, G.-J. Boons and V. V. Popik, *Chem. Sci.*, **2014**, *5*, 1591.

144   S. Arumugam and V. V. Popik, *J. Am. Chem. Soc.*, **2012**, *134*, 8408.

145   M. Glassner, K. K. Oehlenschlaeger, A. Welle, M. Bruns and C. Barner-Kowollik, *Chem. Commun.*, **2013**, *49*, 633.

146   T. Tischer, T. K. Claus, K. K. Oehlenschlaeger, V. Trouillet, M. Bruns, A. Welle, K. Linkert, A. S. Goldmann, H. G. Börner and C. Barner-Kowollik, *Macromol. Rapid Commun.*, **2014**, *35*, 1121.

147   M. Kaupp, A. S. Quick, C. Rodriguez-Emmenegger, A. Welle, V. Trouillet, O. Pop-Georgievski, M. Wegener and C. Barner-Kowollik, *Adv. Funct. Mater.*, **2014**, *24*, 5649.

148   T. Pauloehrl, A. Welle, K. K. Oehlenschlaeger and C. Barner-Kowollik, *Chem. Sci.*, **2013**, *4*, 3503.

149   J. S. Clovis, A. Eckell, R. Huisgen and R. Sustmann, *Chem. Ber.*, **1967**, *100*, 60.

150   P. Weinberg, U. W. Grummt and C. Csongár, *J. Prakt. Chem.*, **1988**, *330*, 887.

151   P. Weinberg, M. Siegmund, C. Csongár and G. Tomaschewski, *Z. Chem.*, **1988**, *28*, 252.

152   G. Bertrand and C. Wentrup, *Angew. Chem. Int. Ed.*, **1994**, *33*, 527.

153   P. Weinberg, C. Csongar, M. Gessner and G. Tomaschewski, *J. Prakt. Chem.*, **1988**, *330*, 879.

154   M. Dietrich, G. Delaittre, J. P. Blinco, A. J. Inglis, M. Bruns and C. Barner-Kowollik, *Adv. Funct. Mater.*, **2012**, *22*, 304.

155   Y. Wang, C. I. Rivera Vera and Q. Lin, *Organic Letters*, **2007**, *9*, 4155.

156   W. Song, Y. Wang, J. Qu and Q. Lin, *J. Am. Chem. Soc.*, **2008**, *130*, 9654.

157   W. Song, Y. Wang, J. Qu, M. M. Madden and Q. Lin, *Angew. Chem. Int. Ed.*, **2008**, *47*, 2832.

158   Y. Wang, W. J. Hu, W. Song, R. K. V. Lim and Q. Lin, *Organic Letters*, **2008**, *10*, 3725.

159   M. M. Madden, C. I. Rivera Vera, W. Song and Q. Lin, *Chem. Commun.*, **2009**, 5588.

160   Y. Wang, W. Song, W. J. Hu and Q. Lin, *Angew. Chem. Int. Ed.*, **2009**, *48*, 5330.

161   W. Song, Y. Wang, Z. Yu, C. I. R. Vera, J. Qu and Q. Lin, *ACS Chem. Biol.*, **2010**, *5*, 875.

162   J. Wang, W. Zhang, W. Song, Y. Wang, Z. Yu, J. Li, M. Wu, L. Wang, J. Zang and Q. Lin, *J. Am. Chem. Soc.*, **2010**, *132*, 14812.

163   Z. Yu, R. K. V. Lim and Q. Lin, *Chem. Eur. J.*, **2010**, *16*, 13325.

164   Z. Yu, L. Y. Ho, Z. Wang and Q. Lin, *Bioorg. Med. Chem. Lett.*, **2011**, *21*, 5033.

165   T. Tischer, C. Rodriguez-Emmenegger, V. Trouillet, A. Welle, V. Schueler, J. O. Mueller, A. S. Goldmann, E. Brynda and C. Barner-Kowollik, *Adv. Mater.*, **2014**, *26*, 4087.

166   C. Rodriguez-Emmenegger, C. M. Preuss, B. Yameen, O. Pop-Georgievski, M. Bachmann, J. O. Mueller, M. Bruns, A. S. Goldmann, M. Bastmeyer and C. Barner-Kowollik, *Adv. Mater.*, **2013**, *25*, 6123.

167   E. Blasco, M. Piñol, L. Oriol, B. V. K. J. Schmidt, A. Welle, V. Trouillet, M. Bruns and C. Barner-Kowollik, *Adv. Funct. Mater.*, **2013**, *23*, 4011.

168 L. Stolzer, A. S. Quick, D. Abt, A. Welle, D. Naumenko, M. Lazzarino, M. Wegener, C. Barner-Kowollik and L. Fruk, *Chem. Commun.*, **2015**, *51*, 3363.

169 C. J. Dürr, P. Lederhose, L. Hlalele, D. Abt, A. Kaiser, S. Brandau and C. Barner-Kowollik, *Macromolecules*, **2013**, *46*, 5915.

170 A. Hufendiek, C. Barner-Kowollik and M. A. R. Meier, *Polym. Chem.*, **2015**, *6*, 2188.

171 S. Arndt and H.-A. Wagenknecht, *Angew. Chem. Int. Ed.*, **2014**, *53*, 14580.

172 T. Wang, Y. Wu, S. L. Kuan, O. Dumele, M. Lamla, D. Y. W. Ng, M. Arzt, J. Thomas, J. O. Mueller , C. Barner-Kowollik and T. Weil, *Chem. Eur. J.*, **2015**, *21*, 228.

173 A. Padwa, *Acc. Chem. Res.*, **1976**, *9*, 371.

174 E. Albrecht, J. Mattay and S. Steenken, *J. Am. Chem. Soc.*, **1997**, *119*, 11605.

175 A. Padwa, M. Dharan, J. Smolanoff and S. I. Wetmore, *J. Am. Chem. Soc.*, **1973**, *95*, 1945.

176 A. Padwa, M. Dharan, J. Smolanoff and S. I. Wetmore, *J. Am. Chem. Soc.*, **1973**, *95*, 1954.

177 A. Padwa, J. Smolanoff and S. I. Wetmore, *J. Org. Chem.*, **1973**, *38*, 1333.

178 A. Padwa and S. I. Wetmore, *J. Org. Chem.*, **1974**, *39*, 1396.

179 N. J. Turro, D. A. Hrovat, I. R. Gould, A. Padwa, W. Dent and R. J. Rosenthal, *Angew. Chem. Int. Ed.*, **1983**, *22*, 625.

180 R. K. V. Lim and Q. Lin, *Chem. Commun.*, **2010**, *46*, 7993.

181 V. V. Rostovtsev, L. G. Green, V. V. Fokin and K. B. Sharpless, *Angew. Chem. Int. Ed.*, **2002**, *41*, 2596.

182 R. K. Iha, K. L. Wooley, A. M. Nyström, D. J. Burke, M. J. Kade and C. J. Hawker, *Chem. Rev.*, **2009**, *109*, 5620.

183 H. Nandivada, X. Jiang and J. Lahann, *Adv. Mater.*, **2007**, *19*, 2197.

184 S. K. Mamidyala and M. G. Finn, *Chem. Soc. Rev.*, **2010**, *39*, 1252.

185 X.-L. Sun, C. L. Stabler, C. S. Cazalis and E. L. Chaikof, *Bioconjugate Chem.*, **2006**, *17*, 52.

186 H. C. Kolb and K. B. Sharpless, *Drug Discovery Today*, **2003**, *8*, 1128.

187 G. von Maltzahn, Y. Ren, J.-H. Park, D.-H. Min, V. R. Kotamraju, J. Jayakumar, V. Fogal, M. J. Sailor, E. Ruoslahti and S. N. Bhatia, *Bioconjugate Chem.*, **2008**, *19*, 1570.

188 Q. Wang, T. R. Chan, R. Hilgraf, V. V. Fokin, K. B. Sharpless and M. G. Finn, *J. Am. Chem. Soc.*, **2003**, *125*, 3192.

189 J. Dommerholt, S. Schmidt, R. Temming, L. J. A. Hendriks, F. P. J. T. Rutjes, J. C. M. van Hest, D. J. Lefeber, P. Friedl and F. L. van Delft, *Angew. Chem. Int. Ed.*, **2010**, *49*, 9422.

190 E. M. Sletten and C. R. Bertozzi, *Organic Letters*, **2008**, *10*, 3097.

191 A. A. Poloukhtine, N. E. Mbua, M. A. Wolfert, G.-J. Boons and V. V. Popik, *J. Am. Chem. Soc.*, **2009**, *131*, 15769.

192 A. Poloukhtine and V. V. Popik, *J. Org. Chem.*, **2003**, *68*, 7833.

193 N. K. Urdabayev, A. Poloukhtine and V. V. Popik, *Chem. Commun.*, **2006**, 454.

194 S. V. Orski, A. A. Poloukhtine, S. Arumugam, L. Mao, V. V. Popik and J. Locklin, *J. Am. Chem. Soc.*, **2010**, *132*, 11024.

195 C. D. McNitt and V. V. Popik, *Org. Biomol. Chem.*, **2012**, *10*, 8200.

196 N. C. Yang, R. L. Loeschen and D. Mitchell, *J. Am. Chem. Soc.*, **1967**, *89*, 5465.

197 N. C. Yang, M. Kimura and W. Eisenhardt, *J. Am. Chem. Soc.*, **1973**, *95*, 5058.

198 S. C. Freilich and K. S. Peters, *J. Am. Chem. Soc.*, **1981**, *103*, 6255.

199 D. Sun, S. M. Hubig and J. K. Kochi, *J. Org. Chem.*, **1999**, *64*, 2250.

200 S. J. Harris, D. Murdock, M. P. Grubb, I. P. Clark, G. M. Greetham, M. Towrie and M. N. R. Ashfold, *J. Phys. Chem. A*, **2014**, *118*, 10240.

201 A. G. Griesbeck and S. Stadtmueller, *J. Am. Chem. Soc.*, **1990**, *112*, 1281.

202 *J. Am. Chem. Soc.*, **1991**, *113*, 6923.

203 W. Adam, V. R. Stegmann and S. Weinkötz, *J. Am. Chem. Soc.*, **2001**, *123*, 2452.

204 A. G. Griesbeck, S. Bondock and M. S. Gudipati, *Angew. Chem. Int. Ed.*, **2001**, *40*, 4684.

205 M. Abe, M. Terazawa, K. Nozaki, A. Masuyama and T. Hayashi, *Tetrahedron Lett.*, **2006**, *47*, 2527.

206 B. Pintér, F. De Proft, T. Veszprémi and P. Geerlings, *J. Chem. Sci.*, **2005**, *117*, 561.

207 X.-L. Liu, J.-B. Wang, Y. Tong and Q.-H. Song, *Chem. Eur. J.*, **2013**, *19*, 13216.

208 M. Conradi and T. Junkers, *Macromolecules*, **2011**, *44*, 7969.

209 A. Ethirajan, L. Baeten, M. Conradi, K. Ranieri, B. Conings, H.-G. Boyen and T. Junkers, *Polym. Chem.*, **2013**, *4*, 4010.

210 M. Conradi and T. Junkers, *J. Photochem. Photobiol.*, **2013**, *259*, 41.

211 W. E. Farneth and D. G. Johnson, *J. Am. Chem. Soc.*, **1984**, *106*, 1875.

212 L. Zalotai, T. Berces and F. Marta, *J. Chem. Soc., Faraday Trans.*, **1990**, *86*, 21.

213 A. Joseph and D. E. Falvey, *Photochem. Photobiol. Sci.*, **2002**, *1*, 632.

214 M. K. Cichon, S. Arnold and T. Carell, *Angew. Chem. Int. Ed.*, **2002**, *114*, 793.

215 A. Joseph, G. Prakash and D. E. Falvey, *J. Am. Chem. Soc.*, **2000**, *122*, 11219.

216 K. Nakabayashi, J.-i. Kojima, K. Tanabe, M. Yasuda and K. Shima, *Bull. Chem. Soc. Jpn.*, **1989**, *62*, 96.

217 M. A. Miranda and M. A. Izquierdo, *J. Am. Chem. Soc.*, **2002**, *124*, 6532.

218 R. Pérez-Ruiz, M. A. Izquierdo and M. A. Miranda, *J. Org. Chem.*, **2003**, *68*, 10103.

219 X. Ma and Y. Xia, *Angew. Chem. Int. Ed.*, **2014**, *126*, 2630.

220 T. Pauloehrl, A. Welle, M. Bruns, K. Linkert, H. G. Börner, M. Bastmeyer, G. Delaittre and C. Barner-Kowollik, *Angew. Chem. Int. Ed.*, **2013**, *52*, 9714.

221 T. Pauloehrl, G. Delaittre, M. Bruns, M. Meißler, H. G. Börner, M. Bastmeyer and C. Barner-Kowollik, *Angew. Chem. Int. Ed.*, **2012**, *51*, 9181.

222 D. Voll, T. Junkers and C. Barner-Kowollik, *J. Polym. Sci., Part A: Polym. Chem.*, **2012**, *50*, 2739.

223 Y. Yagci, S. Jockusch and N. J. Turro, *Macromolecules*, **2010**, *43*, 6245.

224 T. J. A. Wolf, D. Voll, C. Barner-Kowollik and A.-N. Unterreiner, *Macromolecules*, **2012**, *45*, 2257.

225 D. Voll, A. Hufendiek, T. Junkers and C. Barner-Kowollik, *Macromol. Rapid Commun.*, **2012**, *33*, 47.

226 D. Voll, D. Neshchadin, K. Hiltebrandt, G. Gescheidt and C. Barner-Kowollik, *Macromolecules*, **2012**, *45*, 5850.

227 E. Frick, H. A. Ernst, D. Voll, T. J. A. Wolf, A.-N. Unterreiner and C. Barner-Kowollik, *Polym. Chem.*, **2014**, *5*, 5053.

228 M. A. B. Meador, M. A. Meador, L. L. Williams and D. A. Scheiman, *Macromolecules*, **1996**, *29*, 8983.

229 M. A. Meador, *Polyimides by photochemical cyclopolymerization*, US Patent, US 6,974,855 B1, **2005**.

230 Y. Musa and M. P. Stevens, *J. Polym. Sci., Part A: Polym. Chem.*, **1972**, *10*, 319.

231 Y. Nakayama and T. Matsuda, *J. Polym. Sci., Part A: Polym. Chem.*, **2005**, *43*, 3324.

232 C. Pac, M. Ihama, M. Yasuda, Y. Miyauchi and H. Sakurai, *J. Am. Chem. Soc.*, **1981**, *103*, 6495.

233 J. Xuan and W.-J. Xiao, *Angew. Chem. Int. Ed.*, **2012**, *51*, 6828.

234 C. K. Prier, D. A. Rankic and D. W. C. MacMillan, *Chem. Rev.*, **2013**, *113*, 5322.

235 D. Ravelli, D. Dondi, M. Fagnoni and A. Albini, *Chem. Soc. Rev.*, **2009**, *38*, 1999.

236 Y. Miyake, K. Nakajima and Y. Nishibayashi, *J. Am. Chem. Soc.*, **2012**, *134*, 3338.

237 D. P. Hari, P. Schroll and B. König, *J. Am. Chem. Soc.*, **2012**, *134*, 2958.

238 T. P. Yoon, M. A. Ischay and J. Du, *Nat Chem*, **2010**, *2*, 527.

239 S. Maity, M. Zhu, R. S. Shinabery and N. Zheng, *Angew. Chem. Int. Ed.*, **2012**, *51*, 222.

240 M. Rueping, D. Leonori and T. Poisson, *Chem. Commun.*, **2011**, *47*, 9615.

241 Y.-Q. Zou, L.-Q. Lu, L. Fu, N.-J. Chang, J. Rong, J.-R. Chen and W.-J. Xiao, *Angew. Chem. Int. Ed.*, **2011**, *50*, 7171.

242 J. Xuan, X.-D. Xia, T.-T. Zeng, Z.-J. Feng, J.-R. Chen, L.-Q. Lu and W.-J. Xiao, *Angew. Chem. Int. Ed.*, **2014**, *53*, 5653.

243 M. A. C. Stuart, W. T. S. Huck, J. Genzer, M. Muller, C. Ober, M. Stamm, G. B. Sukhorukov, I. Szleifer, V. V. Tsukruk, M. Urban, F. Winnik, S. Zauscher, I. Luzinov and S. Minko, *Nat. Mater.*, **2010**, *9*, 101.

244 S. Trakhtenberg, J. C. Warner, R. Nagarajan, F. F. Bruno, L. A. Samuelson and J. Kumar, *Chem. Mater.*, **2006**, *18*, 2873.

245 Y. Chujo, K. Sada, R. Nomura, A. Naka and T. Saegusa, *Macromolecules*, **1993**, *26*, 5611.

246 A. S. Hoffman, *Adv. Drug Deliv. Rev.*, **2002**, *54*, 3.

247 W. E. Hennink and C. F. van Nostrum, *Adv. Drug Deliv. Rev.*, **2002**, *54*, 13.

248 C.-M. Chung, Y.-S. Roh, S.-Y. Cho and J.-G. Kim, *Chem. Mater.*, **2004**, *16*, 3982.

249 K. Saito, L. R. Ingalls, J. Lee and J. C. Warner, *Chem. Commun.*, **2007**, 2503.

250 J. Jiang, B. Qi, M. Lepage and Y. Zhao, *Macromolecules*, **2007**, *40*, 790.

251 J.-C. Boyer, C.-J. Carling, B. D. Gates and N. R. Branda, *J. Am. Chem. Soc.*, **2010**, *132*, 15766.

252 Y. Chen and K.-H. Chen, *J. Polym. Sci., Part A: Polym. Chem.*, **1997**, *35*, 613.

253 G. Kaur, P. Johnston and K. Saito, *Polym. Chem.*, **2014**, *5*, 2171.

254 P. Froimowicz, H. Frey and K. Landfester, *Macromol. Rapid Commun.*, **2011**, *32*, 468.

255 W. G. Kim, *J. Appl. Polym. Sci.*, **2008**, *107*, 3615.

256 M. Nagata and Y. Yamamoto, *J. Polym. Sci., Part A: Polym. Chem.*, **2009**, *47*, 2422.

257   Y. Inaki and H. Hiratsuka, *J. Photopolym. Sci. Technol.*, **2000**, *13*, 739.

258   A. P. Somlai, R. A. Cozad, K. A. Page, H. R. Williams, D. Creed and C. E. Hoyle, *Photochem. Photobiol. Sci.*, **2008**, *7*, 578.

259   M. Ouchi, N. Badi, J.-F. Lutz and M. Sawamoto, *Nat. Chem.*, **2011**, *3*, 917.

260   J. Willenbacher, K. N. R. Wuest, J. O. Mueller, M. Kaupp, H.-A. Wagenknecht and C. Barner-Kowollik, *ACS Macro Lett.*, **2014**, 574.

261   V. San Miguel, C. G. Bochet and A. del Campo, *J. Am. Chem. Soc.*, **2011**, *133*, 5380.

262   K. Hiltebrandt, T. Pauloehrl, J. P. Blinco, K. Linkert, H. G. Börner and C. Barner-Kowollik, *Angew. Chem. Int. Ed.*, **2015**, *54*, 2838.

263   J.-F. Lutz, M. Ouchi, D. R. Liu and M. Sawamoto, *Science*, **2013**, *341*.

264   N. Badi and J.-F. Lutz, *Chem. Soc. Rev.*, **2009**, *38*, 3383.

265   N. Zydziak, F. Feist, B. Huber, J. O. Mueller and C. Barner-Kowollik, *Chem. Commun.*, **2015**, *51*, 1799.

266   A. S. Quick, J. Fischer, B. Richter, T. Pauloehrl, V. Trouillet, M. Wegener and C. Barner-Kowollik, *Macromol. Rapid Commun.*, **2013**, *34*, 335.

267   C. D. Muller, A. Falcou, N. Reckefuss, M. Rojahn, V. Wiederhirn, P. Rudati, H. Frohne, O. Nuyken, H. Becker and K. Meerholz, *Nature*, **2003**, *421*, 829.

268   K. Yoshida and E. H. Greener, *J. Dent.*, **1994**, *22*, 296.

269   E. Reichmanis and L. F. Thompson, *Chem. Rev.*, **1989**, *89*, 1273.

270   G. Oster, G. K. Oster and H. Moroson, *J. Polym. Sci., Part A: Polym. Chem.*, **1959**, *34*, 671.

271   L. Tang, B. Qu and X. Shen, *J. Appl. Polym. Sci.*, **2004**, *92*, 3371.

272   F. Fallani, G. Ruggeri, S. Bronco and M. Bertoldo, *Polym. Deg. Stab.*, **2003**, *82*, 257.

273   B. Rånby, *Mat. Res. Innovat.*, **1998**, *2*, 64.

274   A. Harada and Q. Tran-Cong, *Macromolecules*, **1997**, *30*, 1643.

275   M. Yan, S. X. Cai, M. N. Wybourne and J. F. W. Keana, *Bioconjugate Chem.*, **1994**, *5*, 151.

276   T. Miyashita, M. Nakaya and A. Aoki, *Thin Solid Films*, **1998**, *327–329*, 833.

277   H. Park, D.-C. Han, D.-H. Han, S.-J. Kim, W.-E. Lee and G. Kwak, *Macromolecules*, **2011**, *44*, 9351.

278   A. Bacher, C. H. Erdelen, W. Paulus, H. Ringsdorf, H.-W. Schmidt and P. Schuhmacher, *Macromolecules*, **1999**, *32*, 4551.

279   K. S. Schanze, T. S. Bergstedt and B. T. Hauser, *Adv. Mater.*, **1996**, *8*, 531.

280   X. Deng and K. Y. Wong, *Macromol. Rapid Commun.*, **2009**, *30*, 1570.

281   J. D. Gelorme, R. J. Cox and S. A. R. Gutierrez, *Photoresist composition and printed circuit boards and packages made therewith*, US Patent, US4882245 A, **1989**.

282   M. Jamal, A. M. Zarafshar and D. H. Gracias, *Nat. Commun.*, **2011**, *2*, 527.

283   A. Charas and J. Morgado, *Curr. Phys. Chem.*, **2012**, *24*, 241.

284   D. C. Müller, T. Braig, H.-G. Nothofer, M. Arnoldi, M. Gross, U. Scherf, O. Nuyken and K. Meerholz, *Chem. Phys. Chem.*, **2000**, *1*, 207.

285   M. V. S. N. Maddipatla, D. Wehrung, C. Tang, W. Fan, M. O. Oyewumi, T. Miyoshi and A. Joy, *Macromolecules*, **2013**, *46*, 5133.

286   L. A. Connal, R. Vestberg, C. J. Hawker and G. G. Qiao, *Adv. Funct. Mater.*, **2008**, *18*, 3315.

287   A. L. Barbarini, D. L. Reyna and D. M. Martino, *Green Chem. Lett. Rev.*, **2010**, *3*, 231.

288   J. R. Bianchini, K. Saito, T. B. Balin, V. Dua and J. C. Warner, *J. Polym. Sci., Part A: Polym. Chem.*, **2007**, *45*, 1296.

289   X.-Y. Hong, J.-Q. Xiao, Z. Zhou and R.-X. Pei, *J. Polym. Sci., Part A: Polym. Chem.*, **1984**, *22*, 3289.

290   B. Domercq, R. D. Hreha, Y.-D. Zhang, N. Larribeau, J. N. Haddock, C. Schultz, S. R. Marder and B. Kippelen, *Chem. Mater.*, **2003**, *15*, 1491.

291   R. Yamaguchi and S. Sato, *J. Photopolym. Sci. Technol.*, **2008**, *21*, 203.

292   X.-C. Li, T.-M. Yong, J. Grüner, A. B. Holmes, S. C. Moratti, F. Cacialli and R. H. Friend, *Synth. Met.*, **1997**, *84*, 437.

293   A. Kumar, S.-Y. Jang, J. Padilla, T. F. Otero and G. A. Sotzing, *Polymer*, **2008**, *49*, 3686.

294   L. Qiu, Q. Xu, W. H. Lee, X. Wang, B. Kang, G. Lv and K. Cho, *J. Mater. Chem.*, **2011**, *21*, 15637.

295   V. S. Khire, A. W. Harant, A. W. Watkins, K. S. Anseth and C. N. Bowman, *Macromolecules*, **2006**, *39*, 5081.

296   M. Natali, S. Begolo, T. Carofiglio and G. Mistura, *Lab on a Chip*, **2008**, *8*, 492.

297   A. R. Davis, J. A. Maegerlein and K. R. Carter, *J. Am. Chem. Soc.*, **2011**, *133*, 20546.

298   F. Baycan Koyuncu, A. R. Davis and K. R. Carter, *Chem. Mater.*, **2012**, *24*, 4410.

299   J. Lee, H. Han, J. Lee, S. C. Yoon and C. Lee, *J. Mater. Chem.*, **2014**, *2*, 1474.

300   B. J. Adzima, C. J. Kloxin, C. A. DeForest, K. S. Anseth and C. N. Bowman, *Macromol. Rapid Commun.*, **2012**, *33*, 2092.

301   F. G. Schmidt, S. Hilf, C. Barner-Kowollik, N. Guimard, K. K. Oehlenschlaeger and J. Mueller, **2013**.

302   A. S. Quick, H. Rothfuss, A. Welle, B. Richter, J. Fischer, M. Wegener and C. Barner-Kowollik, *Adv. Funct. Mater.*, **2014**, *24*, 3571.

303   E. Zhao, H. Li, J. Ling, H. Wu, J. Wang, S. Zhang, J. W. Y. Lam, J. Z. Sun, A. Qin and B. Z. Tang, *Polym. Chem.*, **2014**, *5*, 2301.

304   C. Lang, D. Voll, A. J. Inglis, N. Dingenouts, A. S. Goldmann, L. Barner and C. Barner-Kowollik, *Macromol. Chem. Phys.*, **2011**, *212*, 831.

305   C. Lang, K. Pahnke, C. Kiefer, A. S. Goldmann, P. W. Roesky and C. Barner-Kowollik, *Polym. Chem.*, **2013**, *4*, 5456.

306   W. H. Carothers, *Trans. Faraday Soc.*, **1936**, *32*, 39.

307   M. Beija, M.-T. Charreyre and J. M. G. Martinho, *Prog. Polym. Sci.*, **2011**, *36*, 568.

308   O. P. Lee, A. T. Yiu, P. M. Beaujuge, C. H. Woo, T. W. Holcombe, J. E. Millstone, J. D. Douglas, M. S. Chen and J. M. J. Fréchet, *Adv. Mater.*, **2011**, *23*, 5359.

309   S. Burattini, B. W. Greenland, D. H. Merino, W. Weng, J. Seppala, H. M. Colquhoun, W. Hayes, M. E. Mackay, I. W. Hamley and S. J. Rowan, *J. Am. Chem. Soc.*, **2010**, *132*, 12051.

310   Z. Xu, N. J. Singh, J. Lim, J. Pan, H. N. Kim, S. Park, K. S. Kim and J. Yoon, *J. Am. Chem. Soc.*, **2009**, *131*, 15528.

311   T. Gruendling, M. Kaupp, J. P. Blinco and C. Barner-Kowollik, *Macromolecules*, **2010**, *44*, 166.

312   A. S. Goldmann, M. Glassner, A. J. Inglis and C. Barner-Kowollik, *Macromol. Rapid Commun.*, **2013**, *34*, 810.

313   S. Sinnwell, A. J. Inglis, T. P. Davis, M. H. Stenzel and C. Barner-Kowollik, *Chem. Commun.*, **2008**, 2052.

314   L. Nebhani, S. Sinnwell, C. Y. Lin, M. L. Coote, M. H. Stenzel and C. Barner-Kowollik, *J. Polym. Sci., Part A: Polym. Chem.*, **2009**, *47*, 6053.

315   A. J. Inglis, M. H. Stenzel and C. Barner-Kowollik, *Macromol. Rapid Commun.*, **2009**, *30*, 1792.

316   S. Sinnwell, A. J. Inglis, M. H. Stenzel and C. Barner-Kowollik, *Macromol. Rapid Commun.*, **2008**, *29*, 1090.

317   K. K. Oehlenschlaeger, J. O. Mueller, N. B. Heine, M. Glassner, N. K. Guimard, G. Delaittre, F. G. Schmidt and C. Barner-Kowollik, *Angew. Chem. Int. Ed.*, **2013**, *52*, 762.

318   P. G. Sammes, *Tetrahedron*, **1976**, *32*, 405.

319   C. Barner-Kowollik, *Macromol. Rapid Commun.*, **2009**, *30*, 1625.

320   M. W. Farber, J. R. Worns, *Syndiotactic polybutadiene composition for a photosensitive printing plate*, European Patent, EP0076588 A3, **1981**.

321   R. K. Y. Shikinami, R. Kimura, Y. Yoshikawa, K. Iida, K. Hata, *Radiation process for producing 1,2-polybutadiene foamed products*, US Patent, US4144153 A, **1979**.

322   A. Kassu, J.-M. Taguenang and A. Sharma, *Appl. Opt.*, **2007**, *46*, 489.

323   C. Decker and T. N. T. Viet, *Macromol. Chem. Phys.*, **1999**, *200*, 1965.

324   C. Decker and T. Nguyen Thi Viet, *J. Appl. Polym. Sci.*, **2000**, *77*, 1902.

325   C. Decker and T. Nguyen Thi Viet, *Polymer*, **2000**, *41*, 3905.

326   V. Barboiu and M. I. Avadanei, *Polymer*, **2008**, *49*, 4687.

327   G. T. Carroll, L. Devon Triplett, A. Moscatelli, J. T. Koberstein and N. J. Turro, *J. Appl. Polym. Sci.*, **2011**, *122*, 168.

328   V. Barboiu and M. I. Avadanei, *J. Photochem. Photobiol.*, **2011**, *222*, 170.

329   D. H. Carey and G. S. Ferguson, *Macromolecules*, **1994**, *27*, 7254.

330   M. I. Avadanei, *J. Macromol. Sci., Phys.*, **2011**, *51*, 313.

331   C. Decker and T. N. T. Viet, *Macromol. Chem. Phys.*, **1999**, *200*, 358.

332   C. Decker and T. Nguyen Thi Viet, *J. Appl. Polym. Sci.*, **2001**, *82*, 2204.

333   W. Kern and K. Hummel, *Macromol. Chem. Phys.*, **1993**, *194*, 2641.

334   V. T. Kagiya and K. Takemoto, *J. Macromol. Sci. A: Chem.*, **1976**, *10*, 795.

335   G. T. Carroll, N. J. Turro and J. T. Koberstein, *J. Colloid Interface Sci.*, **2010**, *351*, 556.

336   R.-Q. Png, P.-J. Chia, J.-C. Tang, B. Liu, S. Sivaramakrishnan, M. Zhou, S.-H. Khong, H. S. O. Chan, J. H. Burroughes, L.-L. Chua, R. H. Friend and P. K. H. Ho, *Nat. Mater.*, **2010**, *9*, 152.

337   R. K. V. Lim and Q. Lin, *Chem. Commun.*, **2010**, *46*, 1589.

338   H. Mehenni, V. Pourcelle, J.-F. Gohy and J. Marchand-Brynaert, *Austr. J. Chem.*, **2012**, *65*, 193.

339   M. A. Tasdelen and Y. Yagci, *Angew. Chem. Int. Ed.*, **2013**, *52*, 5930.

340   P. Weinberg, C. Csongár and G. Tomaschewski, *Z. Chem.*, **1987**, *27*, 407.

341   C. Csongar, P. Weinberg, M. Gessner and G. Tomaschewski, *J. Prakt. Chem.*, **1987**, *329*, 1111.

342   P. Weinberg, C. Csongár and U.-W. Grummt, *J. Photochem. Photobiol.*, **1989**, *50*, 11.

343   S. Ito, Y. Tanaka, A. Kakehi and K.-I. Kondo, *Bull. Chem. Soc. Jpn.*, **1976**, *49*, 1920.

344   C. Rodriguez-Emmenegger, C. M. Preuss, B. Yameen, O. Pop-Georgievski, M. Bachmann, J. O. Mueller, M. Bruns, A. S. Goldmann, M. Bastmeyer and C. Barner-Kowollik, *Adv. Mater.*, **2013**.

345   X.-C. Gao, H. Cao, L.-Q. Zhang, B.-W. Zhang, Y. Cao and C.-H. Huang, *J. Mater. Chem.*, **1999**, *9*, 1077.

346   M. Schäfer, M. Drayß, A. Springer, P. Zacharias and K. Meerholz, *Eur. J. Org. Chem.*, **2007**, *2007*, 5162.

347   R. Darkow, U. Hartmann and G. Tomaschewski, *React. Funct. Polym.*, **1997**, *32*, 195.

348   C. J. Dürr, P. Lederhose, L. Hlalele, D. Abt, A. Kaiser, S. Brandau and C. Barner-Kowollik, *Macromolecules*, **2013**, *46*, 5915.

349   T. Pauloehrl, A. Welle, K. K. Oehlenschlaeger and C. Barner-Kowollik, *Chem. Sci.*, **2013**, *4*, 3503.

CURRICULUM VITAE

Date of birth: 01/12/1986

Place of birth: Worms, Germany

Nationality: German

Education and professional experience

02/2012 - 05/2015   Doctoral studies in chemistry under the supervision of
                        Prof. Dr. Christopher Barner-Kowollik
                        Karlsruhe Institute of Technology (KIT), Germany
                        "Modular Light-Induced Ligation in Polymer Science"

12/2014 - 03/2015   Research period under the supervision of Dr. James
                        Blinco
                        Queensland University of Technology (QUT), Queensland,
                        Brisbane, Australia

10/2011   Diploma in Chemistry under the Supervision of Prof. Dr.
                        Christopher Barner-Kowollik
                        Karlsruhe Institute of Technology (KIT), Germany
                        "Photo-Induced Diels-Alder Chemistry and its Application"

04/2007 - 10/2011   Studies in Chemistry
                        Universität Karlsruhe (TH) (later: Karlsruhe Institut of
                        Technology (KIT)), Germany

07/2006 - 03/2007   Civilian Service
                        Johanniter, Viernheim (Germany)

06/2006   High School Certificate
                        Heppenheim, Germany

PUBLICATIONS AND CONFERENCE CONTRIBUTIONS

Peer reviewed journal articles

14. b) Effiziente Photochemie für die räumlich aufgelöste Oberflächen-funktionalisierung

G. Delaittre, A. S. Goldmann, J. O. Mueller, C. Barner-Kowollik, *Angew. Chem.* **2015**, *in press.*

14. a) Efficient Photochemistries for Spatially Resolved Surface Functionalization

G. Delaittre, A. S. Goldmann, J. O. Mueller, C. Barner-Kowollik, *Angew. Chem. Int. Ed.* **2015**, *in press.*

13. b) Durch sichtbares Licht induzierte Klick-Chemie

J. O. Mueller, F. G. Schmidt, J. P. Blinco, C. Barner-Kowollik, *Angew. Chem.* **2015**, DOI: 10.1002/ange.201504716R1.

13. a) Visible-Light-Induced Click Chemistry

J. O. Mueller, F. G. Schmidt, J. P. Blinco, C. Barner-Kowollik, *Angew. Chem. Int. Ed.* **2015**, DOI: 10.1002/anie.201504716.

12. Photo-Induced Sequence Defined Macromolecules via Hetero Bifunctional Synthons

N. Zydziak, F. Feist, B. Huber, J. O. Mueller, C. Barner-Kowollik, *Chem. Commun.* **2015**, *51*, 1799-1802.

11. **A Disulfide Intercalator Toolbox for Site-Directed Protein Chemistry**

T. Wang, Y. Wu, S. L. Kuan, O. Dumele, M. Lamla, D. Y. W. Ng, M. Arzt, J. Thomas, J. O. Mueller , C. Barner-Kowollik , T. Weil, *Chem. Eur. J.* **2014**, *21*, 228-238.

10. **Fluorescent Polymers from Non-Fluorescent Photoreactive Monomers**

J. O. Mueller, D. Voll, F. G. Schmidt, G. Delaittre, C. Barner-Kowollik, *Chem. Commun.* **2014**, *50*, 15681-15684.

9. **Adaptable Hetero Diels–Alder Networks for Fast Self-Healing under Mild Conditions**

K. K. Oehlenschlaeger, J. O. Mueller, J. Brandt, S. Hilf, A. Lederer, M. Wilhelm, R. Graf, M. L. Coote, F. G. Schmidt, C. Barner-Kowollik, *Adv. Mater.* **2014**, *26*, 3561-3566.

8. **Photochemical Design of Functional Fluorescent Single-Chain Nanoparticles**

J. Willenbacher, K. N. R. Wuest, J. O. Mueller, M. Kaupp, H.-A. Wagenknecht, C. Barner-Kowollik, *ACS Macro Lett.* **2014**, 574-579.

7. **Photo-Patterning of Non-Fouling Polymers and Biomolecules on Paper**

T. Tischer, C. Rodriguez-Emmenegger, V. Trouillet, A. Welle, V. Schueler, J. O. Mueller, A. S. Goldmann, E. Brynda, C. Barner-Kowollik, *Adv. Mater.* **2014**, *26*, 4087-4092.

6. **Sunlight-Induced Crosslinking of 1,2-Polybutadienes: Access to Fluorescent Polymer Networks**

J. O. Mueller, N. K. Guimard, K. K. Oehlenschlaeger, F. G. Schmidt, C. Barner-Kowollik, *Polym. Chem.* **2014**, *5*, 1447-1456.

5. **Controlled Cell Adhesion on Poly(dopamine) Interfaces Photo-patterned with Non-Fouling Brushes**

C. Rodriguez-Emmenegger, C. M. Preuss, B. Yameen, O. Pop-Georgievski, M. Bachmann, J. O. Mueller, M. Bruns, A. S. Goldmann, M. Bastmeyer, C. Barner-Kowollik, *Adv. Mater.* **2013**, *25*, 6123-6127.

4. **Fast and Catalyst-Free Hetero-Diels-Alder Chemistry for Cyclable Bonding/Debonding on Demand Material Design**

K. K. Oehlenschlaeger, N. K. Guimard, J. Brandt, J. O. Mueller, C. Y. Lin, S. Hilf, A. Lederer, M. L. Coote, F. G. Schmidt, C. Barner-Kowollik, *Polym. Chem.* **2013**, *4*, 4348-4355.

3. **Harnessing Entropy to Direct the Bonding/Debonding of Polymer Systems on Reversible Chemistry**

N. K. Guimard, J. Ho, J. Brandt, C. Y. Lin, M. Namazian, J. O. Mueller, K. K. Oehlenschlaeger, S. Hilf, A. Lederer, F. G. Schmidt, M. L. Coote, C. Barner-Kowollik, *Chem. Sci.* **2013**, *4*, 2752-2759.

2. b) **Lichtinduzierte Modulare Ligation von Konventionellen RAFT Polymeren**

K. K. Oehlenschlaeger,[‡] J. O. Mueller,[‡] N. B. Heine, M. Glassner, N. K. Guimard, G. Delaittre, F. G. Schmidt, C. Barner-Kowollik, *Angew. Chem.* **2013**, *125*, 791-796. [‡] both authors contributed equally.

2. a) **Light-Induced Modular Ligation of Conventional RAFT Polymers**

K. K. Oehlenschlaeger,[‡] J. O. Mueller,[‡] N. B. Heine, M. Glassner, N. K. Guimard, G. Delaittre, F. G. Schmidt, C. Barner-Kowollik, *Angew. Chem. Int. Ed.* **2013**, *52*, 762-766. [‡] both authors contributed equally.

1. **Highly Orthogonal Functionalization of ADMET Polymers via Photo-Induced Diels-Alder Reactions**

M. Winkler, J. O. Mueller, K. K. Oehlenschlaeger, L. Montero de Espinosa, M. A. R. Meier, C. Barner-Kowollik, *Macromolecules* **2012**, *45*, 5012-5019.

Patents

4. **Durch sichtbares Licht induzierte Polymerisation bzw. Vernetzung mittels Azirin-Verbindungen**

F.-G. Schmidt, C. Barner-Kowollik, J. Blinco, J. Müller, *IP-nr. to be advised.*

3. **Photo-induced Crosslinking of Double Bond-containing Polymers by Means of a Pericyclic Reaction**

   F.-G. Schmidt, S. Hilf, C. Barner-Kowollik, N. Guimard, K. Öhlenschläger, J. Müller, *International Patent PCT*, US **2014**0323648 A1.

2. **Functional Materials with Reversible Crosslinking**

   C. Barner-Kowollik, K. Öhlenschläger, S. Hilf, F.-G. Schmidt, N. Guimard, J. Müller, *International Patent PCT*, WO/**2014**/090492.

1. **Photoinduzierte Vernetzung von Doppelbindungen-enthaltenden Polymeren mittels pericyclischer Reaktion**

   C. Barner-Kowollik, N. Guimard, S. Hilf, J. Müller, K. Öhlenschläger, F.-G. Schmidt, *International Patent PCT*, WO/**2013**/104486.

Book chapter

1. **Advanced Strategies for Spatially Resolved Surface Design via Photochemical Methods**

   A. S. Goldmann, G. Delaittre, J. O. Mueller, C. Barner-Kowollik **2015**, in *Dyes and Chromophores in Polymer Science* (eds J. Lalevee, J. P. Fouassier), John Wiley & Sons, Hoboken, USA. DOI: 10.1002/9781119006671.ch9.

Invited talk and conference contributions

3. **Advanced Light-Induced Ligation Techniques for Application in Polymer Science**

   Queensland University of Technology (QUT), Brisbane, Australia

2. **Modular Light-Induced Crosslinking**

   BASF Research Forum Europe **2014**, Antwerp, Belgium

1. **Light-Induced Modular Ligation of Conventional RAFT Polymers**

   Macromolecular Colloquium **2013**, Freiburg, Germany

DANKSAGUNGEN –

ACKNOWLEDGEMENTS

An erster Stelle möchte ich Prof. Dr. Christopher Barner-Kowollik danken. Außer der Tatsache, dass er mir ermöglicht hat in seiner Gruppe zu arbeiten, bin ich vor allem für die Art und Weise seiner Betreuung dankbar, die sich durch das mir entgegengebrachte Vertrauen in meine eigenen Fähigkeiten auszeichnet und mir dadurch ermöglicht hat selbständig Forschungsprojekte zu gestalten und durchzuführen. Besonders beeindruckt haben mich sein vorgelebter Enthusiasmus für die Forschung sowie die Hingabe, mit der er seine Gruppe führt.

Ich danke meinen Kooperationspartnern von Evonik Industries für die hervorragende Zusammenarbeit. Insbesondere Dr. Friedrich-Georg Schmidt, aber auch Dr. Stefan Hilf, Dr. Markus Pridöhl und Dr. Christian Meier danke ich für die vielen gemeinsamen Meetings, die sich stets durch produktive und zielgerichtete Diskussionen ausgezeichnet haben und dadurch mit neuen Impulsen und Sichtweisen für einen positiven Einfluss auf meine Arbeit gesorgt haben.

Very special thanks to everyone who has contributed to the publications I have (co)authored, including collaboration partners as well as post-docs, fellow Ph.D. students and undergraduate students from our group.

A big thank you goes to the entire macroarc research group as well as its former members! Zunächst seien Anja Goldmann, Maria Schneider, Peter Gerstel und Vincent Schüler erwähnt, die mit ihrem großen organisatorischen Einsatz effektive Forschungsarbeit erst ermöglichen. Als nächstes danke ich ganz besonders meinen Evonik-Teamkollegen Kim Öhlenschläger und Kai Pahnke. Abgesehen von der höchst produktiven wissenschaftlichen Zusammenarbeit bin ich euch vor allem für die gute Stimmung abseits der Arbeit dankbar. Importantly, I want to thank Nathalie Guimard for teaching me the English language as well as scientific work and writing

at the beginning of my time in this group. The present thesis would not be in the state it is if it wasn't for you. Desweiteren möchte mich bei allen Labor- und Bürokollegen bedanken, die aufzuzählen auf Grund der wechselnden Besetzung nahezu ein Ding der Unmöglichkeit ist. Unser fließender Übergang zwischen professioneller Forschungsarbeit zu entspanntem, ungezwungenem Umgang miteinander ist bemerkenswert und macht die Arbeit in dieser Gruppe so angenehm.

Many thanks to Dr. James Blinco for part-time supervision during my research period at the Queensland University of Technology in Brisbane. Moreover, I thank Prof. Dr. Stephen Blanksby and Dr. David Marshall for plenty of productive and informative discussions concerning mass spectrometry. In the context of my stay in Australia, I acknowledge the Karlsruhe House of Young Scientists (KHYS) for financial support. Still in the context of supporting my research, I thank Paul Lederhose for his great help with pretty much everything concerning laboratory issues in M6. Besides thanking everyone I have forgotten so far but who contributed to making my research at the QUT successful, I want to give very warm thanks to all the friends I have made in Brisbane. I thank everyone in the free radical group as well as my sharehouse roommates for the great time I had in Brisbane.

In direktem Bezug auf die vorliegende Arbeit möchte ich mich bei Elena Frick, Michael Kaupp, Katrin Kockler, Alex Schenzel, Dominik Voll, Kai Pahnke und Nils Jasinsky sowie meinem Bruder Torbjörn für ihre Mühe beim Korrekturlesen bedanken.

An letzter Stelle stehend und doch mit am wichtigsten sind meine Danksagungen, die in Richtung meines sozialen Umfelds abseits der Arbeit gehen. Zunächst möchte ich mich ganz allgemein bei Familie und Freunden für deren Geduld mit mir bedanken. Vielen Dank, dass ihr mir meine limitierte Fähigkeit rechtzeitig an persönliche Nachrichten und Termine zu denken nachseht bzw. sie kompensiert. Ein herzliches Dankeschön an meine Familie sowie meine Freundin Nina für das Verständnis und die Unterstützung, die ihr mir entgegenbringt. Ein weiterer Punkt, der mir persönlich sehr wichtig ist, hat mit Ausgleich und Ablenkung von der Arbeit zu tun, was für mich essentiell zur Lebensqualität beiträgt und dementsprechend auch die allgemeine Stimmung beeinflusst. In diesem Zusammenhang bedanke ich mich erneut bei meinen Eltern, meinem Bruder, Nina und ihrer Familie, meinen Freunden aus der Heimat und Karlsruhe, Tischtenniskollegen aus Lorsch und Karlsruhe, meinen

früheren Kommilitonen, der Doppelkopfrunde, aber auch all meinen neu gewonnenen Freunden innerhalb der Gruppe, die beim gemeinsamen Sport treiben, Kaffeepausen oder einem Feierabendbier zum Kraft tanken beigetragen haben.

Hiermit bestätige ich wahrheitsgemäß, dass ich die vorliegende Arbeit im Rahmen der Betreuung von Prof. Dr. Christopher Barner-Kowollik, selbstständig verfasst und keine anderen als die angegebenen Quellen und Hilfsmittel verwendet habe.

Karlsruhe, den 01.06.2015

Jan Müller